THE NORTH PACIFIC FROM GLACIAL TO MODERN: ASSEMBLAGES, ISOTOPES AND CO_2

Ben Justin Taylor

A Thesis Submitted for the Degree of PhD
at the
University of St Andrews

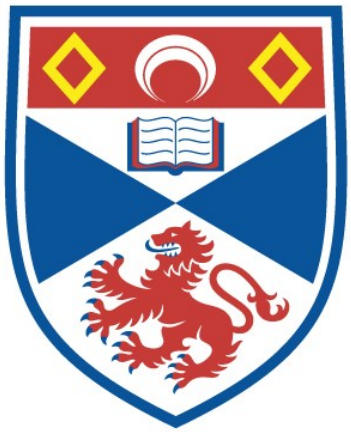

2019

Candidate's declaration

I, Ben Justin Taylor, do hereby certify that this thesis, submitted for the degree of PhD, which is approximately 50,000 words in length, has been written by me, and that it is the record of work carried out by me, or principally by myself in collaboration with others as acknowledged, and that it has not been submitted in any previous application for any degree.

I was admitted as a research student at the University of St Andrews in September 2014.

I received funding from an organisation or institution and have acknowledged the funder(s) in the full text of my thesis.

Date Signature of candidate

Supervisor's declaration

I hereby certify that the candidate has fulfilled the conditions of the Resolution and Regulations appropriate for the degree of PhD in the University of St Andrews and that the candidate is qualified to submit this thesis in application for that degree.

Date Signature of supervisor

Permission for publication

In submitting this thesis to the University of St Andrews we understand that we are giving permission for it to be made available for use in accordance with the regulations of the University Library for the time being in force, subject to any copyright vested in the work not being affected thereby. We also understand, unless exempt by an award of an embargo as requested below, that the title and the abstract will be published, and that a copy of the work may be made and supplied to any bona fide library or research worker, that this thesis will be electronically accessible for personal or research use and that the library has the right to migrate this thesis into new electronic forms as required to ensure continued access to the thesis.

I, Ben Justin Taylor, confirm that my thesis does not contain any third-party material that requires copyright clearance.

The following is an agreed request by candidate and supervisor regarding the publication of this thesis:

Printed copy

No embargo on print copy.

Electronic copy

No embargo on electronic copy.

Date Signature of candidate

Date Signature of supervisor

Underpinning Research Data or Digital Outputs

Candidate's declaration

I, Ben Justin Taylor, hereby certify that no requirements to deposit original research data or digital outputs apply to this thesis and that, where appropriate, secondary data used have been referenced in the full text of my thesis.

Date Signature of candidate

Abstract

Investigating past changes in Earth's climate can provide useful information for assessing future climate change scenarios. Planktic foraminifera preserved in marine sediment are commonly used as a tool to reconstruct past environmental change. Here I present a combination of modern census and multinet data from the North Pacific, a new compilation of global census data, a new global calibration for Mg/Ca ratios in *Neogloboquadrina pachyderma*, and foraminifera assemblage, trace element, and boron isotope data from the North Pacific spanning the last deglaciation.

New modern census data from the North Pacific shows that two key sub-polar proxy carrying species, *N. pachyderma* and *Globigerina bulloides*, predominantly live between 0-50 m in the water column. Global planktic foraminifera diversity is observed to be driven primarily by sea surface temperature, with upwelling and ocean productivity providing key secondary roles. In the North Pacific, a preservation bias of *N. pachyderma* over *G. bulloides* is observed when comparing multinet and core-top samples, highlighting the importance of tracking dissolution during downcore studies. To improve the use of Mg/Ca ratios in *N. pachyderma* downcore, I produced a new global calibration with a temperature sensitivity of 6 % per °C. This calibration was combined with boron isotope and Mg/Ca data from sediment core MD02-2489 to investigate changes in North Pacific circulation, productivity, and CO_2 during the last deglaciation. Two intervals of high surface CO_2 were observed, the first during Heinrich Stadial 1, where deep ventilation mixed CO_2 and nutrients throughout the water column. The second occurred during the Bølling-Allerød, where stratification pooled nutrients and CO_2 in surface waters, leading to enhanced productivity and CO_2 outgassing. Overall, this thesis improves the use of planktic foraminifera as tools for investigating past climate change and highlights the role of the North Pacific in deglacial CO_2 release.

General acknowledgements

Firstly, I would like to thank my supervisors James Rae and Andrea Burke. I could not have hoped for two more enthusiastic, invested, and truly excellent supervisors. You have inspired me to do more and do better and have made this PhD a thoroughly enjoyable experience. Watching the STAiG lab grow from just three people and a mass spec, to the thriving group it is now has been great to witness.

That brings me to my second group of thanks, the STAiG team. I'd like to thank Will Gray for excellent (and endless) discussions regarding the North Pacific, for teaching me R, and all the lab support and advice. I thank Jess Crumpton-Banks, the first PhD student to join me in STAiG and my lab buddy for the past four years, you helped me through a lot of long lab days and were always keen for a beer at the end. Thank you to Rosanna Greenop, you have been an excellent guide throughout my PhD, I think myself, Jess, and Eloise can safely say you have made our PhD experiences that much better. Thank you, Eloise Littley, for always keeping a calm head and having the best set of columns in the world. Thanks also to the rest of the STAiG team past and present: Paul Savage; Bob Steele; Dan Nita; Rhian Rees-Owen; Laura Crick; Natalya Zainva-James.

There are many people outside of St Andrews who have provided help, support and samples throughout my PhD and I would like to thank some of them here. Rainer Gersonde, Andrea Ablemann, Edith Maier, and Oliver Esper are thanked for hosting me at the Alfred-Wegner Institute, providing core-top and multinet samples from the SO202 INOPEX cruise, and for excellent discussions regarding planktic foraminifera in the North Pacific. For teaching me planktic foraminifera taxonomy, genetics, and generally all things foraminifera, I thank Kate Darling. I also thank Lucas Jonkers for providing me with compiled Mg/Ca data, as well as Alan Mix and those at Oregon State University for providing core-top samples from the EW0408 cruise. Michael Sarnthein is thanked for in depth discussions about North Pacific circulation and CO_2, and for providing samples from sediment core MD02-2489. I would also like to thank the Natural Environment Research Council for funding this PhD.

On a personal note, I would like to thank Mum and Dad for being ever supportive of me moving to the other end of the country and for having a full fridge ready whenever I came home. My brother, Lyndon, I thank for distracting me with football and FIFA during the holidays. I'd also

like to thank Dev, Sonny, Lawrence, Sam, Ballen, Paddy, Ben, and Christian for their support and "interest" throughout. Finally, I'd like to thank Imy for the never-ending support and for making St Andrews such a special place that I'll never forget.

I also want to thank all within the School of Earth and Environmental Science at the University of St Andrews as well as the wider postgraduate community. From Halloween and Burn's night, to Friday evening Miller Club, I have had a fantastic four years with you all, and one that will not be forgotten in a hurry.

Funding

This work was supported by the Natural Environment Research Council [NE/L002590/1].

Table of contents

1. Introduction 12
1.1 Global climate change: 800,000 years to present 12
1.2 CO_2 and the carbon cycle in seawater 14
1.3 Reconstructing past environmental change 16
1.4 Changes in CO_2 circulation during the last deglaciation 21
1.5 Thesis structure 23
1.6 References 23
2. Distribution and ecology of planktic foraminifera in the North Pacific: Implications for paleo-reconstructions 31
2.1 Introduction 32
2.2 Oceanographic Setting 33
2.3 Materials and Methods 34
2.3.1 SO202 INOPEX cruise study area 34
2.3.2 CTD deployments 36
2.3.3 Multinet samples 36
2.3.4 Surface sediment samples 37
2.3.5 Plankton net samples 37
2.3.6 Compilation of North Pacific core-top assemblage data 38
2.3.7 Sediment trap data 38
2.4 Results 38
2.4.1 Subarctic Front 38
2.4.2 North East Pacific (Alaskan Coastal Current) 39
2.4.3 Sub-tropical gyre 40
2.4.4 North West Pacific (Kamchatka Current, Oyashio Current) 40
2.4.5 Bering Sea (Alaskan Coastal inflow water, Bering slope water) 41
2.5 Discussion 43
2.5.1 Geographic distribution of planktic foraminifera in the North Pacific 43
2.5.2 Ecology and Distribution of *G. bulloides* in North Pacific waters 49
2.5.3 Ecology and Distribution of *N. pachyderma* in the subpolar North Pacific 56
..... 60
2.5.4 Dissolution and seasonality in North Pacific core top assemblages 61
2.6 Conclusions and implications for downcore records 62
2.6.1 Ecological drivers in subpolar species 62
2.6.2 Implications for geochemical records 64

2.6.3 Dissolution bias in sediments 64
2.7 Acknowledgments 65
2.8 References 65
2.9 Supplementary figures and tables 72
3. Drivers of planktic foraminifera distribution in the modern ocean 76
3.1 Introduction 77
3.1.1 Modern distribution of planktic foraminifera 77
3.1.2 Seasonality and habitat depth of modern planktic foraminifera 78
3.1.3 Planktic foraminifera and the carbon cycle 79
3.1.4 Paleo-reconstructions with planktic foraminifera census data 80
3.1.5 Global distribution, ecology, and drivers of planktic foraminifera 81
3.2 Methods 81
3.2.1 Global database of planktic foraminifera census data 81
3.2.2 Environmental data 82
3.2.3 Regression and redundancy analysis 83
3.3 Results 83
3.3.1 Global foraminifera database 83
3.3.2 Environmental data 85
3.3.3 Redundancy Analysis 86
3.4 Discussion 87
3.4.1 Global distribution of major planktic foraminifera species 87
3.4.2 Ecological drivers of species abundance 97
3.4.3 Temperature, upwelling and nutrient controls on planktic foraminifera 100
3.4.4 Faunal zones of interest 106
3.4.5 Dissolution bias in planktic foraminifera assemblages 112
3.5 Conclusions 115
3.6 References 119
4. A global calibration for Mg/Ca in the planktic foraminifera Neogloboquadrina pachyderma 130
4.1 Introduction 131
4.2 Methods 132
4.2.1 North Pacific sample collection and Mg/Ca analysis 132
4.2.2 Global data compilation 133
4.2.3 Surface and bottom water parameters 135
4.2.4 Results 135
4.3 Discussion 136

4.3.1 A global Mg/Ca temperature calibration for *N. pachyderma* 136
4.3.2 Additional surface controls on Mg/Ca in *N. pachyderma* 139
4.3.3 Bottom water controls on Mg/Ca ratios 141
4.4 Conclusions 142
4.5 References 143
4.6 Supplementary figures 148
5. Pulses of deglacial CO_2 release from the sub-polar North Pacific 150
5.1 Introduction 151
5.1.1 Deglacial CO_2 in the North Pacific 151
5.1.2 Regional Oceanography 152
5.2 Methods 153
5.2.1 Sediment core and age control 153
5.2.2 Planktic foraminifera census counts 154
5.2.3 Trace element and boron isotope analysis 154
5.2.4 pH and CO_2 calibration and calculations 155
5.3 Results 157
5.3.1 Planktic foraminifera census data 157
5.3.2 Trace element data 158
5.3.3 Boron isotope data 159
5.4 Discussion 159
5.4.1 CO_2, circulation, and productivity during Heinrich Stadial 1 161
5.4.2 Stratification, nutrients and CO_2 during the Bølling-Allerød 165
5.4.3 Younger Dryas and Holocene in the North Pacific 168
5.5 Conclusion 169
5.6 References 170
5.7 Supplementary information 177
6. Summary and outlook 180
7. Appendix 183
7.1 Appendix 1: Trace element ratios from North Pacific core-tops 183
7.2 Appendix 2: Trace element ratios from glacial to Holocene 194
7.3 Appendix 3: Glacial sedimentology of marine sediment core ODP 887 201
7.4 Appendix 4: Benthic-planktic radiocarbon offsets from ODP 887B 206

Chapter 1

1. Introduction

1.1 Global climate change: 800,000 years to present

Our global climate is changing. Atmospheric CO_2 levels have increased dramatically since the industrial revolution and are projected to increase further throughout the next century (IPCC, 2013). This unprecedented rise in CO_2 has affected many aspects of our planet's climate system. From rising temperatures, to ocean acidification and coral bleaching, anthropogenic CO_2 rise has left its mark on our planet. The reconstruction of past climate change can help to further our understanding of what the future might hold by providing a means to investigate the causes, consequences, and processes associated with rising CO_2 levels.

The most direct measurement of past atmospheric CO_2 comes from Antarctic ice cores. These records stretch back over the past 800,000 years and paint a unique picture of past changes in climate (Petit *et al.,* 1999; Pepin *et al.,* 2001; Monnin *et al.,* 2001; EPICA community members, 2004; Siegenthaler *et al.,* 2005; Jouzel *et al.,* 2007; Luthi *et al.,* 2008) (Figure 1.1). Over the past 800,000 years, CO_2 has varied in a cyclical fashion punctuated by abrupt jumps in both directions (Figure 1.1). Alongside CO_2, deuterium isotopes from Antarctic ice cores have been used to reconstruct past atmospheric temperatures (Figure 1.1) (Jouzel *et al.,* 2007). As CO_2 and temperature varied in tandem, they clearly define periods of high CO_2 and high temperature, known as interglacials, and periods of low CO_2 and temperature, known as glacials (Figure 1.1). Interglacial periods are short-lived events involving rapid increases in CO_2 over timescales of 5-20 ky, whilst glacial periods are longer and exhibit a more gradual reduction in atmospheric CO_2 over 50-100 kys (Figure 1.1).

The cause of these glacial-interglacial cycles is widely debated within literature. The cyclical nature of these transitions has lead to the suggestion that orbital cycles play a primary role in the pacing of glacial to interglacial climate change (Imbrie *et al.,* 1992; Jouzel *et al.,* 2007). Three types of orbital cycle have effected earth' climate over the past 65 million years (Zachos *et al.,* 2008). Eccentricity, operating on cycles of 400 ka and 100 ka, is defined by the shape of earth's orbit. Obliquity, occurring on 41 kyr cycles, reflects the tilt of the earth on its axis. Finally, precession, which operates on a 21 kyr cycle is a reflection on the earth's "wobble" on its axis. The inter-play of these Milankovitch cycles primarily effects the solar insolation received by the earth and therefore has a profound effect on global climate (Broecker *et al.,* 1969; Zachos *et al.,* 2008). Over the past 1.2 million years the pacing of glacial-interglacial cycles has shifted from a

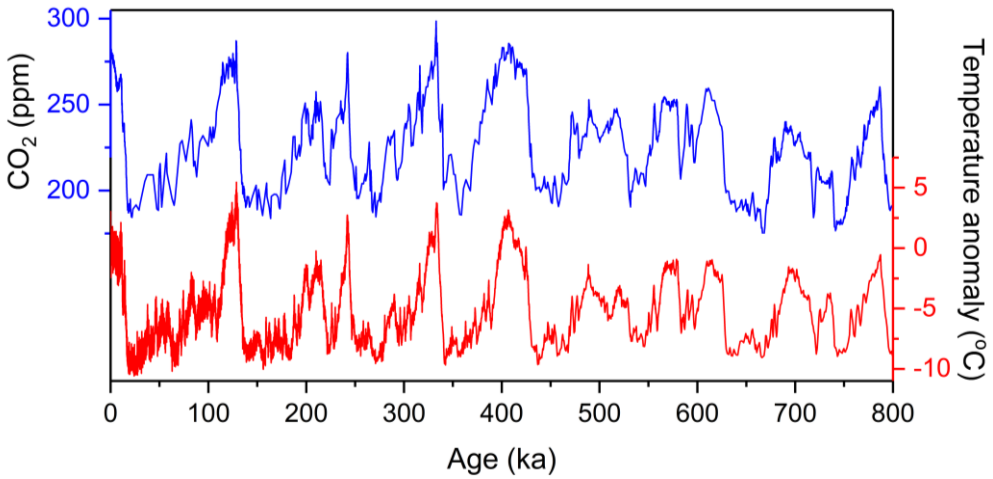

Figure 1.1: CO_2 (blue) and temperature reconstructions (red) from the Antarctic ice core Dome C (Jouzel et al., 2007). Temperature anomaly is reconstructed using Deuterium isotopes.

largely 41 kyr (obliquity) periodicity to the 100 kyr periodicity that has existed for the past 600,000 years (Figure 1.1) (Tziperman and Gildor, 2003; Jouzel *et al.*, 2007; Hönisch *et al.*, 2009). The fact that these orbital cycles show such coherence with glacial-interglacial transitions suggests that the first order control on the pacing of these climate events is orbitally driven (Kohfeld and Ridgewell, 2009).

Although eccentricity cycles can provide a trigger for recent glacial-interglacial climate, solar insolation changes do not provide the magnitude of forcing required to cause the large shifts in CO_2 and temperature observed in the Antarctic ice core records (Jouzel *et al.*, 2007). Instead, feedbacks within the earth's biogeochemical systems are thought to drive these abrupt shifts in CO_2 and temperature (Kohfeld and Rdigewell, 2009). To determine the cause of changes in atmospheric CO_2 over glacial-interglacial cycles, analysis of the earth's major carbon reservoirs is required (Sigman and Boyle, 2000; Kohfeld and Rdigewell, 2009). Four key reservoirs of carbon exist: the atmosphere; oceans; terrestrial, and sediments and crust (Sigman and Boyle, 2000) (Figure 1.2). Of these, only the oceans interact with the atmosphere on timescales and magnitudes which are comparable to glacial-interglacial changes in CO_2 (Sigman and Boyle, 2000; Kohfeld and Ridgewell, 2009). The role of the oceans in glacial-interglacial climate change is further observed through the comparison of ocean and atmosphere records (Bond *et al.*, 1992; Shackleton, 2000; NGRIP Members, 2004; Lisiecki and Raymo, 2005). Because of the similarities between these records, a number of mechanisms for CO_2 exchange between the oceans and the atmosphere have been proposed (Kohfeld and Ridgewell, 2009). These include changes in ocean temperature, changes in ice volume, ocean circulation, iron fertilization, and changes in sea ice (Kohfeld and Ridgewell, 2000).

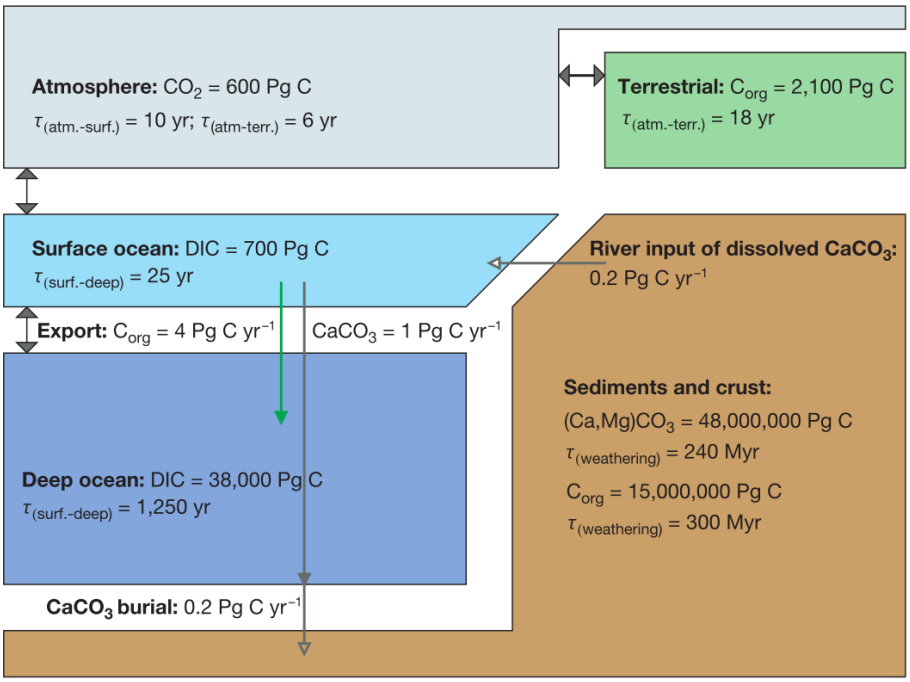

Figure 1.2: Schematic representation of the earth's carbon reservoirs taken from Sigman and Boyle (2000).

1.2 CO_2 and the carbon cycle in seawater

In order to analyse the processes involved in CO_2 exchange between the oceans and the atmosphere, a basic understanding of the carbonate system within seawater is required. Equation 1.1 shows the equilibria within which CO_2 moves between the atmosphere and the oceans, where CO_2 (g) denotes gaseous carbon dioxide and CO_2 denotes dissolved CO_2 (Zeebe and Wolf-Gladrow, 2001). K_0 is the solubility coefficient of CO_2 in seawater which is given by Henry's law and is primarily driven by temperature and salinity (Zeebe and Wolf-gladrow, 2001):

$$CO_2(g) \overset{K_0}{\Leftrightarrow} CO_2 \tag{1.1}$$

When CO_2 dissolves in seawater it is partitioned into three carbonate species, CO_2 ($CO_{2(aq)}$ + H_2CO_3), HCO_3^-, and CO_3^{2-}, the concentrations of which are dependant on two equilibrium constants K_1 and K_2. Equation 1.2 highlights the relationship between these species in seawater:

$$CO_2 + H_2O \overset{K_1}{\Leftrightarrow} HCO_3^- + H^+ \overset{K_2}{\Leftrightarrow} CO_3^{2-} + 2H^+ \tag{1.2}$$

Equilibrium constants K_1 and K_2 are dependent on temperature, salinity and pressure and are related to the concentrations below (Zeebe and Wolf-Gladrow, 2001):

$$K_1^* = \frac{[HCO_3^-][H^+]}{[CO_2]} \tag{1.3}$$

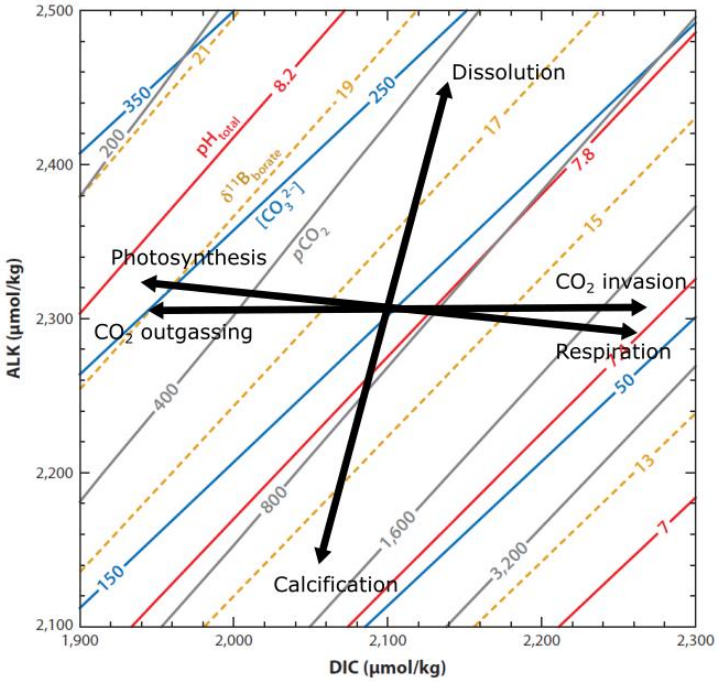

Figure 1.3: ***a)*** *Alkalinity vs DIC and associated changes in ocean properties: blue is CO_3^{2-}; red is pH; dashed yellow is $\delta^{11}B_{borate}$; grey is pCO_2. The black arrows indicate the effects on DIC and ALK of different ocean processes commonly associated with the carbon cycle. Figure was adapted from Foster and Rae (2016).*

$$K_2^* = \frac{[CO_3^{2-}][H^+]}{[HCO_3^-]} \tag{1.4}$$

Together, CO_2, HCO_3^-, and CO_3^{2-} make up the dissolved forms of carbon in seawater. The sum of these constituents is known as dissolved inorganic carbon or DIC (Zeebe and Wolf-Gladrow, 2001). Alongside DIC, alkalinity is another key carbonate system variable which is essential for fully describing the carbonate system. Alkalinity can simply be described as the charge balance within seawater. It is the sum of the positive conservation cations minus the negative conservation cations in seawater. These are normally in the form of strong acids and strong bases meaning weak acids and bases such as $[HCO_3^-]$, $[CO_3^{2-}]$, and $[B(OH)_4^-]$ are left to ensure the charges in seawater are balanced.

Processes involving carbon within the oceans are often described in terms of the change in alkalinity and DIC that they cause. The impact of some of these processes on ocean DIC and alkalinity can be seen in figure 1.3 alongside associated changes in ocean carbonate properties (CO_2, CO_2^{3-}, ph) which are denoted by the diagonal coloured lines in figure 1.3. The most straightforward processes are those which solely affect DIC. CO_2 invasion, CO_2 outgassing, photosynthesis, and respiration simply work to increase or decrease DIC in the oceans; there is no effect on alkalinity since no charged species are exchanged (Figure 1.3). In contrast, the

formation of calcium carbonate will decrease both alkalinity and DIC at a ratio of 2:1. The reason for the ratio can be seen in equation 1.5:

$$Ca^{2+} + CO_3^{2-} \leftrightarrow CaCO_3 \quad (1.5)$$

In equation 1.5, one mole of carbon and one mole of doubly charged Ca^{2+} are removed from seawater and thus alkalinity is affected more than DIC, the same is true for the opposite process of calcium carbonate dissolution (Zeebe and Wolf-Gladrow, 2001). Figure 1.3 also highlights the changes in carbonate species and pH associated with changes in alkalinity and DIC. At high alkalinity and low DIC, pH is high and the predominant carbonate species is [CO_3^{2-}] (Figure 1.3). In contrast, at high DIC and low alkalinity, pH is low and pCO_2 is increased in seawater (Figure 1.3).

1.3 Reconstructing past environmental change

Planktic foraminifera are marine zooplankton that live in the surface ocean and form calcareous chambered tests (Schiebel and Hemleben, 2017). They first appeared in the mid-Jurassic and are now ubiquitous throughout the world's oceans (Caron and Homewood, 1983). In the modern ocean, around 50 extant species of planktic foraminifera exist, with the addition of over 200 genotypes (Schiebel and Hemleben, 2017; de Vargas *et al.*, 2005). Classification to the species level is primarily done through morphological analysis under light microscope with key features

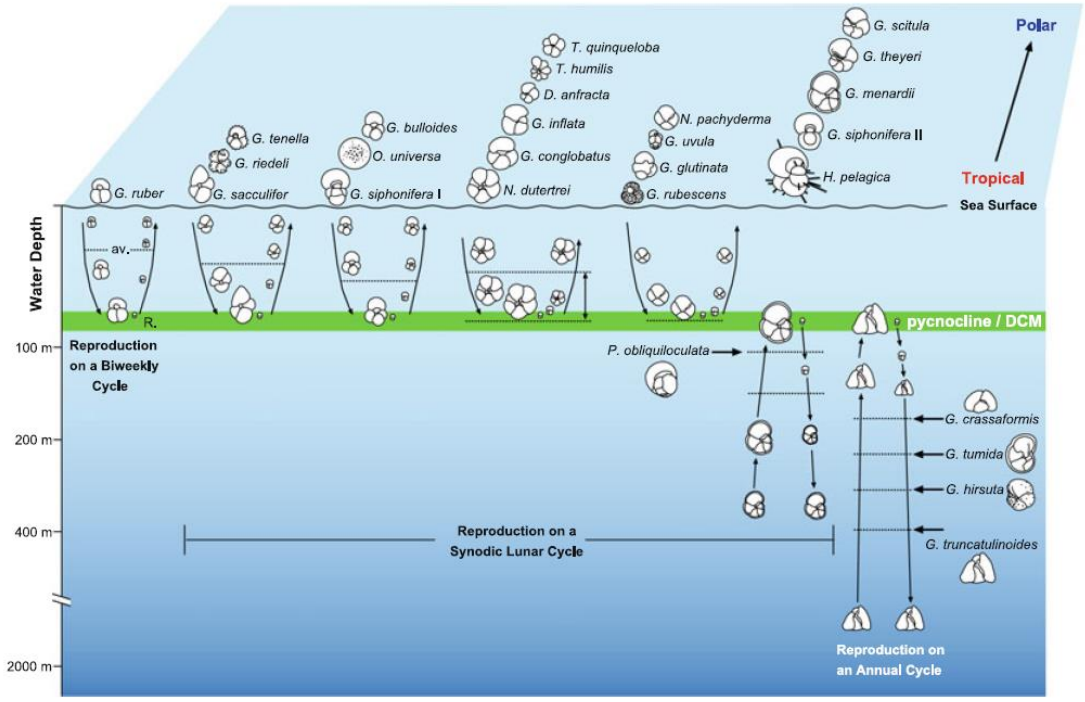

Figure 1.4: Depth habitat and reproduction cycle of different species of planktic foraminifera in the modern ocean. Taken from Schiebel and Hemleben (2017).

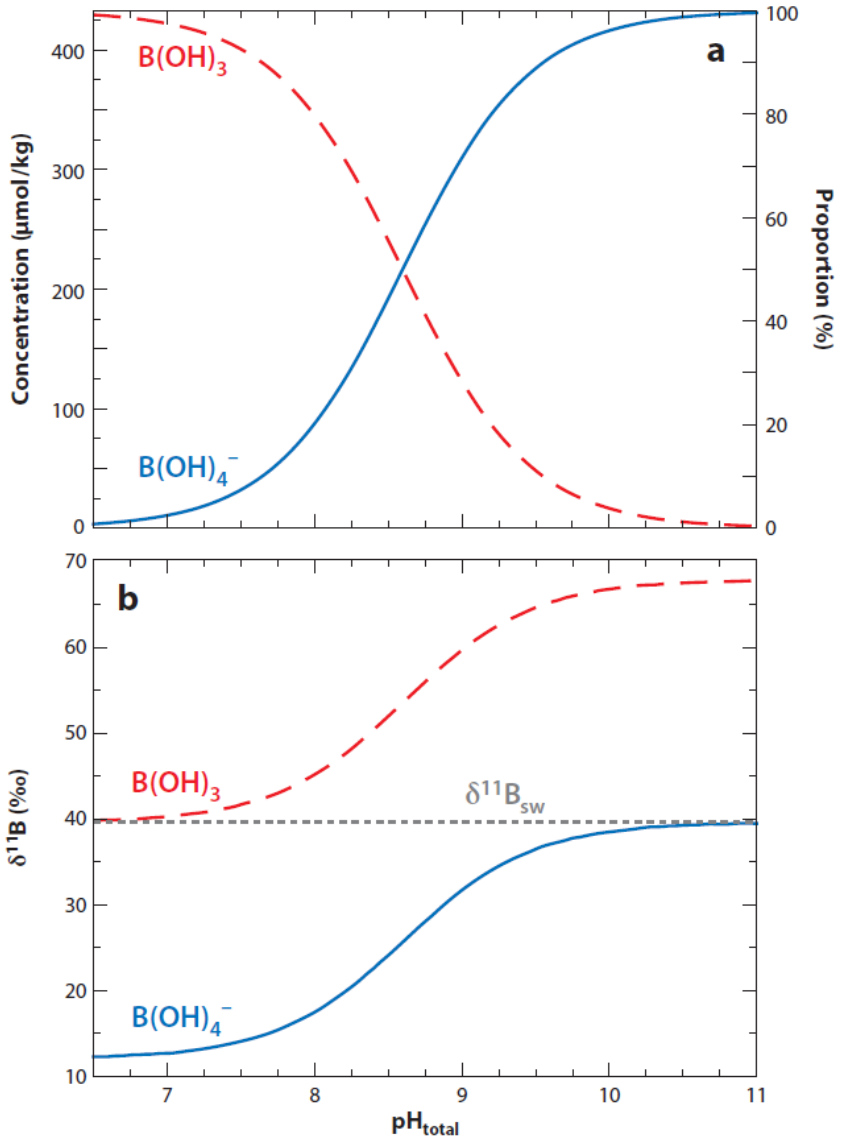

Figure 1.5: From Foster and Rae (2016) showing the ***a)*** *concentration of the different species of boron against pH and* ***b)*** *the $\delta^{11}B$ of the different species of boron against pH.*

including spinose, non-spinose, perforate, and microperforate tests used to characterise planktic foraminifera into distinct groups (Schiebel and Hemleben, 2017). Although most species are found within the top 100 m of the water column, depth habitat can extend down to depths of 400 m for some species (Schiebel and Hemleben, 2005) (Figure 1.4). Figure 1.4 also highlights the varying life cycles of different species of planktic foraminifera. Most species reproduce on a lunar cycle however, some, predominantly deeper dwelling planktic foraminifera, such as *G. truncatulinoides* and *G. tumida* are known to reproduce on an annual cycle (Schiebel and Hemleben, 2017). Individual species of planktic foraminifera are ecologically distinct and thrive in specific environmental niches. This, alongside the fact that deceased tests are deposited in marine sediments over time, make planktic foraminifera a particularly useful tool in the

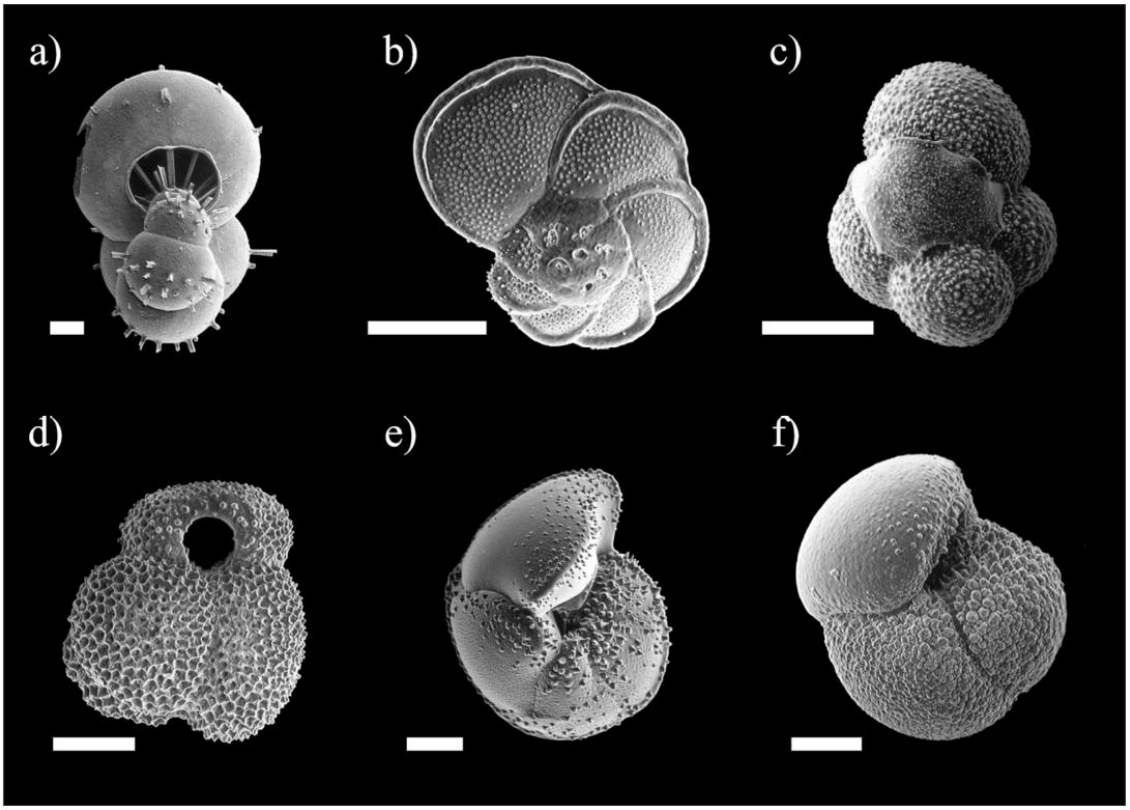

Figure 1.6: Taken from Lončarić (2005). Scanning electron microscope images of six modern planktic foraminifera. ***a)*** *Hastigerina pelagica,* ***b)*** *Globorotalia menardii,* ***c)*** *Globigerinita glutinata,* ***d)*** *Globigerinoides ruber,* ***e)*** *Globorotalia truncatulinoides,* ***f)*** *Globorotalia inflata. Scale bar is 100 µm.*

reconstruction of past environmental change (Coulbourn *et al.*, 1980; Rutherford *et al.*, 1999; Kucera *et al.*, 2005; Taylor *et al.*, 2018; Scheibel and Hemleben, 2017). Planktic foraminifera census data can be used to assess qualitative temperatures, track the movement of gyres and fronts, and assess changes in upwelling and productivity (Taylor *et al.*, 2018). Some examples of modern planktic foraminifera can be seen in figure 1.6 (Lončarič, 2005).

In addition to census data, geochemical analysis of planktic foraminifera can be used to quantitatively assess environmental change in the past (Allen *et al.*, 2016). Trace elements to calcium ratios are commonly used to reconstruct ocean parameters such as temperature, salinity, nutrients, and carbonate system parameters such as pH and CO_3^{2-} (Russell *et al.*, 2004; Allen *et al.*, 2016). The use of Mg/Ca ratios in planktic foraminifera to reconstruct past sea surface temperatures (SSTs) is widely applied (Nürnberg *et al.*, 1996; Elderfield and Gansson, 2000). For these trace elements ratios to be effectively used in paleo-studies, effective ground truthing and calibration is required. This is usually done through core-top calibrations of modern to late Holocene samples or through culture experiments under laboratory conditions (Delaney *et al.*, 1985; Nurnberg, 1995; Elderfield and Gansson, 2000; Anand *et al.*, 2003; Russell *et al.*, 2004; Barker *et al.*, 2005; Allen *et al.*, 2016; Gray *et al.*, 2018a). Core-top and cultures studies of the

incorporation of magnesium into foraminiferal calcite have cited temperature sensitivities of 6-11 %/°C depending on the species used and the calibration method applied (Nurnberg *et al.*, 1995; Elderfield and Gansson, 2000; Barker *et al.*, 2005; Gray *et al.*, 2018a). In addition to Mg/Ca ratios, other trace elements commonly used to reconstruct past environmental change include: B/Ca to reconstruct past ocean pH and CO_3^{2-} (Yu *et al.*, 2013, Allen *et al.*, 2016) and Cd/Ca ratios to reconstruct past ocean phosphate and nutrient contents (Rickaby and Elderfield, 1999; Yu *et al.*, 2013; Allen *et al.*, 2016).

Boron isotopes in planktic foraminifera have become an increasingly popular proxy for reconstructing past ocean pH and CO_2 (Foster and Rae, 2016). Boron has two stable isotopes ^{10}B (~20 %) and ^{11}B (~80 %) and the isotopic variation is reported using the delta notation:

$$\delta^{11}B\ (‰) = \left(\left(\frac{^{11}B/^{10}B\ sample}{^{11}B/^{10}B\ standard}\right) - 1\right) \times 1000 \quad (1.6)$$

Where the standard is the National Institute of Standards and Technology (NIST) Standard reference material (SRM) 951 boric acid. The systematics of boron isotopes in seawater are fully described in Foster and Rae (2016) and Rae (2018). In simple terms, the concentration and isotopic ratios of the two species of boron present in seawater, boric acid $B(OH)_3$ and borate ion $B(OH)_4^-$, varies with pH (Figure 1.5) (Zeebe and Wolf-Gladrow, 2001). Alongside the assumption that only borate ion species is taken up by marine carbonates (Hemming and Hanson, 1992) the $\delta^{11}B$ of planktic foraminifera can be used to reconstruct past changes in pH through equation 1.8, where the $\delta^{11}B$ of seawater ($\delta^{11}B_{sw}$) and the $\delta^{11}B$ of the foraminifera ($\delta^{11}B_{CaCO3}$) are known:

$$pH = pK_B^* - log\left(-\frac{\delta^{11}B_{sw} - \delta^{11}B_{CaCO_3}}{\delta^{11}B_{sw} - \alpha_B\delta^{11}B_{CaCO_3} - \varepsilon_B}\right) \quad (1.7)$$

Where pK_B^* is a constant requiring the input of temperature, salinity and pressure values (the impact of these variables on pK_B* can be seen in Figure 1.5). α_B is the isotopic fractionation which is 1.0272 (Klochko *et al.*, 2006) and ε_B is the fractionation factor which is equal to:

$$\varepsilon_B = (\alpha_B - 1) \times 1000 \quad (1.8)$$

Finally, the $\delta^{11}B_{sw}$ is 39.61 ‰ as measured by Foster *et al.*, (2010). The nature of the carbonate system is such that if any two of the six variables are known, all other components can be calculated (Zeebe-Wolf-Gladrow, 2001). Thus, pH reconstructed through boron isotopes can be used alongside another carbonate parameter, usually alkalinity, to reconstruct past changes in surface ocean pCO_2 (Hemming and Hanson, 1992; Zeebe and Wolf-Gladrow, 2001; Hönisch *et al.*, 2004; Foster *et al.*, 2008; Foster *et al.*, 2010; Henehan *et al.*, 2013; Yu *et al.*, 2013; Foster and Rae, 2016; Rae, 2018).

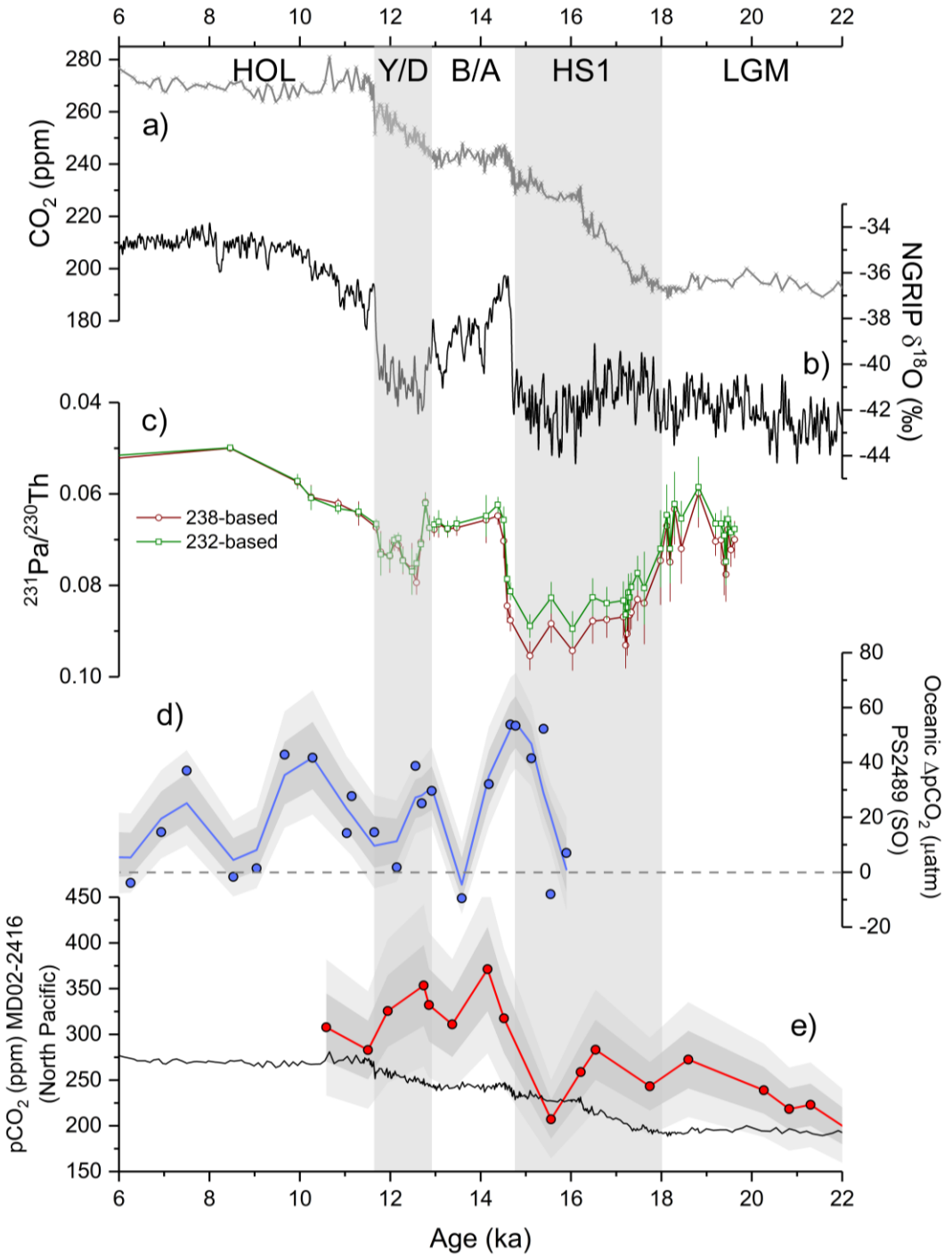

Figure 1.7: Changes in ocean circulation and CO_2 during the last deglaciation. ***a)*** *Atmospheric CO_2 from Antarctic Ice Cores (Marcott et al., 2014; Bereiter et al., 2015).* ***b)*** *$\delta^{18}O$ from Greenland ice core (NGRIP members, 2004).* ***c)*** *$^{231}Pa/^{230}Th$ from the North Atlantic (higher values correspond to weaker AMOC) (McManus et al., 2004).* ***d)*** *$\Delta pCO_{2(sw)}$ from the Southern Ocean calculated from boron isotopes (Martinez-boti et al., 2015).* ***e)*** *$pCO_{2(sw)}$ from the North Pacific (red) from Gray et al., (2018) plotted alongside atmospheric CO_2 from Marcott et al., (2014) (black line). HOL is Holocene; Y/D is Younger Dryas; B/A is Bølling-Allerød; HS1 is Heinrich Stadial 1; LGM is Last Glacial Maximum.*

1.4 Changes in CO_2 circulation during the last deglaciation

The last significant increase atmospheric CO_2 prior to the Anthropocene occurred between the Last Glacial Maximum (~18-23 ka) and the start of the Holocene (11.7 ka) (Figure 1.7). Atmospheric CO_2 rose by ~75 ppm over 7 ka and the period was punctuated by several key intervals characterised by changes in ocean circulation, atmospheric temperature, and atmospheric CO_2. These include: Heinrich Stadial 1 (HS1) between 18-14.7 ka; the Bølling-Allerød (B/A) between 14.7-12.9 ka; the Younger Dryas (Y/D) between 12.9-11.7 ka and the Holocene which began at 11.7 ka (Figure 1.7).

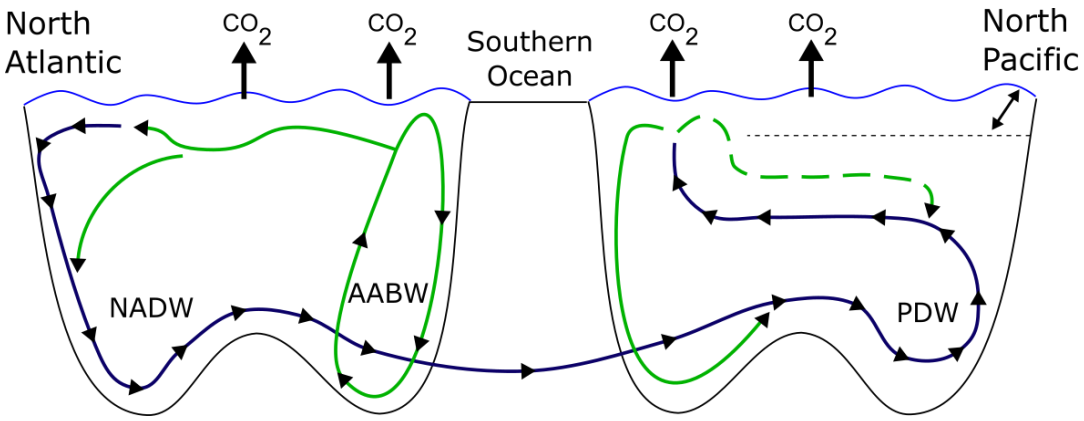

Figure 1.8: Schematic representation of the major ocean circulation pattern in the modern ocean. NADW is North Atlantic Deep Water. AABW is Antarctic Bottom Water. PDW is Pacific Deep Water which is rich in DIC. The figure shows the key regions of surface and deep water interaction in the modern ocean, primarily in the southern ocean, as well as the stratified nature of the modern North Pacific. The major regions of CO_2 outgassing are also depicted.

Ocean circulation has the potential to impact atmospheric CO_2 levels through its ability to control the distribution of nutrients, heat and carbon (Sarmiento and Gruber, 2013). In the modern ocean, North Atlantic Deep Water (NADW) forms in the high-latitude North Atlantic. These waters are nutrient and carbon poor and represent an efficient biological pump whereby nutrients and carbon have been sequestered in the ocean interior through lower latitude productivity (Sigman *et al.*, 2010). This contrasts with the Southern Ocean, where productivity is limited by iron (Boyd *et al.*, 2007) and the formation of Antarctic Bottom Water (AABW) supplies the surface with nutrients and carbon (Sigman *et al.*, 2010). Here, the Southern Ocean represents an inefficient biological pump where nutrients and carbon are not fully utilised by productivity. This leads to "preformed" nutrients being returned to the ocean interior through deep mixing, whilst CO_2 can outgas into the atmosphere (Sigman *et al.*, 2010). In addition to the biological pump, the solubility pump works to sequester carbon in regions where surface ocean temperatures are cool and thus CO_2 solubility is increased. Often, these waters, usually found at high latitudes, are also more dense leading to

active deep water formation, however this is also a function of surface salinity (Sigman and Boyle, 2000).

The biogeochemical relationships between the ocean and the atmosphere mean that tracing changes in ocean circulation in the past can shed light on the causes of deglacial CO_2 rise. The causes of low CO_2 during glacial periods has been related to the stemming of Southern Ocean CO_2 release (Sarmiento and Toggweiler (1984); Siegenthaler and Wenk (1984); Knox and McElroy (1984) and the expansion of the Southern Ocean overturning cell at the expense of NADW (Duplessy *et al.,* 1988; Curry and Oppo, 2005; Ferrari *et al.,* 2014). During the last deglaciation, a major reorganisation of ocean circulation occurred beginning at the onset of HS1. Pa/Th records from McManus *et al.,* (2004) show a large-scale collapse of Atlantic Meridional Overturning Circulation (AMOC) brought about by a shoaling of NADW (Figure 1.7). This reduction in heat transport, possibly triggered by freshwater input from surging icebergs (McManus *et al.,* 2004; Thornalley *et al.,* 2010) is associated with reduced AMOC and is a potential cause of cooling in the Northern Hemisphere during HS1. During this time period there was also ventilation of deep ocean carbon in the Southern Ocean (Burke and Robinson, 2012) highlighting the role of this region in CO_2 release during HS1 (Martinez-Boti *et al.,* 2015). The B/A in the North Atlantic is associated with a reinvigoration of AMOC (McManus *et al.,* 2004) and abrupt increase in atmospheric CO_2 which sees a jump of 12 ppm in 200 years (Marcott *et al.,* 2014).

The role of the North Pacific in deglacial CO_2 is debated within recent literature (Galbraith *et al.,* 2007; Galbraith *et al.,* 2008; Gebhardt *et al.,* 2008; Okazaki *et al.,* 2010; Jaccard and Galbraith, 2011; Jaccard and Galbraith, 2013; Rae *et al.,* 2014; Ren *et al.,* 2015; Maier *et al.,* 2015; Gray *et al.,* 2018b). In the modern ocean, the North Pacific is stratified due to low surface salinity (Warren, 1983) with little interaction between surface and deep waters. As the deep North Pacific stores a large amount of carbon, any past changes in ventilation in this region could lead to CO_2 outgassing and atmospheric CO_2 rise (Rae *et al.,* 2014). Changes in circulation in the North Pacific have been demonstrated through radiocarbon records from Okazaki *et al.,* (2010) and Rae *et al.,* (2014) and suggest increased ventilation during HS1 followed by highly stratified conditions during the B/A. Rae *et al.,* (2014) hypothesize that this HS1 ventilation could contribute to the onset of deglacial CO_2 rise, whilst new boron isotope data from the North West Pacific show that enhanced Ekman Suction during the B/A played a key role in facilitating CO_2 outgassing from this region (Gray *et al.,* 2018b) (Figure 1.7).

1.5 Thesis structure

This Thesis aims to improve the knowledge of North Pacific and global planktic foraminifera ecology now and in the past, and further investigate the role of the North Pacific in deglacial CO_2 release through planktic foraminifera census, trace element and boron isotope data.

Despite their common use in the interpretation of past climate change, planktic foraminifera ecology in the North Pacific has thus far been understudied (Rutherford *et al.*, 1999). This is in part due to a lack of available data, and partly due to poor preservation in North Pacific sediments. In chapters 2 and 3 of this thesis, I examine the distribution and ecology of planktic foraminifera across the North Pacific and globally, with a view to improving the understanding of changes in planktic foraminifera census data downcore. Following this, I investigate the role of the North Pacific in deglacial CO_2 release through new high-resolution boron isotope, census and trace element records from the North East Pacific.

Chapter 2 describes the distribution and ecology of planktic foraminifera in the North Pacific through a newly compiled North Pacific core-top compilation and uses new multinet and core-top data to analyse the key drivers of abundance in two subpolar North Pacific foraminifer *Globigerina bulloides* and *Neogloboquadrina pachyderma*.

Chapter 3 describes a new global compilation of planktic foraminifera census data to fully describe the distribution of 12 major species in the ocean. In addition, I examine the environmental controls on foraminifera abundance through ordination analyses and focus on the faunal and environmental characterises of upwelling regions in the global ocean.

Chapter 4 presents a new global core-top temperature calibration for Mg/Ca ratios in the planktic foraminifer *N. pachyderma*. The calibration uses newly analysed data from the North Pacific alongside previously published data from the North Atlantic and Southern Ocean.

Chapter 5 presents new boron isotope analyses from the North East Pacific to investigate changes in surface CO_2 in the past.

1.6 References

Allen, K.A. et al., 2016. Trace element proxies for surface ocean conditions: A synthesis of culture calibrations with planktic foraminifera. *Geochimica et Cosmochimica Acta*, 193, pp.197–221.

Anand, P., Elderfield, H. & Conte, M.H., 2003. Calibration of Mg/Ca thermometry in planktonic foraminifera from a sediment trap time series. *Paleoceanography*, 18(2).

Barker, S. et al., 2005. Planktonic foraminiferal Mg/Ca as a proxy for past oceanic temperatures: A methodological overview and data compilation for the Last Glacial Maximum. *Quaternary Science Reviews*, 24(7–9 SPEC. ISS.), pp.821–834.

Bond, G. et al., 1992. Evidence for massive discharges of iceberg into the North Atlantic ocean during the last glacial period. *Letters to Nature*, 360, pp.245–249.

Boyd, P.W. et al., 2007. Mesoscale iron enrichment experiments 1993-2005: synthesis and future directions. *Science (New York, N.Y.)*, 315(2007), pp.612–617.

Broecker, W. et al., 1968. Milankovitch Hypothesis Supported by Precise Dating of Coral Reefs and Deep-Sea Sediments. (January), pp.297–300.

Burke, A. & Robinson, L.F., 2012. The Southern Ocean's Role in Carbon Exchange During the Last Deglaciation. *Science*, 335, pp.557–561.

Caron, M. & Homewood, P., 1983. Evolution of early planktic foraminifers. *Marine Micropaleontology1*, 7(6), pp.453–462.

Coulbourn, W.T., Parker, F.L. & Berger, W.H., 1980. Faunal and solution patterns of planktonic foraminifera in surface sediments of the North Pacific. *Marine Micropaleontology*, 5, pp.329–399.

Curry, W.B. & Oppo, D.W., 2005. Glacial water mass geometry and the distribution of d13C of Sigma CO_2 in the western Atlantic Ocean. *Paleoceanography*, 20(1), pp.1–12.

Curry, W.B. & Oppo, D.W., 2005. Glacial water mass geometry and the distribution of $\delta^{13}C$ of ΣCO_2 in the western Atlantic Ocean. *Paleoceanography*, 20(1), pp.1–12.

De Vargas, C. et al., 1997. Phylogeny and rates of molecular evolution of planktonic foraminifera: SSU rDNA sequences compared to the fossil record. *Journal of Molecular Evolution*, 45(3), pp.285–294.

Delaney, M., Bé, A.W.H. & Boyle, E.A., 1985. Li, Sr, Mg, Na in foraminiferal calcite shells from laboratory culture, sediment traps, and sediment cores. *Geochimica Et Cosmochimica Acta*, 49(6), pp.1327–1341.

Duplessy, J.C. et al., 1988. Deep water source variations during the last climatic cycle and their impact on the global deep water circulation. *Paleoceanography*, 3(3), pp.343–360.

Elderfield, H. & Ganssen, G., 2000. Past temperature and $\delta^{18}O$ of surface ocean waters inferred from foraminiferal Mg/Ca ratios. *Nature*, 405(6785), pp.442–445.

EPICA community members, 2004. Eight glacial cycles from an Antarctic ice core. *Nature*, 429, pp.623–628.

Ferrari, R. et al., 2014. Antarctic sea ice control on ocean circulation in present and glacial climates. *Proceedings of the National Academy of Sciences of the United States of America*, 111(24), pp.8753–8.

Foster, G.L., 2008. Seawater pH, pCO_2 and $[CO_2^{-3}]$ variations in the Caribbean Sea over the last 130 kyr: A boron isotope and B/Ca study of planktic foraminifera. *Earth and Planetary Science Letters*, 271(1–4), pp.254–266.

Foster, G.L., Pogge Von Strandmann, P.A.E. & Rae, J.W.B., 2010. Boron and magnesium isotopic composition of seawater. *Geochemistry, Geophysics, Geosystems*, 11(8).

Foster, G.L. & Rae, J.W.B., 2016. Reconstructing Ocean pH with Boron Isotopes in Foraminifera. *Annual Review of Earth and Planetary Sciences*, pp.207–237.

Galbraith, E.D. et al., 2008. Consistent relationship between global climate and surface nitrate utilization in the western subarctic Pacific throughout the last 500 ka. *Paleoceanography*, 23(2), pp.1–11.

Galbraith, E.D. et al., 2007. Carbon dioxide release from the North Pacific abyss during the last deglaciation. *Nature*, 449(7164), pp.890–3.

Gebhardt, H. et al., 2008. Paleonutrient and productivity records from the subarctic North Pacific for Pleistocene glacial terminations I to V. *Paleoceanography*, 23(4).

Gray, W.R. et al., 2018a. The effects of temperature, salinity, and the carbonate system on Mg/Ca in Globigerinoides ruber (white): A global sediment trap calibration. *Earth and Planetary Science Letters*, 482, pp.607–620.

Gray, W.R. et al., 2018b. Deglacial upwelling, productivity and CO_2 outgassing in the North Pacific Ocean. *Nature Geoscience*.

Heinrich, H., 1988. Origin and consequences of cyclic ice rafting in the Northeast Atlantic Ocean during the past 130,000 years. *Quaternary Research*, 29(2), pp.142–152.

Hemming, N.G. & Hanson, G.N., 1992. Boron isotopic composition and concentration in modern marine carbonates. *Geochimica et Cosmochimica Acta*, 56(1), pp.537–543.

Henehan, M.J. et al., 2013. Calibration of the boron isotope proxy in the planktonic foraminifera Globigerinoides ruber for use in palaeo-CO_2 reconstruction. *Earth and Planetary Science Letters*, 364, pp.111–122.

Honisch, B. et al., 2009. Atmospheric Carbon Dioxide Concentration Across the Mid-Pleistocene Transition. *Science*, 324(19), pp.1551–1554.

Hönisch, B. & Hemming, N.G., 2004. Ground-truthing the boron isotope-paleo-pH proxy in planktonic foraminifera shells: Partial dissolution and shell size effects. *Paleoceanography*, 19(4), pp.1–13.

Imbrie, J. et al., 1992. Linear Responses to Milankovitch Forcing ulate new observational and modelling efforts. *Palaontogische Zeitschrift*, 7(6), pp.701–738.

IPCC et al., 2013. IPCC, 2013: Climate Change 2013: The Physical Science Basis. Contribution of Working Group I to the Fifth Assessment Report of the Intergovernmental Panel on Climate Change.

Jaccard, S.L. & Galbraith, E.D., 2013. Direct ventilation of the North Pacific did not reach the deep ocean during the last deglaciation. *Geophysical Research Letters*, 40(1), pp.199–203.

Jaccard, S.L. & Galbraith, E.D., 2011. Large climate-driven changes of oceanic oxygen concentrations during the last deglaciation. *Nature Geoscience*, 5(2), pp.151–156.

Jouzel, J. et al., 2007. Orbital and millennial Antarctic climate variability over the past 800,000 years. *Science (New York, N.Y.)*, 317(5839), pp.793–796.

Klochko, K. et al., 2006. Experimental measurement of boron isotope fractionation in seawater. *Earth and Planetary Science Letters*, 248(1–2), pp.261–270.

Knox, F. & McElroy, M.B., 1984. Changes in Atmospheric CO2: Influence of the Marine Biota at High Latitude. *Journal of Geophysical Research*, 89(D3), pp.4629–4637.

Kohfeld, K. & Ridgwell, A., 2009. Glacial-Interglacial Variability in Atmospheric CO_2. *Surface ocean-lower atmosphere processes*, 187, pp.251–286.

Kucera, M. et al., 2005. Reconstruction of sea-surface temperatures from assemblages of planktonic foraminifera: Multi-technique approach based on geographically constrained calibration data sets and its application to glacial Atlantic and Pacific Oceans. *Quaternary Science Reviews*, 24(7–9 SPEC. ISS.), pp.951–998.

Lisiecki, L.E. & Raymo, M.E., 2005. A Pliocene-Pleistocene stack of 57 globally distributed benthic δ 18O records. *Paleoceanography*, 20(1), pp.1–17.

Lončarić, N., 2005. Planktic foraminiferal response to changing SE Atlantic oceanography. PhD Thesis, Vrije Univ., Amsterdam.

Lüthi, D. et al., 2008. High-resolution carbon dioxide concentration record 650,000-800,000 years before present. *Nature*, 453, pp.379–382.

Maier, E. et al., 2015. Deglacial subarctic Pacific surface water hydrography and nutrient dynamics and links to North Atlantic climate variability and atmospheric CO_2. *Paleoceanography*, 30, pp.949–968.

Martínez-Botí, M. a. et al., 2015. Boron isotope evidence for oceanic carbon dioxide leakage during the last deglaciation. *Nature*, 518(7538), pp.219–222.

McManus, J.F. et al., 2004. Collapse and rapid resumption of Atlantic meridional circulation linked to deglacial climate changes. *Nature*, 428(6985), pp.834–837.

Monnin, E. et al., 2001. Atmospheric CO_2 concentrations over the last glacial maximum. *Science*, 291, pp.112–114.

NGRIP Members et al., 2004. High-resolution record of Northern Hemisphere climate extending into the last interglacial period. *Nature*, 431(7005), pp.147–151.

Nürnberg, D., 1995. Magnesium in tests of Neogloboquadrina pachyderma sinistral from high northern and southern latitudes. *Journal of Foraminiferal Research*, 25(4), pp.350–368.

Okazaki, Y. et al., 2010. Deepwater formation in the North Pacific during the Last Glacial Termination. *Science (New York, N.Y.)*, 329(5988), pp.200–4.

Pépin, L. et al., 2001. Hemispheric roles of climate forcings during glacial-interglacial transitions as deduced from the Vostok record and LLN-2D model experiments. *Journal of Geophysical Research Atmospheres*, 106(D23), pp.31885–31892.

Petit, R.J. et al., 1999. Climate and atmospheric history of the past 420,000 years from the Vostok ice core, Antarctica. *Nature*, 399, pp.429–413.

Rae, J.W.B., 2018. *Boron Isotopes in Foraminifera: Systematics, Biomineralisation, and CO2 Reconstruction*, Springer, Cham.

Rae, J.W.B. et al., 2014. Deep water formation in the North Pacific and deglacial CO_2 rise. *Paleoceanography*, 29, pp.645–667.

Ren, H. et al., 2015. Glacial-to-interglacial changes in nitrate supply and consumption in the subarctic North Pacific from microfossil-bound N isotopes at two trophic levels. *Paleoceanography*, 30(9), pp.1217–1232.

Rickaby, R.E.M. & Elderfield, H., 1999. Planktonic foraminiferal Cd/Ca. *Paleoceanography*, 14(3), pp.293–303.

Russell, A.D. et al., 2004. Effects of seawater carbonate ion concentration and temperature on shell U, Mg, and Sr in cultured planktonic foraminifera. *Geochimica et Cosmochimica Acta*, 68(21), pp.4347–4361.

Rutherford, S., D'Hondt, S. & Prell, W., 1999. Environmental controls on the geographic distribution of zooplankton diversity. *Nature*, 400(6746), pp.749–753.

Sarmiento, J.L. & Toggweiler, J.R., 1984. A new model for the role of the oceans in determining atmospheric PCO2. *Nature*, 308(5960), pp.621–624.

Sarmiento, J. & Gruber, N., 2013. Ocean biogeochmical dynamic, *Princeton University Press.*

Schiebel, R. & Hemleben, C., 2017. Planktic foraminifers in the modern ocean, *Springer Berlin Heidelberg*.

Schiebel, R. & Hemleben, C., 2005. Modern planktic foraminifera. *Palaontogische Zeitschrift*, 79(1), pp.135–148.

Shackleton, N.J., 2000. The 100,000 Year Ice-Age Cycle Identified and Found to Lag Temperature, Carbon Dioxide, and Orbital Eccentricity, 289(5486), pp.1897–1902.

Siegenthaler, U. & Wenk, T., 1984. Rapid atmospheric CO_2 variations and ocean circulation. *Nature*, 308(5960), pp.624–626.

Siegenthaler, U., Stocker, T.F. & Monnin, E. et al., 2005. Stable Carbon Cycle – Climate Relationship During the Late Pleistocene. *Science*, 2(310), pp.1313–1317.

Sigman, D.M., Hain, M.P. & Haug, G.H., 2010. The polar ocean and glacial cycles in atmospheric CO(2) concentration. *Nature*, 466(7302), pp.47–55.

Sigman, D. & Boyle, E., 2000. Glacial/interglacial variations in atmospheric carbon dioxide. *Nature*, 407(October), pp.859–869.

Taylor, B.J. et al., 2018. Distribution and ecology of planktic foraminifera in the North Pacific: Implications for paleo-reconstructions. *Quaternary Science Reviews*, 191, pp.256–274.

Thornalley, D.J.R., McCave, I.N. & Elderfield, H., 2010. Freshwater input and abrupt deglacial climate change in the North Atlantic. *Paleoceanography*, 25(1), pp.1–16.

Tziperman, E. & Gildor, H., 2003. On the mid-Pleistocene transition to 100-kyr glacial cycles and the asymmetry between glaciation and deglaciation times. *Paleoceanography*, 18(1), pp. 1001-1008.

Yu, J. et al., 2013. Calibration and application of B/Ca, Cd/Ca, and δ11B in Neogloboquadrina pachyderma (sinistral) to constrain CO_2 uptake in the subpolar North Atlantic during the last deglaciation. *Paleoceanography*, 28(2), pp.237–252.

Zachos, J., 2008. Trends, Rhythms, and Aberrations in Global Climate 65 Ma to Present. 686(2001), pp.686–694.

Zeebe, R.E and Wolf-Gladrow, D., 2001. CO_2 in Seawater: Equilibrium, Kinetics, Isotopes. *Elsevier*.

Chapter 2

2. Distribution and ecology of planktic foraminifera in the North Pacific: Implications for paleo-reconstructions

This chapter was published in Quaternary Science Reviews in May 2018 with the citation: ***Taylor, B.J.,*** *Rae, J.W., Gray, W.R., Darling, K.F., Burke, A., Gersonde, R., Abelmann, A., Maier, E., Esper, O. and Ziveri, P., 2018. Distribution and ecology of planktic foraminifera in the North Pacific: Implications for paleo-reconstructions. Quaternary Science Reviews, 191, pp.256-274. https://doi.org/10.1016/j.quascirev.2018.05.006. Taylor performed the analyses, made the figures, and wrote the paper, with input and comments from all other authors.*

Abstract

Planktic foraminifera census data have been used to reconstruct past temperatures through transfer functions, as well as changes in ocean ecosystems, chemistry and circulation. Here we present new multinet and core-top census data from 15 sites in the Subpolar North Pacific. We combine these with previous data to provide an up to date compilation of North Pacific planktic foraminifera assemblage data. Our compilation is used to define 6 faunal zones: the subpolar zone; transitional zone; upwelling zone; subtropical zone; east equatorial zone; west equatorial zone; based on the distribution of 10 major species of planktic foraminifera. Two species of planktic foraminifera *Neogloboquadrina pachyderma* and *Globigerina bulloides* provide the basis for many subpolar paleo-reconstructions. Through the analysis of new multinet and CTD data we find that *G. bulloides* and *N. pachyderma* are predominantly found within 0-50 m of the water column and coincide with high food availability. *N. pachyderma* also shows a strong temperature control and can thrive in food poor waters where temperatures are low. Both species bloom seasonally, particularly during the spring bloom of March to June, with *G. bulloides* exhibiting greater seasonal variation. We suggest that percentage abundance of *N. pachyderma* in paleo-assemblages can be used to assess relative changes in past temperature, with *G. bulloides* abundance more likely to reflect changes in food availability. By comparing our core-top and multinet data, we also find a dissolution bias of *G. bulloides* over *N. pachyderma* in the North Pacific, which may enrich assemblages in the latter species.

2.1 Introduction

Planktic foraminifera provide a key tool in studies of past changes in climate. Foraminiferal species assemblages may track a variety of oceanographic conditions, including temperature, salinity and nutrients, while the geochemistry of foraminiferal calcite can be used to reconstruct quantitative changes in ocean temperature and chemistry through time. However, downcore studies using foraminifera can only be justified if modern calibrations are well established, giving context to paleo-records. The upper water column may vary vertically, seasonally and spatially across the global ocean and it is therefore of prime importance that modern assemblages are fully understood in order to disentangle downcore signals.

Planktic foraminifera are known to exhibit variable depth distribution and seasonal abundance, thus identifying constraints on these variables has become vital to the interpretation of paleo-data (Schiebel and Hemleben, 2017). Early work using plankton tows and isotopic data suggested that planktic foraminifera are most abundant at chlorophyll maxima and that species were vertically stratified in accordance with their temperature preferences (Fairbanks and Wiebe, 1980; Fairbanks *et al.,* 1982; Hemleben *et al.,* 1989). The vertical distribution of planktic foraminifera in the North Pacific and globally has been linked to phytoplankton productivity and food availability which are in turn related to variations in the pycnocline and thermocline. In the North-West Pacific, recent literature highlights the role of nutrients and seasonal changes in the thermocline as key drivers of foraminiferal abundance (Mohiuddin *et al.,* 2002; Kuroyanagi *et al.,* 2002; Eguchi *et al.,* 2003; Mohiuddin *et al.,* 2004; Mohiuddin *et al.,* 2005; Kuroyanagi *et al.,* 2008). Despite this, large regional variations in depth preference and abundance have been observed within individual species, suggesting that there are regional discrepancies in the North Pacific assemblages which are not accounted for in paleo-records (Kuroyanagi *et al.,* 2002; Field, 2004; Iwasaki *et al.,* 2017). Three key species of planktic foraminifera dominate high-latitude assemblages in the North Pacific, *Neogloboquadrina pachyderma, Globigerina bulloides* and *Turborotalita quinqueloba*. Note that here and throughout, we refer to *N. pachyderma* sinistral as *N. pachyderma*, and previous references to *N. pachyderma* dextral as *Neogloboquadrina incompta* (Darling et al, 2006). *T. quinqueloba* is ubiquitous throughout subpolar and polar waters but is often under-represented in assemblage counts, due to its small size (Kandiano and Bauch, 2002). For this reason, it is rarely used in paleoceanographic reconstructions, unless a size fraction of >125 μm is used. Seasonally resolved data from the North East Pacific records the apparent affinity of specific species, particularly *G. bulloides,* to the spring upwelling conditions off the coast of southern California and Vancouver (Sautter and Thunell, 1989; Thunell and Sautter, 1991), which is accompanied by high phytoplankton abundance (Thunell and Honjo, 1987). In

contrast, Davis *et al.*, (2016) demonstrate the upwelling affinity of *N. pachyderma* over *G. bulloides* in the California coastal upwelling further to the north. Such contrasting differences between adjacent regional assemblages imposes complexity, which can be used to further refine paleoceanographic reconstructions.

Although detailed compilations of planktic foraminifera assemblages are available globally, the North Pacific is poorly represented (Rutherford *et al.*, 1999; Fenton *et al.*, 2016, Siccha and Kucera, 2017). The North Pacific has abyssal depths of > 5500 m, resulting in poor preservation of foraminiferal calcite (Peterson, 1966; Berger, 1970). The lack of preservation, particularly in core-top material, has meant that the distribution and paleoecological significance of planktic foraminifera in the North Pacific is poorly constrained. The difficulty of constraining dissolution effects on sediment also impacts upon the use of North Pacific census data in downcore records (Berger, 1970). North Pacific planktic foraminiferal provinces, or faunal zones, were originally characterised by Bradshaw (1959) and further constrained by Coulbourn *et al.*, (1980). The zones: subarctic; transitional; central and equatorial were defined broadly by the relative abundance of *N. pachyderma*, *T. quinqueloba*, *G. bulloides*, *Globorotalia inflata* and *Globigerinoides ruber* in core-top samples (Coulbourn *et al.*, 1980).

In this study, we generate new planktic foraminifera assemblage data from plankton tows and core tops collected from 15 sites across the subpolar North Pacific. We combine these data with previously published planktic foraminifera core top, multinet and sediment trap assemblage data from the North Pacific, to characterise the ocean conditions associated with modern planktic foraminifera assemblages. This evidence is then used to constrain the depth habitat of individual subpolar species, for the better understanding of paleo-records. To do so, we first address the gap in North Pacific census data, particularly prevalent in the subpolar gyre (Rutherford *et al.*, 1999), by re-evaluating North Pacific planktic foraminifera faunal provinces using our new data compilation. We then focus in detail on the two key subpolar North Pacific proxy carriers, *G. bulloides* and *N. pachyderma*. Through assessment of their dominant ecological drivers in the surface ocean, we suggest how best to interpret both the assemblage and geochemical records of these species downcore. Surface water and sediment assemblages are then compared, highlighting the effects of both seasonality and dissolution as potential biases within the sediment record.

2.2 Oceanographic Setting

Oceanographic currents in the North Pacific are dominated by two large-scale gyres: the subpolar gyre and the subtropical gyre, separated by the Subarctic Front, which is marked by a pronounced latitudinal sea surface temperature gradient (Figure 2.1). This gradient is also seen within salinity

and nutrient records, with the subpolar gyre exhibiting higher nutrients and low salinity, whilst the subtropical gyre is comparatively saltier and nutrient poor (Locarnini *et al.*,2013; Zweng *et al.,* 2013; Garcia *et al.,* 2014).

The subpolar gyre can be further split into the West Pacific Gyre and the Alaskan Gyre (Harrison *et al.,* 2004). The West Pacific Gyre is a high nutrient low chlorophyll zone (HNLC) which is fed predominantly by cool, nutrient rich waters from the Sea of Okhotsk and the Kamchatka Current (Locarnini *et al.*,2013; Garcia *et al.,* 2014). The southern extent of this gyre is the Subarctic Current, a region along the Subarctic Front characterised by the confluence of a number of current systems (Figure 2.1). These include the warm Kuroshio Current originating from the subtropical gyre, the cold Oyashio Current originating from the West Pacific Gyre together with a number of minor currents (Yasuda, 2003; Figure 2.1). The Subarctic Current and Kuroshio Extension define, in part, the Subarctic Front (Figure 2.1) which roughly follows 40°N latitude zonally across the North Pacific. In the eastern North Pacific, the California Current splits towards the south in the Subtropical Gyre, whilst the Alaskan Current forms the eastern limb of the Alaskan Gyre (Figure 2.1). The Alaskan gyre, also a HNLC zone, is more nutrient limited than the West Pacific gyre (Harrison *et al.,* 2004) and thus productivity is reduced. It feeds the Bering Sea which consists primarily of the Bering Slope current in the east and the Kamchatka current to the west (Figure 2.1) (Stabeno and Reed, 1994). In the Subtropical Gyre, the California Current extends southward to the equator where it forms the North Pacific Equatorial Current. In the east Equatorial Pacific, the North Pacific Equatorial Current is characterised by upwelling of cooler nutrient rich waters (Locarnini *et al.*,2013; Zweng *et al.,* 2013; Garcia *et al.,* 2014), contributing to the formation of the east equatorial upwelling region where productivity is high (Wyrtki, 1981). The current continues along the equator to the west, where it enters the West Pacific warm pool (Yan *et al.,* 1992) and continues to form the western limb of the Kuroshio Current.

2.3 Materials and Methods

2.3.1 SO202 INOPEX cruise study area

Multinet and multicore samples from the SO202 INOPEX cruise (2009) with the German RV *Sonne* (Gersonde, 2012) were analysed from 15 North Pacific sites (6 multicore and 9 multinets) in combination with hydrographic CTD data (Table 2.1). The site locations range from the Subarctic Front through the Subpolar Gyre to the Bering Sea (Figure 2.1). The spatial variation between the sites means the diverse regional hydrography affects individual sites differently (Figure 2.1). Those lying within the Subarctic frontal region (sites SO202-02-40, SO202-05-34 and SO202-05-33) are predominantly bathed in waters derived from the westward extension of

the Kuroshio Current. Sites SO202-04-27 and SO202-02-31 are influenced by the Alaskan Coastal Current, and sites SO202-05-02, SO202-02-06 and SO202-02-07 in the northwest Pacific are associated with the cooler Kamchatka Current and outflow from the Sea of Okhotsk. The Bering Sea sites (SO202-04-10, SO202-03-13, SO202-04-14, SO202-04-15), located along Bower's Ridge, the Aleutian Basin and proximal to the Bering Slope, are subject to inflow waters from the Alaskan Current and waters that form the initial stages of the Bering Slope Current. Data were also compiled from core-top sites spanning down to 20° S latitude.

Station No.	Lat (dec)	Long (dec)	Date	Depth (m)	Area
Multinet					
SO202-05-**02**	46.97	156.98	12/07/2009	0-1000	off Kurile-Kamchatka Trench
SO202-04-**10**	52.74	179.85	20/07/2009	0-1000	southern Bowers Ridge
SO202-03-**13**	54.98	177.96	22/07/2009	0-1000	northern Bowers Ridge
SO202-04-**14**	56.79	178.82	22/07/2009	0-1000	central Aleutian Basin
SO202-04-**15**	59.51	-179.85	24/07/2009	0-1000	N-bering Slope Pervenets/ Navarin Canyons
SO202-04-**27**	54.30	-149.60	02/08/2009	0-1000	Patton Seamount
SO202-02-**31**	49.68	-152.55	05/08/2009	0-1000	Seamount East SAP
SO202-05-**33**	45.08	-174.14	10/08/2009	0-1000	North of Chinook Trough
SO202-05-**34**	40.89	-177.68	12/08/2009	0-1000	East of southern Emperor Trough
Multicore					
SO202-02-**06**	51.90	166.49	16/07/2009	3422	Obruchev Rise
SO202-02-**07**	51.27	167.70	16-17/07/2009	2349	Detroit Seamount
SO202-04-**13**	54.98	177.96	22/07/2009	1383	northern Bowers Ridge
SO202-01-**27**	54.30	-149.60	02/08/2009	2916	Patton Seamounts
SO202-05-**31**	49.68	-152.55	05/08/2009	3744	Seamount East SAP
SO202-02-**40**	38.41	160.34	18/08/2009	3462	N Shatsky Rise
CDISK-IV Plankton nets					
KM1712-**St.1**	22.75	-157.98	03/08/2017	0-300	Station ALOHA
KM1712-**St.2**	27.74	-155.25	06/08/2017	0-300	Subtropical gyre
KM1712-**St.3**	35.27	-151.00	13/08/2017	0-250	Transition zone
KM1712-**St.4**	41.76	-148.26	17/08/2017	0-200	Transition zone
KM1712-**St.5**	49.82	-149.22	24/08/2017	0-150	Subpolar gyre
Sediment Traps					**Reference**
50N	50.00	165.00	1997-2001	3260	Kuroyanagi et al.,2008
40N	40.00	165.00	1997-2000	2986	Kuroyanagi et al.,2008
Papa	50.10	-144.90	1982-1986	3858	Sautter and Thunell, 1989
AB	53.50	176.90	1990-1999	3198	Asahi and Takahashi, 2007
SA	49.00	174.00	1990-1999	4812	Asahi and Takahashi, 2007

Table 2.1: Key station information for sites in this study alongside station information for compiled sediment trap data. Note that numbers in bold refer to station numbers used in Figure 2.1. CTD data was also collected for all of the multinet sites. Station information for the core-top compilation can be found within the supplementary information.

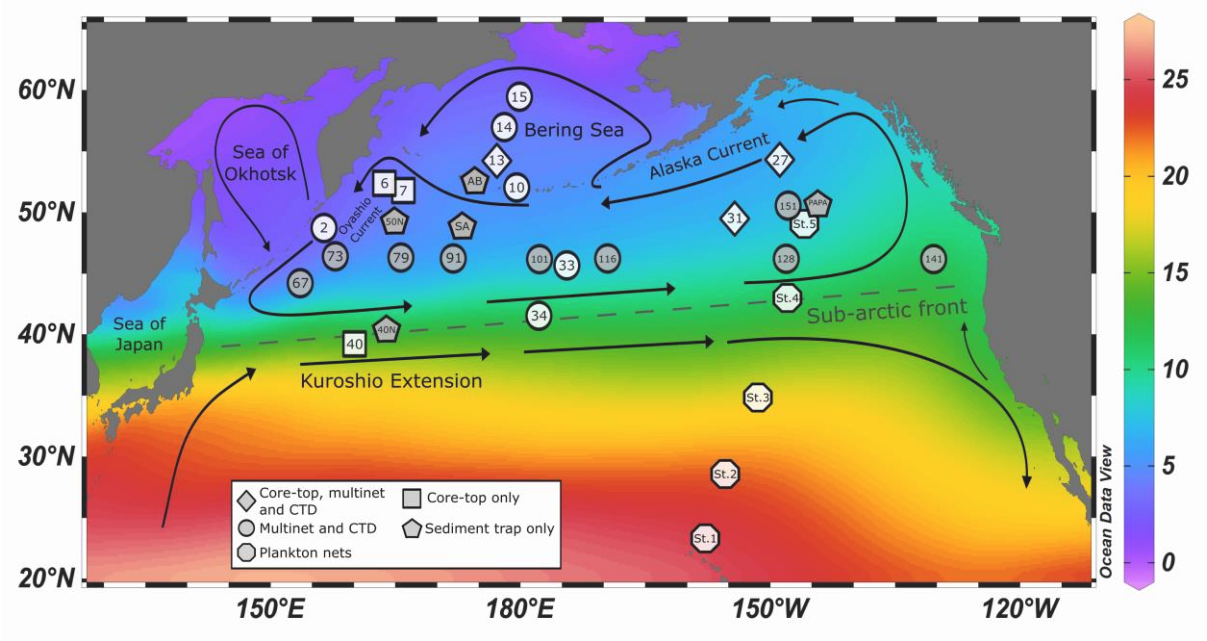

Figure 2.1: Hydrographic map showing the major current systems in the North Pacific and the sites used in this study. Arrows represent the direction of the major current systems in the North Pacific based on Gersonde (2012) and background colours represent mean annual temperature from 1955-2012 in degrees Celsius based on data from the world ocean atlas 2013 (Locarini et al., 2013). Diamonds show sites where core-top and multinet material was available; circles show sites where only multinet material was available; octagons show plankton net sites; squares show sites where only core-top material was available; pentagons show sites where sediment trap data was compiled. White shapes indicate new sites presented in this study, whilst grey shapes indicate sites where data was compiled from previous studies (Sautter and Thunell, 1989; Takahashi et al., 2000; Asahi and Takahashi, 2007; Kuroyanagi et al., 2008). Numbers here refer to the numbers in station numbers in bold listed in Table 2.1.

2.3.2 CTD deployments

A Seabird 911 CTD device was used to record hydrographic conditions down to a depth of 6000 m. The CTD was lowered through the water column at speeds of up to 0.5 m/s and carried a fluorimeter to measure chlorophyll fluorescence and derive phytoplankton concentration. At multinet sites, temperature, salinity, oxygen and chlorophyll-α concentration (calculated from phytoplankton fluorescence) were recorded down to 1000 m. The CTD data were usually collected within 3 hours of the multinet deployment and are available within the supplementary information and through the PANGAEA database.

2.3.3 Multinet samples

The multinet device collected samples at five depth intervals (1000-500 m; 500-300 m; 300-150 m; 150-50 m and 0-50 m) using a mesh size of 55 µm and an aperture area of 0.25 m^2 (Gersonde, 2012). The multinet was lowered to 1000 m depth and raised through the water column at a speed of 0.3 m/s. Plankton samples were collected in cod end beakers (1 litre, 41 µm mesh size) and

then transferred into 1 litre bottles and fixed in a seawater solution containing 2% formalin by volume (formalin is 37% formaldehyde w/w) and buffered with hexamethylenetetramine at pH = 8.1 onboard. In preparation for foraminifera assemblage work, each depth interval was wet sieved between 160-500 µm to remove larger organisms. Foraminifera were then wet picked under the light microscope and all species were counted. For each depth interval, foraminifera standing stocks were calculated using equation 1, where Z is the distance the multinet travelled through a particular interval:

$$\text{Foraminifera standing stock } (m^3) = (\#\ \text{foraminifera}) / (Z * 0.25) \quad (1)$$

No distinction was made between living and dead specimens.

2.3.4 Surface sediment samples

Multicore material from six new subpolar sites (Figure 2.1) was collected using a 12 tube (60 cm x 6 cm) multicorer (MUC) (Gersonde, 2012). The samples represent the 1-2 cm interval from one tube and approximately 20 cc of the sediment material was utilised to provide sufficient foraminifera for the assemblage counts. The core-material is stored at the Alfred Wegner Institute in Bremerhaven, Germany.

Samples were wet sieved (63 µm) to remove the fine clay fraction, placed in a petri dish and dried in an oven at <50 °C for 6-12 hours. Following drying, the coarse fraction (>63 µm) was transferred to a glass vial. The sample was then sieved at greater than 150 µm and split with micro-splitter to greater than 300 planktic foraminifera, a number shown to provide an accurate assessment of relative abundance within an assemblage (Schiebel and Hemleben, 2017). Foraminiferal species were then counted using a stereo microscope and the percentage species abundances for each sample calculated (for taxonomy see supplementary information).

2.3.5 Plankton net samples

Plankton net samples were collected along a transect from Hawaii to Alaska during August 2017 as part of the CDisK-IV (KM1712) cruise on R/V Kilo Moana. The transect was designed to sample subtropical, transition zone and subpolar waters. A 0.5 m diameter net with 90 µm mesh size was used throughout the cruise. The sampling strategy was designed to capture an integrated sample of all foraminifera living throughout the upper water column. The net was towed from the surface down to a specified maximum depth within the water column, and then back to the surface in a continuous manner. The maximum depth was determined from the florescence profile of a preceding CTD cast and was selected to ensure the net sampling captured the base of the chlorophyll maximum, and ranged from 150 m in the north to 300 m in the south in these samples.

After collection, samples were preserved in a 4% formalin seawater solution, buffered to a pH of ~8.1 with hexamethylenetetramine (Schiebel and Hemleben, 2017). Samples were split with a falsom splitter and all foraminifera >125 µm were identified to species level.

2.3.6 Compilation of North Pacific core-top assemblage data

To obtain an overview of the distribution pattern of planktic foraminifers preserved in North Pacific surface sediment record we merged our subarctic data set with previously published data from the subtropical Pacific, the Equatorial Pacific and the South China Sea presented in the MARGO database (Kucera *et al.,* 2005) and by Coulbourn *et al.,* (1980). The MARGO database was filtered to include only samples from the north and equatorial Pacific and the South China Sea. For consistency and accuracy, samples with fewer than 300 specimens were removed from the database. A baseline of 300 foraminifera is widely used within census studies and provides a fraction that is statistical representational of the sample as a whole (Schiebel and Hemleben, 2017). Substantial effort was made in this study to manually digitise the assemblage data from Coulbourn *et al.,* (1980), and the same filtering parameters were used to select sites from this database. All three datasets were then combined to produce a new North Pacific planktic foraminifera assemblage database containing 770 sites.

For each of the 770 sites of our compilation, hydrographic data (temperature, salinity, oxygen and phosphate) was estimated using ODV's 3D estimation tool and the World Ocean Atlas 2013 (1955-2012) (Boyer *et al.,* 2013). Mean annual surface water data was derived for surface temperature (Locarnini *et al.,* 2013), salinity (Zweng *et al.,* 2013), oxygen (Garcia *et al.,* 2013) and phosphate content (Garcia *et al.,* 2013).

2.3.7 Sediment trap data

We consider planktic foraminifera assemblage data from five previously published sediment trap sites in the North Pacific (Figure 2.1): sites 40N (1997-2000) and 50N (1997-2001) in the Northwest Pacific (Kuroyanagi *et al.,* 2008); site SA in the central subpolar Pacific (Asahi and Takahashi, 2007) collected between 1990-1999; station PAPA in the Northeast Pacific (Sautter and Thunell, 1989) collected between 1982-1986 and site AB in the Bering Sea (Asahi and Takahashi, 2007) collected between 1990-1999 (Table 2.1). As sediment trap data was collected over multiple years, values were averaged to produce comparable datasets between sites. In these cases, the standard error was calculated to constrain annual variability.

2.4 Results

2.4.1 Subarctic Front

Sites SO202-05-33 and SO202-05-34 lie on the eastward extension of the Subarctic Front (Figure 2.1). Both sites exhibit highest foraminifera abundance within the top 50 m of the water column coinciding with maximum chlorophyll levels and a seasonal thermocline. Total foraminifera standing stocks at Site SO202-05-34 was high with 24.8 shells/m^{-3} and lower at Site SO202-05-33 with 15.1 shells/m^{-3} (Figure 2.2). Site SO202-05-34 has a much more diverse foraminiferal assemblage than SO202-05-33 and is dominated by 7 species: *N. dutertrei* (25 %), *N. incompta* (23 %), *G. inflata* (13 %), *G. bulloides* (8.9 %), *T. quinqueloba* (8.4 %), *N. pachyderma* (8.3 %) and *G. siphonifera* (6.8 %). Site SO202-05-34 shows the highest abundance of *N. incompta* and *G. inflata* for any of our multinets, reflecting the southerly location of this site. The more northerly Site SO202-05-33 is dominated by only three species: *G. bulloides* (74.8 %), *N. pachyderma* (12.5 %) and *G. glutinata* (8.1 %). Hydrographically, sites SO202-05-33 and SO202-05-34 differ significantly, with site SO202-05-34 exhibiting higher SST (sea surface temperature) of 16.4°C compared with 13.3°C at site SO202-05-33. Surface salinity is higher at site SO202-05-34 (33.9 p.s.u compared to 32.8 p.s.u), reflecting the location of site SO202-05-34 at the northern rim of the subtropical gyre.

Core-top site SO202-02-40 is located further west than sites SO202-05-33 and SO202-05-34 and occupies the northern limb of the Kuroshio Current (Figure 2.1). Its assemblage is dominated by 5 species of planktic foraminifera: *N. incompta* (42.6 %), *G. inflata* (18.3 %), *N. pachyderma* (15.8 %), *G. bulloides* (9 %) and *G. siphonifera* (7.3 %) (Figure 2.2). As with site SO202-05-34, the high abundance of *N. incompta*, *G. inflata* and *G. siphonifera* reflect the warmer temperatures at this site. Plankton net assemblages from site St. 4 comprise of two main planktic foraminifera species, *N. incompta* (46.2 %) and *N. dutertrei* (42.6 %) (Figure 2.2). Site St. 4 is found on the Sub-arctic front (Figure 2.1).

2.4.2 North East Pacific (Alaskan Coastal Current)

Sites SO202-04-27 and SO202-02-31 are located in the North East Pacific, an area dominated by the Alaskan coastal current and the North East Pacific gyre (Figure 2.1). Total foraminiferal standing stocks at site SO202-04-27 is the highest of any of our multinets and is mainly confined to the first 50 m of the water column. Maximum foraminiferal abundance is clearly associated with high chlorophyll levels (Figure 2.2). In contrast, site SO202-02-31 in the centre of the gyre shows lower total foraminiferal standing stocks (5-10 shells/m^{-3}), with the highest flux coming in the 50-150 m depth interval. Chlorophyll levels here are markedly lower than at site SO202-04-27 (Figure 2.2). The proportionate assemblage of species at the two sites are also quite different. Site SO202-04-27 is characterised by only two species, *G. bulloides* (41.4 %) and *N. pachyderma* (50.3 %), while Site SO202-02-31 has significant abundances of four species: *G. bulloides* (44.8

%), *N. pachyderma* (20.5 %), G. *glutinata* (20.1 %) and *T. quinqueloba* (13.3 %). Core-top assemblage data from site SO202-02-31 shows a reduction in diversity compared to the multinet, with only two species with high abundance: *N. pachyderma* (67.9 %) and *G. bulloides* (29.8 %). Both multinet and core-top counts from site SO202-04-27 are characterized by two species: *N. pachyderma* (50.28 % multinet, 93.68 % core-top) and *G. bulloides* (41.4 % multinet, 6.3 % core-top) (Figure 2.2). Site St. 5 is located close to Station PAPA and site SO202-04-27 (Figure 2.1). It exhibits close to equal contributions from four species: *N. pachyderma* (33.2 %); *T. quinqueloba* (24.4 %); *N. incompta* (23.7 %); *G. bulloides* (17.9 %) (Figure 2.2).

Hydrologically the two sites exhibit similar surface oxygen and temperature (11-12°C) values at the surface and high oxygen values down to ~100 m. Site SO202-02-31 has lower salinity (32.5 p.s.u.) at 10 m than Site SO202-04-27 (32.8 p.s.u), alongside greater numbers of foraminifera at 50-150m depth compared with 0-50 m at site SO202-04-27. There are major differences between the two sites in terms of chlorophyll. At site SO202-04-27, chlorophyll levels indicate a high phytoplankton bloom, peaking at around 50 m (0.7 µg/L), which is double that of the maximum at site SO202-02-31 at 10 m depth (0.35 µg/L).

2.4.3 Sub-tropical gyre

Plankton net St. 3 is located just below the Sub-arctic front. It is primarily influences by southbound waters of the Kuroshio Extension. Two species are present in high abundance in this sample: *G. ruber* (53.63 %) and *N. incompta* (31.88 %). Site St. 2 is located on the eastern limb of the sub-tropical gyre (Figure 2.1) and is characterised by six species of planktic foraminifera: *T. sacculifer* (24.21 %), *G. ruber* (24.21 %), *G. crassaformis* (14.74 %), *G. siphonifera* (12.63 %), *G. calida* (10. 53 %) and *G. radians* (7.37 %) (Figure 2.2). Site St. 1 is located off the coast of Hawaii (Figure 2.1) and is characterised by five species: *T. sacculifer* (33.24 %), *G. tenella* (22.46 %), *G. ruber* (22.16 %), *G. rubescens* (7.78 %) and *G. siphonifera* (5.09 %) (Figure 2.2).

2.4.4 North West Pacific (Kamchatka Current, Oyashio Current)

Site SO202-05-02 is located in the North West Pacific and reflects hydrological influences from the Kamchatka and Oyashio currents with the addition of outflow water from the Sea of Okhotsk (Figure 2.1). Overall total foraminifera flux is low at site SO202-05-02, with the greatest abundance found in the 0-50 m depth interval (Figure 2.2). Only three species are abundant (>5 %) in the multinet assemblage: *N. pachyderma* (70.7 %), *G. bulloides* (16.5 %) and *N. incompta* (5.4 %). Compared to the North East Pacific, *N. pachyderma* is present in proportionately much greater numbers within the total assemblage. Chlorophyll levels peak at 35 m in the water column (0.4 µg/L), and SST is nearly 3°C colder than in the North East Pacific with a seasonal thermocline

present in the first 50 m. Similar to site SO202-02-31, site SO202-05-02 has a deep oxygen maximum down to 125 m, reflecting a deeper winter mixed layer.

Core-tops were collected from sites SO202-02-06 and SO202-02-07 also in the North West Pacific. Both sites indicate a dominance of *N. pachyderma* with site SO202-02-06 exhibiting 96.8 % and no other species over 5 % abundance. Site SO202-02-07 has 89.7 % *N. pachyderma* with *G. bulloides* showing a relative abundance of 9.4 % (Figure 2.2).

2.4.5 Bering Sea (Alaskan Coastal inflow water, Bering slope water)

Multinets SO202-04-10, SO202-03-13, SO202-04-14 and SO202-04-15 were collected in the Bering Sea between the Aleutian Islands and the Bering Slope (Figure 2.1). The sites are predominantly bathed in waters derived through inflow from the Alaskan Coastal Current as well as the initial stages of the Bering Slope current (Figure 2.1). Total foraminiferal flux was highest at sites SO202-04-14 and SO202-03-13 where foraminifera populations were predominantly found in the top 50 m of the water column alongside chlorophyll-α levels of 0.2-0.4 µg/L (Figure 2.2). Both sites also exhibit a notable abundance of planktic foraminifera just below the chlorophyll maxima. Sites SO202-04-10 and SO202-04-15 show much lower standing stocks of foraminifera (<5 shells/m^{-3}) (Figure 2.2). In both cases, foraminifera are found slightly below the chlorophyll maxima in the 50-150 m depth interval (Figure 2.2). Sites SO202-04-10, SO202-03-13 and SO202-04-14 are dominated by two species of planktic foraminifera. Site SO202-04-14 has 65.04 % *N. pachyderma* and 32.3 % *G. bulloides*. Site SO202-03-13 has 52.9 % *N. pachyderma* and 40.4 % *G. bulloides*, whilst site SO202-04-10 has 54 % *N. pachyderma* and 44.52 % *G. bulloides*. Site SO202-04-15 is the only Bering Sea site to exhibit additional species >5 % in its assemblage: *N. pachyderma* (65.1 %), *G. bulloides* (25.6 %) and G. *glutinata* (9.3 %). Core-top assemblage counts from site SO202-03-13 show a sole dominance of *N. pachyderma* (99.4 %).

Hydrographically, sites in the Bering Sea have similar water column profiles. Sea surface temperatures range from 7-8 °C with a seasonal thermocline from 25-50 m. A key feature of Bering Sea sites is the very deep oxygen maximum zone, often extending below 200 m, as well as low temperatures and salinities reflecting a deep winter mixed layer. Chlorophyll levels are low at sites SO202-03-13 and SO202-04-15 compared to the other multinets at sites SO202-04-10 and SO202-04-14 (Figure 2.2).

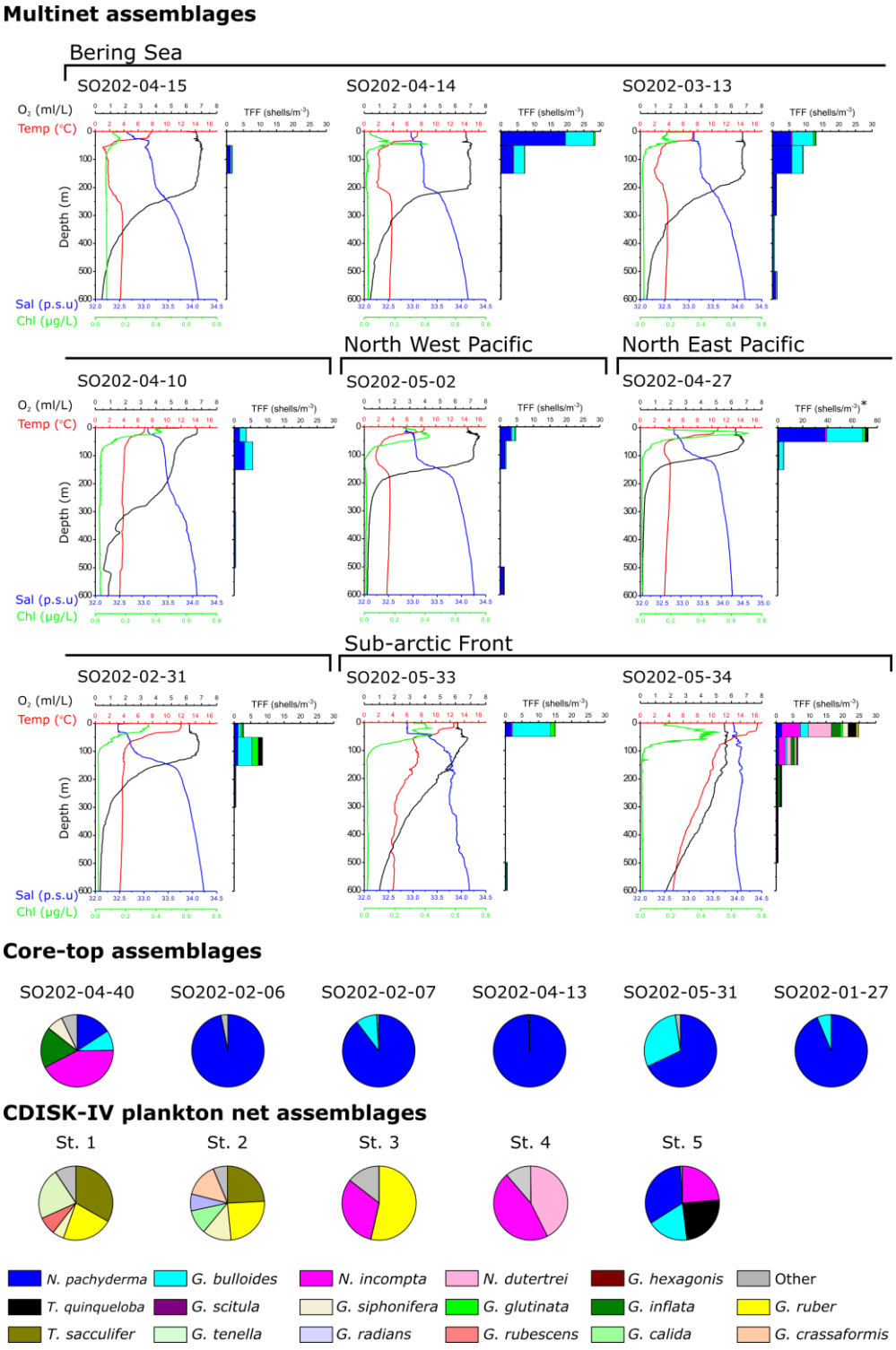

*Figure 2.2: Vertical profiles down to 600 m of total foraminifera flux (TFF) and CTD data from 9 new sites in the North Pacific. CTD data comprises of four variables: temperature (red line) in °C; oxygen concentration (black line) in ml/L; salinity (dark blue line) in p.s.u. and chlorophyll concentration (green line) in µg/L which was calculated using florescence data. TFF is given in shells/m^{-3} where different coloured bars represent different planktic foraminifera species, as denoted in the key. TFF is presented for five multinet depth intervals: 0-50 m; 50-150 m; 150-300 m; 300-500 m and 500-1000 m. Pie charts denoting core-top assemblages for 6 new sites in the subpolar North Pacific are displayed from East to West with accurate locations displayed in figure 2.1. Pie charts denoting plankton net assemblages for 5 new sites are displayed from South to North with accurate locations displayed in figure 2.1. *note different TFF scale due to very high abundance of foraminifera at this site SO202-04-27.*

2.5 Discussion

We use our new data and compiled core-top database to re-evaluate planktic foraminifera faunal zones in the North Pacific. We also discuss dissolution bias within the sediment record and suggest that although North Pacific planktic foraminifera assemblages are influenced by dissolution, and specific species abundances within a sample may be biased, the overall pattern of faunal distribution is not seriously affected, and paleo-assemblages provide a particularly useful tool to track large-scale changes in surface ocean circulation. We then focus our discussion on the spatial, seasonal and depth distribution of the key proxy carrying species in the subpolar zone, *N. pachyderma* and *G. bulloides.* Understanding seasonal, spatial and water column drivers of abundance within these species is increasingly important with regards to interpreting both paleo-assemblage and geochemical data. A better understanding of these drivers will allow paleoceanographers to better use foraminiferal assemblages downcore to track changes in paleoenvironmental conditions. For geochemists, knowledge about seasonal preference and depth habitat are vitally important, particularly when reconstructing ocean conditions such as temperature and pH.

2.5.1 Geographic distribution of planktic foraminifera in the North Pacific

In addition to *N. pachyderma* and *G. bulloides*, which dominate the subpolar zone, 8 other indicator species of planktic foraminifera define the other regional zones in the North and Equatorial Pacific (Figure 2.3). Bradshaw (1959) and Coulbourn *et al.,* (1980) initially characterised 4 major faunal regions within the North Pacific: sub-arctic; transitional; central and equatorial. These were based predominantly on distributions of 5 species of planktic foraminifera: *N. pachyderma, G. bulloides, T. quinqueloba, G. ruber* and *G. inflata* (Bradshaw, 1959; Coulbourn *et al.,* 1980). We suggest updated zones based on our larger compilation of core-top data. The faunal zones (subpolar, transitional, upwelling, subtropical, western equatorial and eastern equatorial) are broadly defined by the spatial distribution of *N. pachyderma*; *G. bulloides*; *G. inflata; N. incompta; G. ruber; P. obliquiloculata; G. tumida; N. dutertrei; T. sacculifer; G. menardii* (Figure 2.3). Although core-top assemblages may be somewhat affected by corrosive North Pacific waters, as defined below (surface water comparison) we find that dissolution has little effect on the overall pattern of faunal zones.

2.5.1.1 Subpolar Zone

The North Pacific subpolar zone is located north of the subpolar front at 40°N (Figure 2.3). It is defined by the subpolar gyre with its southern boundary occurring on the eastward limb of the Kuroshio current. Surface water temperatures in the subpolar zone range from 2-10°C (based on

annual averages from WOA13). The subpolar zone is characterised by two species of planktic foraminifera: *N. pachyderma* which is found throughout the region, and *G. bulloides* which is most abundant in the Gulf of Alaska.

2.5.1.2 Transitional Zone

The transitional zone occupies the boundary between the subpolar and subtropical gyres (Figure 2.3). Surface waters flowing through this region are typically a mix of the Kuroshio and Oyashio currents (Yasuda, 2003). Annual average SSTs in the region are 8-15°C (WOA13). The transitional zone is characterised by two species of foraminifera: *G. inflata,* which exhibits the highest abundance in the transitional zone and *N. incompta* which is present in lower abundances. It is difficult to characterise the extension of this zone into the central Pacific, due to the lack of core-top sites with available foraminifera data. However, based on our multinet samples and those of Iwasaki *et al.,* (2017), both species are prevalent across the central North Pacific along the Kuroshio extension. The link between the transitional zone and the subpolar front mean that changes in the abundance of these transitional species through time could be used as a sensitive tracer of gyre circulation and strength.

2.5.1.3 Upwelling Zone

In the North East Pacific, the Subarctic Front splits southward through the formation of the California current, a low temperature, low salinity current (Lynn and Simpson, 1987). This region is typified by significant upwelling, particularly during winter months (Huyer, 1983). *N. incompta* is most prevalent in this zone with *G. bulloides* and *N. dutertrei* also apparent (Figure 2.3).

2.5.1.4 Subtropical Zones

The subtropical zone represents the region between 35°N and 15°N in the North Pacific with an equivalent zone in the southern hemisphere (Figure 2.3). A warm water zone influenced by waters from the subtropical gyre with surface water temperatures between 18 and 27°C (WOA13), it is the most faunally diverse zone in the North Pacific in terms of planktic foraminifera. Species counts range from 7 to 29 (suppl. Figure 2.12), with *G. ruber* being the most consistently abundant species across the region (Figure 2.3). Other species include *T. sacculifer, G. siphonifera*, and *G. calida*.

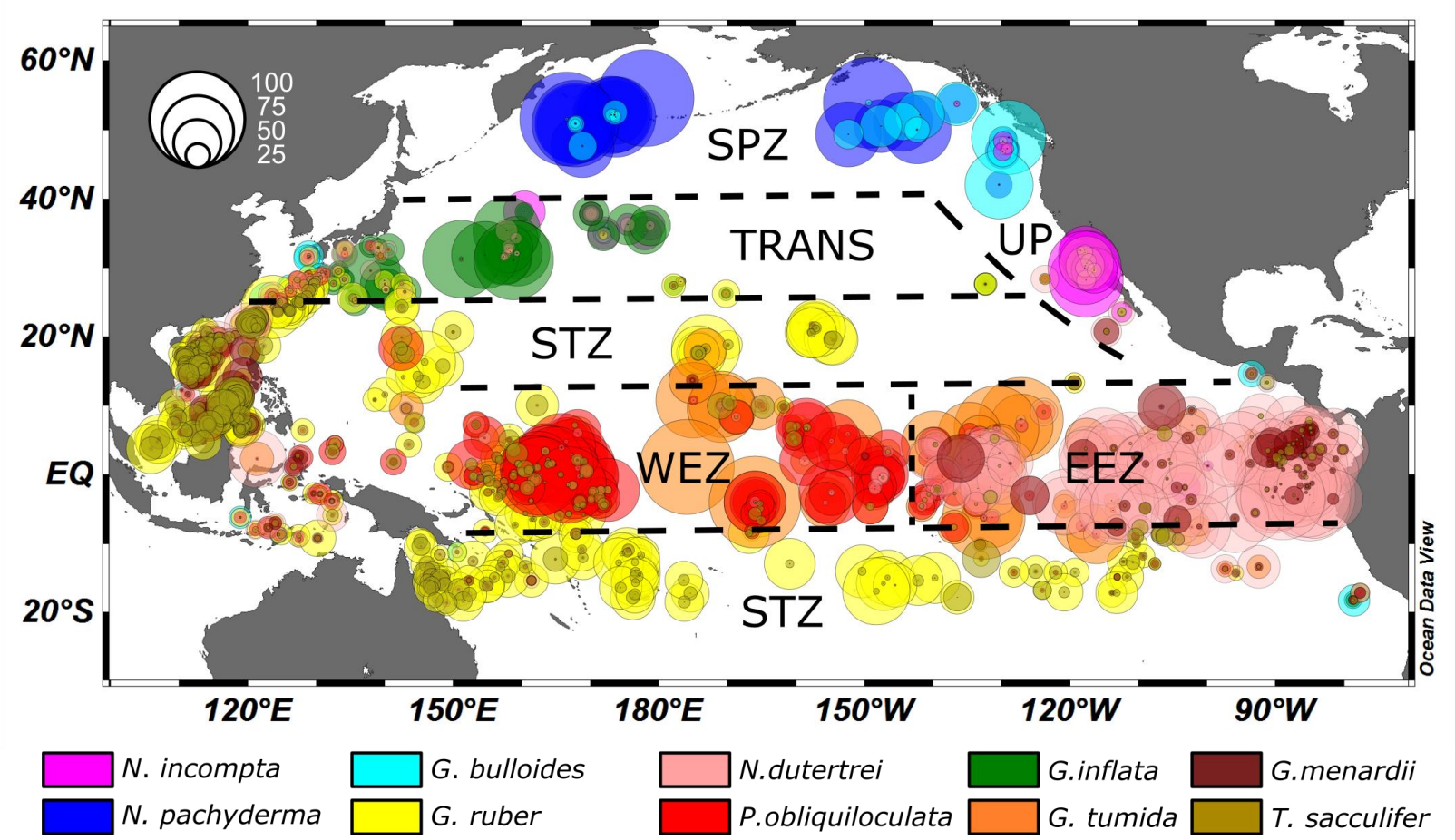

Figure 2.3: Distribution and abundance of North Pacific planktic foraminifera based on new subpolar North Pacific sites and compiled data from Coulbourn et al., 1980 and Kurcera et al., 2005. Size of bubbles represent percentage abundance of planktic foraminifera and colour represents different species of planktic foraminifera, as denoted by the key. Six faunal zones are described based on the distribution of 10 major species of planktic foraminifera: SPZ is the subpolar zone; TRANS is the transitional zone; UP is the upwelling zone; STZ is the subtropical zone; WEZ is the west equatorial zone; EEZ is the east equatorial zone.

2.5.1.5 West Equatorial Zone

The west equatorial zone is located between 15°N and 15°S in the North Pacific (Figure 2.3). Annual surface water temperatures range from 25°C to 30°C (WOA13). Two species of planktic foraminifera dominate in this region, *P. obliquiloculata* and *G. tumida*. *P. obliquiloculata* populations are thought to expand in response to winter temperatures (Tolderland and Bé, 1971) as well as living deep in the water column at depths of 200 m. *G. tumida*, is not commonly observed within surface water samples and its high abundance within the sediment may be a result of dissolution bias. In addition to these two species, *G. menardii* and *T. sacculifer* are also present throughout this region in moderate abundances (Figure 2.3).

2.5.1.6 East Equatorial Zone

The East Equatorial zone refers to the region east of 140°W in the Equatorial zone (Figure 2.3). The region exhibits a broader temperature range than the West Equatorial zone (20-30°C), due to seasonal changes in upwelling which bring cooler nutrient rich waters to the surface. The zone is dominated by *N. dutertrei*. *N. dutertrei* is thought to flourish in upwelling conditions near to gyre margins in warm tropical to subtropical waters (Imbrie and Kipp, 1971; Bé, 1977; Kroon and Ganssen, 1989; Brummer 2000)), which is consistent with very high abundance of *N. dutertrei* in the East Equatorial zone. *G. menardii* is also found in relatively high abundances in this region (Figure 2.3).

In a key observation regarding the relationship between the east equatorial zone and the west equatorial zone is the dominance of three key species in different regions: *P. obliquiloculata* in the west; *G. tumida* in the central and N. dutertrei in the east. This could have significant implications for the reconstruction of the El Nino Southern Oscillation (ENSO) in the past. It is likely that during the dramatic shifts in surface ocean conditions observed during ENSO, the relatively distribution of these species may reflect this change and could thus provide a sensitive means by which to track ENSO variability in the past.

2.5.1.7 Surface water comparison

The zones described above are based on our compilation of surface sediment samples, which may be affected by dissolution. To test resemblance of surface water assemblages to these zones we analysed five plankton net samples from a transect spanning from Hawaii to Station PAPA in the North East Pacific during the CDISK-IV cruise (Figure 2.4). In addition, this transect fills a gap in the sediment record likely due to poor foraminiferal preservation (Figure 2.3).

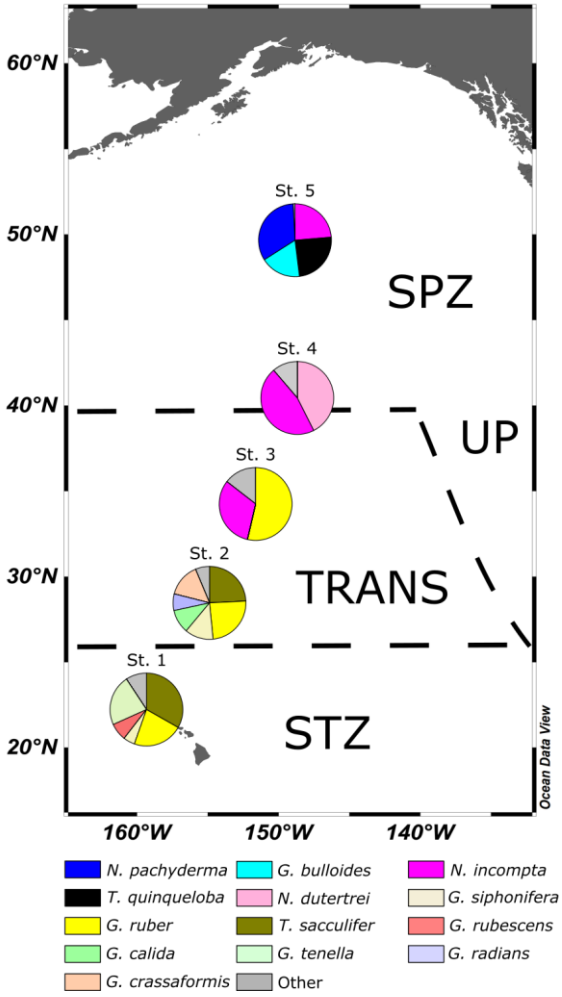

Figure 2.4: Pie charts showing new assemblage data from 5 plankton nets taken during the CDISK-IV KM1712 cruise. The map is overlain with faunal zones depicted in figure 2.3 indicating the validity of the zones within surface water samples. SPZ is the Sub-Polar Zone; UP is the Upwelling Zone; TRANS is the Transitional Zone; STZ is the Sub-Tropical Zone.

The plankton net samples show good agreement with our proposed faunal zones. Site St. 1 in the Subtropical Zone shows high species diversity with the dominant species *G. ruber* and *T. sacculifer*, typical of this faunal zone. A high abundance of *T. sacculifer* and *G. ruber* is also found at site St. 2 which lies on the border between the transitional and subtropical zones. Sites St. 3 and St. 4 see a decrease in assemblage diversity with only two species in high abundance. The dominance of the transitional species *N. incompta* over *G. inflata* at this location (Figure 2.3), suggests *N. incompta* may be the dominant transitional species in the eastern Transitional zone. The *N. dutertrei* identified at the transitional site St. 4 (41°N) is highly likely to be the cooler water *N. dutertrei* genetic type Ic, identified off the California coast by Darling et al, (2003) and reflects the warmer regional SSTs of the summer months. Site St. 5 shows a clear transition to Subpolar Zones species. *N. pachyderma* has the highest abundance, though is not as predominant

as in the core-top data, likely due to the combination of warm summer collection temperatures and dissolution (see below).

The key differences between our net samples and the surface sediment compilation include higher diversity at mid to lower latitudes, greater abundance of smaller foraminifera, and increased abundance of some temperate species at mid to high latitudes (Figure 2.3 and 2.4). There are three reasons these differences might occur. Firstly, the smaller sampling size of >125 µm used in the plankton nets meant increased numbers of smaller species such as *G. rubescens, G. tenella* and *T. quinqueloba* were present. Secondly, the plankton net samples were collected during summer months where warmer surface waters allow the more temperate genetic types of both *G. ruber* (St. 3) and *N. dutertrei* (St. 4) to frequent the higher latitude waters (Darling et al, 2003; 2008). Thirdly, dissolution in corrosive North Pacific waters is likely to reduce diversity in sediment samples and bias samples somewhat towards dissolution resistant species. However, despite these potential biases, overall net samples show patterns consistent with core tops, adding confidence to this zonation.

2.5.2 Ecology and Distribution of *G. bulloides* in North Pacific waters

G. bulloides is primarily found within the subpolar and transitional zones of the global ocean (Tolderlund and Bé, 1971; Bé and Hutson, 1977; Coulbourn *et al.,* 1980), forming a substantial portion of mid to high latitude assemblages (Kucera, 2007). It can be found in association with both upwelling and non-upwelling regions (Curry *et al.,* 1992; Darling *et al.,* 2003; Davis *et al.,* 2016; Mallo *et al.,* 2017) and represents an important proxy carrier for paleoclimatic records (Schiebel and Hemleben, 2017). In the North Atlantic, *G. bulloides* has been observed to tolerate temperature ranges of between 5-30 °C (Źarić *et al.,* 2005; Kucera, 2007). However much of this extreme temperature range may be explained by the presence of different cryptic species of *G. bulloides* (Darling *et al.,* 2008), where different genotypes are adapted to different environmental conditions. It is therefore key that depth habitat, seasonality and ecology are regionally resolved for this species.

The relationship between the vertical distribution of *G. bulloides* and the physical state of the water column can be determined from our multinet data. Our data shows the highest *G. bulloides* standing stocks are between 0-50 m. In most cases, this coincides with maximum chlorophyll-α concentration in the water column (Figure 2.5), indicative of high food availability. This relationship is typified at site SO202-04-27 where *G. bulloides* peaks at 28.64 tests/m^{-3} between 0-50 m, the highest of any site in this study, with surface temperatures of 8°C (0-50 m) and a chlorophyll-α peak of 0.7 µg/L. Similarly, where surface chlorophyll-α is low, such as site SO202-02-31 (0.35 µg/L), *G. bulloides* abundance is also low. This suggests that within the upper 50 m of the water column, *G. bulloides* abundance is primarily driven by food availability. Kuroyanagi and Kawahata (2004) also show *G. bulloides* predominantly residing between 20-40 m in the water column in the North West Pacific and Field (2004) link the peak occurrence of *G. bulloides* with chlorophyll maximum at sites along the California margin. Bird *et al.,* (2017) cite *G. bulloides* as an opportunistic feeder, preying on zoo- and phytoplankton, as well as bacterioplankton.

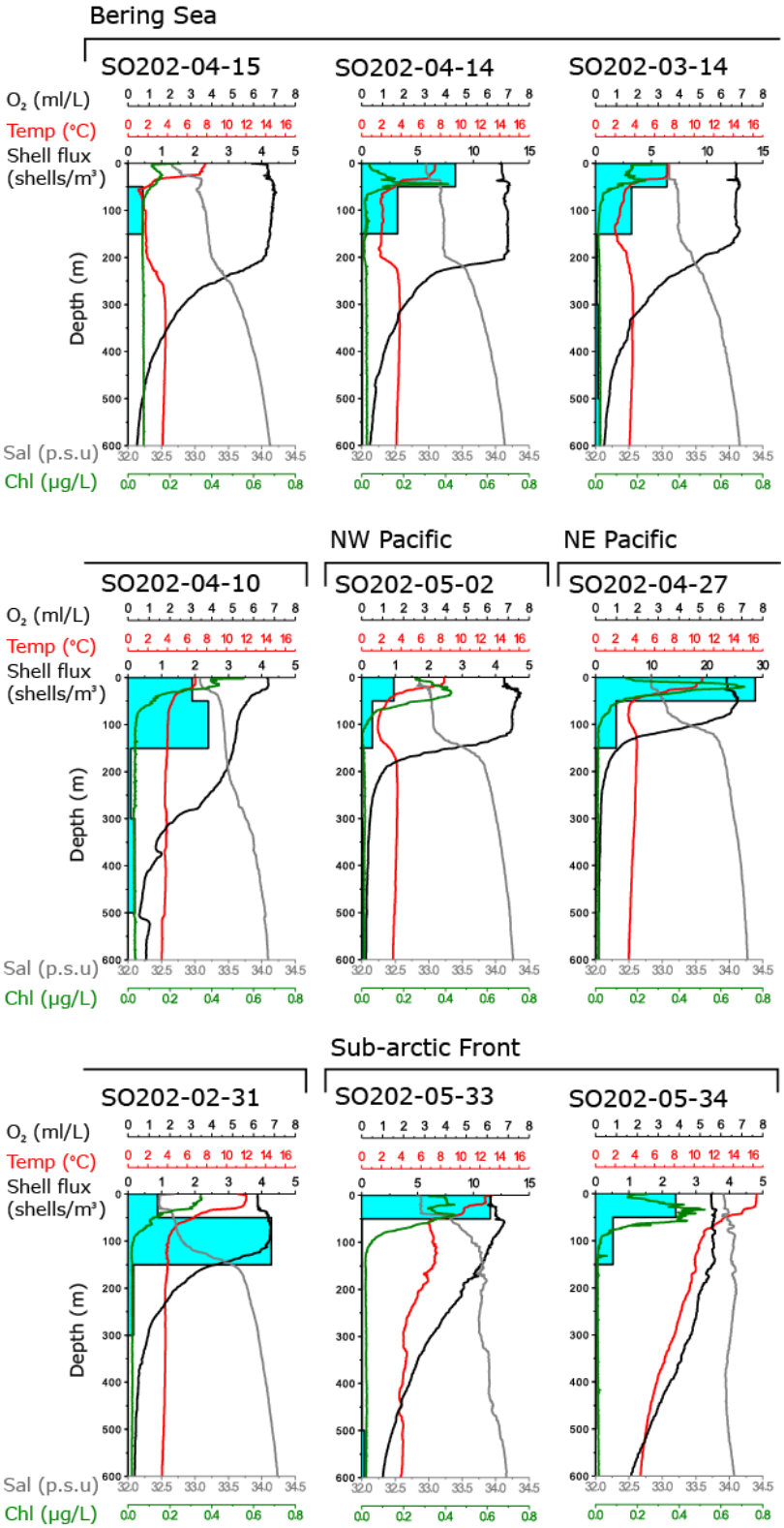

Figure 2.5: Vertical profile of G. bulloides flux and CTD data to 600 m from 9 new sites in the North Pacific. G. bulloides flux is shown at 5 depth intervals: 0-50 m; 50-150 m; 150-300 m; 300-500 m; 500-1000 m. CTD data include: oxygen concentration (black line) in ml/L; temperature (red line) in °C; salinity (grey line) in p.s.u; chlorophyll concentration (green line) in µg/L, derived from fluorescence data. Light blue bars indicate the shell flux (shells/m^3) of G. bulloides, note variable shell flux scales depending on site.

A number of sites within this study indicate that some populations of *G. bulloides* may live deeper in the water column, below the chlorophyll maximum. Sites in the North East Pacific (SO202-04-27 and SO202-02-31), Bering Sea (SO202-04-10, SO202-03-13 and SO202-04-14) all have standing stocks of *G. bulloides* greater than 2 tests/m^{-3} down to 150 m depths, whilst at site SO202-04-15 (the most northerly site in the Bering Sea), a small standing stock of *G. bulloides* occurs between 50-150 m (Figure 2.5). The exact size and prominence of these deeper dwelling populations are difficult to quantify as some specimens at our sites may represent deceased foraminifera which have recently sunk through the water column. Despite this, Iwasaki *et al.,* (2017) indicate several North Pacific sites where deeper dwelling *G. bulloides* are observed (see *supplementary information*). Their study includes 5 sites with *G. bulloides* abundances greater than 2 tests/m^3 between 50-100 m and 4 sites with *G. bulloides* >100m (Iwasaki *et al.,* 2017) (see *supplementary information*). The fact that Iwasaki *et al.,* (2017) also find small populations of deep-dwelling *G. bulloides* suggests the influence of deceased on our dataset is reduced.

Both our sites and those cited by Iwasaki *et al.,* (2017), indicate that *G. bulloides* can live below the chlorophyll maximum but at reduced abundances compared to the photic zone. At our sites, deep dwelling *G. bulloides* are associated with a deep oxygen maximum zone, reflecting deep winter mixing (Roden, 1985). Schiebel *et al.,* (2001) and Freeland *et al.,* (1997) suggest that a deeper mixed layer could increase the entrainment of deep water nutrients from intermediate waters into the mixed layer, a mechanism used to explain a deeper depth habit for *G. bulloides* by Iwasaki *et al.,* (2017). This coupled with mixing of nutrient and food rich surface waters to depth could explain deeper dwelling *G. bulloides* at our sites. Recent work by Bird *et al.,* 2017, which demonstrates the first observation of bacteria within *G. bulloides* type IId off California, also suggests that *G. bulloides* may use bacteria as a potential food source. This could help explain the survival of deeper dwelling populations, where light limits the availability of conventional food sources. Deeper dwelling *G. bulloides* are often found at our sites where surface waters (0-50 m) have lower salinity. This is particularly prevalent at site SO202-02-31 and could explain the deeper dwelling *G. bulloides* at this site, where salinity increases below the chlorophyll maximum (Figure 2.5). Despite the evidence that *G. bulloides* may inhabit waters below the chlorophyll maximum, it is important to stress that the majority of sites in this study show the maximum abundance of *G. bulloides* in the top 50 m of the water column (Figure 2.5), an important factor when interpreting geochemical and census data downcore.

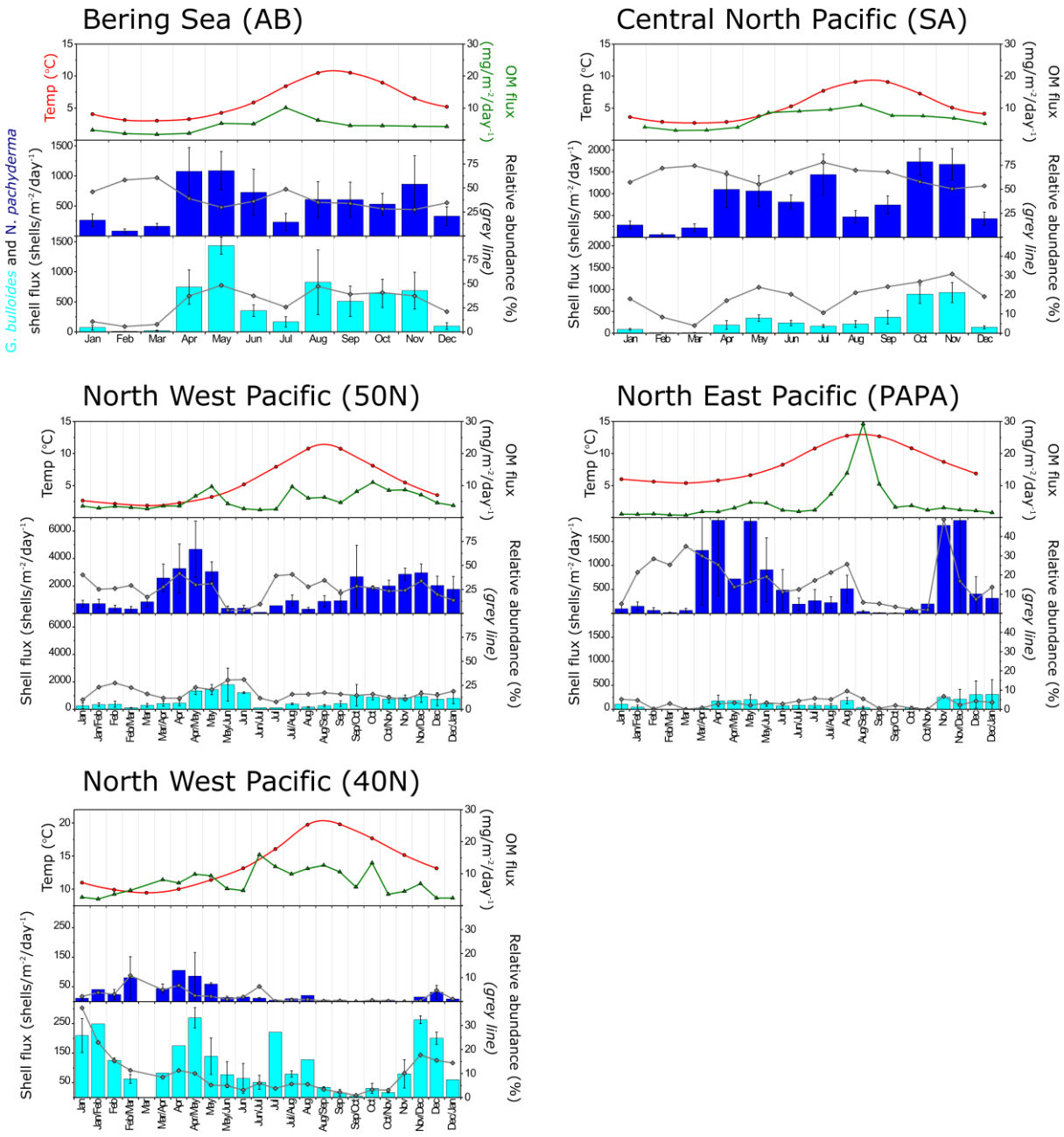

Figure 2.6: Compiled sediment trap and hydrological data from five sites in the North Pacific. All sites contain monthly or bi-weekly data on shell flux (shells/m^{-2}/day^{-1}) of N. pachyderma (dark blue bars) and G. bulloides (light blue bars) as well as the relative abundance (%) of each species in the assemblage. Where multiple years of sediment trap data was available from the same site, the data was averaged with error bars defining the standard error. Organic matter flux (mg/m^{-2}/day^{-1}) was also compiled for each sediment trap (green line). Monthly temperature was derived for each site using ocean data view's 3D estimation tool and the world ocean atlas 2013 monthly datasets (red line). Sediment trap data for each site was compiled from the following publications: Site AB (Bering Sea) and SA (central Pacific) (1990-1999) from Takahashi et al., 2000, Asahi and Takahashi, 2007; Sites 40N (1997-2000) and 50N (1997-2001) (North West Pacific) from Kuroyanagi et al., 2008; Station PAPA (1982-1986) from Sautter and Thunell, 1989.

To aid the interpretation of paleo-records, it is particularly important to understand the seasonal changes in oceanographic conditions which drive planktic foraminiferal abundance. Mean bi-weekly sampling of *G. bulloides* in sediment traps from the North West Pacific (Kuroyanagi *et al.,* 2008) demonstrate the diverse seasonal hydrography of the region (sites 40N and 50N, Figure 2.6). In the North West Pacific at 50 °N, *G. bulloides* is found throughout the year, with peak abundance occurring between April and June (Kuroyanagi *et al.,* 2008). This represents the onset of the spring phytoplankton bloom, driven by reduced light limitation and increased stratification, combined with abundant nutrients that were previously brought to the surface by deep winter mixing (Kuroyanagi *et al.,* 2008). This supports the use of *G. bulloides* as an indicator of productivity, a conclusion also reached by several recent modelling studies (Źarić *et al.,* 2005; Fraile *et al.,* 2008; Lombard *et al.,* 2011; Jonkers and Kučera, 2015). Despite an increase in *N. pachyderma* flux during this period, the relative abundance, and overall flux, of *G. bulloides* still increases. Although this effect is muted, it further supports the use of *G. bulloides* relative abundance in tracking changes in productivity in the past. The *G. bulloides* flux at 40°N (site 40N) in the North West is more variable than at site 50N, with two abundance peaks occurring in winter (November-February) and in late spring (April-May) (Figure 2.6). Although organic matter flux peaks from July through to October, it does not correlate with the peaks in *G. bulloides* abundance (Kuroyanagi *et al.*, 2008) (Figure 2.6). This variability is likely caused by the fact that the sediment trap lies on the interface between the Oyashsio (cold) and Kuroshio (warm) currents. This zone is characterised by strong eddy activity as well as influence from minor currents such as the Tsushima Warm Current (Yasuda, 2003). Horizontal transport of nutrients from rich subpolar waters, driven primarily by intra-annual wind stress variability (Ayers and Lozier, 2010), add to the confluence of ecological signals around the Kuroshio extension. The variable influences of these different systems are likely to drive the variability in annual *G. bulloides* flux, making it difficult to disentangle a particular driver of flux at this latitude. In addition, the high SSTs observed throughout the year at Site 40°N is likely to contribute to the lack of *G. bulloides* flux seen here in comparison with the other more northerly sites.

Sediment trap data from the central North Pacific and Bering Sea also show *G. bulloides* abundances associated with spring and summer increases in productivity, with very low abundances recorded during winter months (December to March) (Asahi and Takahashi, 2007). Peaks in *G. bulloides* in both traps tend to track increases in organic matter flux (Asahi and Takahashi, 2007), again suggesting a preference for eutrophic environments. This relationship is demonstrated by the prominent increase in *G. bulloides* relative abundance at the onset of the spring bloom in the Bering Sea. In the North East Pacific at Station PAPA, sediment trap data shows very low *G. bulloides* abundance over a four year period (Reynolds and Thunell, 1989).

Small increases in *G. bulloides* were observed during April and May, in line with a small rise in organic matter flux, suggesting ties to food availability. However, no response in *G. bulloides* abundance was observed during the large increase in organic matter between August and September (Figure 2.6), which may imply summer temperatures (>12.5°C) at this site rise above those tolerated by *G. bulloides*. The large increase in organic matter at station PAPA could also represent a plankton bloom of little dietary use to *G. bulloides*. Across the Pacific, the seasonal abundance of *G. bulloides* is largely tied to phytoplankton blooms and food availability, with *G. bulloides* numbers minimal or absent during the winter months, when organic matter flux is very low. Overall, the relative abundance of *G. bulloides* responds positively to the onset of the spring phytoplankton bloom, particularly at the higher latitude sites. Conversely, when assemblages become more diverse at lower latitude sites, this signal is muted.

G. bulloides has often been linked to upwelling zones (Reynolds and Thunell, 1980; Thiede, 1975; Sautter and Thunell, 1992; Field, 2004). However, its affinity with upwelling conditions in the

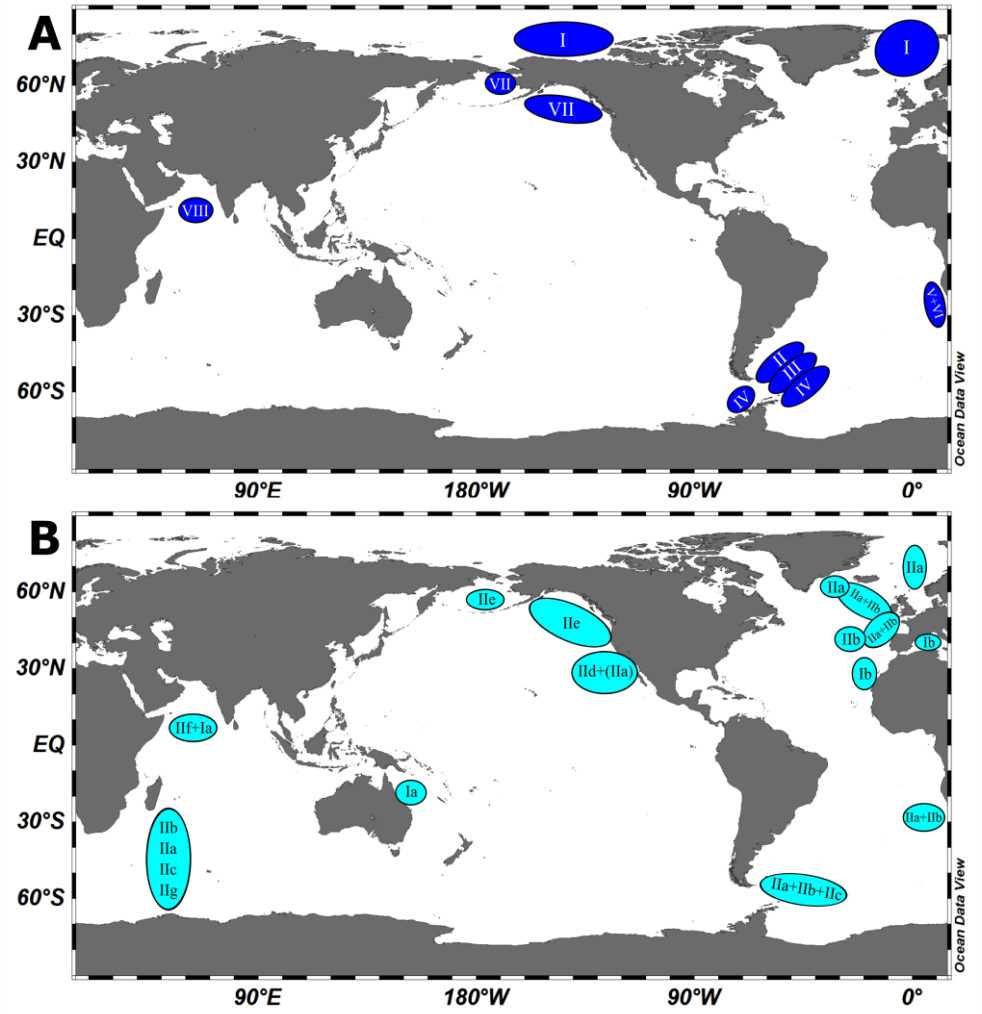

Figure 2.7: Map showing global distribution of genotypes of two species of planktic foraminifera (A) N. pachyderma and (B) G. bulloides based on Darling et al., 2008 and Morard et al., 2013.

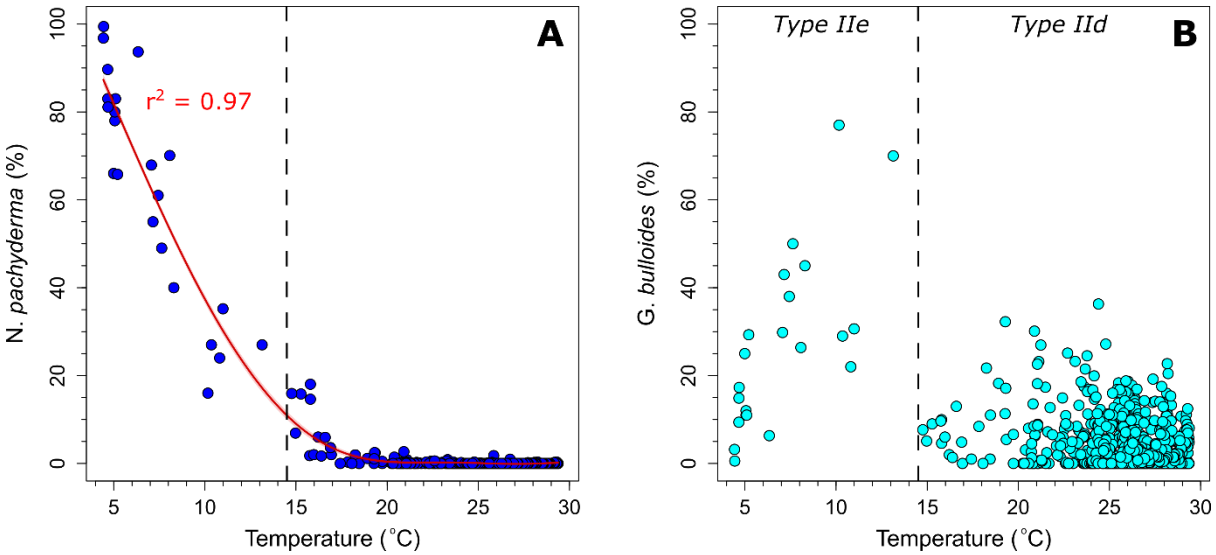

Figure 2.8: Scatter plot of planktic foraminifera species against sea surface temperature (SST). (A) Percentage abundance of N. pachyderma from new core-top compilation plotted against SSTs from world ocean atlas 2013 (Locarnini et al., 2013) derived using Ocean Data View's 3D estimation tool. We used a generalized additive model (GAM) from the 'mgcv' package in R to determine the relationship shown by the red line in A. (B) Percentage abundance of G. bulloides from core-top new compilation plotted against SSTs from the world ocean atlas 2013 (Locarnini et al., 2013) derived using Ocean Data View's 3D estimation tool. Two populations of G. bulloides can extracted from the plot: a low temperature population, likely comprising of genotype IIe and a high temperature population, likely comprising of genotypes IIa and IId (based on cryptic species distribution work by Darling et al., 2008).

North East Pacific is debated within recent literature. In the North-East Pacific, increased *G. bulloides* flux was observed during upwelling conditions (Reynolds and Thunell, 1980; Thiede, 1975; Sautter and Thunell, 1992; Field, 2004). However, other studies cite little dependence of *G. bulloides* on upwelling (Davis *et al.*, 2016; Iwasaki *et al.*, 2017). The recent work by Davis *et al.*, (2016) from the North Pacific showed decreased abundance of *G. bulloides* during periods of enhanced mixing on the central California shelf. In this region, upwelling is characterised by nutrient rich cold waters which may be below the temperature tolerance of *G. bulloides* type IId, leading to a reduction in abundance despite high nutrient levels.

The discovery of several genetically distinct genotypes of *G. bulloides* now sheds new light on the wide-ranging ecologies of regionally distributed *G. bulloides* (Figure 2.7). *Globigerina bulloides* genotypes fall into two clear highly divergent groups which are related to their ecologies (Darling & Wade, 2008; Morard at al, 2013; Darling *et al.*, 2017). The Type I genotypes (2 types) are associated with warmer waters and the Type II genotypes (7 types) are associated with cooler high latitude and transitional upwelling waters. The full temperature-specific range of the *G. bulloides* genotypes identified to date is shown in Sadekov *et al.*, (2016). Three genotypes have

been identified in the North Pacific, two of which are potentially endemic to the region (Fig. 6). The first is the transitional genotype Type IId, which has only been identified to date in the California Current (Darling et al, 2003). The second is genotype Type IIe, which has only been identified in the subpolar waters of the North Pacific and Bering Sea at latitudes greater than 40°N (Darling *et al.*, 2007). A single specimen of the subpolar and transition North Atlantic and Southern Ocean genotype Type IIa was identified off California in January (Darling et al, 2003), which possibly represents the winter population in the region (Davis et al, 2016). Uncertainty regarding the upwelling affinity of North Pacific *G. bulloides* is likely due to the differing ecological preferences of these different genotypes.

The separation of transitional and sub-polar genotypes is clearly demonstrated within our assemblage compilation. When the abundance of *G. bulloides* is plotted alongside SST, two clear populations can be seen (Figure 2.8). A mid-latitude population with a temperature range of 14.5-30°C is likely to represent the genotype IId and a high-latitude population with a temperature range of 5-14.5°C represents genotype IIe (Figure 2.8). Examples of *G. bulloides* as upwelling indicators in the North East Pacific are predominantly constrained to latitudes between 30-35°N (Sautter and Thunell, 1992; Field, 2004). Only genotype IId has been found at these latitudes in both upwelling waters and more stable summer water columns in the Santa Barbara Channel (Darling et al, 2003).

2.5.3 Ecology and Distribution of *N. pachyderma* in the subpolar North Pacific

N. pachyderma is found in high abundance in the polar and subpolar oceans and is frequently found in association with upwelling systems in the mid to low latitudes (Darling et al, 2017). Eight cryptic genotypes are currently recognised which are regionally distributed (Darling and Wade, 2008; Darling et al, 2017). Type I dominates the Arctic and North Atlantic oceans, Type II, III and IV are found only in the Antarctic water masses. Types V and VI appear isolated within the Benguela upwelling system, Type VII within the eastern North Pacific and Type VIII off the Oman margin in the Arabian Sea (Figure 2.7; Darling and Wade, 2007; Darling et al, 2017). There are clear ecological differences between the different cryptic species of *N. pachyderma* (Darling et al, 2004), and this is particularly important in the Antarctic region where 3 genetically distinct genotypes have been identified, with little morphological difference to separate them (Darling and Wade, 2008). As yet, genotyping coverage of the North Pacific subpolar region is incomplete in the far western region, but only one genotype of *N. pachyderma* (Type VII) has been identified to date throughout the eastern region and the Bering Sea (Darling et al, 2007). It would be

expected that the anticlockwise subpolar gyre circulation (Figure 2.1) would also carry the *N. pachyderma* Type VII into western subpolar waters.

The vertical distribution of *N. pachyderma* in North Pacific waters varies with regional hydrography (Figure 2.9). The North East Pacific is typified by site SO202-04-27, where cool summer surface temperatures (10°C) combine with high chlorophyll-α levels and a shallow seasonal thermocline. Here, *N. pachyderma* is most abundant in the top 50 m of the water column. *N. pachyderma* is also found at 0-50 m in the Bering Sea, where low chlorophyll-α is compensated for by cold surface temperatures (7-8°C) which are optimal for *N. pachyderma* (Reynolds and Thunell, 1986, Kuroyanagi and Kawahata, 2004). Although *N. pachyderma* responds most consistently to cool surface temperatures (<10°C), it can flourish in warmer surface waters (10-14°C) when food availability is high (site SO202-04-27). Kuroyanagi and Kawahata (2004) argue that *N. pachyderma* abundance is associated with the pycnocline in the North West Pacific. Within our sites, there is some evidence of high *N. pachyderma* abundance within the shallow seasonal pycnocline, a region also commonly associated with high chlorophyll-α values. Overall, our sites suggest that *N. pachyderma* vertical abundance distribution is controlled primarily by food availability, but they can also flourish in cooler temperatures where competition for food is likely to be limited. Spatially *N. pachyderma* abundance is strongly linked to temperature in the North Pacific (Figure 2.7a). This striking relationship provides excellent evidence that percentage abundance *N. pachyderma* can be used to track qualitative changes in temperature downcore.

N. pachyderma is also observed to live deeper in the water column at our sites as well as those published by Iwasaki *et al.,* (2017) (Figure 2.9 and *supplementary information*). This is particularly prevalent in the Bering Sea, where 3 sites show >2 m^{-3} abundance between 50-150 m. In the North West Pacific three sites from Iwasaki *et al.,* (2017) show *N. pachyderma* living down to 300 m in the water column (see *supplementary information*). As with *G. bulloides,* where deep dwelling *N. pachyderma* are observed in our multinets they are commonly associated with deep oxygen maxima and a deep winter mixed layer. This could be a result of increased winter mixing bringing up nutrient rich waters (Schiebel *et al.,* 2001; Iwasaki *et al.,* 2017), as well as mixing of food (phytoplankton) from the surface waters down to depth. Nutrients are higher in general throughout the year in the North West Pacific and are higher still during winter months (Garcia *et al.,* 2013). In addition, deeper dwelling populations could be linked to low surface salinities at 0-50 m, which may be outside the preferential salinity range of *N. pachyderma*. Interestingly, King and Howard (2003) found that *N. pachyderma* in the Southern Ocean could live down to depths of 200 m when the mixed layer was deep, allowing deeper penetration of food and nutrients. A combination of these mechanisms may be present in the North Pacific and

explain why some of our sites show an increase of deep dwelling *N. pachyderma* and *G. bulloides* at locations where a deep-winter mixed layer is observed (Figure 2.9). However, overall our sites suggest a predominantly near surface habitat (0-50 m) for *N. pachyderma* which is reflected in other studies from this region (Kuroyanagi *et al.,* 2004; Iwasaki *et al.,* 2017), as well as the North Atlantic (Pados and Spielhagen, 2014) and Southern Ocean (King and Howard, 2003; Kohfeld *et al.,* 1996).

In the subpolar North West Pacific, *N. pachyderma* is abundant throughout the year and peaks predominantly during the spring phytoplankton bloom between April and May when organic matter flux is high (Kuroyanagi *et al.,* 2008) (Figure 2.6). Only during later summer months does *N. pachyderma* abundance drop whilst organic matter flux remains high (Figure 2.6), possibly reflecting SST's that are above the ecological range for this species. On the subpolar front at 40°N latitude, *N. pachyderma* again peaks between April and May. Its abundance throughout the rest of the year is very low, reflecting SST as the limiting factor in *N. pachyderma* abundance. In the North East Pacific, subpolar seasonal trends in *N. pachyderma* mirror those in the west, but with a lower overall abundance (Sautter and Thunell, 1989). Predominantly, high abundances occur during spring (March-April) and tail off into summer months as SSTs rise. A second increase in *N. pachyderma* occurs during November, where *N. pachyderma* may be responding to a combination of low SSTs and reduced competition for food as light and temperature limit productivity.

As a subpolar species, *N. pachyderma* relative abundance in the North Pacific is tied closely to temperature (Figure 2.8) and latitude. Darling *et al.,* (2004 and 2007) cite a temperature range of 3 to 14 °C, which correlates well with relative abundance seen in our core-top compilation, whilst Kuroyanagi and Kawahata (2004) cite 5-8°C as the optimum temperature range for *N. pachyderma*. We find a temperature tolerance of up to 16°C, at which point *N. pachyderma* relative abundance drops below 10% (Figure 2.8). We also find that at <8°C, a temperature suggested by Reynolds and Thunell (1986) and Kuroyanagi and Kawahata (2004) as being close to optimum conditions, *N. pachyderma* has relative abundance of >50% (Figure 2.8). It is important to note that *N. pachyderma* abundance is also likely to be controlled partly by the temperature tolerance of its food source.

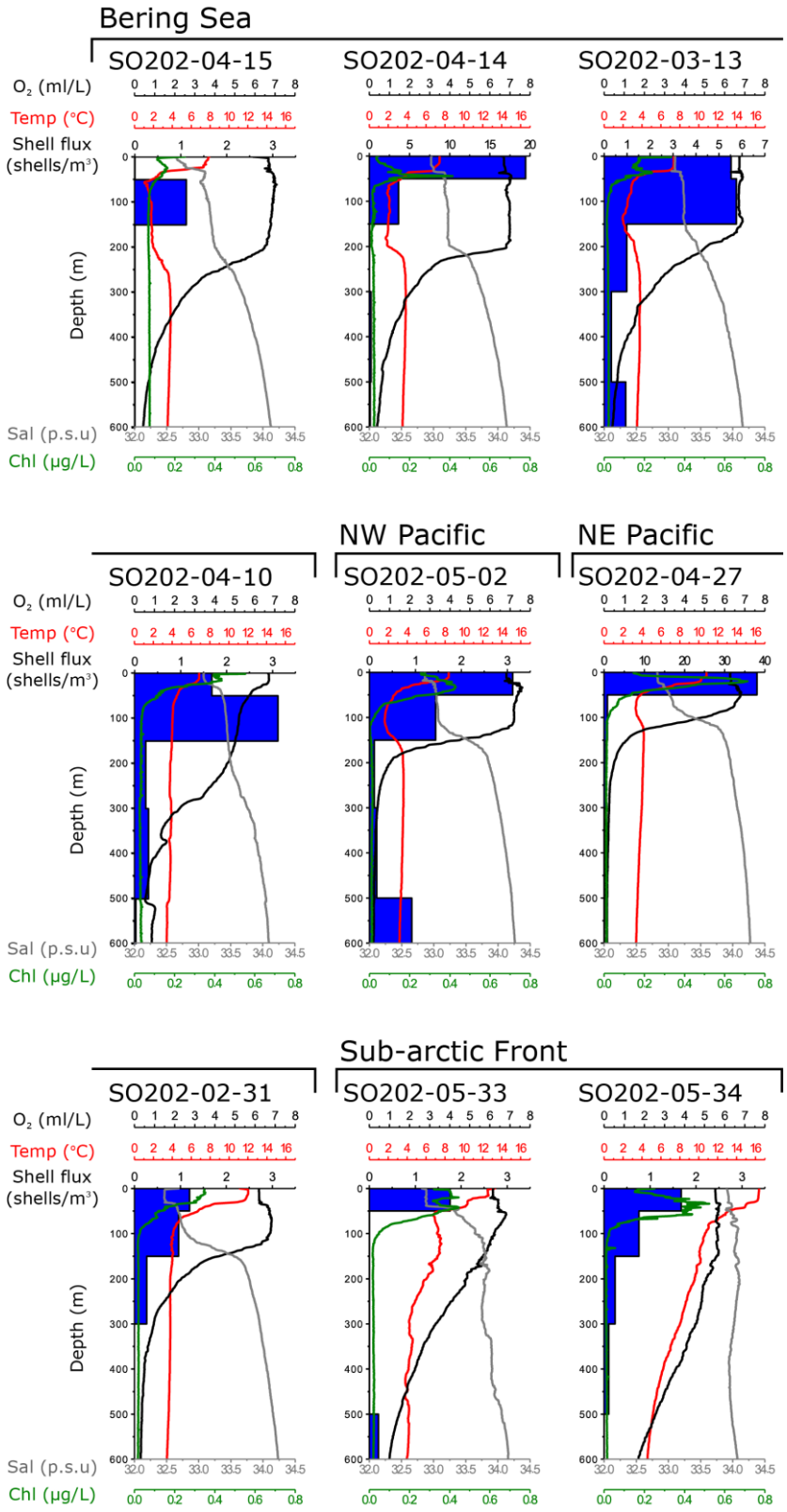

Figure 2.9: Vertical profile of N. pachyderma and CTD data to 600 m from 9 new sites in the North Pacific. CTD data include: oxygen concentration (black line) in ml/L; temperature (red line) in °C; salinity (grey line) in p.s.u; chlorophyll concentration (green line) in µg/L, derived from fluorescence data. Dark blue bars indicate the shell flux (shells/m^3) of N. pachyderma, note variable shell flux scales depending on site.

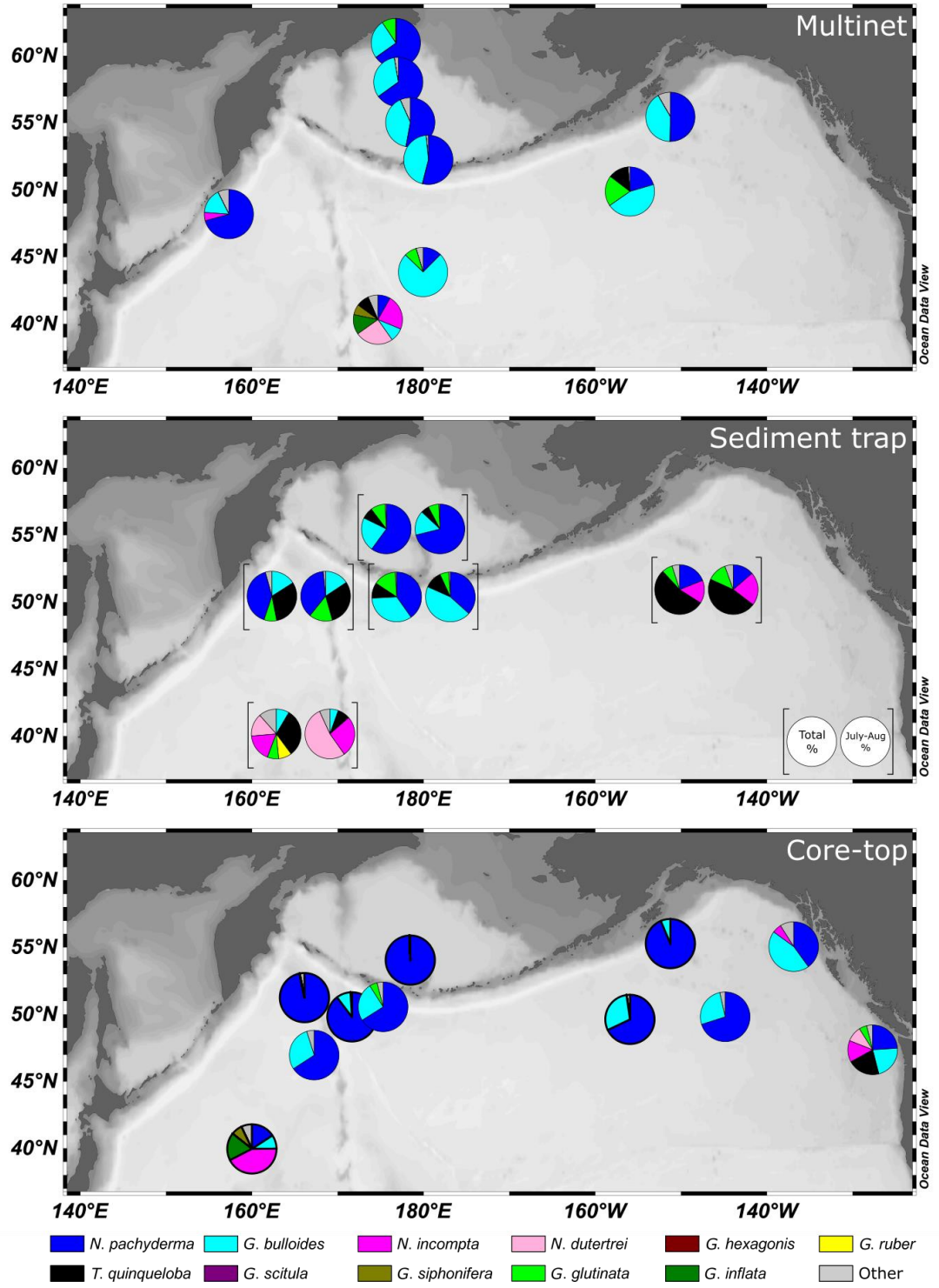

Figure 2.10: Bathymetric maps with pie charts comparing percentage abundance of planktic foraminifera in new multinets, compiled sediment trap data and core-top data from the same or adjacent sites in the North Pacific. Multinet pie charts show the average relative abundance for 0-500 m in the water column taken in July and August. Sediment trap data shows the average abundance over the course of the sediment trap (total %) adjacent to the average abundance during only July and August (July-Aug %). The similarity between the two sets of sediment trap data suggest little influence of seasonality on our multinets. Core-top data includes new data from our sites (bold pie charts) and data from adjacent sites taken from our core-top compilation. Note the reduction in diversity exhibited in subpolar North Pacific sites and the bias of preservation towards N. pachyderma over G. bulloides when comparing multinets to core-tops.

2.5.4 Dissolution and seasonality in North Pacific core top assemblages

Preferential dissolution of certain species of planktic foraminifera in seafloor sediment samples has the potential to bias paleo-assemblage data. By comparing core-tops and multinets from the same and nearby sites, we observe possible dissolution driven increase in *N. pachyderma* over *G. bulloides* abundance in core-top sediments, with up to 31% reduction (Site SO202-03-13, Bering Sea) in *G. bulloides* and up to 44% increase in *N. pachyderma* (Figure 2.10). Differences between multinet and core-top assemblages could be driven by two factors: dissolution or seasonality. We tested the possible effect of seasonality on our multinet samples by comparing annual sediment trap assemblages with assemblages based only on July-August (the time when our multinet were collected) (Figure 2.10 and 2.11). Figure 2.11 highlights a lack of obvious offset between summer and annual assemblages allowing us to conclude that the major driver of change within our core-tops is dissolution. In the North Pacific, under-saturated deep waters offer the potential to assess the influence of dissolution (Berger *et al.,* 1982), especially in combination with abundance data from tows and sediment traps. Sautter and Thunell (1989) also reported an increase in *N. pachyderma* relative to other species when comparing sediment trap samples to core-top samples, and although they rule out water column dissolution through analysis of surface and deep trap material, it is likely that sediment pore-water dissolution does take place. Despite being widely prevalent in the compiled sediment trap data (Figure 2.10), *T. quinqueloba* is absent from the majority of our multinet and core-top samples. Whilst this may partly be reflecting dissolution of small *T. quinqueloba* specimens in corrosive North Pacific deep waters, it is more likely that the smaller sieve size used in sediment trap studies (>125 μm) compared with core-top studies (>150 μm) causes the offset. The fact that both surface water (multinet) and sediment (core-top) samples show a lack of *T. quinqueloba* further illustrates this point.

Assessment of dissolution in the deep North Pacific was previously attempted by Coulbourn *et al.,* (1980), through similarity assessments of well-preserved near surface samples to samples situated deeper in the water column. Species were also ranked for dissolution resistance by region, allowing for dissolution indices to be calculated for each core-top sample (Coulbourn *et al.*, 1980). Coulbourn *et al.,* (1980) rank *N. pachyderma* and *G. bulloides* as 1 and 5 respectively, with 1 being highly dissolution resistant, suggesting that *N. pachyderma's* more compact test morphology could leave it less susceptible to dissolution, as suggested by our dataset. Conversely, a foraminifera like *G. bulloides* with a more bulbous test structure and larger surface area is likely to be more susceptible to dissolution in corrosive waters. The overarching outcome from Coulbourn *et al.,* (1980) is that dissolution is complex and difficult to account for in marine sediments and is likely to increase the error on transfer functions derived from assemblages, as

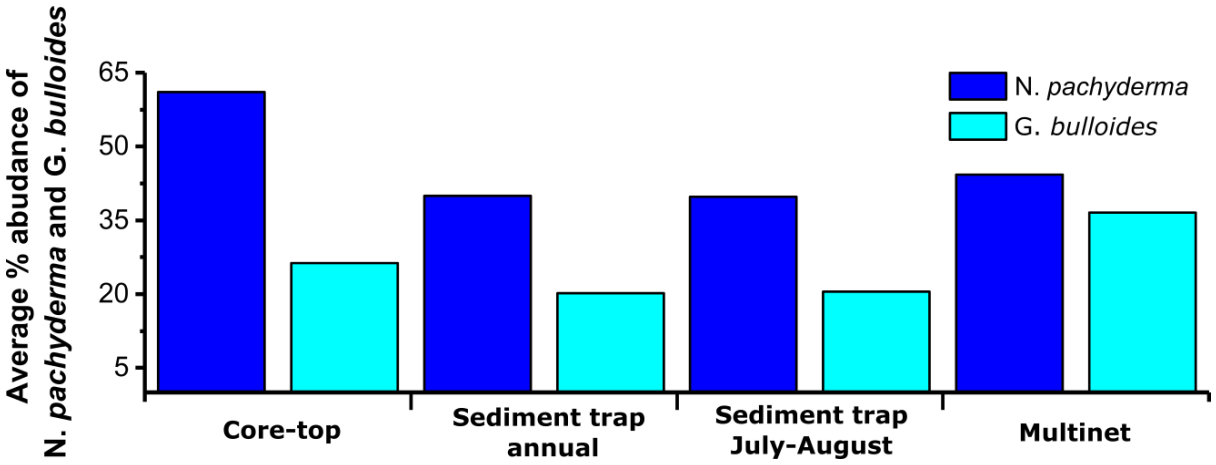

Figure 2.11: Average percentage abundance of N. pachyderma and G. bulloides compared between Core-top, sediment trap and multinet data. Relative abundances of N. pachyderma (dark blue bar) and G. bulloides (light blue bar) were averaged for all sites seen in Figure 2.10. This figure highlights the lack of difference between July-August sediment trap and annual sediment trap abundances compared to a larger difference between Core-top and multinet abundance of G. bulloides. This suggests the cause of these discrepancies is likely due to sediment dissolution rather than seasonality.

well as skew potential ecological observations. However local dissolution analysis from the Western Equatorial Pacific suggests that although dissolution above 3000 m does occur, it has only minor influence on assemblages (Berger *et al.*,1982). Below 3400 m, Berger *et al.*, (1982) note that dissolution is more pronounced and that assemblages below 4000 m should be classed as residual assemblages and reflect the impacts of higher dissolution. Similarly, a water column dissolution experiment by Peterson (1966) cites a depth of 3700 m for the onset of increased dissolution in central North Pacific sediments. Within our dataset we see substantial changes in assemblage at considerably shallower depths (1383 m) than reported by Berger *et al.*, (1982) and Peterson (1966). This is likely due to the highly corrosive nature of intermediate depth water in the North Pacific. The overall impact of dissolution on faunal assemblages in planktic foraminifera is a bias towards the preservation of dissolution resistant species (Ruddiman *et al.*, 1967) such as *N. pachyderma, G. inflata* and *N. dutertrei* in the North Pacific (Schiebel and Hemleben, 2017). This has the potential to bias estimates of surface hydrography based on assemblage and should be taken into account when interpreting such records.

2.6 Conclusions and implications for downcore records

2.6.1 Ecological drivers in subpolar species

Analyses of new core-top and multinet data in combination with published core-top, sediment trap and multinet data allow us to better constrain the ecological drivers of the two key subpolar species of planktic foraminifera *G. bulloides* and *N. pachyderma* in the North Pacific.

In the subpolar North Pacific, *G. bulloides* is tied closely to food availability in the water column and is largely associated with the chlorophyll maximum. This trend is also observed within sediment trap data, where seasonal decreases in organic matter flux are associated with very low *G. bulloides* abundance. The use of *G. bulloides* relative abundance is therefore a useful productivity indicator for downcore interpretation. However, it is important to note that abundance of *N. pachyderma* is also tied to food availability and thus the percentage abundance of *G. bulloides* may not necessarily respond prominently to changes in food availability or productivity in the region, as both species may respond in parallel. Additional proxies such as percentage opal or temperature proxies used alongside relative abundance provide the best combination to obtain a more meaningful interpretation of the *G. bulloides* data within paleo-records. The calculation of mass accumulation rates (MAR) or planktic foraminifera per gram of sediment may also allow for a more robust use of *G. bulloides* when interpreting productivity changes.

The close relationship between *N. pachyderma* and temperature in the North Pacific (Figure 2.8) is striking. Multinet data demonstrates that *N. pachyderma* can flourish in colder waters even when food availability is low, likely due to decreased competition. This relationship is further demonstrated in our core-top compilation, where the largest relative *N. pachyderma* abundances are recorded in the coldest waters. We estimate a temperature range for the North Pacific subpolar *N. pachyderma* of 4-16 °C, with relative abundance dropping below 50 % at > 8°C. Food availability also controls *N. pachyderma* numbers, but it is less important than with *G. bulloides*. As with *G. bulloides*, calculating planktic foraminifera accumulation rates may be the best way to assess the significance of paleo-assemblages.

A key feature of our core-top compilation is the existence of a species-specific transitional zone occupying the region between the subpolar and subtropical gyres. The domination of *G. inflata* and *N. incompta* provide a potential tool to assess the strength and position of the two gyres in the past. For core sites located within the transition zone, any shifts in assemblage away from these species could be used to interpret influences from waters derived from either the subtropical or subpolar gyre.

The regional distribution of three equatorial species: *P. obliquiloculata; G. tumida* and *N. dutertrei* is significant and could provide a means with which to construct ENSO variability in the past. To fully investigate this relationship, modern studies of foraminifera distribution during ENSO and non-ENSO years would provide the basis for utilisation of this relationship in paleo-records.

2.6.2 Implications for geochemical records

Accurate use of geochemical proxies in planktic foraminifera requires knowledge of their ecology, particularly depth habitat and seasonality. The subpolar genotype of *N. pachyderma* found in the North Pacific, resides predominantly in the top 50 m of the water column and is likely to reflect near-surface conditions. Where a deeper depth habit is observed, it is associated with a deep winter mixed layer, homogenising the water column such that conditions remain similar to those in the surface. Seasonally *N. pachyderma* flux does vary regionally, however, it often exhibits peaks in abundance during spring and late summer/autumn. The similarity in temperature during these two periods gives further credibility to the use of *N. pachyderma* in paleo-temperature reconstructions.

G. bulloides is often used to reconstruct sea surface temperatures through Mg/Ca ratios. We find that *G. bulloides* predominantly resides in the top 50 m of the water column and is therefore likely to record sea surface conditions. Seasonal deep mixing also allows it to frequent greater depths, but at lower abundances. Seasonally, *G. bulloides* blooms in both spring and late autumn in the subpolar North Pacific. However, temperature signatures observed at these periods are not dissimilar and should not discourage geochemists from using *G. bulloides* to reconstruct sea surface temperatures down core. Two genotypes of *G. bulloides* dominate the North Pacific waters (Types IIe and IId), of these, Type IIe is confined to the subpolar zone whilst Types IId is found off the California margin throughout the year in both upwelling and non-upwelling waters (Darling *et al.,* 2003). However, the genotype Type IIa has been identified in the winter in the south eastern coastal zone and is thought a potential member of the winter assemblage (Davies et al, 2017). It is therefore important to note that when analysing foraminifera on the boundary of these zones, multiple genotypes of ecologically distinct *G. bulloides* may be present in the assemblage.

2.6.3 Dissolution bias in sediments

Planktic foraminifera abundance and flux have been widely used as proxies for paleoenvironmental change (Bond *et al.,* 1993; Barker *et al.,* 2009; Barker *et al.,* 2015). In the Atlantic and Southern oceans, true polar conditions are achieved at high latitudes, normally resulting in 95-100% abundance of *N. pachyderma* during cold periods (Bond *et al.,* 1993) with increased abundances of transitional and warmer water species (*G. bulloides, G. inflata, G. ruber, G. hirsuta)* occurring during warm time-intervals such as the Bølling-Allerød (Baker *et al.,* 2009). Our comparison of North Pacific core-tops to multinets from the same region shows preferential preservation of *N. pachyderma* over more dissolution prone species such as *G. bulloides*. This has the potential to bias reconstructions that suggest more abundant polar waters during stadial

conditions in the Atlantic (Bond *et al.*, 1993), especially if these are accompanied with influx of more corrosive waters at depth. This warrants increased caution when assessing paleo-assemblage records, particularly at sites where deep water masses are known to be corrosive. Despite this, we find that broadly our defined faunal zones are unaffected by dissolution, however the details of assemblages within zones are more susceptible to dissolution bias.

2.7 Acknowledgments

We thank the crew of the scientific research vessel Sonne and those who participated in the SO202 INOPEX cruise for their assistance with the collection of multinet samples. We thank the crew of the Kilo Moana and science team of CDISK-IV (KM1712), led by Will Berelson and Jess Adkins, for their assistance with the collection of the plankton tows and an enjoyable cruise. We also thank members of the CALMED project (CTM2016-79547-R), and the Generalitat de Catalunya (MERS, 2017 SGR 1588). We are also thankful to all the people at the Alfred Wegner Institute who helped prepare the multinet samples, and to Heidi Block, Alasdair Murphy, Rory Abernathy, and Joshua Cook for assistance in preparing CDISK-IV net samples in the St Andrews lab. Funding was providied through a NERC Research Training Support Grant awarded NE/L002590/1 to Ben Taylor and NERC grant NE/N011716/1 awarded to James Rae and Andrea Burke. All supplementary data related to this article can be found within the supplementary information and is available on the PANGAEA database.

2.8 References

Asahi, H. & Takahashi, K., 2007. A 9-year time-series of planktonic foraminifer fluxes and environmental change in the Bering sea and the central subarctic Pacific Ocean, 1990-1999. *Progress in Oceanography*, 72(4), pp.343–363.

Ayers, J.M. & Lozier, M.S., 2010. Physical controls on the seasonal migration of the North Pacific transition zone chlorophyll front. *Journal of Geophysical Research: Oceans*, 115(5), pp.1–11.

Barker, S. *et al.,* 2015. Icebergs not the trigger for North Atlantic cold events. *Nature*, 520(7547), pp.333–336.

Barker, S. *et al.,* 2009. Interhemispheric Atlantic seesaw response during the last deglaciation. *Nature*, 457, pp.1097–1102.

Bé, A.W.H. & Hutson, W.H., 1977. Ecology of Planktonic Foraminifera and Biogeographic Patterns of Life and Fossil Assemblages in the Indian Ocean Ecology of planktonic foraminifera and biogeographic patterns of life and fossil assemblages in the Indian Ocean.

Micropaleontology, 23(4), pp.369–414.

Berger, W.H., 1970. Planktonic Foraminifera: Selective solution and the lysocline. *Marine Geology*, 8(2), pp.111–138.

Berger, W.H., Bonneau, M.--C. & Parker, F.L., 1982. Foraminifera on the deep-sea floor: lysocline and dissolution rate. *Oceanologica acta*, 5(2), pp.249–258.

Bond, G., Broecker, W., Johnsen, S., McManus, J., Lbeyrie, L., Jouzel, J., Bonani, G. 1993. Correlations between climate records from North Atlantic sediments and Greenland ice. *Nature*, 363, pp.143–147.

Bradshaw, J.S., 1959. Ecology of living planktonic foraminifera in the North and equatorial Pacific Ocean. *Foraminiferal Research*, 10, pp.25–64.

Conan, S.M.H., Brummer, G.J.A., 2000. Fluxes of planktic foraminifera in response to monssonal upwelling on the Somalia Basin margin. *Deep Sea Research Part II: Tropical Studies in Oceanography.* 47(9-11), pp. 2207-2227.

Coulbourn, W.T., Parker, F.L. & Berger, W.H., 1980. Faunal and solution patterns of planktonic foraminifera in surface sediments of the North Pacific. *Marine Micropaleontology*, 5, pp.329–399.

Curry, W.B. *et al.*, 1992. Foraminiferal production and monsoonal upwelling in the Arabian Sea: evidence from sediment traps. *Geological Society, London, Special Publications*, 64(1), pp.93–106.

Darling, K.F. *et al.*, 2003. Seasonal distribution of genetic types of planktonic foraminifer morphospecies in the Santa Barbara Channel and its paleoceanographic implications. *Paleoceanography*, 18(2), pp.1–10.

Darling, K.F. *et al.*, 2004. Molecular evidence links cryptic diversification in polar planktonic protists to Quaternary climate dynamics. *Proceedings of the National Academy of Sciences*, 101(20), pp.7657–7662.

Darling, K.F. *et al.*, 2006. A resolution for the coiling direction paradox in Neogloboquadrina pachyderma. *Paleoceanography*, 21(2), pp.1–14.

Darling, K.F., Kucera, M. & Wade, C.M., 2007. Global molecular phylogeography reveals persistent Arctic circumpolar isolation in a marine planktonic protist. *Proceedings of the National Academy of Sciences of the United States of America*, 104(12), pp.5002–5007.

Darling, K.F. & Wade, C.M., 2008. The genetic diversity of planktic foraminifera and the global distribution of ribosomal RNA genotypes. *Marine Micropaleontology*, 67(3–4), pp.216–238.

Darling et al, 2017. Genetic diversity and ecology of the planktonic foraminifers Globigerina bulloides, Turborotalita quinqueloba and Neogloboquadrina pachyderma off the Oman margin during the late SW Monsoon. Marine Micropaleontology, 137, pp. 64-77. https://doi.org/10.1016/j.marmicro.2017.10.006.

Davis, C. V. *et al.*, 2016. Seasonality in Planktic Foraminifera of the Central California Coastal Upwelling Region. Biogeosciences Discussions, pp.5139–5150.

Eguchi, N.O. *et al.*, 2003. Seasonal variations in planktonic foraminifera at three sediment traps in the Subarctic, Transition and Subtropical zones of the central North Pacific Ocean. Marine Micropaleontology, 48(1–2), pp.149–163.

Fairbanks, R.G. *et al.*, 1982. Vertical distribution and isotopic fractionation of living planktonic foraminifera from the Panama Basin. Nature, 298(5877), pp.841–844.

Fairbanks, R.G. & Wiebe, P.H., 1980. Forminifera and chlorophyll maximum: Vertical distribution, seasonal succession and paleoceanographic distributuion. Science, 209(4464), pp.1524–1526.

Fenton, I.S. *et al.*, 2016. Environmental Predictors of Diversity in Recent Planktonic Foraminifera as Recorded in Marine Sediments. Plos One, 11(11).

Field, D.B., 2004. Variability in vertical distributions of planktonic foraminifera in the California current: Relationships to vertical ocean structure. Paleoceanography, 19(2).

Fraile, I. *et al.*, 2008. Predicting the global distribution of planktonic foraminifera using a dynamic ecosystem model. Biogeosciences. 5, pp. 891-911.

Freeland, H. *et al.*, 1997. Evidence of change in the winter mixed layer in the Northeast Pacific Ocean. Deep Sea Research Part I: Oceanographic Research Papers, 44(12), pp.2117–2129.

Garcia, H.E. *et al.*, 2014. World Ocean Atlas 2013, Volume 4 : Dissolved Inorganic Nutrients (phosphate, nitrate, silicate). NOAA Atlas NESDIS 76, 4(September), p.27.

Gersonde, R. 2012. The Expedition of the Research Vessel "Sonne" to the subpolar North Pacific and the Bering Sea in 2009 (SO202-INOPEX). Reports on Polar and Marine Research 643, 323 pp (http://epic.awi.de/30138/).

Harrison, P.J. *et al.,* 2004. Nutrient and plankton dynamics in the NE and NW Gyres of the subarctic Pacific Ocean. Journal of Oceanography, 60(3), pp.93–117.

Hemleben, C., Spindler, M. & Anderson, R.O., 1989. Modern Planktonic Foraminifera, Springer-Verlag New York Inc.

Huyer, A., 1983. Coastal upwelling in the California Current System. Progress In Oceanography, 12(3), pp.259–284.

Imbrie, J. & Kipp, N., 1971. A new micropalaeontological method for quantitiative paleoclimatology: Application to late Pleistocene Carribean core V28-238. In K. K. Turekian, ed. The late Cenozoic Glacial Ages. Yale Univ. Press, New Haven, Conn, pp. 77–181.

Iwasaki, S. *et al.,* 2017. Horizontal and vertical distributions of planktic foraminifera in the subarctic North Pacific. Marine Micropaleontology.

Jonkers, L. & Kucera, M., 2015. Global analysis of seasonalitiy in the shell flux of extant planktonic Foraminifera. Biogeosciences. 12, pp. 2207-2226.

Kandiano, E.S. & Bauch, H.A., 2002. Implications of planktic foraminiferal size fractions for the glacial-interglacial paleoceanogeaphy of the polar North Atlantic. Journal of Foraminiferal Research. 22(3).

King, A.L. & Howard, W.R., 2003. Planktonic foraminiferal flux seasonality in Subantarctic sediment traps: A test for paleoclimate reconstructions. Paleoceanography, 18(1), pp.1–17.

Kohfeld, K.E. *et al.,* 1996. Neogloboquadrina pachyderma (sinistral coiling) as paleoceanographic tracers in polar oceans: Evidence from northeast water polynya plankton tows, sediment traps, and surface sediments. Paleoceanography, 11(6), pp.679–699.

Kroon, D., Ganssen, G., 1989. Northern Indian Ocean upwelling cells and the stable isotope compostiion of living planktonic foraminifers. Deep Sea Research Part A. Oceanographic Research Papers. 36(8), pp. 1219-1236.

Kucera, M., 2007. Planktonic Foraminifera as Tracers of Past Oceanic Environments. In Proxies in Late Cenozoic Paleoceanography. pp. 213–262.

Kucera, M. *et al.,* 2005. Reconstruction of sea-surface temperatures from assemblages of planktonic foraminifera: Multi-technique approach based on geographically constrained calibration data sets and its application to glacial Atlantic and Pacific Oceans. Quaternary

Science Reviews, 24(7–9 SPEC. ISS.), pp.951–998.

Kuroyanagi, A. *et al.*, 2002. Seasonal changes in plankotnic foraminifera in the North Pacific Ocean: sediment trap experiments from subarctic and subtropical gyres. Deep-Sea Research II, 49, pp.5627–5645.

Kuroyanagi, A. *et al.*, 2008. Seasonal to interannual changes in planktonic foraminiferal assemblages in the northwestern North Pacific: Sediment trap results encompassing a warm period related to El Niño. Palaeogeography, Palaeoclimatology, Palaeoecology, 262(1–2), pp.107–127.

Kuroyanagi, A. & Kawahata, H., 2004. Vertical distribution of living planktonic foraminifera in the seas around Japan. Marine Micropaleontology, 53(1–2), pp.173–196.

Locarnini, R.A. *et al.*, 2013. World Ocean Atlas 2013. Vol. 1: Temperature. S. Levitus, Ed., A. Mishonov Technical Ed.; NOAA Atlas NESDIS 73, pp. 40.

Lombard, F. *et al.*, 2011. Modelling planktic foraminifer growth and distribution using an ecophysiological multi-species approach. Biogeosciences. 8, pp. 853-873.

Lynn, R.J. & Simpson, J.J., 1987. The California Current system: The seasonal variability of its physical characteristics. Journal of Geophysical Research, 92(C12), p.12947.

Mallo M, Ziveri P , Mortyn G, Schiebel R, Grelaud M. 2017. Low planktic foraminiferal diversity and abundance observed in a 2013 West-East Mediterranean Sea transect, Biogeosciences, 14, pp. 2245-2266.

Mohiuddin, M.M. *et al.*, 2004. Seasonality of biogenic particle and planktonic foraminifera fluxes: Response to hydrographic variability in the Kuroshio Extension, northwestern Pacific Ocean. Deep-Sea Research Part I: Oceanographic Research Papers, 51(11), pp.1659–1683.

Mohiuddin, M.M., Nishimura, A. & Tanaka, Y., 2002. Regional and interannual productivity of biogenic components and planktonic foraminiferal fluxes in the northwestern Paci¢c Basin. Marine Micropaleontology, 45.

Mohiuddin, M.M., Nishimura, A. & Tanaka, Y., 2005. Seasonal succession, vertical distribution, and dissolution of planktonic foraminifera along the Subarctic Front: Implications for paleoceanographic reconstruction in the northwestern Pacific. Marine Micropaleontology, 55(3–4), pp.129–156.

Morard, R. *et al.*, 2013. Ecological modeling of the temperature dependence of cryptic species

of planktonic Foraminifera in the Southern Hemisphere. Palaeogeography, Palaeoclimatology, Palaeoecology, 391, pp.13–33.

Olsen, A. *et al.,* 2016. The global ocean data analysis project version 2 (GLODAPv2) - An internally consistent data product for the world ocean. Earth System Science Data, 8(2), pp.297–323.

Pados, T. & Spielhagen, R.F., 2014. Species distribution and depth habitat of recent planktic foraminifera in Fram Strait, Arctic Ocean. Polar Research, 33(Ehrenberg 1861).

Peterson, M.N., 1966. Calcite: rates of dissolution in a vertical profile in the central pacific. Science, 154(3756), pp.1542–1544.

Prell, W.L. & Curry, W.B., 1981. Faunal and isotopic indices of monsoonal upwelling: Western Arabian Sea. Oceanologica Acta, 4, pp.91–98.

Roden, G.I., 1995. Aleutian Basin of the Bering Sea: Thermohaline, oxygen, nutrient, and current structure in July 1993. Journal of Geophysical Research, 100(C7), p.13539.

Ruddiman, W.F. & Heezan, B.C., 1967. Differential solution of Planktonic Foraminifera. Deep Sea Research and Oceanographic Abstracts, 14(6), pp.801–802.

Rutherford, S., D'Hondt, S. & Prell, W., 1999. Environmental controls on the geographic distribution of zooplankton diversity. Nature, 400(6746), pp.749–753.

Sadekov, A.Y. *et al.,* 2016. Geochemical imprints of genotypic variants of Globigerina bulloides in the Arabian Sea. Paleoceanography, 31(10), pp.1440–1452.

Sautter, R, L. & Thunell, R.C., 1989. Seasonal succession of planktonic foraminifera; results from a four-year time-series sediment trap experiment in the Northeast Pacific. Journal of Foraminiferal Research, 19(4), pp.253–267.

Schiebel, R. *et al.,* 2001. Planktic foraminiferal production stimulated by chlorophyll redistribution and entrainment of nutrients. Deep-Sea Research Part I: Oceanographic Research Papers, 48(3), pp.721–740.

Schiebel, R., 2002. Planktic foraminiferal sedimentation and the marine calcite budget. Global Biogeochem. Cycles, 16(4), p.1065.

Schiebel, R. & Hemleben, C., 2017. Planktic foraminifers in the modern ocean, Springer Berlin Heidelberg.

Siccha, M. & Kucera, M., 2017. Data Descriptor : ForCenS , a curated database of planktonic

foraminifera census counts in marine surface sediment samples. Scientific Data, 4, pp.1–12.

Stabeno, P.J. & Reed, R.K., 1994. Circulation in the Bering Sea Basin Observed by Satellite-Tracked Drifters: 1986–1993. Journal of Physical Oceanography, 24(4), pp.848–854.

Thiede, J., 1975. Distribution of foraminifera in surface waters of a coastal upwelling area. Nature, 253(5494), pp.712–714.

Thunell, R. & Honjo, S., 1987. Seasonal and interannual changes in planktonic foraminiferal production in the North Pacific. Nature, 328, pp.335–337.

Thunell, R.C. & Sautter, R, L., 1991. Planktonic foraminiferal response to upwelling and seasonal hydrographic conditions; sediment trap results from San Pedro Basin, Southern California Bight. Journal of Foraminiferal Research, 21, pp.347–363.

Tolderlund, D.S. & Bé, A.W.H., 1971. Seasonal distribution of planktonic foraminifera in the western North Atlantic. Micropaleontology, 17(3), pp. 297-329.

Wyrtki, K., 1981. An Estimate of Equatorial Upwelling in the Pacific. Journal of Physical Oceanography, 11(9), pp.1205–1214.

Yan, X. *et al.,* 1992. Temperature and Size Variabilities of the Western Pacific Warm Pool. Science. 258 (5088), pp.1643–1645.

Yasuda, I., 2003. Hydrographic structure and variability in the Kuroshio- Oyashio transition area. Journal of Oceanography, 59, pp.389–402.

Žarić, S. *et al.,* 2005. Sensitivity of planktic foraminifera to sea surface temperature and export production as derived from sediment trap data. Marine Micropaleontology, 55(1–2), pp.75–105.

Zweng, M.M. *et al.,* 2013. World Ocean Atlas 2013, Volume 2: Salinity. NOAA Atlas NESDIS, 2(1), p.39.

2.9 Supplementary figures and tables

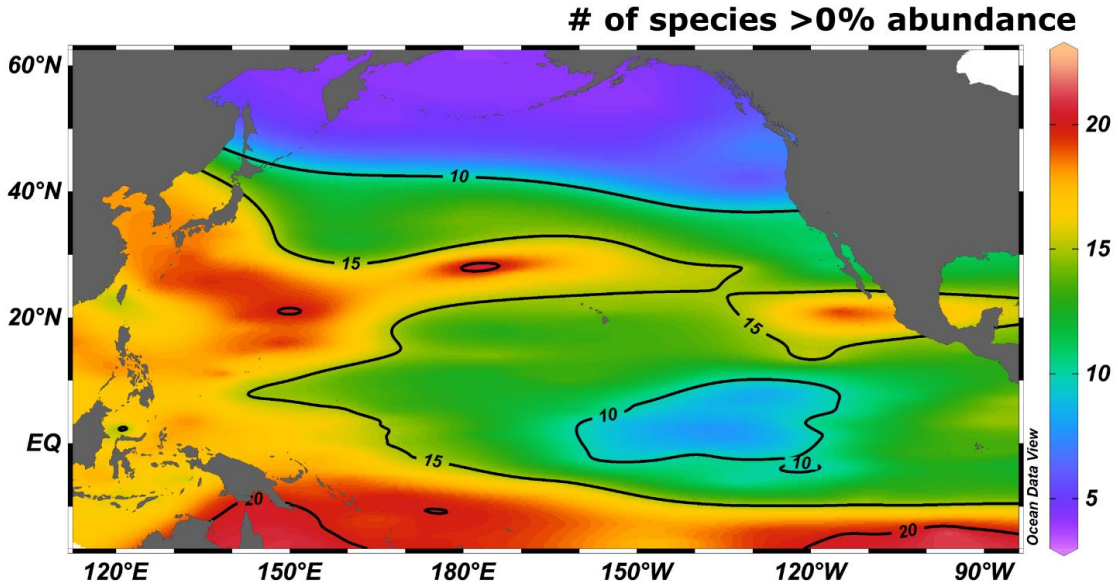

Figure 2.12: Number of species of planktic foraminifera with an abundance greater than 0 % based on our new North Pacific core-top compilation. Colour mapping was created using ODVs weighted averaging tool and contours indicate boundaries of equal species present. Note the high diversity found in the subtropical zone compared with lowest diversity found North of 40°N indicating the subpolar zone. The small patch of low diversity in the east equatorial zone is due primarily to the high relative abundance of N. dutertrei in this region.

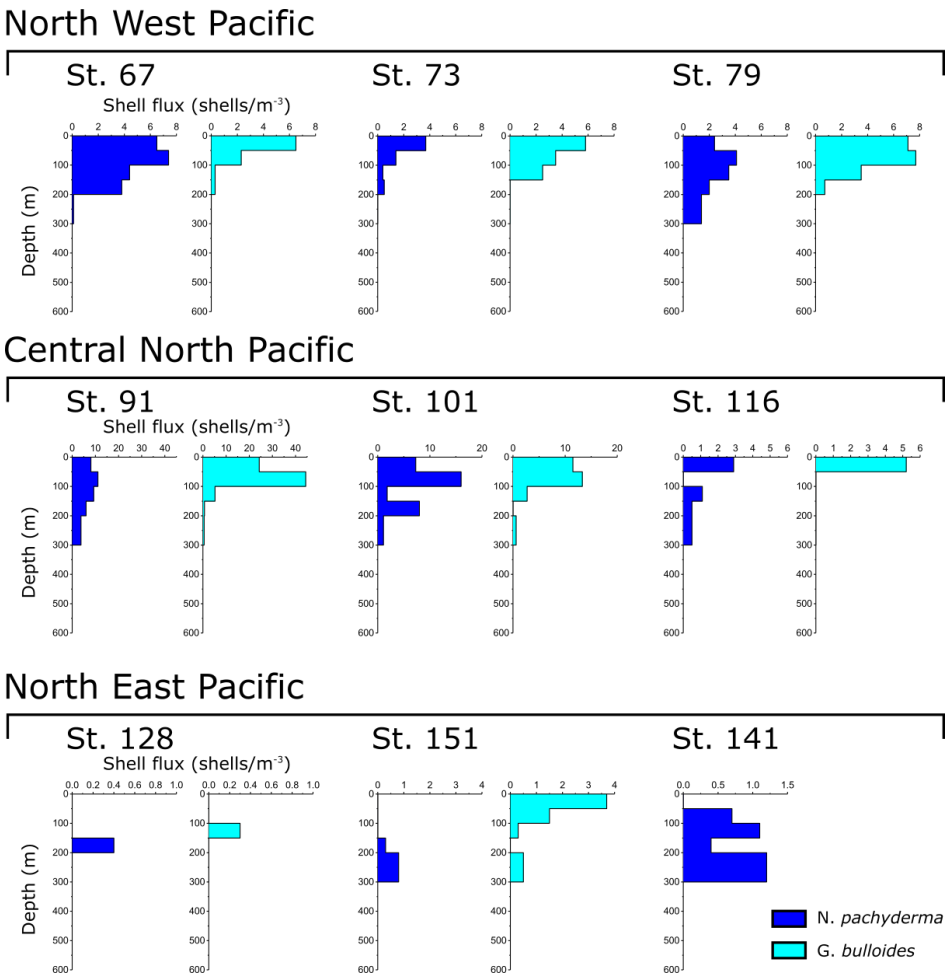

Figure 2.13: Vertical profiles of N. pachyderma (dark blue bars) and G. bulloides (light blue bars) shell flux (shells/m^{-3}) from Iwasaki et al.,, 2017.

Genus	Species	Author, Year
Neogloboquadrina	*pachyderma*	(Ehrenberg, 1861)
Globigerina	*bulloides*	(d'Orbigny, 1826)
Neogloboquadrina	*incompta*	(Cifelli, 1961)
Neogloboquadrina	*dutertrei*	(d'Orbigny, 1839)
Globorotaloides	*hexagonus*	(Natland, 1938)
Turborotalita	*quinqueloba*	(Natland, 1938)
Globorotalia	*scitula*	(Brady, 1882)
Globigerinella	*siphonifera*	(d'Orbigny, 1839)
Globigerinita	*glutinata*	(Egger, 1895)
Globorotalia	*inflata*	(d'Orbigny, 1839)
Globigerinoides	*ruber*	(d'Orbigny, 1839)
Globigerinella	*calida*	(Parker, 1962)
Globoturborotalita	*rubescens*	(Hofker, 1956)
Globoturborotalita	*tenella*	(Parker,1958)
Globigerinella	*radians*	(Egger, 1893)
Globorotalia	*crassaformis*	(Galloway and Wissler, 1927)
Trilobatus	*sacculifer*	(Brady, 1877)

Table 2.2: Taxonomic information for all species identified in new sites within this study including author and date of first description.

Chapter 3

3. Drivers of planktic foraminifera distribution in the modern ocean

This chapter is for submission to Quaternary Science Reviews with the author list: ***Taylor, B.J.,*** *Rae, J.W.B., Gray, W., Darling K., Burke, A. Taylor performed the analyses, made the figures, and wrote the chapter, with input and comments from all other authors.*

Abstract

Planktic foraminifera are commonly used to reconstruct past climates and ocean ecology. By assessing past environmental and ecological changes in the oceans, we can better understand changes that will occur under future climate change scenarios. To aid the interpretation of paleo-records, we present an updated global database of planktic foraminifera census counts containing data from 2903 sites. We use our updated database to identify and describe the distribution of twelve key species of planktic foraminifera which dominate the world's oceans: *N. pachyderma*; *G. bulloides*; *N. incompta*; *T. quinqueloba*; *G. inflata*; *N. dutertrei*; *G. glutinata*; *G. ruber*; *T. sacculifer*; *G. tumida*; *P. obliquiloculata* and *G. menardii*. We utilise multiple regression analysis to assess the relationship between individual species of planktic foraminifera and environmental variables. We find that globally *N. pachyderma* is closely tied to sea surface temperature, and *G. ruber* shows a weak negative relationship with surface ocean phosphate content. Species richness is primarily linked to temperature but also shows a weak correlation to phosphate content suggesting competition for food is a driver of diversity within planktic foraminifera. We used redundancy analysis (RDA) to analyse the variance within faunal assemblages against seven environmental variables (temperature, salinity, phosphate, phosphate gradient, temperature gradient and density gradient). The primary axis of variance within our dataset correlates strongly with temperature, suggesting this is the primary control on variation within planktic foraminifera assemblages. The secondary axis is controlled by several environmental parameters which are linked to upwelling. We use a novel method of plotting foraminiferal assemblage – "bubble plots" – to highlight six faunal regions of particular interest: The North Atlantic; the North East Pacific; the equatorial Pacific; the Chilean margin; the Benguela and Agulhas region; and the Arabian margin. Our analysis of global faunal distribution improves the use of faunal abundances in the reconstruction of past ocean environmental conditions.

3.1 Introduction

3.1.1 Modern distribution of planktic foraminifera

Planktic foraminifera are ubiquitous to the world's oceans (Schiebel and Hemleben, 2017). These single celled zooplankton are environmentally and genetically diverse and are able to occupy a wide range of surface water conditions. Their calcite tests, which are posthumously deposited on the sea floor, can record surface water chemistry and provide a vital tool for the reconstruction of past climates (Hemleben *et al.,* 1989; Schiebel and Hemleben, 2017). There are over 30 extant species of planktic foraminifera and the abundance of different species can be associated with surface ocean conditions to provide a means with which to quantitatively and qualitatively investigate past environmental change (Schiebel and Hemleben, 2017).

Early work regarding the distribution of planktic foraminifera in the modern ocean highlighted several faunal zones characterised by distinct distributions of planktic foraminifera species (Bradshaw *et al.,* 1959; Parker *et al.,* 1971; Be and Hutson, 1977; Coulbourn *et al.,* 1980). These zones, strongly influenced by temperature and latitude, include: the polar zone; subpolar zone; transitional zone; subtropical zone and tropical (equatorial) zone (Bradshaw *et al.,* 1959). Additional upwelling zones were also added later (Hemleben *et al.,* 1989). In the Pacific Ocean, pioneering work by Bradshaw, (1959) was the first to define these faunal zones. Additional core-top sites were added by Coulbourn *et al.,* (1980) and Parker and Berger (1971) who recognised the importance of key species such as *N. pachyderma* and *G. ruber* in defining faunal zones and touched on the importance of dissolution in marine sediments and the possible biasing of core-top planktic foraminifera assemblages (Berger, 1968; Berger and Parker, 1971). In the North Atlantic, detailed work by Ruddiman (1969) and Balsam and Flessa (1978) noted the relationship between planktic foraminifera abundance, diversity, and surface ocean circulation. Ruddiman (1969) noted role of the North Atlantic gyre in smearing the diversity gradient of planktic foraminifera across the North Atlantic. Work by Williams and Johnson (1975) and Bé and Hutson (1977) found similar relationships between assemblage diversity and temperature in the Indian Ocean. These early studies set the baseline for future work on the distribution and diversity of assemblages across the global with the addition of new core-top sites and innovative analytical techniques.

As well as morphotype and species distributions, recent work has highlighted numerous inter-species genotypes whose spatial distributions vary across the globe (Darling *et al.,* 1997; Darling and Wade, 2008; André *et al.,* 2014). Different genotypes of the same species can reflect different surface ocean conditions (Darling and Wade, 2008) and add complexity to the use of paleo-assemblages in environmental reconstruction. In some cases, it is possible to separate these

genotypes based on temperature and other environmental parameters. This is seen in the North Pacific where two genotypes (of a total of 16) type IIe and IId can be clearly distinguished from each other when plotted against surface ocean temperature (Taylor *et al.*, 2018). The distribution of genotypes within several key species are fully described in Darling and Wade (2008) and André *et al.*, (2014), and provide an excellent reference for evaluating potential genotypic differences between assemblages.

The use of statistical methods to characterise planktic foraminiferal diversity across the world's ocean has provided key insights into the main drivers of diversity on a global scale. Rutherford *et al.*, (1999) used compiled planktic foraminifera core-top data from the Brown foraminifera database (Prell *et al.*, 1999) alongside directly measured and remotely sensed environmental data to predict diversity trends in planktic foraminifera. They found that over 90% of planktic foraminifera diversity could be explained by temperature, echoing the key findings of earlier studies by Ruddiman (1969) and Williams and Johnson (1975). Additionally, they noted a secondary peak in foraminiferal diversity at mid-latitudes in all oceans (Rutherford *et al.*, 1999). The conclusions of Rutherford *et al.*, (1999) were re-visited by Fenton *et al.*, (2016) who also found a strong correlation between diversity and sea surface temperature (SST). Fenton *et al.*, (2016) also noted the importance of stratification in foraminifera diversity and noted a possible impact of seasonality on planktic foraminifera diversity. Work by Morey *et al.*, (2005) used Canonical Correspondence Analysis (CCA) to investigate environmental controls on planktic foraminifera assemblages. They found two axes of variation which controlled changes in an assemblage, the first being sea surface temperature (SST) and the second being a combination of surface water parameters which they perceived as ocean fertility (Morey *et al.*, 2005). Interestingly, they noted no influence of dissolution on planktic foraminifera assemblages (Moray *et al.*, 2005), contrasting studies by Berger (1968), Berger and Parker (1970), and Parker *et al.*, (1971) who suggest foraminifera sediments from deep marine environments show evidence of dissolution bias.

3.1.2 Seasonality and habitat depth of modern planktic foraminifera

Planktic foraminifera predominantly reproduce on a lunar cycle with the exception of some species which reproduce on a half lunar or annual cycle (Hemleben *et al.*, 1989). The relatively short life span of the majority of planktic foraminifera means that seasonal changes in water column conditions can be translated into changes in seasonal foraminifera assemblage (Schiebel and Hemleben, 2017). Seasonal variations in planktic foraminifera are often associated with changes in surface ocean productivity, with highest foraminifera standing stocks exhibited during

periods of ocean blooming (Tolderlund and Bé, 1971; Schiebel *et al.*, 2001; Kuroyanagi *et al.*, 2008; Taylor *et al.*, 2018).

Planktic foraminifera have been found in water depths ranging from 0-400 m (Schiebel and Hemleben, 2017). Different species display differing vertical distributions in the surface ocean as well as seasonal variation in depth habitat. Planktic foraminifera have been associated with the deep chlorophyll maximum (Fairbanks and Wiebe, 1980; Field, 2004) which is usually found within the upper 100 m of the water column. However, foraminifera can dwell at much deeper depths depending on food availability and competition, for example *G. truncatulinoides* has been observed to live at much deeper depths (Schiebel and Hemleben, 2005). Knowledge and understanding of habitat depth in planktic foraminifera is essential in the reconstruction of past environmental conditions. This is particularly important for geochemical records where reconstructed water column conditions will depend heavily on the habitat depth of the foraminifera being analysed.

3.1.3 Planktic foraminifera and the carbon cycle

Planktic foraminifera in the modern ocean form an important part of the inorganic and organic carbon cycle. Based on compiled sediment traps and multinet samples, Schiebel (2002) estimated the global planktic foraminiferal calcite flux rate at 100 m depth to be 1.3-3.2 Gt yr^{-1}. This represents between 23-56 % of the total marine $CaCO_3$ flux. Taking into account variations in dissolution from around the globe, Schiebel (2002) estimates that around 25% of planktic foraminifera tests make it to the sea floor and that planktic foraminifera account for between 32 and 80 % of the total deep-marine calcite budget. Despite the large range of this estimation, changes in the calcification and dissolution of planktic foraminifera can have dramatic implications for the global carbon cycle both in terms of changes in ocean alkalinity and DIC (see chapter 1). With regards to organic carbon cycling, planktic foraminifera contain organic matter themselves and feed largely on ocean phytoplankton (Schiebel and Hemleben, 2017). They are thus intrinsically involved in the removal of carbon dioxide from the surface ocean through organic matter formation and the remineralisation of that material at depth.

Dissolution of planktic foraminifera is closely tied to water column carbonate ion concentration (Berger, 1971; Schiebel *et al.*, 2007) with a number of studies noting significant alteration of planktic foraminifera assemblages below water depths of 3500 m (Coulbourn *et al.*, 1980; Berelson *et al.*, 2007). Some attempts have been made to classify the resistivity of foraminifera to dissolution (Berger, 1970; Parker and Berger, 1971; Berger *et al.*, 1982; Dittert *et al.*, 1999). Smaller or more fragile species, such as *G. bulloides*, G. *siphonifera*, and *G. ruber*, tend to be more prone to dissolution, whilst the larger, more compact tests of *N. pachyderma*, *G. tumida*, *S.*

dehiscens are regarded as dissolution resistant and may enrich some assemblages under corrosive conditions (Dittert *et al.,* 1999; Taylor *et al.,* 2018).

3.1.4 Paleo-reconstructions with planktic foraminifera census data

Planktic foraminifera census data have been used to reconstruct past climates due to the affinity of individual species to certain environmental conditions and the relative ease of producing and analysing census counts. Both qualitative and quantitative methods have been used in paleo-reconstructions.

Transfer functions provide a quantitative method for the reconstruction of paleo-environmental variables using planktic foraminifera assemblage data (Schiebel and Hemleben, 2017). First established by Berger (1969) and Imbrie and Kipp (1971), they are most commonly used to reconstruct SSTs in the past. Transfer functions rely on the tightknit association of environmental parameters with certain species of planktic foraminifer (Berger, 1969). Berger (1969) described an equation which utilised the ratios of different species alongside their optimum temperature ranges. This was expanded upon by Imbire and Kipp (1971) who increased the complexity of their transfer functions, adding additional environmental variables into their analyses. Several new techniques have developed since then including: Modern Analogue Techniques (Hutson, 1980); SIMMAX (Pflaumann *et al.,* 1996); Artificial Neural Networks (Malmgren and Nordlund, 1996); and Revised Analogue Method (Waelbroeck *et al.,* 1998).

The Climate Long-Range Mapping and Prediction [CLIMAP] project (CLIMAP Project Members, 1976) used a compiled dataset of global core-top material to reconstruct Last Glacial Maximum (LGM) temperatures using transfer functions. CLIMAP provided a high quality, detailed dataset which has subsequently been incorporated into further studies of modern planktic foraminifera (Kucera *et al.,* 2005; Waelbroeck *et al.,* 2009; Siccha and Kucera, 2017; Taylor *et al.,* 2018). Building on work by the CLIMAP project, the Multiproxy approach for the reconstruction of the glacial ocean surface [MARGO] project introduced additional sites to the global compilation of sediment cores and used four transfer function techniques to reconstruct glacial surface ocean temperatures and help to better define the climatology of the global ocean during the LGM (Kucera *et al.,* 2005).

Planktic foraminifera have also been used to make qualitative interpretations of past climates, and to supplement interpretations based on geochemical analysis. Bond *et al.,* (1993) provides an early example of the role census data can play in paleoclimatic reconstruction. Using the percentage abundance of the polar planktic foraminifera *N. pachyderma* (*N. pachyderma* sinistral until Darling *et al.,* 2003 pointed out the genetic differences between the left and right coiling species *N. pachyderma* and *N. incompta*) Bond *et al.,* (1993) tied changes in atmospheric temperature

recorded by the GRIP ice core project to changes in ocean temperature. This study was key linking the oceans and atmosphere to millennial-scale climate change events. Planktic foraminifera assemblages have also been used to track movements in the polar front during glacial/interglacial cycles (Thompson and Shackleton, 1980). The relative abundance and ratio of polar (cold) and subpolar (warmer) species in down-core studies has been used a sensitive tracer of polar ocean expansion and contraction. This is represented in the early work of Lehman and Keigwin (1992) who used *N. pachyderma* percentage to reconstruct shifts in North Atlantic circulation, and continues with more recent studies by Barker *et al.,* (2009), who investigated the bipolar seesaw and changes in Southern Ocean polar fronts.

3.1.5 Global distribution, ecology, and drivers of planktic foraminifera

For planktic foraminifera census data to be used accurately to investigate past changes in ecology and environments, a thorough understanding of modern planktic foraminifera is required. In this study, we present an updated global compilation of planktic foraminifera census data based on a combination of sites presented in Siccha and Kucera (2017) and additional North Pacific sites from (Taylor *et al.,* 2018). We use this database to describe the global distribution of twelve key species of planktic foraminifera, commenting on key aspects of their distribution including faunal zones and genetic speciation. We then discuss the ecological drivers of individual species based on their association with temperature, salinity, phosphate, and the gradients of temperature and phosphate. We use principal component and redundancy analysis to assess variance within planktic foraminifera assemblages, focusing in detail on upwelling regions as these zones reflect locations where interactions between the deep ocean, surface ocean, and atmosphere are most pronounced. Finally, we assess the role of dissolution in sediment core material based on species diversity, calculated carbonate system parameters, and the abundance of dissolution prone and resistant species.

3.2 Methods

3.2.1 Global database of planktic foraminifera census data

In order to ascertain the key drivers of planktic foraminifera distribution globally, we combined several previously published databases of planktic foraminifera census data to produce a new updated database containing assemblage data from 2903 sites from across the world's oceans. We primarily use data from the newly produced ForCenS database (Siccha and Kucera, 2017) and combine these data with sites from Taylor *et al.,* (2018). The key databases which make these two data compilations are: The Brown foraminiferal database (Prell *et al.,* 1999); the MARGO [Multiproxy Approach for the Reconstruction of the Glacial Ocean surface] database (Kucera *et al.,* 2005); the CLIMAP [Climate: Long range Investigation, Mapping, and Prediction] database,

(CLIMAP Project Members, 2009); and newly digitised data from Coulbourn *et al.,* (1980) published in Taylor *et al.,* (2018). Care was taken to avoid any duplicates within these newly compiled databases. To ensure consistency with published assemblage data (Scheibel and Hemleben, 2017), where foraminifera counts were available sites with fewer than 300 specimens counted were removed from the database. Due to large differences in age calculation between different compiled studies we assume all samples are of late Holocene age (0-5ka) and that accurate age data for some sites can be found alongside all original references in the data tables associated with this study.

3.2.2 Environmental data

Environmental data for each site was generated using Ocean Data View's (ODV) 3D estimation tool (Schlitzer, 2006). To generate surface ocean data, we used annual averages from World Ocean Atlas 2013 (1955-2012) (WOA13) (Boyer *et al.,* 2013). Average temperature (Locarnini *et al.,* 2013), salinity (Zweng *et al.,* 2013) and phosphate (Garcia *et al.,* 2013) levels were estimated for 0-25 m, 0-50 m, 0-100 m, and 0-150 m to account for a broad range of depth habitats in modern planktic foraminifera (Scheibel and Hemleben, 2017). Bottom water carbonate ion and Omega calcite values were calculated for each site in the same manner. The data for carbonate system variables were taken from the Global Ocean Data Analysis Project version 2 (GLODAP V2) (Olsen *et al.,* 2016).

In addition to calculating basic surface water environmental conditions for each site, we also calculated the temperature, phosphate and density gradients over the top 250 m of the water column for each site in our compiled dataset. To achieve this, we calculated the temperature and phosphate at eleven depths at each site (0, 25, 50, 75, 100, 125, 150, 175, 200, 225, 250 m) using ODV's 3D estimation tool (Schlitzer, 2006) and the relevant WOA13 dataset (Locarinini *et al.,* 2013; Garcia *et al.,* 2013). Density was calculated using the *"OCE"* package in R. From this we calculated the temperature, phosphate and density gradients over the top 250 m of the water column which can be used as indicators of upwelling within the ocean (D'Croz *et al.,* 1991). Gradients were calculated by taking the average change in ocean parameter with depth in the top 250 m of the water column. We use phosphate as an indicator of nutrients it is the dominant macro nutrient utilised by organisms in the modern ocean, additionally, most data is available for this parameter (Garcia *et al.,* 2013). We use annual average environmental data to ensure consistency across all our calculated environmental variables. As sediment samples of planktic foraminifera are likely to represent specimens deposited over multiple annual cycles, the use of annual averages also helps to account for this.

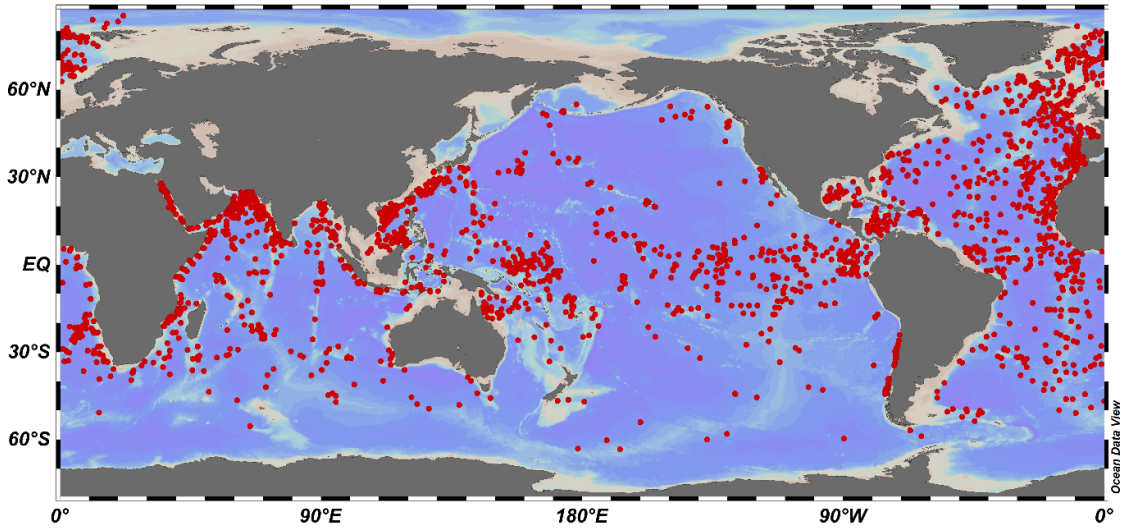

Figure 3.1: Map showing the locations of sites used in this study. Compiled data include those from Taylor et al., 2018 and data from the ForScenS database (Siccha and Kucera, 2017).

3.2.3 Regression and redundancy analysis

We use redundancy analysis (RDA) to analyse the variance within our newly compiled dataset and our calculated environmental surface and bottom water variables. Redundancy analysis extracts the variation within a set of response variables, in this case relative abundances of planktic foraminifera, which can be explained by several explanatory variables, in this case calculated environmental parameters. RDA uses multiple linear regression analysis to produce a matrix of fitted values which are then subjected to principal component analysis (PCA) (Legendre and Legendre, 1998). We transformed our abundance data using ln(percentage abundance + 1) in line with previous work by Morey *et al.*, (2005). Using a log transform helps remove the dominance of a few highly abundant species within the assemblage (Morey *et al.*, 2005). We use the package *"Vegan"* in R to produce our redundancy analysis, full details of which can be found at *https://cran.r-project.org/web/packages/vegan/index.html* (Oksanen *et al.*, 2018). In addition, we use linear, non-linear and multiple regression analysis to analyse the relationships between individual species and calculated environmental parameters.

3.3 Results

3.3.1 Global foraminifera database

Our new global dataset of 2903 sites include data from across the world's oceans (Figure 3.1). Site latitudes range from 85.4°N (dec) to 63.3°S (dec) with longitudes ranging between 188.6°E (dec) and 179.7W (dec). Water depths from which core-tops were retrieved ranged from 41 m to 5480 m below sea level; the average depth of core in this study was 2627.64 m. In total, 39 different species of planktic foraminifera are observed with the addition of two morphotypes, *G.*

crotonensis left and right coiling and *G. truncatulinoides* left and right coiling. At a single site, the maximum number of species observed was 29 and the lowest 1. The average number of species observed at a single site was 16. Figure 3.2 shows the distribution of species counts across the globe averaged. The number of species at a specific site generally decreases towards the poles from the equator. An exception to this is in the East equatorial Pacific where an extensive region of lower species counts between 10-15 exist. The most abundant region of the oceans in terms of species richness is the sub-tropical region of the southern hemisphere where counts are consistently above 20 species in both basins (Figure 3.2). Between 0-30° latitude in both hemispheres, the number of species ranges between 10- 29 (Figure 3.2). Between 30-40° this is generally reduced to between 10-15 species. At latitudes greater than 40° in the northern hemisphere the number of species starts to drop below 10. This is exaggerated in the North Pacific more so than the North Atlantic, where the gradient between greater than and less than 10 species is sharpened (Figure 3.2). In the southern hemisphere, species counts of less than 10 do not appear at latitudes lower than 50°S (Figure 3.2).

Figure 3.3 highlights the occurrence and abundances of the various species of planktic foraminifera present within the database (with more than 50 occurrences). Eight species occur in over 2000 of the 2903 (>70 %) sites within our compilation: *G. bulloides*; *N. dutertrei*; *O. universa*; *G. glutinata*; *G. calida*; *G. ruber*; *G. siphonifera* and *G. sacculifer*. The species with the highest occurrence in our dataset is *G. glutinata* which is present in 90 % of the sites (2601). Seven species occur in less than 100 sites in our database: *B. pumilio*; *G. menardii flexuosa; G. crassula; G. crotonensis; D. anfracta; G. uvula* and *T. iota*. We identify twelve key species of planktic foraminifera based on their average and highest relative abundances within our compiled database. Cold water species *N. pachyderma*, *G. bulloides*, and *T. quinqueloba* have average abundances of 20 %, 13 % and 4 % and highest abundances of 100 %, 77 % and 49 % respectively (Figure 3.3). Temperate species, *G. inflata*, *G. glutinata, N. dutertrei* and *N. incompta* have average relative abundances of 11 %, 11 %, 11 %, and 12 % and highest abundances of 82 %, 60 %, 94 %, and 91 % respectively (Figure 3.3). Warm water species *G. ruber*, *G. sacculifer*, *G. tumida*, *P. obliquiloculata*, *G. menardii* have average abundances of 21 %, 10 %, 5 %, 7 %, and 5 % and highest abundances of 82 %, 58 %, 98 %, 85 %, and 82 % respectively (Figure 3.3).

	RDA1	RDA2	RDA3	RDA4	RDA5	RDA6
Eigenvalue	5.704	1.493	0.620	0.367	0.235	0.078
Proportion Explained	**0.671**	**0.176**	0.073	0.043	0.028	0.009
Cumulative Proportion	**0.671**	**0.847**	0.920	0.963	0.991	1.000

Table 3.1: Eigenvalues and proportion of constrained variance for Redundancy Analysis.

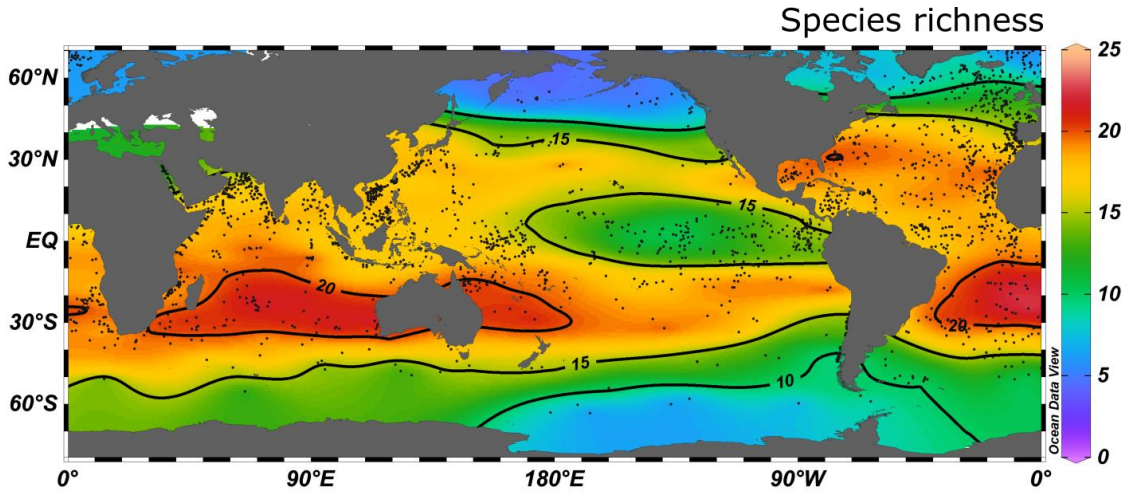

Figure 3.2: Map of species richness created using. Dots show the locations of sites in our study. Data was averaged across the global using Ocean Data Views's surface averaging tool (Schlitzer, 2017).

3.3.2 Environmental data

Planktic foraminifera are known to reside at various water depths depending on their species, genotype, and the geographic region and season they live in (Scheibel and Hemleben, 2017). For this reason, we calculated average water column temperature, salinity, phosphate content for 0-25 m, 0-50 m, 0-100 m and 0-150 m depth for each site in our compiled database. Due to the fact that most species within our dataset have been recorded living within this interval (Schiebel and Hemleben, 2017), we choose to use the 0-50 m depth interval when comparing planktic foraminifera census data to environmental parameters. Data for 0-25 m, 0-100 m, and 0-150 m can be found in the supplementary data tables.

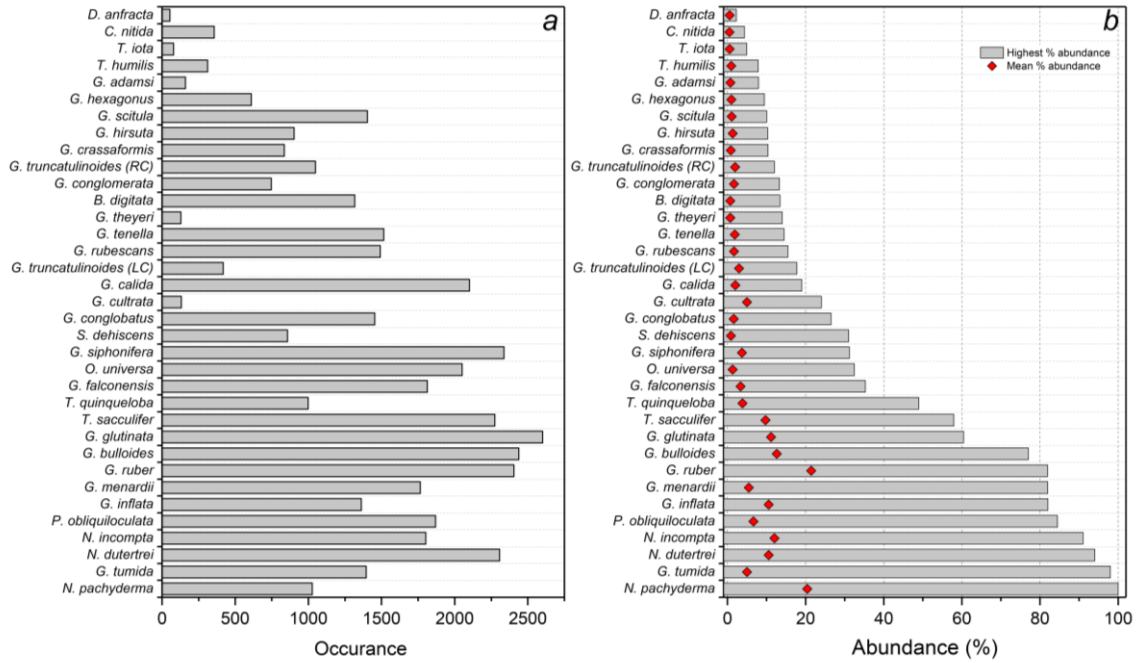

Figure 3.3: Bar charts showing occurrence and percentage abundance for the planktic foraminifera within our global compilation. ***a)*** *Number of times a species appeared at sites in our compiled dataset.* ***b)*** *Shows the highest abundance recorded alongside the mean abundance, the top 12 species for highest abundance are looked at in detail.*

3.3.3 Redundancy Analysis

Our redundancy analysis of planktic foraminifera assemblages and the environmental variables temperature, salinity, phosphate, temperature gradient, phosphate gradient and density gradient identified seven axes of constrained variance. The primary axis, RDA 1 has an eigenvalue of 5.7 and explains 28 % of the total faunal variance as well as 67 % of the constrained variance (the variance accounted for by our explanatory variables) within our dataset (Table 3.1 and Table 3.2). The secondary axis RDA 2 has an eigenvalue of 1.5 and explains 7 % of the total faunal variance and 18 % of the constrained variance (Table 3.1). Together RDA 1, 2, and 3 explain 92 % of the total constrained variance within our data. Site and species scores for all the data in our analyses can be seen in the supplementary data tables. Environmental variable scores for RDA analysis can be seen in table 3.2. The two highest scores for RDA 1 are temperature and oxygen, with scores of -0.98 and 0.87 respectively (Table 3.2). For RDA 2 phosphate content is the highest scoring environmental variable with a score of 0.64 alongside salinity with -0.62 and phosphate and density gradients which score 0.4 and 0.3 respectively (Table 3.2).

3.4 Discussion

	RDA1	RDA2	RDA3	RDA4	RDA5	RDA6
Temperature	**-0.992**	-0.030	0.071	-0.101	0.026	0.000
Phosphate	0.483	**0.728**	0.081	-0.227	-0.128	0.402
Salinity	-0.081	**-0.723**	-0.071	-0.490	-0.352	0.320
Temperature gradient	0.432	-0.322	**-0.414**	-0.342	0.631	-0.151
Phosphate gradient	-0.167	**0.600**	**0.487**	-0.132	-0.591	-0.093
Density gradient	-0.565	0.414	0.079	0.378	-0.599	-0.039

Table 3.2: Environmental variable scores for Redundancy Analysis Axes one to six.

3.4.1 Global distribution of major planktic foraminifera species

Using our updated global planktic foraminifera census database we present a new, detailed visualisation of the twelve most common species of planktic foraminifera and their distribution in the modern ocean (Figures 3.4-3.7). These data allow us to assess the key drivers of species distribution as well as the expected changes in assemblage when analysing material from different ocean basins. The global distribution of all twelve most common planktic foraminifera can be seen together in Figure 3.23. Individual species maps are used to display detailed distributions for each species.

3.4.1.1 *N. pachyderma*

N. pachyderma, also described as *N. pachyderma* sinistral prior to Darling *et al.*, (2003), is the dominant polar and subpolar planktic foraminifera in the modern ocean (Figure 3.4). In line with previous work by Bé (1977), we find it is consistently found at latitudes greater than 40° in both hemispheres and is often present in abundances greater than 90 %. We find a temperature range of -1.4°C and 16.6°C for *N. pachyderma* (where abundance is greater than 25 %). This range compares well with previous studies (Darling *et al.*, 2004; Darling *et al.*, 2007; Kucera *et al.*, 2005b; Kucera, 2007; Darling and Wade, 2008) who cite temperatures ranges for this species between 0 and 18°C. *N. pachyderma* is also known to thrive in upwelling or food rich environments (Darling and Wade, 2008; André *et al.*, 2014; Taylor *et al.*, 2018); this is evidenced in figure 3.4 where *N. pachyderma* can be observed in the North East Pacific and at lower latitudes on the coastal margin of South America. Eight genotypes of *N. pachyderma* exist in the modern ocean (Darling and Wade, 2008; Morard *et al.*, 2013), with a genetic isolation existing between

the North Pacific, North Atlantic, and Indian Ocean. Types IV and I are regarded as subpolar to polar genotypes, whereas types II, III, V, VI, VII are abundant in upwelling and subpolar conditions (Darling and Wade, 2008; Morard *et al.*, 2013). Once genotype, type VIII has been observed within the tropical upwelling region of the Arabian Sea (Darling *et al.*, 2017).

3.4.1.2 *G. bulloides*

G. bulloides is predominantly found in subpolar and polar waters but can be found in abundance at some lower latitude regions (Arabian Sea, South China Sea, and Iberian Margin) (Figure 3.4). In the Southern Ocean, *G. bulloides* is found in the Peruvian and Benguela upwelling zones, and in abundances of 50-75 % at around 50° S (Figure 3.4). In the Northern Hemisphere, *G. bulloides* is abundant along coastal margins notable the Iberian margin, marginal Mediterranean, South East Asia, and the Arabian Sea (Figure 3.4) and has often been associated with upwelling conditions (Prell and Curry, 1982; Curry *et al.*, 1992), although this is debated within recent literature (Davis *et al.*, 2016). We find a temperature range for *G. bulloides* (>25 % abundance) of 5 to 28.4°C in line with work by Źarić *et al.*, (2005) and Kucera (2007). In the North Pacific, food availability is thought to be the primary driver of abundance in *G. bulloides*, this relationship has been seen in core-tops, sediment traps and net material from this region (Taylor *et al.*, 2018). Darling and Wade (2008) describe seven genotypes of G. *bulloides* which may explain the large latitudinal range of the species (0-60°). Unlike *N. pachyderma*, identical genotypes of *G. bulloides* have been found in both the North Atlantic and North Pacific (Darling and Wade, 2008). Although type IIe is restricted to Pacific waters. Type IIe is in direct competition with *N. pachyderma* in the North Pacific, and its abundances is therefore closely linked to temperature (Taylor *et al.*, 2018).

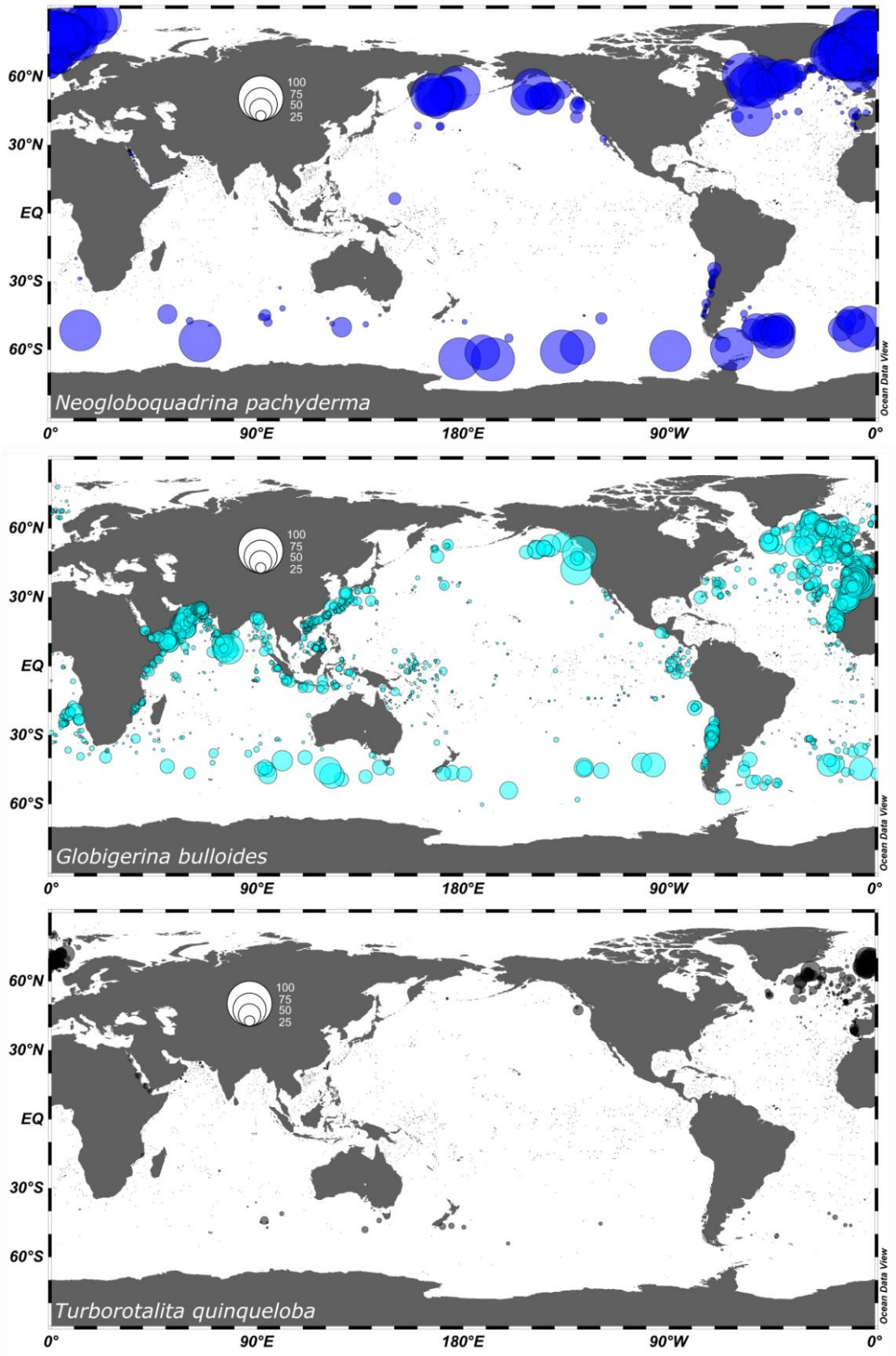

Figure 3.4: Distribution maps for N. pachyderma, G. bulloides, and T. quinqueloba. Size of bubble denotes the percentage abundance of that species at that site.

3.4.1.3 *T. quinqueloba*

T. quinqueloba is a subpolar to polar species of planktic foraminifera predominantly found in the North Atlantic but is seen in small abundances within the North Pacific and Southern Ocean (Figure 3.4). At abundances greater than 25% the temperature range for *T. quinqueloba* is 3.6 to 9.7°C. Due to its small size, *T.* quinqueloba is often underrepresented in core-top material which is usually sieved >150 µm (Taylor *et al.,* 2018). This is likely to reduce the accuracy of temperature and latitudinal ranges for this species when solely based on core-top census data and makes *T. quinqueloba* appear less abundant in our compiled data (Figure 3.4). Often associated with *N. pachyderma* and *G. bulloides,* it makes up a characteristic part of high latitude assemblages. Two genotypes of *T. quinqueloba* and six subtypes exist in the modern ocean with type II found in the North Pacific, Southern Ocean and North Atlantic, and type I found in the Indian Ocean and coastal margin of Australia (Darling and Wade, 2008).

3.4.1.4 *N. incompta*

N. incompta (commonly reported as *N. pachyderma* dextral prior to genetic work by Darling *et al.,* 2006 showing its independent speciation from *N. pachyderma*) is found at mid-high latitudes in the modern ocean (Figure 3.5). In the North Pacific it frequents the transitional and upwelling in the North Atlantic it is ubiquitous between 20-70°N (Figure 3.5). *N. incompta* is particularly abundant in several key upwelling regions including the Benguela upwelling zone, the coastal margin of South America, the Iberian margin, and the eastern North Pacific. It has a broad temperature range (>25 %) of between 1.6 and 21.6°C, slightly larger than that suggested by Kucera *et al.,* (2005b) who cite a range of 7-18°C. Two genotypes of *N. incompta* exist, type I is present in the Atlantic Ocean, whilst type II is only found in the North Pacific (Darling and Wade, 2008). Although *N. incompta* is predominantly a right coiling species, abnormal left coiling specimens can be observed (Darling *et al.,* 2006). Darling *et al.,* (2006) suggest that to distinguish these from the left coiling *N. pachyderma,* assemblages where <3 % of specimens exhibit opposite coiling are likely to reflect the presence of only one species with some abnormal coiling.

3.4.1.5 *G. inflata*

G. inflata is a transitional zone foraminifera commonly found at mid-latitudes between 30-40° in both hemispheres (Figure 3.5). *G. inflata,* is particularly prevalent along the sub-polar front in the North Pacific, where it could be used to trace gyre movement in the past (Taylor *et al.,* 2018), and in the Agulhas and Benguela upwelling regions (Storz *et al.,* 2009). It is noted to thrive in food rich environments and can live down to depths of 100 m depending on food availability (Retailleau *et al.,* 2012). We find a temperature range (>25 %) for this species of 1.6 to 24.2°C,

which is broader than Kucera *et al.,* (2005b) who cite a temperature range of 12-24°C. This is due to several high latitude North Atlantic core-top sites which correspond to very low annual average temperatures (Figure 3.5). Two genotypes of *G. inflata* are recognised by Morard *et al.,* (2013). Type I occurs at lower latitudes whereas type II frequents subpolar to polar regions (Morard *et al.,* 2013).

3.4.1.6 *G.* glutinata

G. glutinata is an unusually large microperforate species of planktic foraminifera (Schiebel and Hemleben, 2017) and the only microperforate to be found in high abundances in core-tops >150 μm. It is found throughout the world's oceans predominantly at mid-equatorial latitudes but can be seen at higher latitudes in the North Atlantic (Figure 3.5), although in lower abundances (Schiebel and Hemleben, 2000). It is most dominant in the Arabian Sea, where it characterises the upwelling fauna in this region (Figure 3.5). Clusters of moderate *G. glutinata* abundance can also be seen in the South China Sea, western Equatorial Pacific, and high latitude North Atlantic (Figure 3.5). At abundances >25 %, *G. glutinata* has a temperature range of 9.5 to 29.3°C in line with estimates from Kucera *et al.,* (2005b). André *et al.,* (2014) describe four genotypes of *G. glutinata* with type I found in the Atlantic Ocean, type II in the Pacific, type IV in the Indian Ocean, and type III occurring in both Atlantic and Pacific oceans. G. *glutinata*'s small size and test structure may mean it could be misidentified as another microperforate species *G. minuta,* or small specimens of the much more common macroperforate species *G. bulloides* (Schiebel and Hemleben, 2017). This could be a problem in the Arabian Sea, where both species occur in high abundances (Figure 3.5).

3.4.1.7 *G. ruber*

G. ruber is the second most common species of planktic foraminifera in our compiled dataset, occurring in 2404 out of 2903 core-tops (Figure 3.6). It also displays the highest mean abundance of all species in our dataset (21.4 %). Figure 3.6 shows that *G. ruber* dominates in subtropical to tropical assemblages, as first reported by Bé (1977). It has clear latitudinal boundaries of 30° in both hemispheres and does not appear at latitudes higher than this. The only equatorial region where it is not present is the eastern equatorial Pacific. Two phenotypes of *G. ruber* exist in the modern ocean, *G. ruber* white and *G. ruber* red (Schiebel and Hemleben, 2017), we show both species together as several of our compiled core-top datasets do not distinguish between them. *G. ruber* pink has only one genotype, whereas *G. ruber* white has four (Darling and Wade, 2008). *G. ruber* white type IIa is also closely related to another tropical planktic foraminifera, *G. conglobatus* (Darling and Wade, 2008). At relative abundances greater than 25 % *G. ruber* has a temperature range between 14.1 and 29.4°C, similar to the range given by Kucera *et al.,* (2005b).

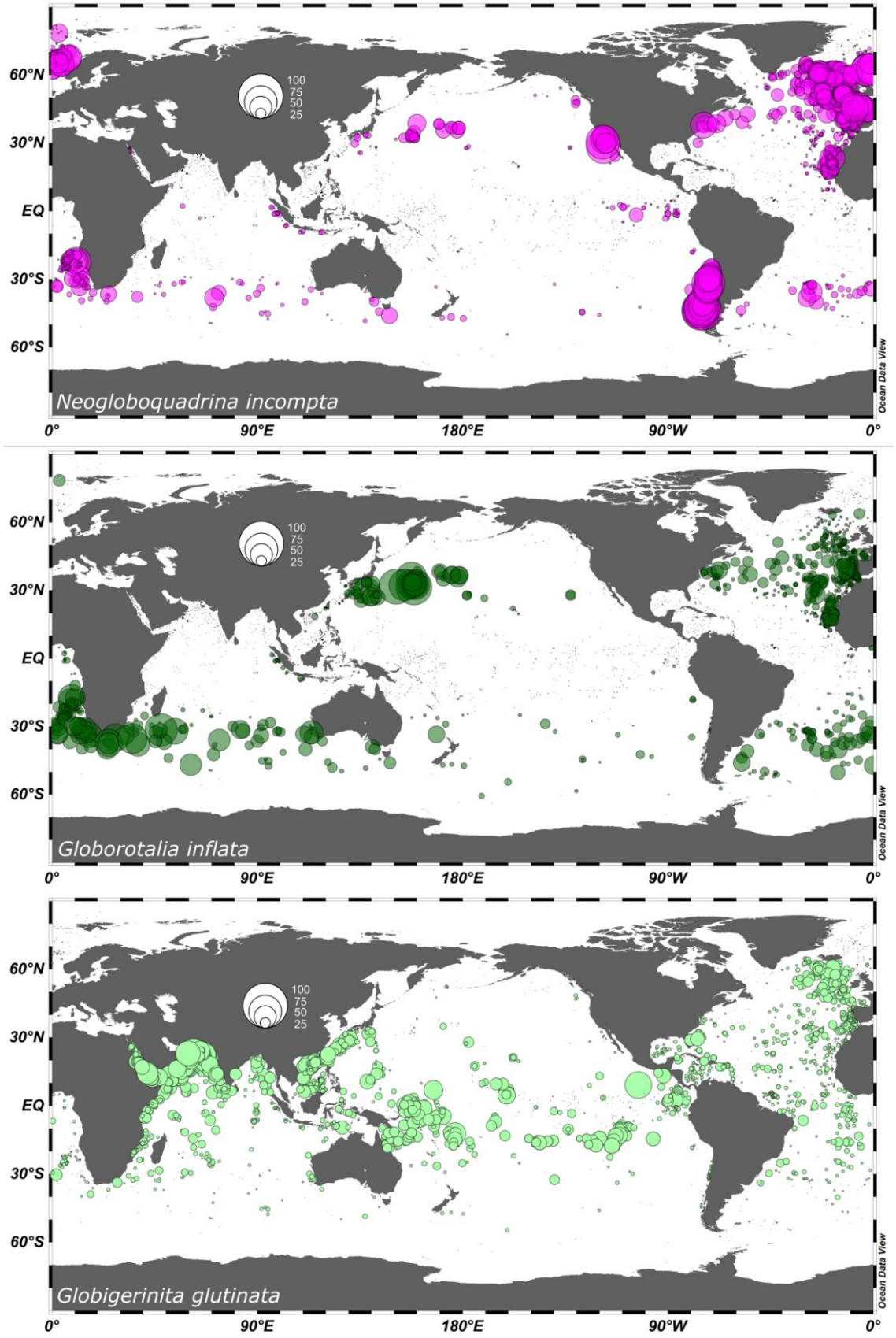

Figure 3.5: Distribution maps for N. incompta, G. inflata, and G. glutinata. Size of bubble denotes the percentage abundance of that species at that site.

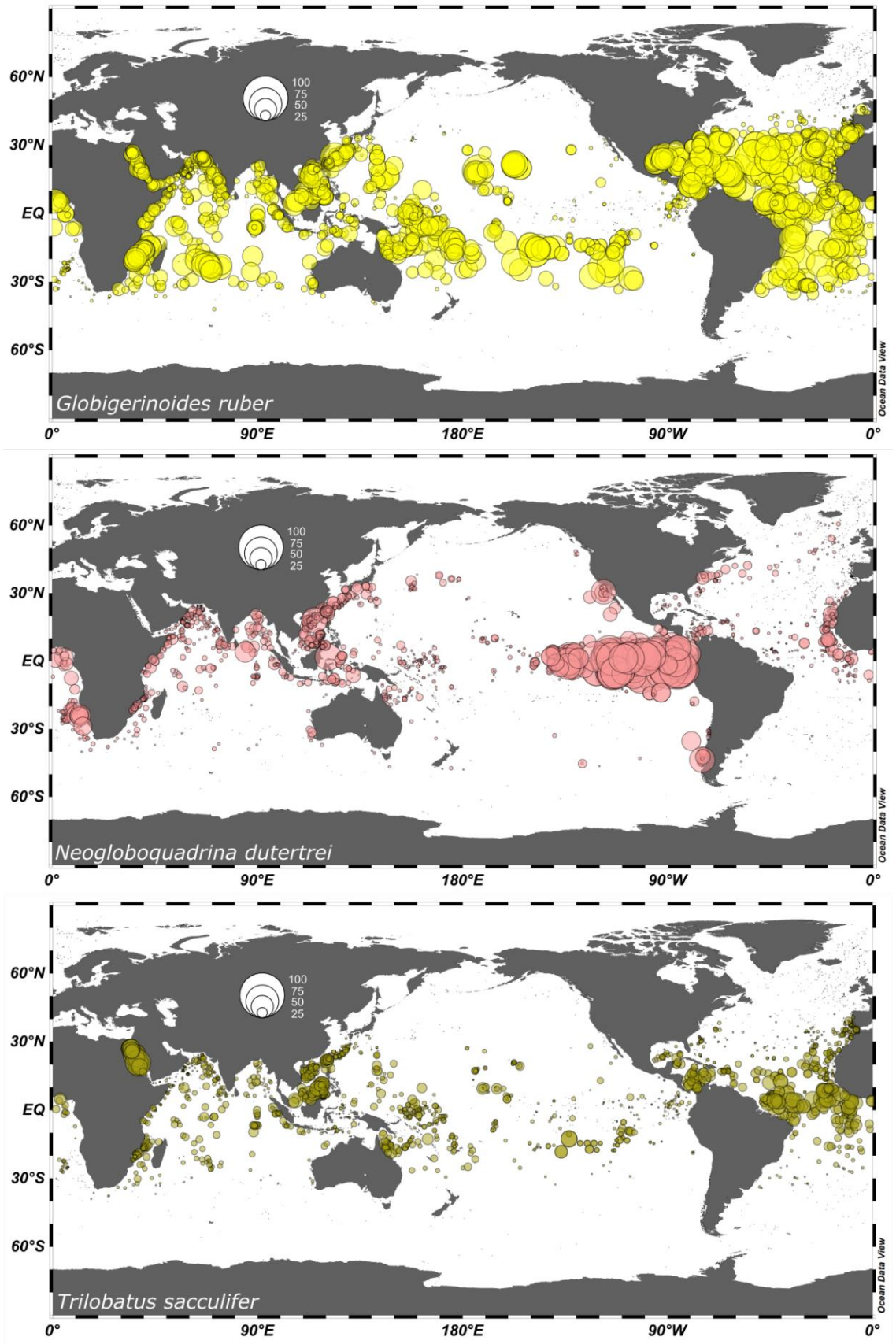

Figure 3.6: Distribution maps for G. ruber, N. dutertrei, and T. sacculifer. Size of bubble denotes the percentage abundance of that species at that site.

3.4.1.8 *N. dutertrei*

N. dutertrei is found in tropical to transitional latitudes in the world's oceans (Figure 3.6) (Bé, 1977). It is most abundant in the east equatorial Pacific, where it dominates the region's assemblages (Figure 3.6) (Taylor *et al.*, 2018). It is also found in high abundance in the Benguela upwelling zone, Iberian margin, South China Sea, and coastal margins of South and North America (Figure 3.6). Its appearance at higher latitudes is likely to reflect warmer water conditions during summer months (Schiebel and Hemleben, 2000). Only one genotype of *N. dutertrei* exists (André *et al.*, 2014), however it is genetically similar to the tropical species *P. obliquiloculata*, *N. pachyderma*, and *N. incompta* (Darling and Wade, 2008). Due to its likeness to *N.* pachyderma, Kipp (1976) define the P-D intergrade, describing a gradation between the morphology of *N. pachyderma* to *N. dutertrei*. The P-D intergrade was further developed by Hilbrecht (1997) and Peeters *et al.*, (1999). We find a temperature range of 12.3 to 28.7°C for *N. dutertrei* (>25 %). This corresponds well to culture studies by Bijma *et al.*, (1990) who reported a temperature tolerance for *N. dutertrei* of 13-33°C.

3.4.1.9 *T. sacculifer*

T. sacculifer (also *G. sacculifer*, Brady, 1877) exhibits moderate abundance at tropical and sub-tropical latitudes (Figure 3.6) (Bé, 1977). It does not dominate assemblages in any ocean region, with its highest abundance recorded at 58 % in the Red Sea (Figure 3.6). Known predominantly as a surface dweller it feeds largely on copepods (Schmuker and Schiebel, 2002; Hemleben *et al.*, 1989). *T. sacculifer* has only one genotype (André *et al.*, 2013), however is known to have a diverse range of morphotypes, primarily defined by abnormal final chamber morphology (Schiebel and Hemleben, 2017), the most distinctive of which is represented by a sac-like final chamber. Unlike most of the previous species discussed, *T. sacculifer* has a narrow temperature range of 23.5 to 28.3°C (>25 %) in line with the 20-27°C range suggested by Kucera *et al.*, (2005b), making it an exclusively tropical species.

3.4.1.10 *P. obliquiloculata*

P. obliquiloculata is a tropical species and has often been described as ubiquitous but rare, with low abundances cited in previous data (Bé, 1977; Li *et al.*, 1997; Schiebel and Hemleben, 2017). However, figure 3.6 indicates its dominance in the central and western Equatorial Pacific, with relative abundances reaching greater than 80%. Abundance of *P. obliquiloculata* is much lower in the Atlantic and Indian Oceans, rarely exceeding 25 %. *P. obliquiloculata* is a deeper dwelling planktic foraminifera, often living below the Deep Chlorophyll Maximum (Bé and Tolderlund, 1971; Watkins *et al.*, 1996), we find a temperature range for the species of 25.2 to 29.3°C (>25

%). Three genotypes of *P. obliquiloculata* exist in the modern ocean (Ujiié *et al.,* 2012). Type I occurs across the world's oceans, whereas type IIa and IIb are found only in the Pacific Ocean (Ujiié *et al.,* 2012). The reasons for the dominance of *P. obliquiloculata* in Equatorial Pacific sediments may be two-fold: firstly, its deeper dwelling habitat allows it to live below the nutrient barren surface waters in the Equatorial Pacific (Murray *et al.,* 1989); secondly, its robust test structure gives it a strong resistance to sediment and water column dissolution (Schiebel and Hemleben, 2017), meaning its abundance in core-top samples are much larger than those collected from plankton tows and traps due to dissolution of other species in this region (Schiebel and Hemleben, 2017).

3.4.1.11 *G. tumida*

G. tumida is a tropical species of planktic foraminifera found in moderate abundances in the Indian and Atlantic Oceans, and in high abundances in the central Equatorial Pacific (Figure 3.7). Although it has been described as rare (Schiebel and Hemleben, 2017), it dominates central equatorial Pacific assemblages, with abundances in excess of 90 % (Figure 3.7). Like *P. obliquiloculata, G. tumida* is known for its robust test and low dissolution susceptibility (Schiebel and Hemleben, 2017). It is therefore likely that its dominance of equatorial Pacific sediment assemblages is somewhat artificial and does not truly reflect surface water assemblages (Dittert *et al.,* 1999). André *et al.,* (2014) describe only one genotype for this species. The temperature range of *G. tumida* based on our calculated SSTs is 24.1 to 28.9°C which similar to other tropical species such as *P. obliquiloculata* and *G. menardii* and in line with previous estimates by Kucera *et al.,* (2005b). *G. tumida* is also regarded as a deeper dwelling species associated with the Deep Chlorophyll Maximum, much like *P. obliquiloculata* (Ravelo and Fairbanks, 1992; Watkins *et al.,* 1996).

3.4.1.12 *G. menardii*

G. menardii is a tropical planktic foraminifera that is found throughout the world's oceans between 25° latitude (Figure 3.7). It is most dominant in the Arabian Sea, Bay of Bengal and South China Sea, with abundances typically between 50 and 80 % (Figure 3.7). Often associated with waters of moderate productivity and food availability (Schiebel *et al.,* 2004), *G. menardii* has a temperature range of 22 to 28.4°C, close to estimates given by Kucera *et al.,* (2005b) for percentages >25 %. Only one genotype of *G. menardii* is known (André *et al.,* 2014), however it is morphologically similar to a number of other tropical and subtropical species such as *G. tumida* and *G. conglomerata* (Schiebel and Hemleben, 2017).

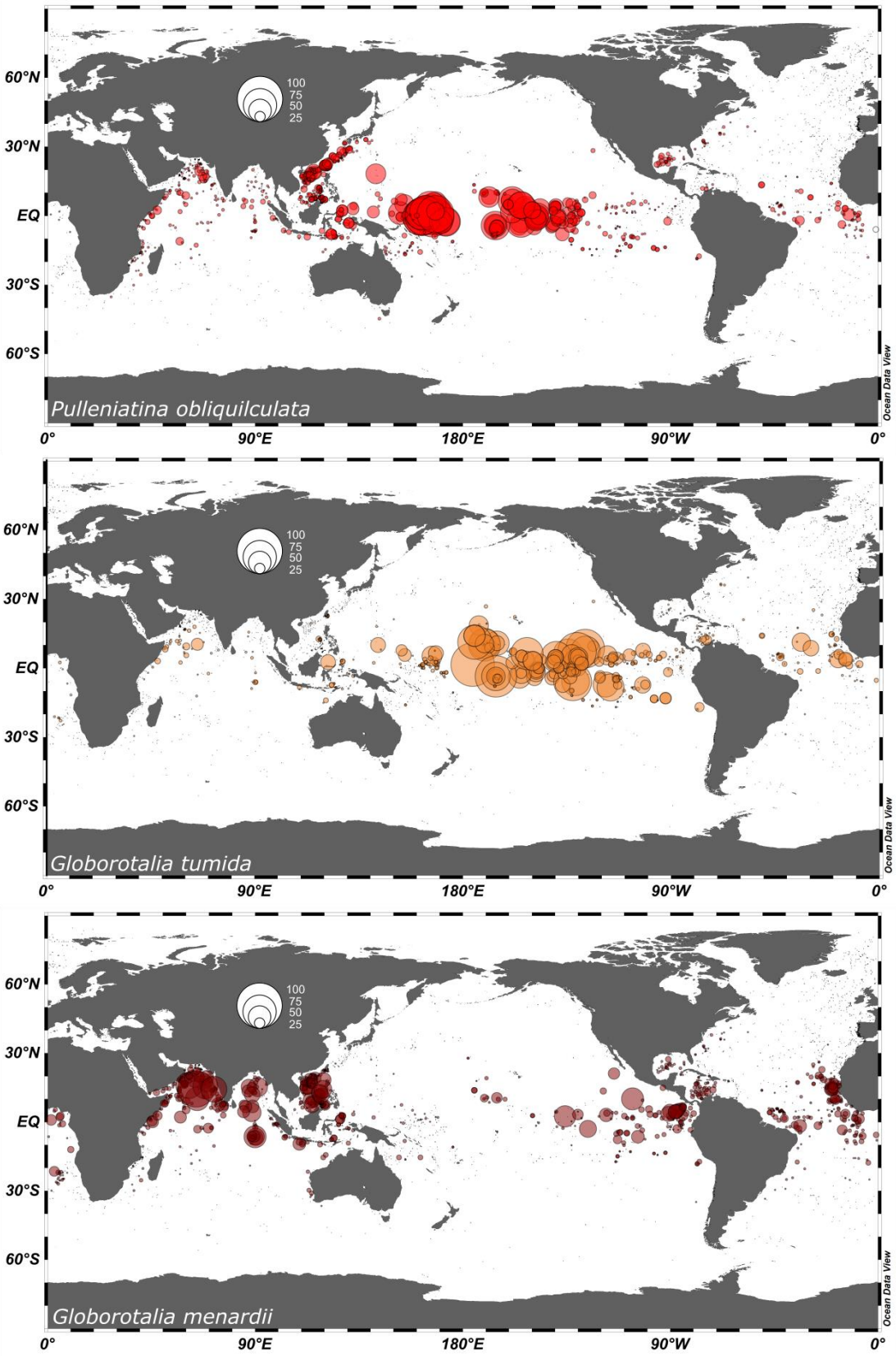

Figure 3.7: Distribution maps for P. obliquiloculata, G. tumida, G. menardii. Size of bubble denotes the percentage abundance of that species at that site.

3.4.2 Ecological drivers of species abundance

The relative abundance of different planktic foraminifera species in core-top samples is dependent on surface ocean and bottom water environmental conditions. Planktic foraminifera census data is often used to qualitatively assess changes in surface environmental conditions in the past. For this to be accurate, knowledge of the effects of different environmental parameters on species abundance in the modern ocean is required. Here we assess the impact of two key environmental variables, temperature and phosphate content, on the relative abundance of two commonly used foraminifera in paleo-reconstructions: *N. pachyderma* and *G. ruber*. These variables have previously been suggested to play a prominent role in planktic foraminifera ecology (Schiebel and Hemleben, 2017).

3.4.2.1 *Temperature control on N. pachyderma*

The relative abundance of polar and subpolar species *N. pachyderma* has commonly been used to assess qualitative changes in temperature (Bond *et al.*, 1992; Bond *et al.*, 1993; Bond *et al.*, 1997) as well as changes in the position of the polar front (Thompson and Shackleton, 1980; Barker *et al.*, 2009). Both methods are based on the assumption that increases in percentage *N. pachyderma* correspond to lower SSTs. Using our estimated SSTs for 0-50 m (Locarnini *et al.*, 2013) we find an excellent correlation between percentage *N. pachyderma* and temperature described by the sigmoidal regression below where T is temperature at 0-50 m (Figure 3.8):

$$N.pachyderma\ \% = \frac{(101.52-0.36)}{(1+\exp((T-6.19)/1.77))} + 0.36 \quad (1)$$

Equation 1 indicates a tight correspondence between percentage *N. pachyderma* and temperature with an $R^2 = 0.94$. This sigmoidal relationship between temperature and *N. pachyderma* is clearly shown in figure 3.8, however several clear outliers can also be seen. Most prominently, a sample containing close to 25 % *N. pachyderma* can be seen at temperatures close to 30°C. This outlier represents the unusual genotype type VIII (Darling and Wade, 2017) which is found only in the Arabian Sea and is associated with upwelling in that region (Darling *et al.*, 2017). This genotype is rare and is not typical of the majority of *N. pachyderma* in the global ocean. When our global temperature calibration is compared to that of the North Pacific (Taylor *et al.*, 2018), several differences are observed (Figure 3.8). At temperatures below 5°C, in our global compilation, the relationship between temperature and *% N. pachyderma* flattens out as the relative abundance of % *N. pachyderma* approaches 100 % (Figure 3.8). This is not seen in the North Pacific (Figure 3.8) due to a lack of polar conditions, with the coldest annual average temperatures observed around 5°C (Locarnini *et al.*, 2013).

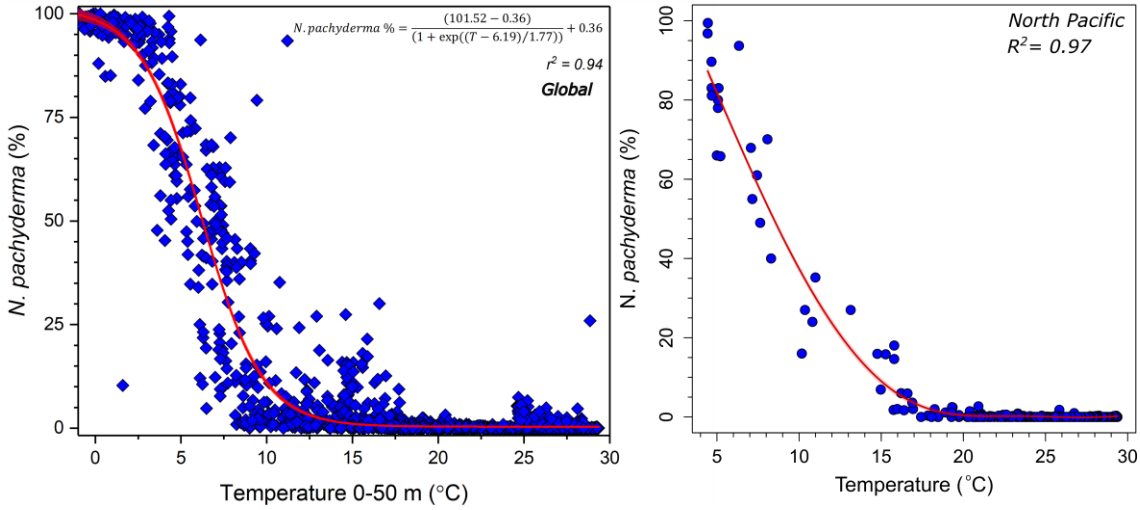

Figure 3.8: Comparison of the relationship between WOA temperature (0-50 m) and percentage N. pachyderma globally and in the North Pacific. A lack of polar conditions in the North Pacific gives a strong exponential fit (right), while globally a sigmoidal fit it more appropriate (left).

To assess the influence of secondary environmental variables on the relative abundance of *N. pachyderma* we use multiple regression analysis. We regress temperature alongside, phosphate content and salinity (all 0-50 m) with the resulting exponential equation taking the form of:

$$N.pachyderma\ \% = \exp(-0.18 * Temp + 0.37\ \pm 0.02 * Phos + 0.12 \pm 0.01 * Sal + 0.14\ \pm 0.6) \quad (2)$$

RSE = 7.43. Our multiple regression shows a negative -18% sensitivity to temperature, a positive 37 % sensitivity to phosphate content, and a 12 % sensitivity to salinity. All the relationships were significant with p = $<10^{-13}$. This suggests multiple controls on the *N. pachyderma*, however when we regress each variable individually against temperature the RSE for phosphate and salinity is much higher (20 and 21.5 respectively).

Overall our regression analysis suggests that the dominant control on the relative abundance of *N. pachyderma* is temperature, with smaller influences from salinity and phosphate content. Several studies also note the importance of food availability for this species as well as upwelling in some regions (Eguchi *et al.*, 1999; Kuroyanagi and Kawahata, 2004; Jonkers *et al.*, 2010; Iwasaki *et al.*, 2017; Darling *et al.*, 2017; Taylor *et al.*, 2018). Upwelling is a complex parameter and difficult to define through a single environmental variable, thus we use redundancy analysis address the importance of upwelling. The sigmoidal relationship we present in equation 1 could in theory be used to quantitatively reconstruct SSTs in the past, however given the potential for multiple controls on species abundance, we instead favour the use of % *N. pachyderma* as a

powerful qualitative indicator of temperature changes in the Polar and Subpolar regions of the global ocean.

3.4.2.2 *Nutrients, productivity and ecological competition in the subtropical ocean*

Several studies highlight the importance of nutrients and food availability for increased planktic foraminifera abundance (Hemleben *et al.,* 1989; Watkins *et al.,* 1996; Schiebel *et al.,* 2001; Kuroyanagi and Kawahata, 2004; Kuroyanagi *et al.,* 2008; Iwasaki *et al.,* 2017; Taylor *et al.,* 2018). As planktic foraminifera commonly prey upon diatoms, copepods, radiolarians and in some cases other foraminifera (Schiebel and Hemleben, 2017), food availability for planktic foraminifera is closely related to the fertility and nutrient content of surface waters. To test the relationship between planktic foraminifera abundance and nutrients, we compared calculated surface water (0-50 m) phosphate content with planktic foraminifera abundance.

No strong relationships exist between individual species of planktic foraminifera and surface water phosphate content. The species with the best correlation is *G. ruber*, which exhibits a weak negative correlation to phosphate values (Figure 3.9). *G. ruber* is a subtropical to tropical species and is most abundant between 20-30° N and S. These waters are low in nutrients but contain the highest species diversity of planktic foraminifera within the global ocean (Rutherford *et al.,* 1999) (Figure 3.9). It is possible, that in these nutrient poor environments where food availability is limited, no one species can establish itself as the dominant planktic foraminifera. This is best highlighted by the relationship between species richness and phosphate content (Figure 3.9). Here, a weak negative correlation exists between nutrients in the surface ocean and the number of species within an assemblage. As *G. ruber* is most abundant in regions of low species richness, it suggests that *G. ruber* is best adapted to low nutrient, food poor conditions. It also points towards *G. ruber* being an opportunistic species, capitalising on sporadic feeding opportunities such as algal blooms. This is in line with studies suggesting a level of adaptability in *G. ruber*, with its ability to thrive in both eutrophic and oligotrophic environments (Kemle-von-Mücke and Hemleben, 1999; Schiebel *et al.,* 2004). In addition, *G. ruber* is known to have algae symbionts and which help it to assimilate nutrients in barren conditions better than non-symbiotic foraminifera (Schiebel and Hemleben, 2017). Indeed, another sub-tropical symbiont bearing species *G. sacculifer* exhibits a similar negative relationship with surface nutrients.

It is widely recognised that species richness is driven primarily by SST (Rutherford *et al.,* 1999; Moray *et al.,* 2005; Fenton *et al.,* 2016). However, in regions where temperatures are comparable such as the east and west subtropical North Pacific, species richness is likely to vary due to secondary factors such as nutrient content and food availability. In the subtropical North Pacific regions where nutrients and food are poor (West Subtropical Pacific), *G. ruber* is consistently

present at moderate abundances and species richness is high (Figure 3.6). This contrasts with the eastern Equatorial Pacific where nutrient content is higher, species richness is reduced, and assemblages are dominated by one species of planktic foraminifera, *N. dutertrei* (Figure 3.6). This relationship highlights the impact that high food availability, which reflects the consumption of nutrient utilising primary producers, can have on species richness within the modern ocean, allowing single species of planktic foraminifera to dominate.

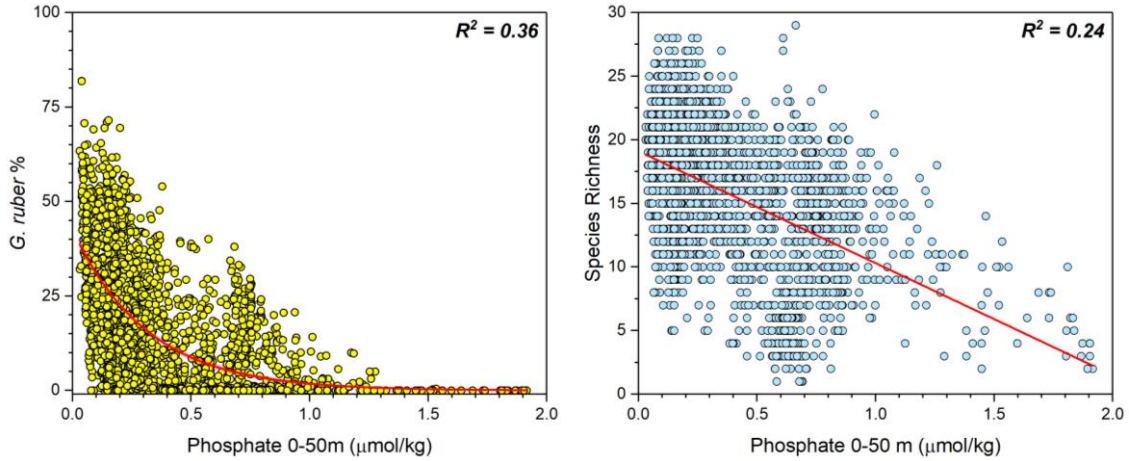

Figure 3.9: Relationship between surface ocean (0-50 m) phosphate content (µmol/kg) and the percentage abundance of G. ruber (left) and species richness (right).

3.4.3 Temperature, upwelling and nutrient controls on planktic foraminifera

Through our redundancy analysis we assess the major drivers of variance within planktic foraminifera assemblage data. We investigate the role of temperature, salinity, and phosphate on variance in our dataset, as well the gradients of temperature, phosphate and density at each site. The latter parameters reflect water column stratification and upwelling.

3.4.3.1 *Temperature controls on variance within planktic foraminifera assemblages*

Our redundancy analysis clearly indicates that the primary driver of variance (RDA axis 1) in planktic foraminifera assemblages is temperature (Figure 3.10). This is demonstrated in the biplot in figure 3.11, with temperature scoring the highest for RDA 1 (-0.992). RDA 1 describes 28 % of the total variance in assemblages and 67 % of the constrained variance, further highlighting the importance of this axis – and temperature – to changes in planktic foraminifera assemblage. This outcome is not novel following the work of Morey *et al.*, 2005, who used Canonical Correspondence Analysis (CCA) to investigate similar relationships between variance and environmental variables. Morey *et al.*, 2005 also found the primary axis of variance was related to temperature with a score of -0.96 and a total variance control of 30.4 %. Their work focused

on the Atlantic and Pacific Oceans and lacked data from the North Pacific and Indian ocean. Despite the inclusion of additional sites and regional data, our results show a remarkable similarity to theirs, with axis 1 from both studies describing a similar proportion of variance and almost identical scores for temperature against the primary axis of variance. This similarity despite our more extensive dataset adds considerable weight to the argument that temperature is the primary driver of faunal variance in the modern ocean. Another output of our RDA is species specific scores for RDA 1 and 2. Species scores shows how much influence the abundance of a particular species had on that particular axis of variance. Figure 3.12 shows that for RDA 1 predominantly cold-water species scored positively, whilst warm water species scored negatively. In addition, *N. pachyderma* and *G. ruber* scored the highest positive and lowest negative values respectively,

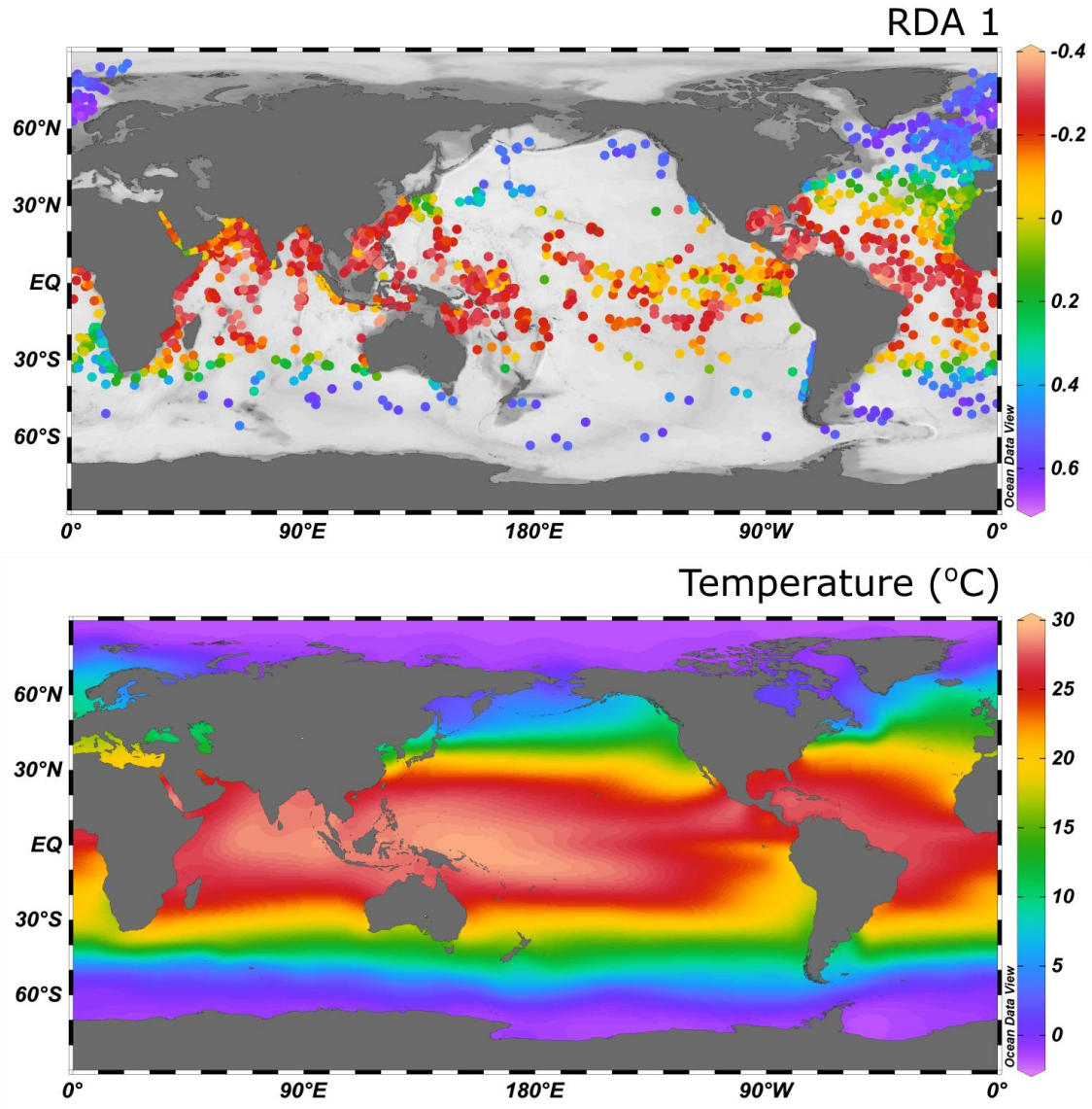

Figure 3.10: Site scores for RDA1 plotted on a world map (top) alongside annual average temperature at 25 m from World Ocean Atlas 13 (Locarnini et al., 2013) (bottom).

indicating that changes in abundance of those species can be linked to temperature in modern assemblages (Figure 3.12).

In addition to work by Morey *et al.* (2005), other studies have highlighted temperature as a key driver of faunal assemblages. Rutherford *et al.* (1999) assessed the drivers of species richness in planktic foraminifera, noting that temperature explained 90 % of the variation in planktic foraminifera diversity in the North Atlantic. More recently, work by Fenton *et al.* (2016) used simultaneous autoregressive models (SARs) to conduct a similar analysis into drivers of diversity. Although they note that planktic foraminifera diversity is likely to be controlled by a number of environmental factors, temperature stands out as the main driver of faunal diversity (Fenton *et al.*, 2016).

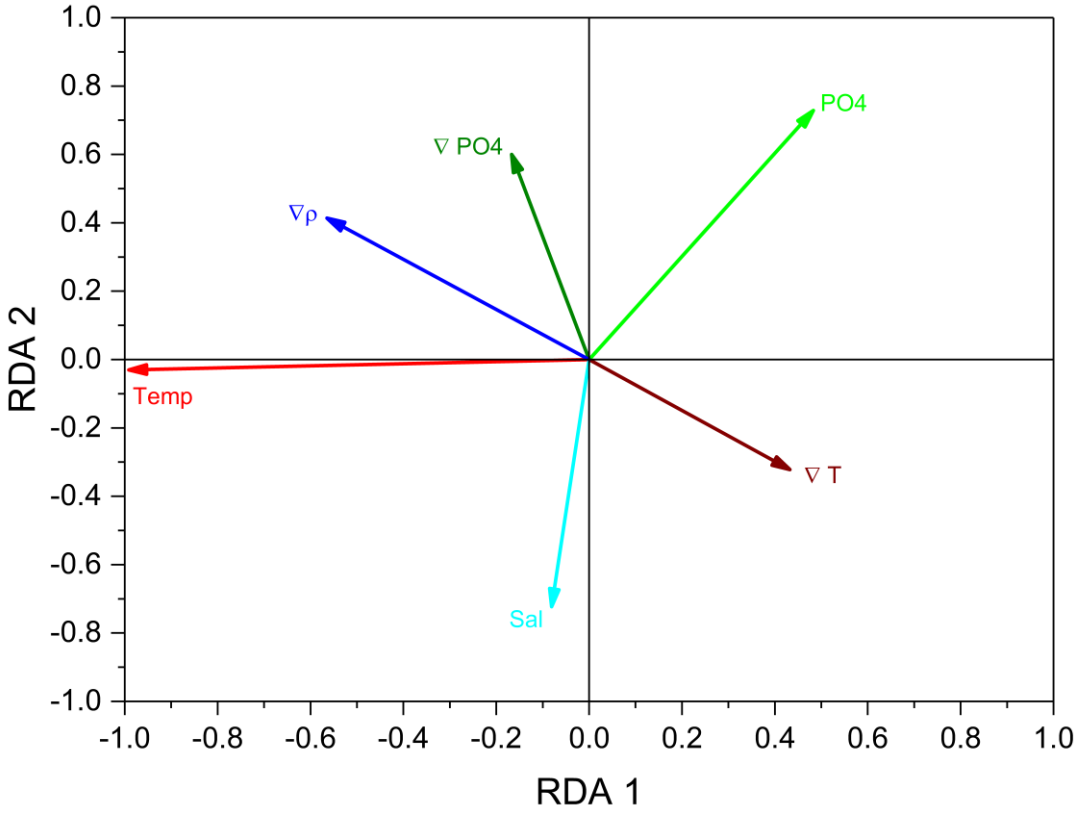

Figure 3.11: Biplot of environmental variables against RDA 1 and RDA2. Temperature (red), salinity (light blue), phosphate (light green), density gradient (dark blue), temperature gradient (brown), and phosphate gradient (dark green).

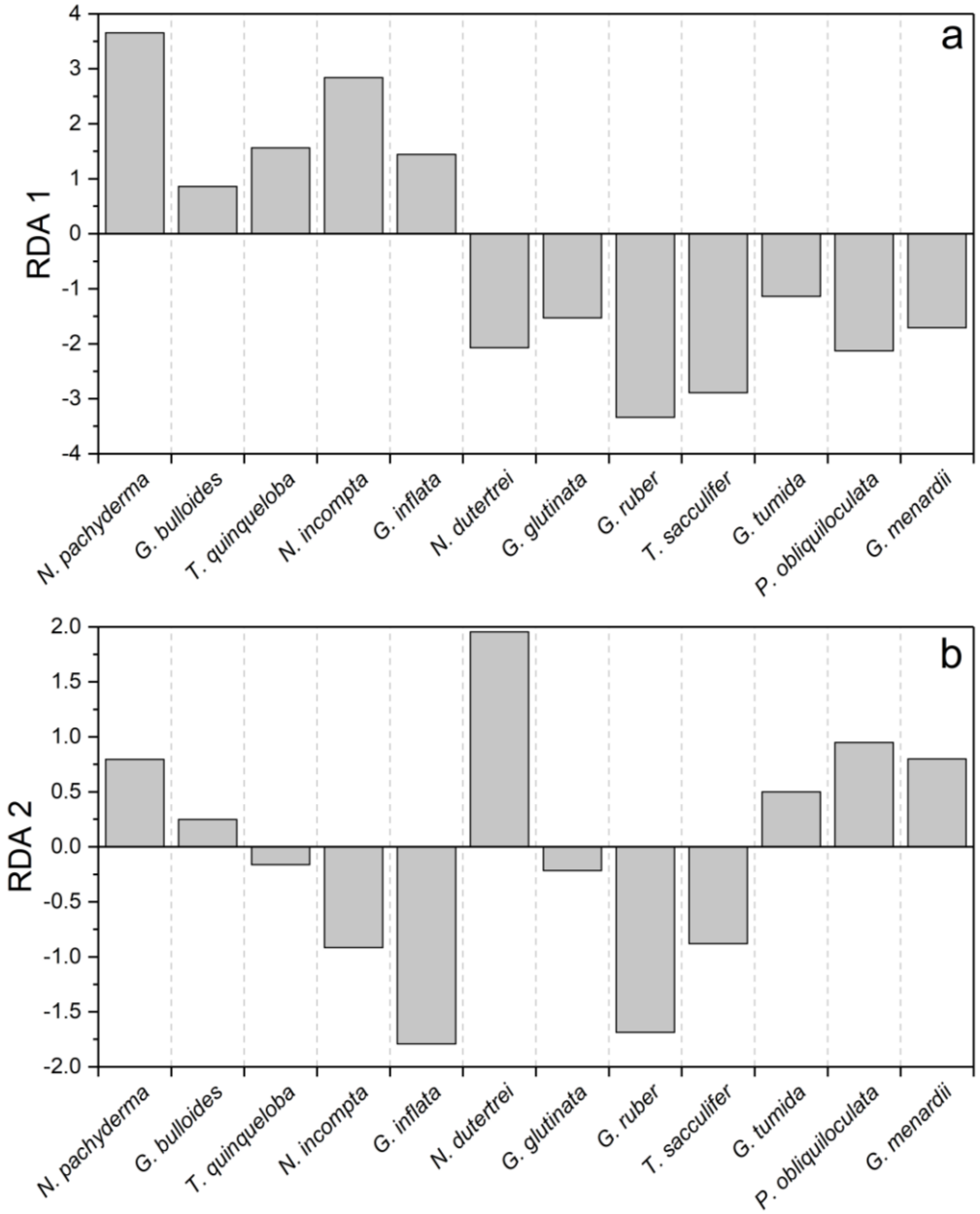

Figure 3.12: Species scores for RDA 1 (top) and RDA 2 (bottom).

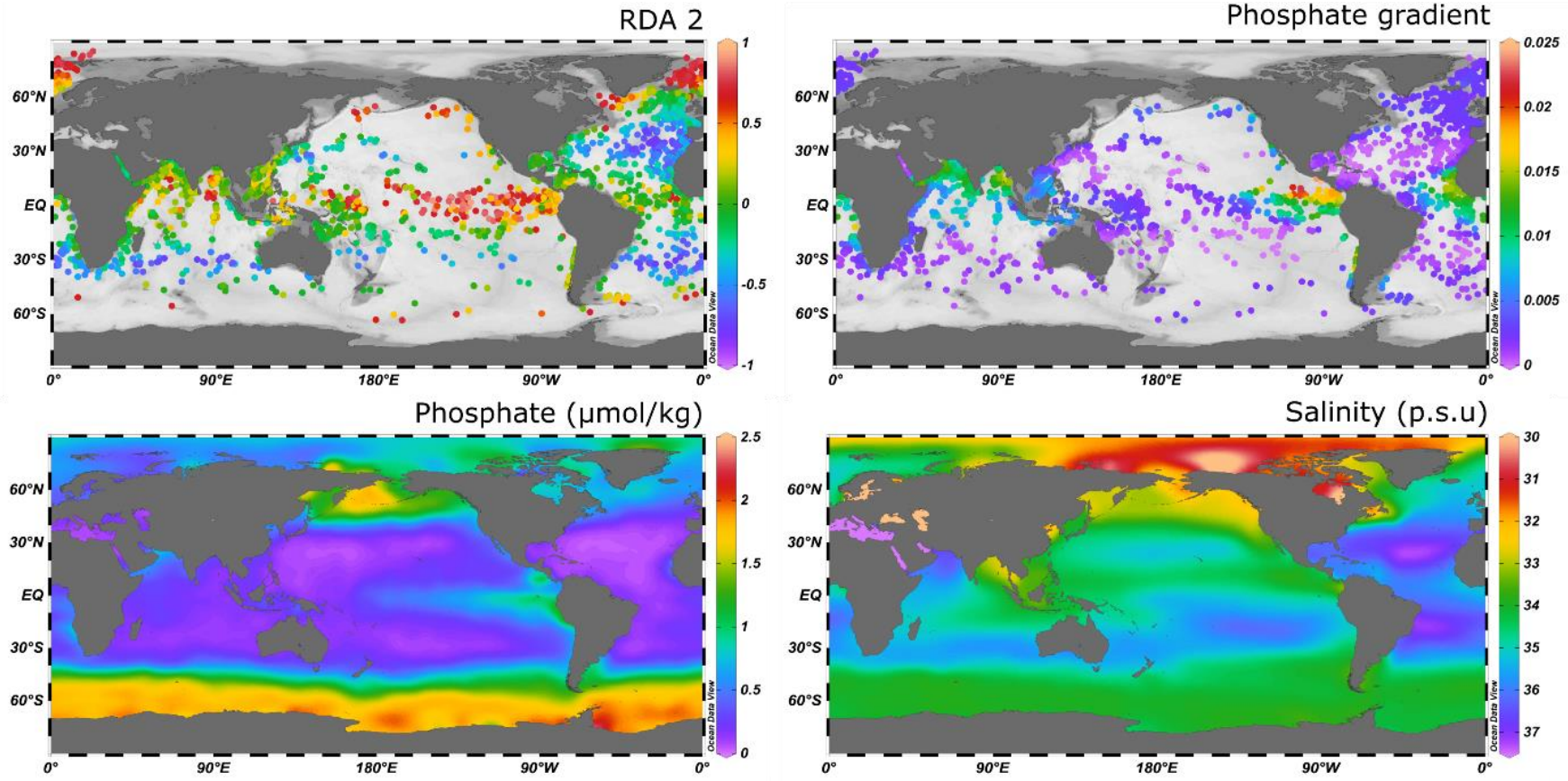

Figure 3.13: Site scores for RDA 2 (top left) alongside calculated phosphate gradient at each site (top right). The bottom two panels show annual average phosphate (bottom left) and salinity (bottom right) at 25 m (Garcia et al., 2014; Zweng et al., 2013).

3.4.3.2 *Nutrients and upwelling controls on assemblage variance*

With RDA 1 explaining 67 % of the constrained variance in our dataset, RDA 2 (18 %) is likely to reflect secondary controls on the variance within planktic foraminifera assemblage data. The biplot in figure 3.11 shows the complexity associated with RDA 2, with no single variable clearly describing the majority of the variance in the data. Four environmental variables show some association with RDA 2: phosphate (0-50 m) has the highest score of 0.728; salinity scores -0.723; the phosphate gradient (a measure of upwelling and stratification) scores 0.600, and the density gradient (primarily association with stratification) scores 0.414. The fact that phosphate content scores highest for RDA 2 suggests a relationship between assemblages and surface water nutrient content. The influence of surface water nutrients and food availability on faunal assemblages was also noticed by Morey *et al.*, (2005). Morey *et al.*, (2005) note the second axis of their CCA corresponded to several environmental parameters which they suggest are predominantly related to ocean fertility (nutrients, productivity and food availability). As well as phosphate content, salinity scores highly against RDA 2 in our analysis. Because phosphate and salinity are the two major controls, alongside minor influences of gradients in phosphate and density, it suggests axis 2 may have some correspondence to exchange with subsurface waters, via upwelling and vertical mixing. Figure 3.13 shows the site scores from RDA 2 with several upwelling regions depicting high scores for RDA 2. The difficulty in characterising different upwelling regions across the global ocean is likely to contribute to multiple environmental influences seen within RDA 2.

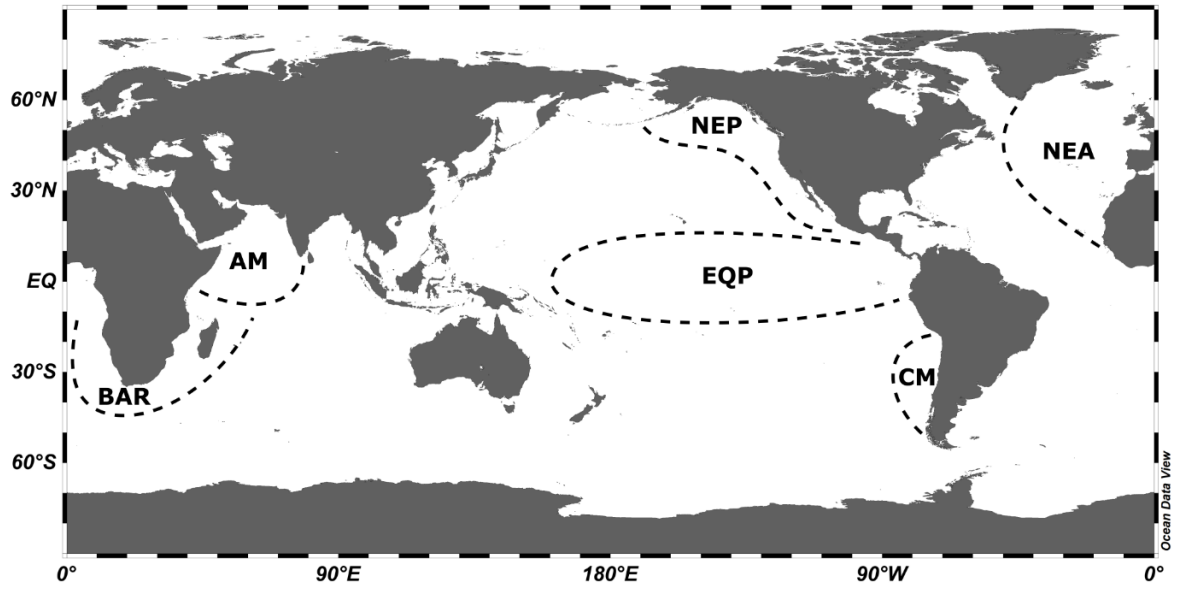

Figure 3.14: Map showing the locations of areas of interest discussed in section 4.3.3. NEP is the North East Pacific; EQP is the Equatorial Pacific; NEA is the North East Atlantic; CM is the Chilean Margin; AM is the Arabian Margin; BAR is the Benguela and Agulhas Region.

3.4.4 Faunal zones of interest

Through our RDA and analysis of census data we highlight six zones of interest, which present a combination of interesting peaks in faunal abundance, unusual appearance of particular species, and unique environmental conditions. These include: the Benguela and Agulhas region (BAR) (Little *et al.*, 1997; Emesis *et al.*, 2017); the North East Pacific (NEP) (Sautter and Thunell, 1991; Hendy *et al.*, 2000); the Equatorial Pacific (EQP) (Loubere and Paul, 2000; Faul *et al.*, 2000); the Arabian margin (AM) (Prell and Curry, 1981; Peeters *et al.*, 2002) and the Chilean margin (Marchant *et al.*, 1999; Haddam *et al.*, 2016). Our zones of interest can be seen in figure 3.14.

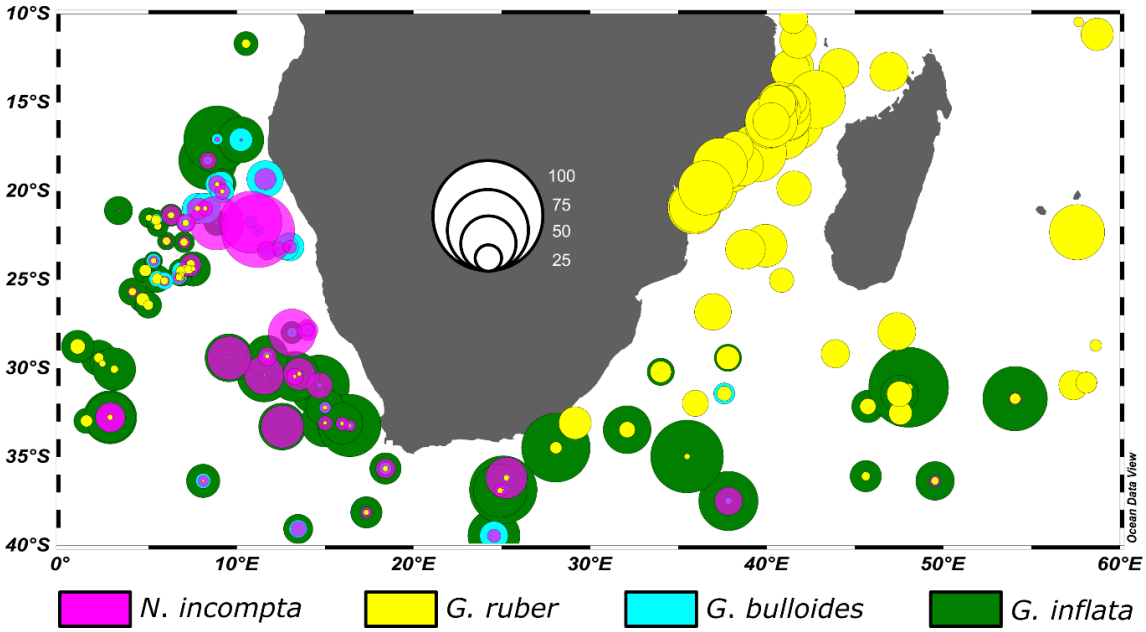

Figure 3.15: Regional bubble plot showing percentage abundance of foraminifera in the Benguela and Agulhas Region (BAR). Four species of planktic foraminifera dominate this region: N. incompta (purple); G. ruber (yellow); G. bulloides (light blue); G. inflata (dark Green). Bubble size denotes the percentage abundance of a particular species at that site.

3.4.4.1 *Benguela and Agulhas region*

The Benguela upwelling system situated on the southwest coastline of Africa. The region is characterised by several different upwelling systems ranging from seasonal to perennial (Hutchings *et al.*, 2009). The Benguela current is fed by consistent eddy currents generated in the Agulhas region (Hutchings *et al.*, 2009). Sites within the Benguela upwelling region score moderately with regards to RDA 2 (Figure 3.13) with southerly sites scoring highest. The predominantly negative scores of sites associated with this region is at odds with other upwelling sites across the global ocean (Figure 3.13), suggesting this region operates in a markedly different

manner. The influence of several distinct upwelling zones within the region (Hutchins *et al.*, 2009) may contribute to this. Faunally, *G. inflata* and *N. incompta* dominate in this region alongside small abundances of *G. bulloides* and *G. ruber* (Figure 3.15). Interestingly, *G. inflata* and *G. ruber* score highly with regards to RDA 2 (Figure 3.12), suggesting they are associated with a combination of phosphate, upwelling, and food availability. *G. inflata* also seem to dominate waters within the Agulhas current, with lower latitude coastal waters, which are still subject to Agulhas eddy activity, seeing higher proportions of *G. ruber*. *G. bulloides* abundance is highest in the northern regions of the upwelling zone and is associated with higher surface phosphate content (Figure 3.13 and Figure 3.15). This is in line with the assumption that *G. bulloides* is an opportunistic species and heavily dependent on food availability (Prell and Curry, 1982; Taylor *et al.*, 2018).

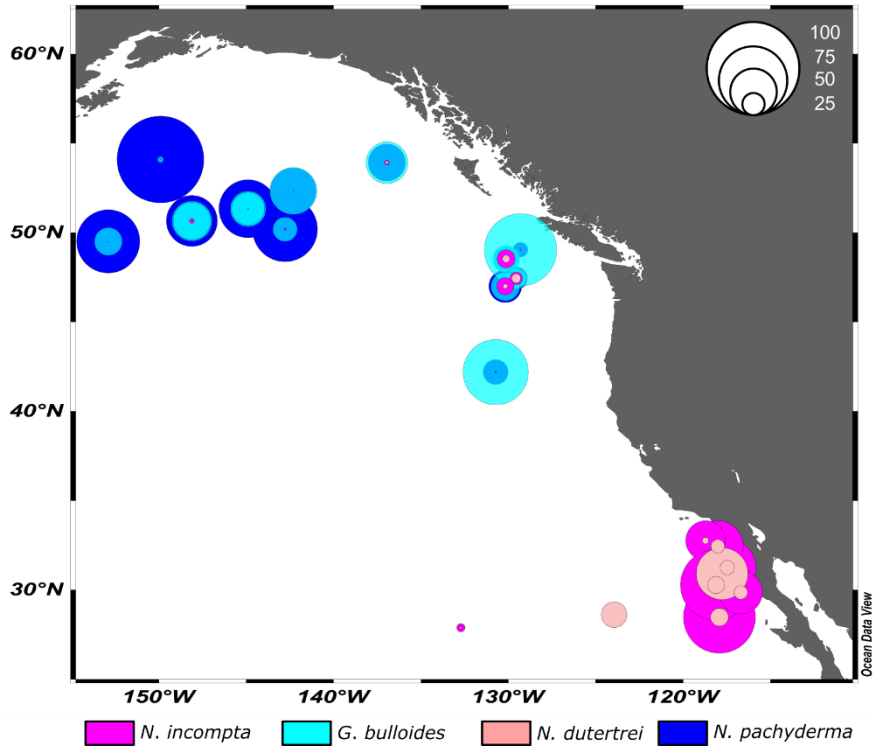

Figure 3.16: Regional bubble plot showing percentage abundance of foraminifera in the North East Pacific (NEP). Key foraminifera present within this region include: N. pachyderma (dark blue); G. bulloides (light blue); N. incompta (purple) and N. dutertrei (pink). Bubble size denotes percentage abundance of a particular species at that site.

3.4.4.2 *North East Pacific*

High nutrients and seasonal upwelling characterise the North East Pacific and California margin (Huyer, 1983; Harrison *et al.*, 2004). Upwelling along the California margin is primarily wind

driven (Huyer, 1983) and impacted by seasonal temperature changes. In the North Pacific subpolar gyre, low surface salinities cause surface stratification (Warren, 1983) for most of the year, with seasonal winter mixing caused by a combination of Ekman suction and lower winter SSTs (Huyer, 1983). Assemblages from sites in the North East Pacific score highly with regards to RDA 2 (Figure 3.13) (~1). This appears to be driven by high levels of surface phosphate combined with very low salinities (~32 p.s.u) (Figure 3.13). In terms of planktic foraminifera species, *G. bulloides* and *G. inflata* are most abundant in the upwelling region (Figure 3.16). *N. pachyderma* is also present at high latitudes and has been noted to have a potential affinity to upwelling and food availability (Davis *et al.*, 2016; Iwasaki *et al.*, 2017; Taylor *et al.*, 2018). *N. dutertrei* is also present in small abundances along the Californian coastal margin (Figure 3.16).

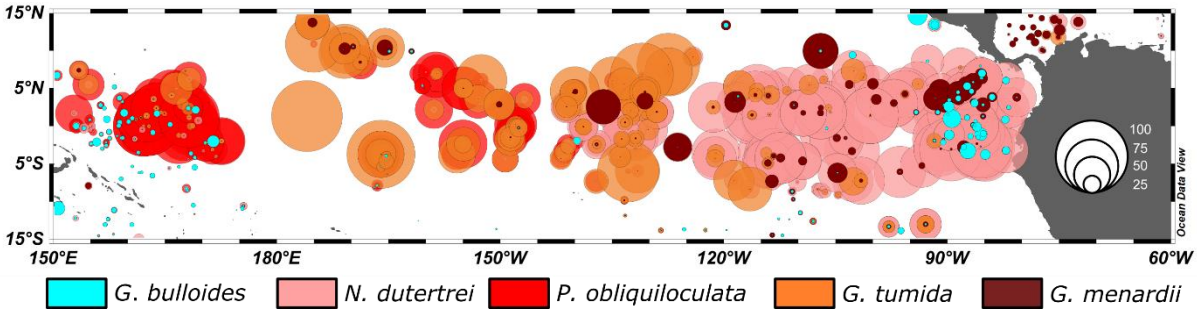

Figure 3.17: Regional bubble plot showing percentage abundance of foraminifera in the Equatorial Pacific. Five species of planktic foraminifera are present in high abundance: G. bulloides (light blue); N. dutertrei (pink); P. obliquiloculata (red); G. tumida (orange); G. menardii (dark red). Bubble size denotes percentage abundance of a particular species at that site.

3.4.4.3 *Equatorial Pacific*

The Equatorial Pacific is dominated by three main species of planktic foraminifera: *P. obliquiloculata* in the western equatorial Pacific, *G. tumida* in the central equatorial Pacific, and *N. dutertrei* in the eastern Equatorial Pacific. In the East Equatorial Pacific (EEP) highly productive waters contribute to between 20-50 % of the biological production in the modern oceans (Barber *et al.*, 1991). Characterised by zonally cool waters and strong upwelling, faunal assemblages score highly with regards to RDA 2 (Figure 3.13). Upwelling in this region is primarily driven by Ekman transport and a shallow thermocline (Wyrtki, 1981) which bring nutrient rich waters to this surface (Figure 3.13). The dominance of *N. dutertrei* in this region, is likely due to a combination of high surface nutrients, high productivity, and moderate to high temperatures. High surface water temperatures mean species usually associated with upwelling and nutrients such as *G. bulloides*, *G. inflata* and *N. incompta* are not present in high abundances. In the central and western Pacific, *P. obliquiloculata* and *G. tumida* are much more dominant.

This is likely because they are usually found to dwell deeper in the water column (100-400 m) (Schiebel and Hemleben, 2017) as surface waters in this region are barren with regards to nutrients. The dominance of *G. tumida* in the central equatorial region could be related to preservation, as its robust shell is able to withstand the corrosive deep waters found here. It is interesting to note that despite high SSTs across the region, small abundances of *G. bulloides* (0-25 %) are present along coastal margins in the east and west equatorial Pacific (Figure 3.17).

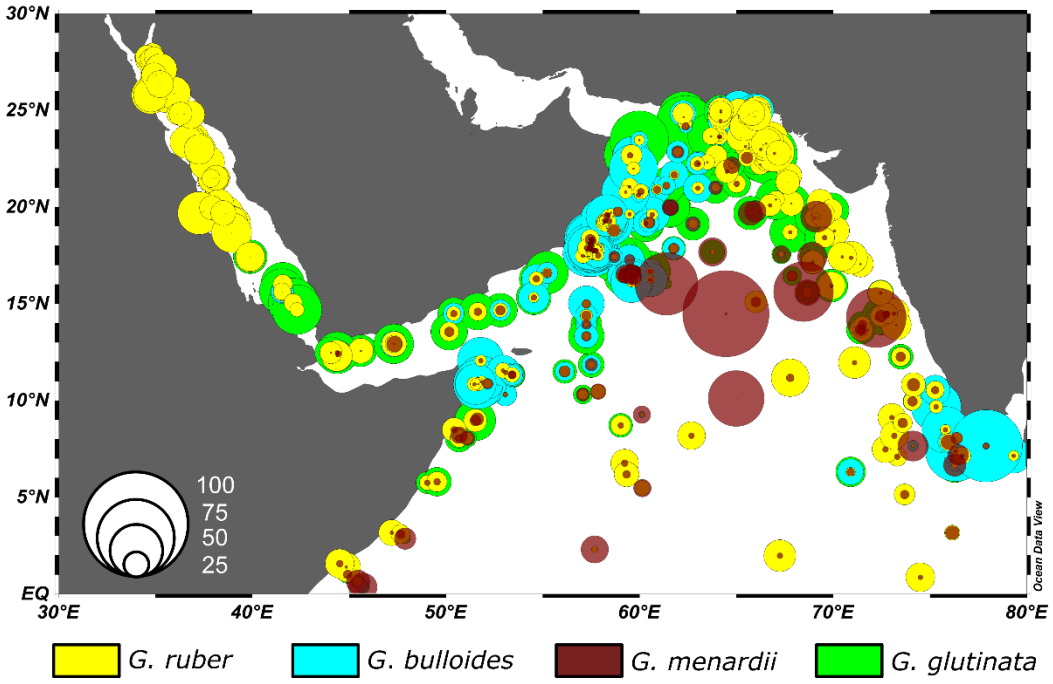

Figure 3.18: Regional bubble plot showing percentage abundance of foraminifera in the Arabian Margin. Foraminifera dominate in this region include: G. ruber (yellow); G. bulloides (light blue); G. menardii (dark red); G. glutinata (light green). Bubble size denotes percentage abundance of a particular species at that site.

3.4.4.4 *Arabian Sea*

The Arabian Sea is a widely documented upwelling region, primarily for its seasonally driven climatology and unusual faunal characteristics (Prell and Curry, 1981; Curry *et al.*, 1992; Peeters *et al.*, 1999; Peeters *et al.*, 2002; Schiebel *et al.*, 2007; Sadekov *et al.*, 2016). Oceanography in the Arabian Sea is dominated by seasonally reversing monsoon conditions (Prell and Curry, 1982; Prell *et al.*, 1992). The fact that this region is highly seasonal may be why it is the only major upwelling zone whose faunal assemblage does not correlate strongly with RDA 2 in our analysis (Figure 3.13). Our RDA is based on annual average data and therefore is unlikely to accurately explain strongly seasonal ecosystems. *G. bulloides* and *G. glutinata* are the dominant species of planktic foraminifera along the coastal margins of the upwelling zone (Figure 3.18), whilst *G. menardii* exhibits very high abundances further from the coast line (Figure 3.18). *G. ruber* is also

consistently abundant across the region as it is across these latitudes globally (Figure 3.18) (Bé *et al.*, 1977). Although not shown on our map (due to its small abundance) the Arabian Sea is home to a cryptic genotype of *N. pachyderma* (type VIII) (Darling and Wade, 2008). Usually found only in polar and subpolar waters, this genotype is inherently linked to the monsoonal upwelling system in the region (Darling and Wade, 2008). Interestingly samples from the Red Sea are dominated by *G. ruber* and *G. glutinata* suggesting these species may have a tolerance for high salinity environments.

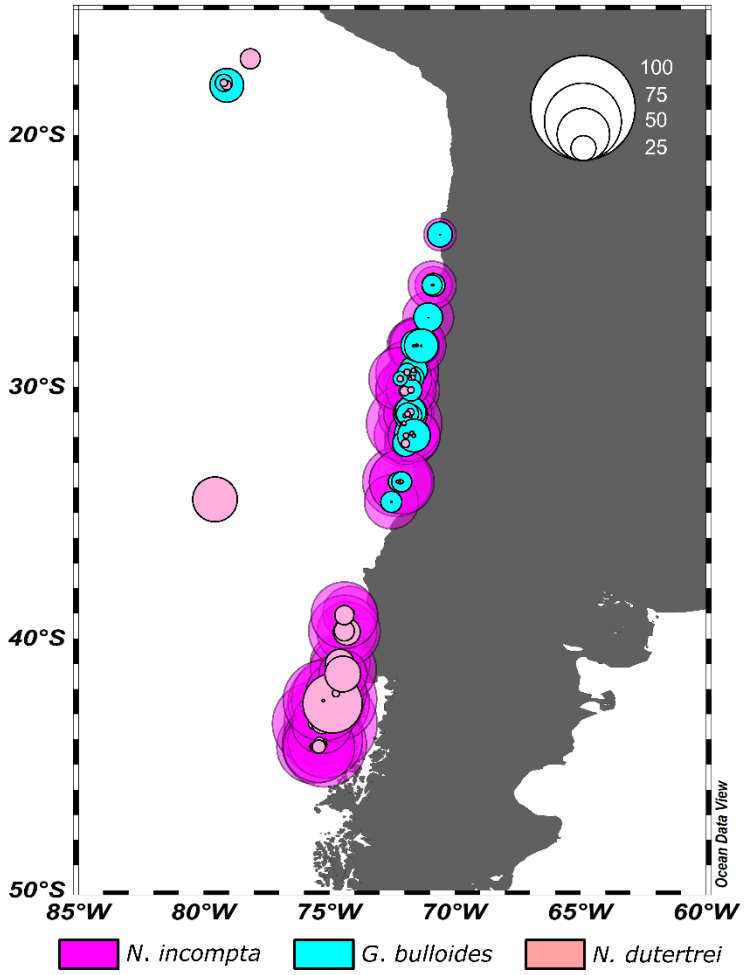

Figure 3.19: Regional bubble plot showing percentage abundance of foraminifera in the Chilean Margin. Three species of planktic foraminifera dominate: N. incompta (purple); G. bulloides (light blue); N. dutertrei (pink). Bubble size denotes percentage the abundance of a particular species at that site.

3.4.4.5 *Chilean margin*

The Chilean margin upwelling zone is a highly productive ocean region dominated by Ekman driven upwelling (Berger *et al.*, 1987; Marchant *et al.*, 1999). Southerly winds are the primary

driver for Ekman suction and are annually constant (Marchant *et al.*, 1999). High phosphate levels alongside moderate phosphate gradients are observed at our study sites in this region (Figure 3.13). Faunal assemblages on the Chilean margin score moderately with regards to RDA 2 (Figure 3.13) suggesting different faunal composition to zones such as the Benguela upwelling system and the East Equatorial Pacific (Figure 3.19). Indeed, faunally, the dominate species in this region is *N. incompta* which exhibits consistently high abundance (50-80 %). *N. dutertrei* is also present, particularly in the higher latitude areas of the upwelling zone. In lower latitudes, *G. bulloides* is once again present in small abundances (0-30 %).

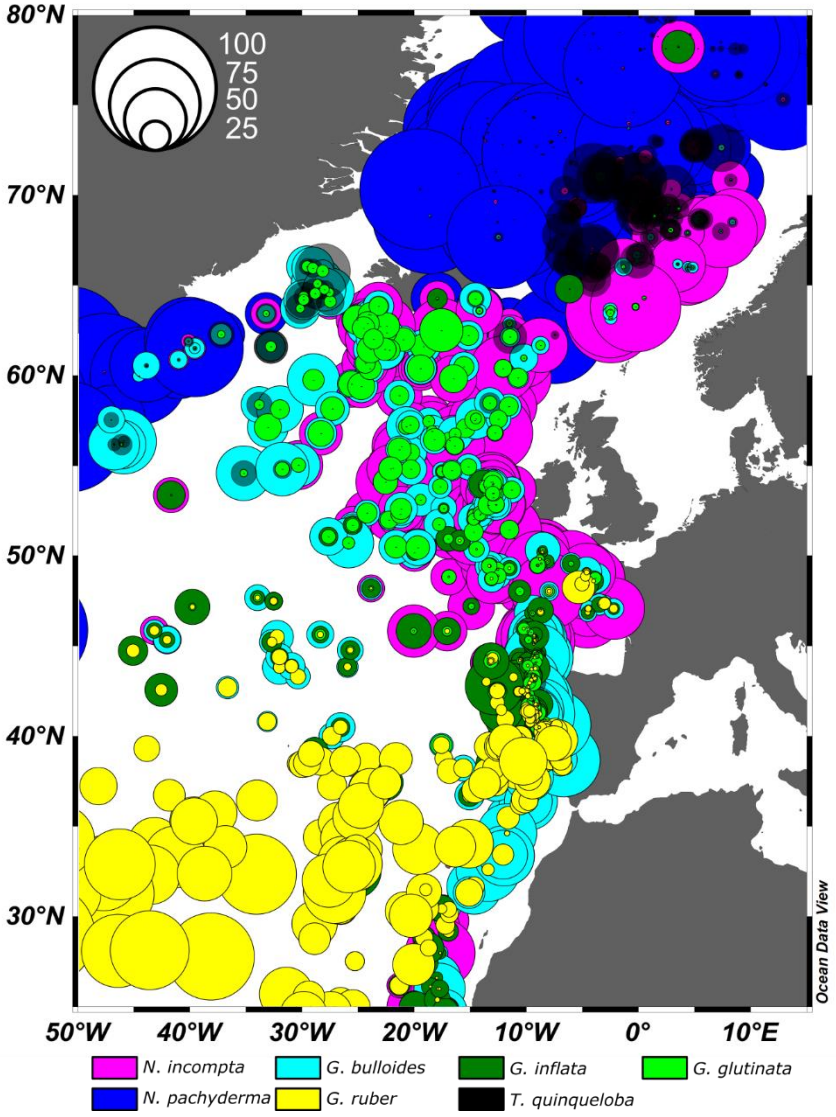

Figure 3.20: Regional bubble plot showing percentage abundance of foraminifera in the North East Atlantic. Seven species of planktic foraminifera dominate this region: N. pachyderma (yellow); T. quinqueloba (black); N. incompta (purple); G. bulloides (light blue); G. inflata (dark green); G. glutinata (light green). Bubble size denotes the percentage abundance of a particular species at that site.

3.4.4.6 *North Atlantic*

The North Atlantic represents a key region for the interaction between the surface and deep ocean, via North Atlantic Deep Water formation, so has been widely studied within paleoclimatology. Within our compiled core-top compilation, seven species of planktic foraminifera dominate above 25° N (Figure 3.20). In the lower latitude open ocean regions *G. ruber* is present in greatest abundance. At latitudes greater than 45° N, *N. incompta* dominates alongside moderate abundances of *G. bulloides* and *G. inflata* (Figure 3.20). In the western North Atlantic, around the Greenland margin, colder surface waters (Locarnini *et al.,* 2013) drive an increased abundance of *N. pachyderma* at latitudes of ~60° N. At latitudes greater than 70° N in the eastern North Atlantic *N. pachyderma* makes up more than 90 % of most assemblages, with smaller influences from *T. quinqueloba* and *N. incompta*. Much of the variation in North Atlantic sediments is driven by temperature. This is highlighted in figure 3.10, where a close correspondence between RDA 1 sites scores and temperature in the North Atlantic is observed. Interestingly, sites along the eastern margin of the North Atlantic are dominated by a high abundance of *G. bulloides*, a known opportunistic species (Darling and Wade, 2008; Taylor *et al.,* 2018), down to lower latitudes of 25° N. This has been attributed to seasonal coastal upwelling between May and September (Salgueiro *et al.,* 2008).

3.4.5 Dissolution bias in planktic foraminifera assemblages

The extent to which planktic foraminifera tests dissolve prior to burial depends on the calcite saturation state ($\Omega_{calcite}$) of the water column, the sedimentation rate, and the species of planktic foraminifera in question (Berger, 1968; Berger, 1971). To accurately reconstruct past climates using planktic foraminifera census data, it is important to consider the effects of dissolution (Berger, 1968). However, quantifying the effects of dissolution has proven difficult, especially when detailed knowledge of species dissolution susceptibility and bottom water carbonate saturation conditions are absent. Berger *et al.,* (1982) note that key indicators of dissolution included the amount of fragmentation of foraminifera tests and the species diversity of assemblages when compared to expected values. Recent studies also note foraminifera residence times within undersaturated zones at the sediment-water interface may influence dissolution rates across the globe (De Villiers, 2005), as well as shell weight loss that occurs as the foraminifera sinks through the water column (Schiebel *et al.* 2007). It is this combination of drivers that adds complexity to the analysis of foraminifera dissolution.

It is difficult to extract a quantitative dissolution index from our database due to the large amount of data present, lack of foraminifera accumulation data, and lack of fragmentation data. However, we have performed additional analyses to assess the findings of previous studies. One method of

assessing dissolution involves the characterisation of planktic foraminifera depending on their dissolution susceptibility (Berger, 1973; Haddam, 2016). Dissolution susceptibility is defined as the easy at which a foraminifera is dissolved in seawater and is primarily a qualitative term. Berger (1973) proposed a solution index determined by taking the ratio of solution resistant species against the remainder of the assemblage. Haddam *et al.,* (2016) also investigated dissolution through species characterisation. They used three tiers of characterisation: dissolution-sensitive species; moderately sensitive species and dissolution-resistant species to assess the changing relative abundance of all species with ocean depth. We assess the relative abundance of six key species of planktic foraminifera against estimated bottom water $\Omega_{calcite}$ to assess the relationship between different species and dissolution. From the twelve most abundant species in the global ocean we use the three most susceptible species *G. ruber, T. sacculifer,* and *G. bulloides* and the three most resistant species *G. tumida, N. pachyderma, P.obliquiloculata* (as given by Schiebel and Hemleben, 2017). When compared to ocean $\Omega_{calcite}$ we find clear association between high relative abundances of the three dissolution-resistant species and low $\Omega_{calcite}$ suggesting an enrichment of these species at very low $\Omega_{calcite}$ (Figure 3.21). This is typified by *G. tumida* where abundances above 25 % are only found at $\Omega_{calcite}$ lower than 1 (Figure 3.21). Interestingly, those species regarded as highly susceptible to dissolution do not exhibit an obvious relationship with $\Omega_{calcite}$. These species are found at higher $\Omega_{calcite}$ but, apart from *T. sacculifer,* their abundance remains high at lower $\Omega_{calcite}$ (Figure 3.21). This likely reflects the dominance of surface ocean conditions over dissolution bias in marine sediments.

We also assess how species richness may be affected by planktic foraminifera dissolution. We would expect that as $\Omega_{calcite}$ decreases, species richness in core-top planktic foraminifera assemblages would decrease as dissolution susceptible species are removed. However, we see no relationship with either $\Omega_{calcite}$ or core depth in our database (Figure 3.22). This may be because species richness is often the same for multiple sites within our dataset, clouding possible trends in the data. To combat this, we calculated the average abundance of a sample which provides an indirect method for assessing species richness (Figure 3.22). A high average abundance corresponds directly to lower species richness, as few species dominate, with low average abundance reflecting high species richness (Figure 3.22). When this is plotted against $\Omega_{calcite}$ we see a more obvious trend with high average abundances associated with low $\Omega_{calcite}$ (Figure 3.22). Despite this, there are still several low average abundance (high richness) sites occurring at low $\Omega_{calcite}$, suggesting the relationship between $\Omega_{calcite}$ and average abundance is more complex.

Our analysis adds weight to the early work of Berger (1968), Berger (1970), Dittert *et al.,* 1999 and Schiebel and Hemleben (2017) suggesting clear differences in dissolution susceptibility of

individual species and that planktic assemblages from low $\Omega_{calcite}$ regions are likely to be affected by dissolution and be enriched in dissolution resistant species. This has key implications for down-core studies, particularly in high latitude areas such as the North Atlantic, where the abundance of *N. pachyderma* is used to track changes in polar front movement and ocean temperature (Bond *et al.*, 1993; Barker *et al.*, 2009; Barker *et al.*, 2015). Work by Taylor *et al.*, (2018) showed a dissolution bias of *N. pachyderma* over warmer species such as *G. bulloides*. During glacial and stadial periods with corrosive bottom waters (Yu *et al.*, 2014), this bias may be increased, leading to a possible over estimation of *N. pachyderma* abundance. With this in mind, it is important to take into account potential dissolution bias when assessing changes in planktic foraminifera assemblages in the past.

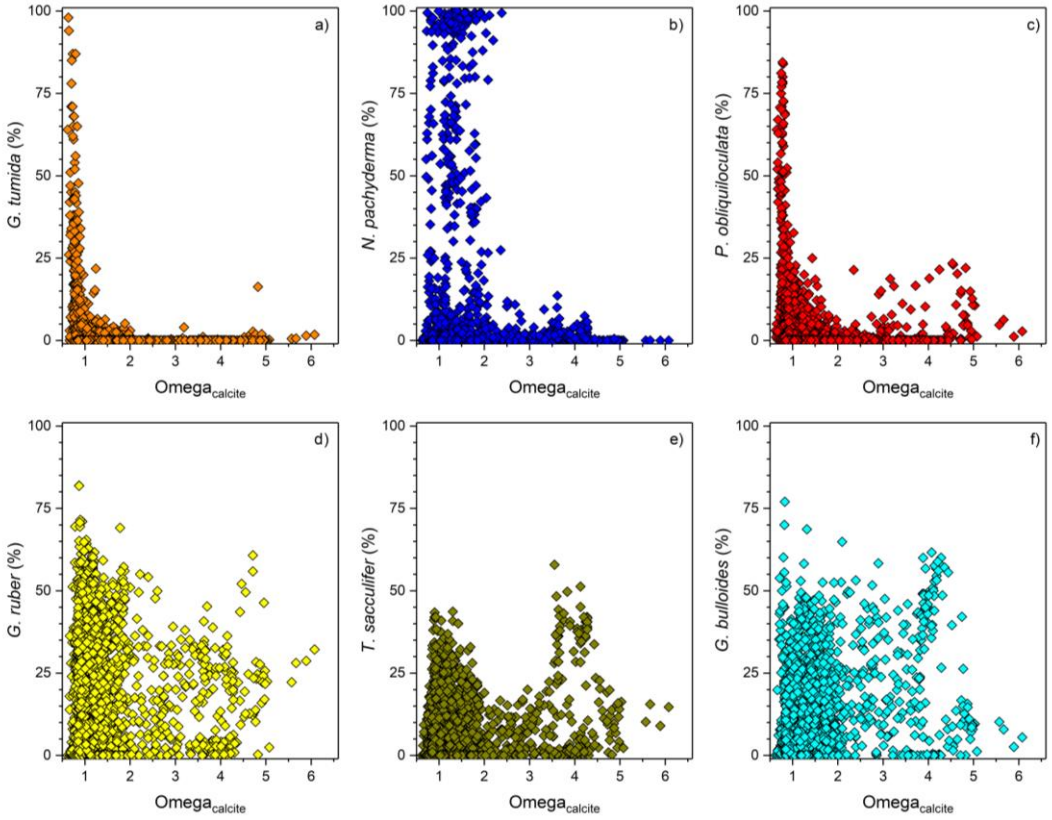

Figure 3.21: Planktic foraminifera species vs bottom water Omega calcite. ***a-c****) Dissolution resistant species of planktic foraminifera (Schiebel and Hemleben, 2017), G. tumida (orange), N. pachyderma (dark blue), P. obliquiloculata (red).* ***d-f****) Dissolution susceptible species (Schiebel and Hemleben, 2017), G. ruber (yellow), T. sacculifer (gold), G. bulloides (light blue).*

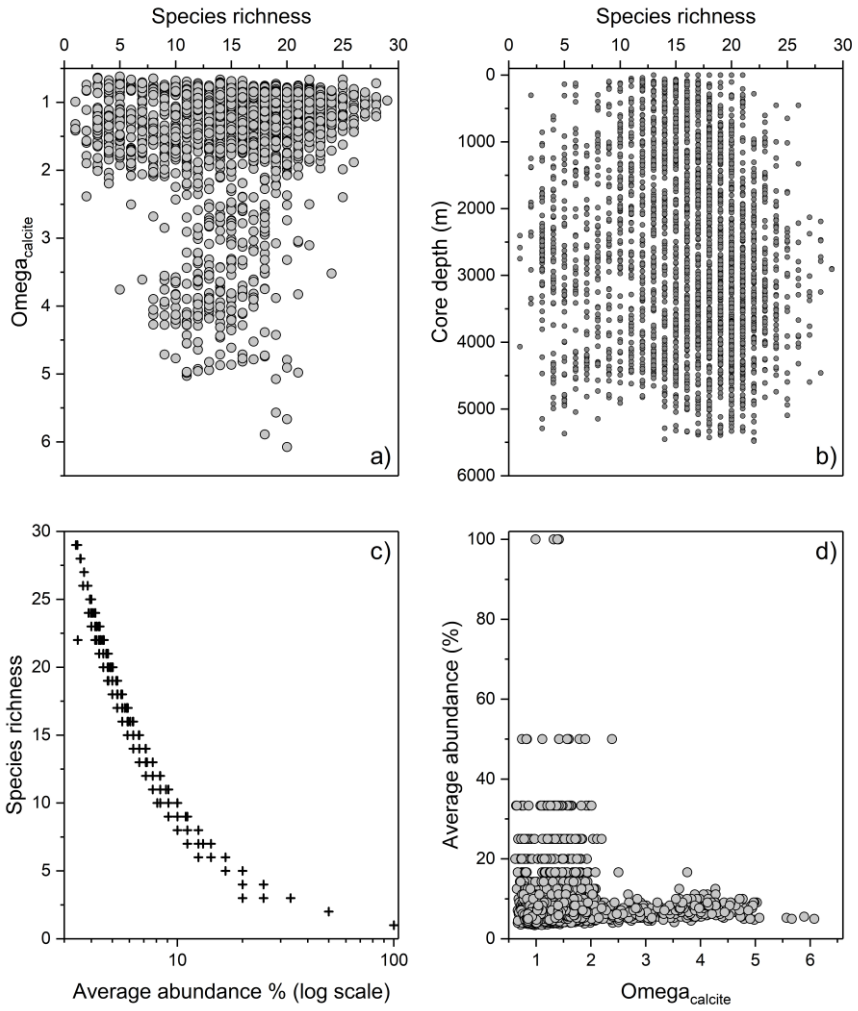

Figure 3.22: Cross plots highlighting the influence of dissolution on planktic foraminifera assemblages. ***a)*** *Bottom water omega calcite plotted against species richness for each site in our global compilation.* ***b)*** *Species richness plotted against core depth (m).* ***c)*** *Highlights the relationship between average abundance (%) and species richness for the sites within our study.* ***d)*** *Average abundance plotted alongside Omega calcite showing high average abundance occurring at sites with low bottom water Omega calcite.*

3.5 Conclusions

Using our updated database of planktic foraminifera census data and estimated environmental variables we describe in detail the distribution of the twelve major species of planktic foraminifera in the modern ocean. In addition, we evaluate the key ecology drivers of individual species of planktic foraminifera and assess how these drivers affect variance in the whole planktic foraminifera assemblage.

The global distributions of the twelve most abundant species of planktic foraminifera are shown together in figure 3.23. Following on from Bé (1977), *N. pachyderma*, *G. bulloides* and *T. quinqueloba* dominate the polar and sub-polar oceans with *N. incompta*, *G. inflata* and *G. bulloides* most commonly found in transitional waters (Figure 3.23). In sub-tropical waters, *G. ruber* is most consistently abundant whilst *G. glutinata* and *G. menardii* are prominent in the Arabian Sea (Figure 3.23). *P. obliquiloculata* and *G. tumida* dominate assemblages in the central and western equatorial Pacific, whilst *N. dutertrei* is most abundant in the East Equatorial Pacific (Figure 3.23). In the tropical Atlantic, *G. ruber* and *T. sacculifer* are the two most dominant species (Figure 3.23).

The only major species of planktic foraminifera to show a strong relationship with any environmental variable is *N. pachyderma*. We find a sigmoidal relationship between the relative abundance of *N. pachyderma* and temperature between 0-50 m in the water column ($R^2 = 0.94$). This demonstrates the use of percentage *N. pachyderma* as a potentially semi-quantitative tool in reconstruction of past temperatures. Caution should still be taken when using percentage changes in *N. pachyderma* to reconstruct past climates, as dissolution can bias assemblages towards high percentages of this species. *G. ruber* percentage abundance and overall species richness have a weak negative relationship with phosphate content in the surface ocean ($R^2 = 0.36$ and $R^2 = 0.24$). This suggests that in low nutrient environments competition is spread relatively evenly through the assemblage with no single species dominating and *G. ruber* making up a consistently high proportion of the assemblage. The opposite is true in high nutrient waters where one species is more likely to dominate an assemblage – this is seen in the EEP where *N. dutertrei* is highly abundant. This relationship also suggests that *G. ruber* can capitalise on intermittent feeding opportunities within water that is usually nutrient poor.

Through redundancy analysis we investigated environmental controls on variance within planktic foraminifera assemblages. We found that, in line with previous work of Morey *et al.*, (2005), the primary axis of variance (RDA 1) was controlled strongly by temperature (Figure 3.10). The species which are most important to this correlation (the species with the highest RDA scores) are *N. pachyderma* and *N. incompta*, which characterise cold waters, and *G. ruber* and *T. sacculifer* which characterise warm waters (Figure 3.12). The secondary axis of variance (RDA 2) is more complex and is likely to reflect several environmental parameters including phosphate content, salinity, and phosphate gradient. The combination of these environmental parameters and the site scores for our study area suggest RDA 2 is linked to upwelling (Figure 3.13). The species scoring highest for RDA 2 are *G. inflata*, a known upwelling species (Schiebel and Hemleben, 2017), *G. ruber*, and *N. dutertrei*.

We look in detail at six regions of interest in the modern ocean: Benguela; EEP; North East Pacific; Arabian Sea, Chilean margin and the North Atlantic. The first five regions are all characterised by upwelling. These upwelling regions show extensive differences in hydrology and faunal assemblage. Upwelling controls on faunal variance are also represented in our redundancy analysis, which does an impressive job of highlighting the major perennial upwelling centres such as the southern Benguela upwelling region and the East Equatorial Pacific. However, it struggles to definitively pick out the Arabian margin upwelling region which may be because of the highly seasonal upwelling regime which operates in that area. In the North Atlantic, temperature is the dominant control on species distribution and variance within assemblages, except along the Iberian margin, which is characterised by seasonal upwelling and has increased abundances of *G. bulloides* and *N. incompta*.

Dissolution of planktic foraminifera from core-top assemblages adds additional complexity to the use of census data in paleo-reconstructions. Although we find no significant relationship between dissolution resistant species and bottom water omega values, we do see increased abundance of these species at low omega values. In addition, we see a similar relationship when comparing average relative abundance in an assemblage to bottom water omega. Whilst, dissolution may be difficult to characterise in planktic foraminifera assemblages, it is an important factor to bear in mind when reconstruction past ocean environments.

The characterisation of faunal assemblages and upwelling zones in the modern ocean has implications for paleo-reconstructions. The strong control of temperature on faunal assemblages promotes the use of changes in assemblage to trace past temperature change, and the identification of key upwelling species for specific regions means that these can be used as indicators of changes in paleo-upwelling, a key variable when investigating past changes in CO_2 and ocean fertility. This study provides a firm basis for future work through the publication of a new global foraminifera database and provides insight into key proxies favourable to working with foraminifera. Temperature and ocean productivity or fertility are clearly observed to be closely linked to changes in foraminifera assemblage. Using assemblage data alongside geochemical proxies for temperature and productivity has the potential to vastly enhance the reliability of both types of proxies and can be used to scrutinise interpretations. Future work should focus on further calibrations using different criteria. This could include looking at summer vs winter trends or zonal changes in temperature to investigate upwelling in more detail.

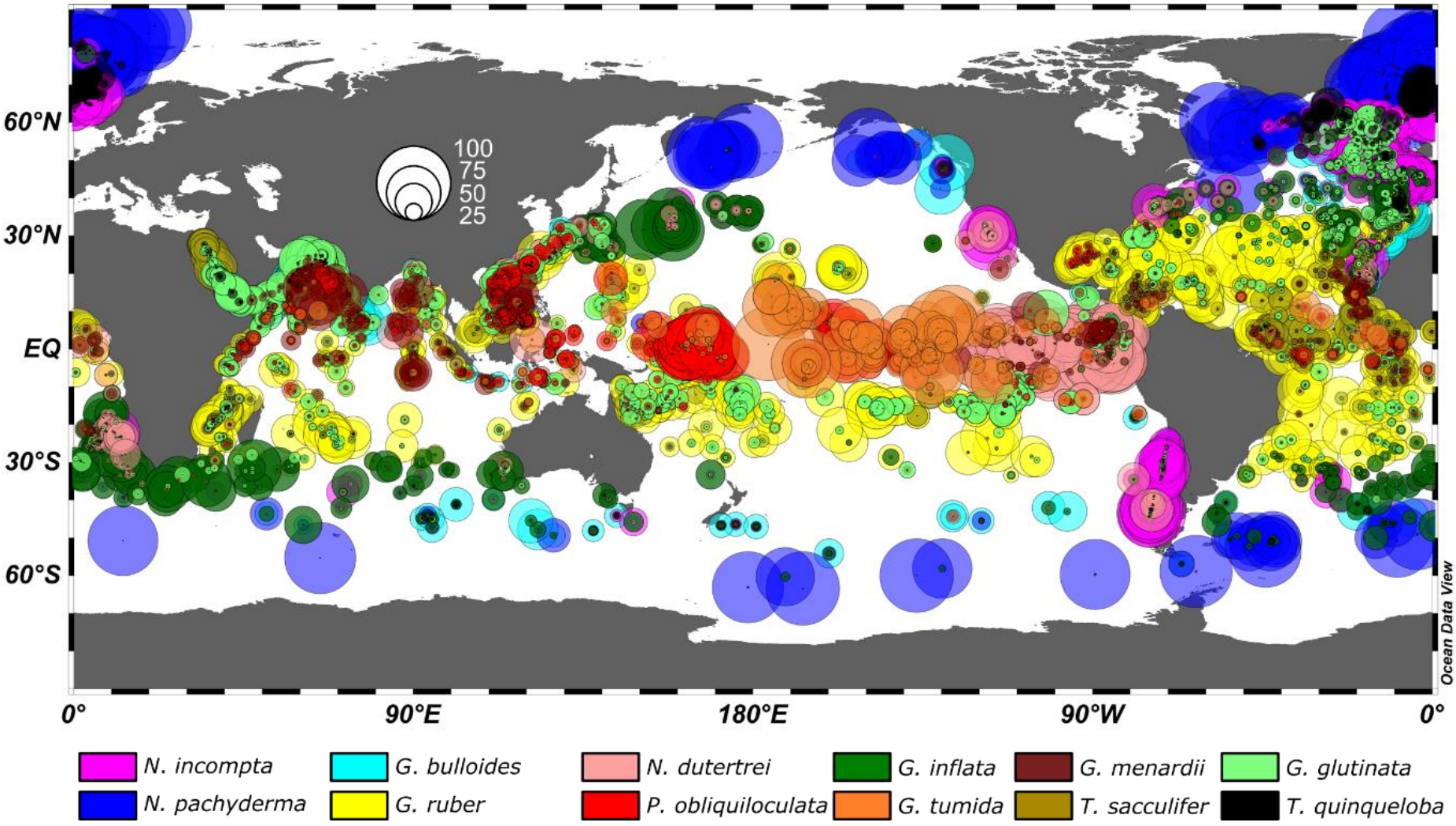

Figure 3.23: Global distribution of 12 species of planktic foraminifera in the modern ocean based on core-top assemblages. Bubble size denotes the percentage abundance of a particular species in an assemblage. Bubble colour denotes different species of planktic foraminifera. Not all species of planktic foraminifera found in modern core-tops are represented on this map.

3.6 References

André, A. et al., 2014. SSU rDNA divergence in planktonic foraminifera: Molecular taxonomy and biogeographic implications. *PLoS ONE*, 9(8).

Balsam, W.L. & Flessa, K.., 1978. Patterns of planktonic foraminiferal abundance and diversity in surface sediments of the western North Atlantic. *Marine Micropaleontology*, 3(3), pp.279–294.

Barber, R.T. & Chavez, F., 1991. Regulation of Primary Productivity Rate in the Equatorial Pacific. *Limnology Oceanography*, 36(8), pp.1803–1815.

Barker, S. et al., 2015. Icebergs not the trigger for North Atlantic cold events. *Nature*, 520(7547), pp.333–336.

Barker, S. et al., 2009. Interhemispheric Atlantic seesaw response during the last deglaciation. *Nature*, 457, pp.1097–1102.

Bé, A.W.H., 1977. An ecological, zoogeographic and taxonomic review of recent planktonic foraminifera. *Oceanic micropaleontology*, pp.1–100.

Bé, A.W.H. & Hutson, W.H., 1977. Ecology of Planktonic Foraminifera and Biogeographic Patterns of Life and Fossil Assemblages in the Indian Ocean Ecology of planktonic foraminifera and biogeographic patterns of life and fossil assemblages in the Indian Ocean *. *Micropaleontology*, 23(4), pp.369–414.

Berelson, W.M. et al., 2007. Relating estimates of CaCO3production, export, and dissolution in the water column to measurements of CaCO3rain into sediment traps and dissolution on the sea floor:A revised global carbonate budget. *Global Biogeochemical Cycles*, 21(1), pp.1–15.

Berger, W.H., Bonneau, M.--C. & Parker, F.L., 1982. Foraminifera on the deep-sea floor: lysocline and dissolution rate. *Oceanologica acta*, 5(2), pp.249–258.

Berger, W.H. & Parker, F.L., 1970. Diversity of planktonic foraminifera in deep-sea sediments. *Science*, 168(3937), pp.1345–1347.

Berger, W.H., 1968. Planktonic Foraminifera: selective solution and paleoclimatic interpretation. *Deep Sea Research and Oceanographic Abstracts*, 15(1), pp.31–43.

Berger, W.H., 1987. *Productivity and organic carbon flux. Part I. Overview and maps of primary production and export production*, Scripps Inst. Oceanography.

Bijma, J., Faber, W.W. & Hemleben, C., 1990. Temperature and salinity limits for growth and survival of some planktonic foraminifers in laboratory cultures. *The Journal of Foraminiferal Research*, 20(2), pp.95–116.

Bond, G. et al., 1993. Correlations between climate records from North Atlantic sediments and Greenland ice. *Nature*, 363, pp.143–147.

Bond, G. et al., 1992. Evidence for massive discharges of iceberg into the North Atlantic ocean during the last glacial period. *Letters to Nature*, 360, pp.245–249.

Bond, G. et al., 1997. A pervasive Millenial-Scale Cycle in North Atlantic Holocene and Glacial Climates. *Science*, 278(November), pp.1257–1266.

Boyer, T.P. et al., 2013. World Ocean Database 2013.

Bradshaw, J.S., 1959. Ecology of living planktonic foraminifera in the North and equatorial Pacific Ocean. *Foraminiferal Research*, 10, pp.25–64.

Bradshaw, J.S., 1959. Ecology of living planktonic foraminifera in the North and equatorial Pacific Ocean. Foraminiferal Research, 10, pp.25–64.

Chapman, M.R., 2010. Seasonal production patterns of planktonic foraminifera in the NE Atlantic Ocean: Implications for paleotemperature and hydrographic reconstructions. *Paleoceanography*, 25(1).

CLIMAP Project Members., 1976. Climate Long-Range Investigation, Mapping and Prediction Project.

Curry, W.B. et al., 1992. Foraminiferal production and monsoonal upwelling in the Arabian Sea: evidence from sediment traps. *Geological Society, London, Special Publications*, 64(1), pp.93–106.

Darling, K.F. et al., 2004. Molecular evidence links cryptic diversification in polar planktonic protists to Quaternary climate dynamics. *Proceedings of the National Academy of Sciences*, 101(20), pp.7657–7662.

Darling, K.F. et al., 2006. A resolution for the coiling direction paradox in Neogloboquadrina pachyderma. *Paleoceanography*, 21(2), pp.1–14.

Darling, K.F. et al., 2003. Seasonal distribution of genetic types of planktonic foraminifer morphospecies in the Santa Barbara Channel and its paleoceanographic implications. *Paleoceanography*, 18(2), pp.1–10.

Darling, K.F. & Wade, C.M., 2008. The genetic diversity of planktic foraminifera and the global distribution of ribosomal RNA genotypes. *Marine Micropaleontology*, 67(3–4), pp.216–238.

Darling, K.F. et al., 1997. Planktic foraminiferal molecular evolution and their polyphyletic origins from benthic taxa. *Marine Micropaleontology*, 30(4), pp.251–266.

Darling, K.F. et al., 2017. Genetic diversity and ecology of the planktonic foraminifers Globigerina bulloides, Turborotalita quinqueloba and Neogloboquadrina pachyderma off the Oman margin during the late SW Monsoon. *Marine Micropaleontology*, 137(April), pp.64–77.

Davis, C. V. et al., 2016. Seasonality in Planktic Foraminifera of the Central California Coastal Upwelling Region. *Biogeosciences Discussions*, pp.5139–5150.

D'Croz, L., Del Rosario, J.B. & Gomaz, J.A., 1991. Upwelling and phytoplankton in the Bay of Panama. *Rev. Biol. Trop.*, 39(2), pp.233–241.

De Villiers, S., 2005. Foraminiferal shell-weight evidence for sedimentary calcite dissolution above the lysocline. *Deep-Sea Research Part I: Oceanographic Research Papers*, 52(5), pp.671–680.

Dittert, N. & et al., 1999. Carbonate dissolution in the deep-sea: methods, quantification and paleoceanographic application. In *Uses of proxies in paleoceanography*. Springer Berlin Heidelberg, pp. 255–284.

Eguchi, Nobuhisa O. Kawahata, H., Taira, A., 1999. Seasonal response of planktonic foraminifera to surfce ocean conditions: Sediment trap results from the central North Pacific Ocean. *Journal of Oceanography*.

Fairbanks, R.G. & Wiebe, P.H., 1980. Foraminifera and chlorophyll maximum: Vertical distribution, seasonal succession and paleoceanographic distribution. *Science*, 209(4464), pp.1524–1526.

Faul, K., Ravelo, A.C. & Delaney, M., 2000. Reconstructions of upwelling, productivity, and photic zone depth in the eastern equatorial Pacific Ocean using planktonic foraminiferal stable isotopes and abundances. *Foraminiferal Research*, 30(2), pp.110–125.

Fenton, I.S. et al., 2016. Environmental Predictors of Diversity in Recent Planktonic Foraminifera as Recorded in Marine Sediments. *Plos One*, 11(11).

Field, D.B., 2004. Variability in vertical distributions of planktonic foraminifera in the California current: Relationships to vertical ocean structure. *Paleoceanography*, 19(2).

Garcia, H.E. et al., 2014. World Ocean Atlas 2013, Volume 4 : Dissolved Inorganic Nutrients (phosphate, nitrate, silicate). *NOAA Atlas NESDIS 76*, 4(September).

Haddam, N.A. et al., 2016. Improving past sea surface temperature reconstructions from the Southern Hemisphere oceans using planktonic foraminiferal census data. *Paleoceanography*, 31(6), pp.822–837.

Harrison, P.J. et al., 2004. Nutrient and plankton dynamics in the NE and NW Gyres of the subarctic Pacific Ocean. *Journal of Oceanography*, 60(3), pp.93–117.

Hemleben, C., Spindler, M. & Anderson, R.O., 1989. *Modern Planktonic Foraminifera*, Springer-Verlag New York Inc.

Hendy, I.L. et al., 2004. Intermittent existence of a southern Californian upwelling cell during submillennial climate change of the last 60 kyr. *Paleoceanography*, 19(3), pp.1–15.

Hilbrecht, H., 1997. Morphologic gradation and ecology in Neogloboquadrina pachyderma and N. dutertrei (planktic foraminifera) from core top sediments. *Marine Micropaleontology*, 31(1–2), pp.31–43.

Hutchings, L. et al., 2009. The Benguela Current: An ecosystem of four components. *Progress in Oceanography*, 83(1–4), pp.15–32.

Hutson, W.H., 1980. The Agulhas current during the Late Pleistocene: Analysis of modern faunal analogs. *Science*, 207(4426), pp.64–66.

Huyer, A., 1983. Coastal upwelling in the California Current System. *Progress In Oceanography*, 12(3), pp.259–284.

Imbrie, J. & Kipp, N., 1971. A new micropalaeontological method for quantitative paleoclimatology: Application to late Pleistocene Caribbean core V28-238. In K. K. Turekian, ed. *The late Cenozoic Glacial Ages*. Yale Univ. Press, New Haven, Conn, pp. 77–181.

Iwasaki, S. et al., 2017. Horizontal and vertical distributions of planktic foraminifera in the subarctic North Pacific. *Marine Micropaleontology*.

Jonkers, L. et al., 2010. Seasonal stratification, shell flux, and oxygen isotope dynamics of leftcoiling N. pachyderma and T. quinqueloba in the western subpolar North Atlantic. *Paleoceanography*, 25(2), pp.1–13.

Kemle-vin-Mucke, S. & Hemleben, C., 1999. Planktic Foraminifera. In E. Boltovskoy, ed. *South Atlantic zooplankton*. Backhuys Publishers, Leiden, pp. 43–67.

Kipp, N., 1976. New transfer function for estimating past sea-surface conditions from sea-bed distribution of planktonic foraminiferal assemblages in the North Atlantic. *Geological Society of America, Memoir*, 145, pp.3–41.

Kucera, M., 2007. Planktonic Foraminifera as Tracers of Past Oceanic Environments. In *Proxies in Late Cenozoic Paleoceanography*. pp. 213–262.

Kucera, M. et al., 2005. Multiproxy approach for the reconstruction of the glacial ocean surface (MARGO). *Quaternary Science Reviews*, 24(7–9 SPEC. ISS.), pp.813–819.

Kucera, M. et al., 2005b. Reconstruction of sea-surface temperatures from assemblages of planktonic foraminifera: Multi-technique approach based on geographically constrained calibration data sets and its application to glacial Atlantic and Pacific Oceans. *Quaternary Science Reviews*, 24(7–9 SPEC. ISS.), pp.951–998.

Kuroyanagi, A. & Kawahata, H., 2004. Vertical distribution of living planktonic foraminifera in the seas around Japan. *Marine Micropaleontology*, 53(1–2), pp.173–196.

Kuroyanagi, A. et al., 2008. Seasonal to interannual changes in planktonic foraminiferal assemblages in the northwestern North Pacific: Sediment trap results encompassing a warm period related to El Niño. *Palaeogeography, Palaeoclimatology, Palaeoecology*, 262(1–2), pp.107–127.

Legendre, P. & Legendre, L., 1998. *Numerical Ecology*, Elsevier B.V.

Lehman, S.J. & Keigwin, L.D., 1992. Sudden changes in North Atlantic circulation during the last deglaciation. *Nature*, 356(6372), pp.757–762.

Li, B., Jian, Z. & Wang, P., 1997. Pulleniatina obliquiloculata as a paleoceanographic indicator in the southern Okinawa Trough during the last 20,000 years. *Marine Micropaleontology*, 32, pp.59–69.

Little, M.G. et al., 1997. Rapid palaeoceanographic changes in the Benguela Upwelling System for the last 160,000 years as indicated by abundances of planktonic foraminifera. *Palaeogeography, Palaeoclimatology, Palaeoecology*, 130(1–4), pp.135–161.

Locarnini, R.A. et al., 2013. *World Ocean Atlas 2013. Vol. 1: Temperature.*

Lončarić, N. et al., 2006. Oxygen isotope ecology of recent planktic foraminifera at the central Walvis Ridge (SE Atlantic). *Paleoceanography*, 21(3), pp.1–18.

Loubere, P., 2000. Marine control of biological production in the eastern equatorial Pacific Ocean. *Nature*, 406(August), pp.497–500.

Malmgren, B. & Nordlund, U., 1996. Application of artificial neural network to chemostratigraphy. *Paleoceanography*, 11(4), pp.505–512.

Marchant, M., Hebbeln, D. & Wefer, G., 1999. High resolution planktic foraminiferal record of the last 13,300 years from the upwelling area off Chile. *Marine Geology*, 161(2–4), pp.115–128.

Mohtadi, M., Hebbeln, D. & Marchant, M., 2005. Upwelling and productivity along the Peru-Chile Current derived from faunal and isotopic compositions of planktic foraminifera in surface sediments. *Marine Geology*, 216(3), pp.107–126.

Morard, R. et al., 2013. Ecological modelling of the temperature dependence of cryptic species of planktonic Foraminifera in the Southern Hemisphere. *Palaeogeography, Palaeoclimatology, Palaeoecology*, 391, pp.13–33.

Morey, A.E., Mix, A.C. & Pisias, N.G., 2005. Planktonic foraminiferal assemblages preserved in surface sediments correspond to multiple environment variables. *Quaternary Science Reviews*, 24(7–9 SPEC. ISS.), pp.925–950.

Murray, J.W. et al., 1989. Nutrient assimilation, export production and234Th scavenging in the eastern equatorial Pacific. *Deep Sea Research Part A, Oceanographic Research Papers*, 36(10), pp.1471–1489.

Oksanen, J. & et al., 2018. Package "vegan."

Olsen, A. et al., 2016. The global ocean data analysis project version 2 (GLODAPv2) - An internally consistent data product for the world ocean. *Earth System Science Data*, 8(2), pp.297–323.

Parker, F.L. & Coulbourn, W.T., 1971. Faunal and solution patterns of planktonic foraminifera in surface sediments of the South Pacific. *Deep-sea research*, 18, pp.73–107.

Peeters, F.J.C., Brummer, G.J.A. & Ganssen, G., 2002. The effect of upwelling on the distribution and stable isotope composition of Globigerina bulloides and Globigerinoides ruber (planktic foraminifera) in modern surface waters of the NW Arabian Sea. *Global and Planetary Change*, 34(3–4), pp.269–291.

Peeters, F. et al., 1999. A size analysis of planktic foraminifera from the Arabian Sea. *Marine Micropaleontology*, 36, pp.31–63.

Pflaumann, U. et al., 1996. A modern analog technique to deduce Atlantic sea surface temperatures from planktonic foraminifera in deep-sea sediments. *Paleoceanography*, 11(1), pp.15–35.

Prell, W.L. & Curry, W.B., 1981. Faunal and isotopic indices of monsoonal upwelling: Western Arabian Sea. *Oceanologica Acta*, 4, pp.91–98.

Prell, W.L. et al., 1999. The Brown University Foraminiferal Data Base (BFD). *PANGAEA*.

Ravelo, A.C. & Fairbanks, R.G., 1992. Oxygen isotopic composition of multiple species of planktonic foraminifera: Records of the modern photic zone temperature gradient. *Paleoceanography*, 7(6), pp.815–831.

Retailleau, S. et al., 2012. Canyon Heads and River Plumes: How Might They Influence Neritic Planktonic Foraminifera Communities in the Se Bay of Biscay? *The Journal of Foraminiferal Research*, 42(3), pp.257–269.

Ruddiman, W.F., 1969. Recent Planktonic Foraminifera: Dominance and Diversity in North Atlantic Surface Sediments. *Science*, 164(3884), pp.1164–1167.

Rutherford, S., D'Hondt, S. & Prell, W., 1999. Environmental controls on the geographic distribution of zooplankton diversity. *Nature*, 400(6746), pp.749–753.

Sadekov, A.Y. et al., 2016. Geochemical imprints of genotypic variants of Globigerina bulloides in the Arabian Sea. *Paleoceanography*, 31(10), pp.1440–1452.

Salgueiro, E. et al., 2008. Planktonic foraminifera from modern sediments reflect upwelling patterns off Iberia: Insights from a regional transfer function. *Marine Micropaleontology*, 66(3–4), pp.135–164.

Sarmiento, J. & Gruber, N., 2013. *Ocean biogeochmical dynamic*, Princeton University Press.

Schiebel, R. & Hemleben, C., 2017. *Planktic foraminifers in the modern ocean*, Springer Berlin Heidelberg.

Schiebel, R., 2002. Planktic foraminiferal sedimentation and the marine calcite budget. *Global Biogeochem. Cycles*, 16(4), p.1065.

Schiebel, R. et al., 2007. Planktic foraminiferal dissolution in the twilight zone Ralf. *Deep-Sea Research II*, 54, pp.676–686.

Schiebel, R. & Hemleben, C., 2005. Modern planktic foraminifera. *Palaontogische Zeitschrift*, 79(1), pp.135–148.

Schiebel, R. & Hemleben, C., 2000. Interannual variability of planktic foraminiferal populations and test flux in the eastern North Atlantic Ocean (JGOFS). *Deep-Sea Research Part II: Topical Studies in Oceanography*, 47(9–11), pp.1809–1852.

Schiebel, R. et al., 2001. Planktic foraminiferal production stimulated by chlorophyll redistribution and entrainment of nutrients. *Deep-Sea Research Part I: Oceanographic Research Papers*, 48(3), pp.721–740.

Schiebel, R. et al., 2004. Distribution of diatoms, coccolithophores and planktic foraminifers along a trophic gradient during SW monsoon in the Arabian Sea. *Marine Micropaleontology*, 51(3–4), pp.345–371.

Schlitzer, R., 2017. Ocean Data View.

Schmuker, B. & Schiebel, R., 2002. Planktic foraminifers and hydrography of the eastern and northern Caribbean Sea. *Marine Micropaleontology*, 46(3–4), pp.387–403.

Siccha, M. & Kucera, M., 2017. Data Descriptor : ForCenS , a curated database of planktonic foraminifera census counts in marine surface sediment samples. *Scientific Data*, 4, pp.1–12.

Storz, D. et al., 2009. Seasonal and interannual variability of the planktic foraminiferal flux in the vicinity of the Azores Current. *Deep-Sea Research Part I: Oceanographic Research Papers*, 56(1), pp.107–124.

Taylor, B.J. et al., 2018. Distribution and ecology of planktic foraminifera in the North Pacific: Implications for paleo-reconstructions. *Quaternary Science Reviews*, 191, pp.256–274.

Thompson, P. & Shackleton, N.J., 1980. North Pacific paleoceanography: late Quaternary coiling variation of planktonic foraminifer Neogloboquadrina pachyderma. *Nature*, 287(30), pp.829–833.

Tolderlund, D.S. & Bé, A.W.H., 1971. Seasonal distribution of planktonic foraminifera in the western North Atlantic. *Micropalaeontology*, 17(3), pp. 297-329.

Ujiié, Y. et al., 2012. Longitudinal differentiation among pelagic populations in a planktic foraminifer. *Ecology and Evolution*, 2(7), pp.1725–1737.

Waelbroeck, C. et al., 2009. Constraints on the magnitude and patterns of ocean cooling at the Last Glacial Maximum. *Nature Geoscience*, 2(2), pp.127–132.

Waelbroeck, C. et al., 1998. Improving past sea surface temperature estimates based on planktonic fossil faunas. *Paleoceanography*, 13(3), pp.272–283.

Warren, B. a., 1983. Why is no deep water formed in the North Pacific? *Journal of Marine Research*, 41(2), pp.327–347.

Watkins, J.M., Mix, A.C. & Wilson, J., 1996. Living planktic foraminifera: Tracers of circulation and productivity regimes in the central equatorial Pacific. *Deep-Sea Research Part II: Topical Studies in Oceanography*, 43(4–6), pp.1257–1282.

Williams, D. & Johnson, W.., 1975. Diversity of Recent Planktonic Foraminifera in the Southern Indian Ocean and Late Pleistocene Paleotemperatures. *Quaternary Research*, 5, pp.237–250.

Wyrtki, K., 1981. An Estimate of Equatorial Upwelling in the Pacific. *Journal of Physical Oceanography*, 11(9), pp.1205–1214.

Yu, J. et al., 2013. Calibration and application of B/Ca, Cd/Ca, and $\delta^{11}B$ in Neogloboquadrina pachyderma (sinistral) to constrain CO_2 uptake in the subpolar North Atlantic during the last deglaciation. *Paleoceanography*, 28(2), pp.237–252.

Yu, J., Anderson, R.F. & Rohling, E.J., 2014. Deep ocean carbonate chemistry and glacial-interglacial atmospheric CO2 changes. *Oceanography*, 27(1), pp.16–25.

Žarić, S. et al., 2005. Sensitivity of planktic foraminifera to sea surface temperature and export production as derived from sediment trap data. *Marine Micropaleontology*, 55(1–2), pp.75–105.

Zweng, M.M. et al., 2013. World Ocean Atlas 2013, Volume 2: Salinity. *NOAA Atlas NESDIS*, 2(1), p.39.

Chapter 4

4. A global calibration for Mg/Ca in the planktic foraminifera Neogloboquadrina pachyderma

This chapter is for submission to Biogeosciences with the author list: ***Taylor, B.J.,*** *Rae, J.W.B., Gray, W., Burke, A., Gersonde, R. Taylor performed the analyses, made the figures, and wrote the chapter, with input and comments from all other authors.*

Abstract

Changes in sea surface temperature (SST) have a profound influence on ocean ecosystems and global climate. A better understanding of how ocean temperatures varied in the past can help us understand the processes associated with temperature change in the future. The Mg/Ca ratio of planktic foraminiferal calcite is one of the most widely applied SST proxies. Due to the biological mediation of Mg uptake into foraminiferal calcite, modern calibration studies are required to assess the sensitivity of Mg/Ca ratios to changes in temperature and secondary influences. We present a calibration for the high latitude planktic foraminifera *Neogloboquadrina pachyderma* using new Mg/Ca data from the North Pacific and compiled global data. Our global sea surface temperature calibration takes the form of $Mg/Ca = 0.641 \pm 0.025 * e^{0.061 \pm 0.003 * T}$ with a sensitivity of 6.1 % (RSE = 0.250). We observe a slightly lower sensitivity than suggested by previous region-specific calibrations (8-10 %); however, the temperature sensitivity in our calibration compares well with a recently published global calibration for *Globigerinoides ruber* (Gray *et al.*, 2018a). In addition to temperature, we assess the influence of salinity, surface ocean carbonate chemistry, water depth, and bottom water calcite-saturation ($\Omega_{calcite}$) on Mg/Ca through multiple regression analysis. We find no significant influence of salinity or surface ocean carbonate chemistry in our dataset, however the range in surface ocean pH is very limited. We see no relationship between depth and Mg/Ca, however a significant sensitivity of -41% to bottom water $1/\Omega_{calcite}$ is observed, suggesting some influence of bottom water carbonate conditions on the preservation of Mg/Ca signatures in foraminiferal calcite.

4.1 Introduction

Mg/Ca ratios in planktic foraminifera are commonly used to reconstruct past ocean sea surface temperatures (SST) (Lea et al., 2000; Visser et al., 2003; Stott et al., 2004; Gray et al., 2018b). However, in common with other geochemical proxies hosted by planktic foraminifera, Mg/Ca ratios are typically influenced by biologically-induced "vital effects", adding complexity to geochemical reconstructions (Erez, 1978). To this end, species-specific calibrations against modern oceanographic and laboratory conditions are essential to ground truth geochemical proxies for use in paleoclimatology. The relationships between planktic foraminiferal Mg/Ca and environmental parameters have been assessed using core-tops (e.g. Elderfield and Gansson, 2000; Dekens et al., 2002; Vazquez-Riveiros et al., 2016), sediment traps and plankton tows (e.g. Anand et al., 2003; Pak et al., 2004; Jonkers et al., 2013; Gray et al., 2018a), as well as laboratory cultures (Lea et al., 1999; Russell et al., 2004; Allen et al., 2016; Evans et al., 2016). In most studies, the temperature sensitivity of Mg/Ca ranges between 6-10 % per °C (Gray et al., 2018a). Additional variables such as salinity and carbonate chemistry also influence Mg/Ca, with a sensitivity of ~3 to 5% per salinity unit (Nürnberg et al, 1996; Lea et al., 1999; Hönisch et al., 2013; Gray et al., 2018a), and ~-5 to -10 % per 0.1 pH unit (Lea et al., 1999; Russel et al., 2004; Evans et al., 2015; Gray et al., 2018a). The Mg/Ca of planktic foraminiferal calcite has also been demonstrated to be affected by post depositional dissolution (Brown et al., 1996; Regenberg et al. 2014).

The availability of planktic foraminifera species for Mg/Ca paleothermometry is markedly reduced in high-latitude records due to the decreased diversity of species found in these regions (Rutherford *et al.*, 1999; Fenton *et al.*, 2016; see Chapters 2 and 3). In sub-polar zones only two species, *Globigerina bulloides* and *Neogloboquadrina pachyderma*, are commonly used to reconstruct past ocean temperatures (Barker *et al.*, 2005; Gebhardt et al., 2008; Barker *et al.*, 2009; Thornalley *et al.*, 2009; Thornalley *et al.*, 2011; Riethdorf *et al.*, 2013; Ujiie *et al.*, 2016; Gray et al., 2018b), and during cold glacial conditions often only *N. pachyderma* is available, due to its colder temperature preference (Lombard et al., 2009). It is thus crucial to accurately calibrate the Mg/Ca proxy in this species.

Calibrations for the use of Mg/Ca ratios in *N. pachyderma* based on core-top material have often been focussed on particular geographic areas, including: Nürnberg (1995), Norwegian Sea; Elderfield and Ganssen (2000), North Atlantic; Meland et al. (2006), Nordic Sea; and Vazquez Riveiros et al., (2016), Southern Ocean. In addition to these, Jonkers et al. (2013) show seasonal variability in *N. pachyderma* Mg/Ca ratios based on sediment trap material in the North Atlantic. Here, we present the first core-top measurements of Mg/Ca in *N. pachyderma* collected in the North Pacific Ocean (eight core-tops and one new multinet site) and, by comparing our new data

to previous studies, propose a new global calibration for Mg/Ca in *N. pachyderma* using climatological data.

4.2 Methods

4.2.1 North Pacific sample collection and Mg/Ca analysis

Trace element analysis was undertaken on eight core-top sites and one multinet site from the North Pacific (Figure 4.1, Table 4.1). Four samples came from the SO202 INOPEX cruise which sailed in 2009 on the Vessel SONNE (SO202-01-27, SO202-02-07, SO202-04-13, SO202-04-27 [multinet], SO202-05-31) (Gersonde, 2012) and two samples were collected during the EW0408 cruise which sailed in 2004 on the research vessel Maurice Ewing (EW0408-15, EW0408-68). Two further samples were collected on the HLY0902 cruise which sailed in 2009 on the vessel USCGC Healy (HLY0902-19, HLY0902-24). Samples were washed and sieved between 150 and 250 µm. Roughly 400 specimens of *N. pachyderma* per site were picked for analysis and samples were crushed and cleaned to remove clay material and organic matter as described by Rae et al. (2011), adapting the method of Barker *et al.*, (2003). Samples were then analysed for Mg/Ca ratios on an Agilent 7500 ICP-MS in the STAiG laboratory at the University of St Andrews, with a long-term precision ±0.02 mmol/mol (1.25 %) (2σ).

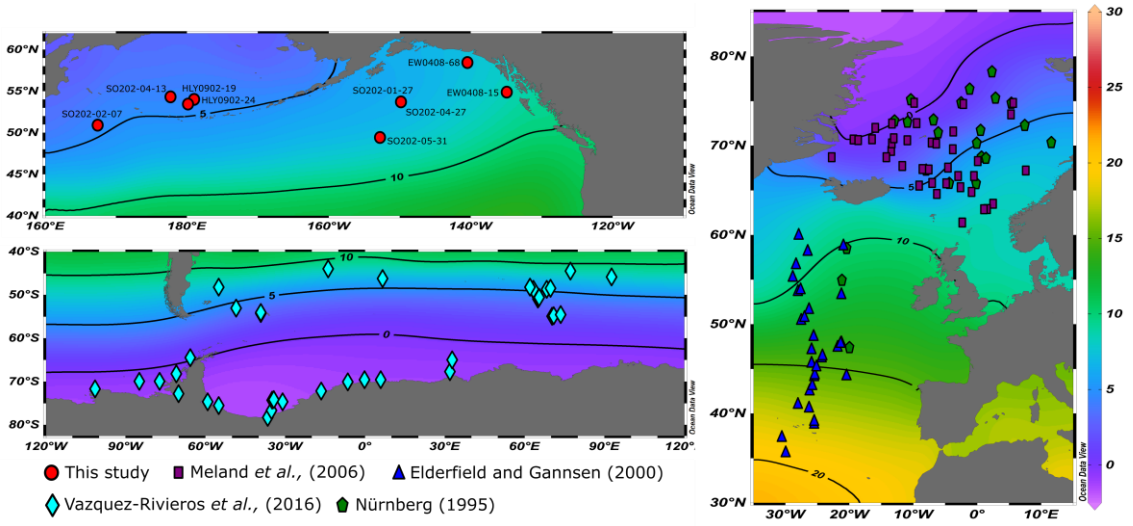

Figure 4.1: Site map showing location of samples used in this study. Samples from the North Pacific (red) indicate newly generated data. The light blue diamonds in Southern Ocean samples are those from Vazquez-Rivieros et al., (2016). Dark blue triangles from the North Atlantic are from Elderfield and Ganssen (2000). Purple squares are from Meland et al., 2006 and dark green pentagons are from Nürnberg (1995). Background colours are annual average temperatures from WOA13 (Locarnini et al., 2013).

4.2.2 Global data compilation

We compiled published Mg/Ca data from 131 sites across the world's oceans. Published data included: 22 sites from Nurnberg *et al.*, (1995); 32 sites from Elderfield and Ganssen (2000); 38 sites from Vazquez Riveiros *et al.*, (2016); and 39 sites from Meland *et al.*, (2006) (Figure 4.1). Including our new data from the North Pacific (Figure 4.1, Table 4.1), our dataset (140 samples total) covers the three key high latitude oceans, the North Atlantic, North Pacific and Southern Ocean, and therefore provides a wide range of conditions with which to assess the controls on Mg/Ca in *N. pachyderma*.

Site	Device	lat (dec)	long (dec)	depth (m)	Mg/Ca mmol/mol
EW0408-68	*MUC*	55.55	-134.71	296	0.89
EW0408-15	*MUC*	59.44	-140.25	238	0.98
HLY0902-19	*MUC*	54.61	-178.72	855	1.33
HLY0902-24	*MUC*	54.00	-179.59	714	1.22
SO202-02-07	*MUC*	51.27	167.69	2349	0.78
SO202-04-13	*MUC*	54.97	177.95	1386	0.70
SO202-04-27	*Multinet*	54.29	-149.59	0-500	1.31
SO202-01-27	*MUC*	54.29	-149.59	2921	0.77
SO202-05-31	*MUC*	49.67	-152.54	3744	0.69

Table 4.1: New North Pacific multicore (core-top) and multinet sites used within this study

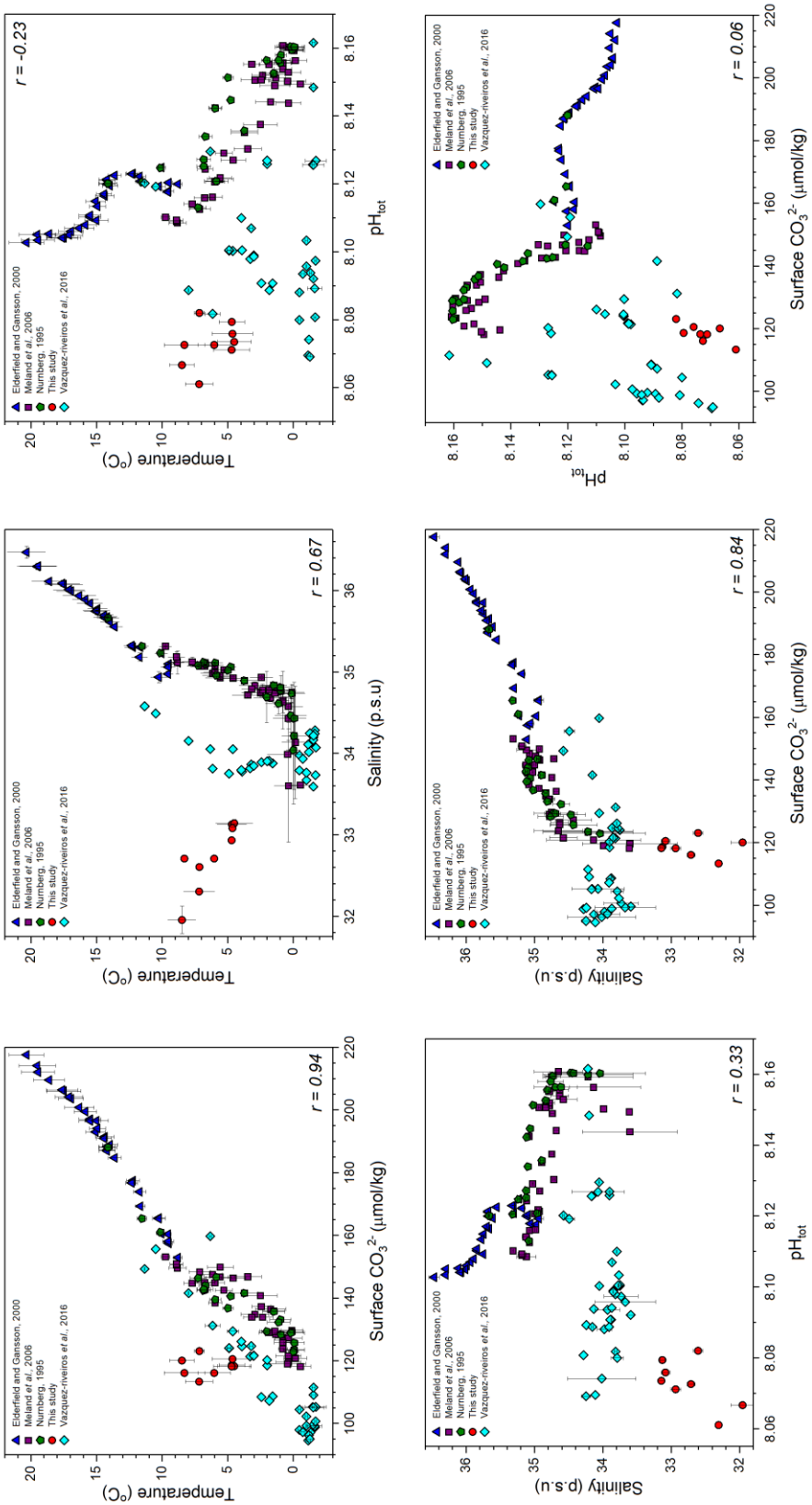

Figure 4.2: Covariance between calculated environmental variables for all sites within our compilation colour coded by study reference. Error bars indicate 2SD uncertainty calculated for WOA13 data.

4.2.3 Surface and bottom water parameters

Recent studies from the North Atlantic and North Pacific suggest *N. pachyderma* lives between 0-50 m in the water column, close to the base of the mixed layer (Jonkers *et al.,* 2010; Iwasaki *et al.,* 2017; Taylor *et al.,* 2018), so we use data from 0-50 m to calculate our surface environmental variables. To calculate temperature and salinity data for each of the new and previously published sites we extracted monthly temperatures and salinity at 5 m depth intervals from World Ocean Atlas 13 (Locarnini *et al.,* 2013; Zweng *et al.,* 2013) and averaged these to produce annual values for 0-50 m (± 2σ). For sites where no data was available we used ODVs 3D estimation tool (Schlitzer, 2006) to generate annual average temperatures between 0-50 m. Water column carbonate system data (pH, carbonate ion and Omega calcite) were calculated using alkalinity and dissolved inorganic carbon data from the Global Ocean Data Analysis Project version 2 (GLODAP V2) (Key *et al.,* 2004), and calculated for our sites between 0-50 m in the surface ocean, and at the depth of the core-top for bottom water parameters, using ODV's 3D estimation tool (Schlitzer, 2006). Carbonate ion and pH were then calculated using the *R* package *"seacarb"*, combining in-situ temperature, salinity, and pressure from WOA13, alongside alkalinity and DIC data. Although no uncertainty data is obtained from ODV's 3D estimation tool, poor estimates indictor by the program were removed. We use both linear and non-linear as well as single and multivariate regression analysis to determine the relationship between Mg/Ca ratios and temperature as well as the secondary environmental variables.

4.2.4 Results

Calculated hydrographic variables covered a wide range of values due to the large-scale geographic variation of the sites in our compiled dataset (Figure 4.2). Average temperature between 0-50 m ranged between -1.7°C and 20.3°C with an average temperature of 5.9°C. The coldest sites were located in Southern Ocean whilst the warmest temperatures occurred at sites in the mid-latitude North Atlantic (Figure 4.1). Salinity values ranged from 31.9 (p.s.u) in the North Pacific to 36.5 (p.s.u) in the North Atlantic, with average salinity of 34.6 (p.s.u). The calculated surface (0-50 m) carbonate variables, pH and CO_3^{2-}, ranged between 8.05 - 8.21 and 96.2 - 219.21 respectively. Bottom water $\Omega_{calcite}$ was lowest in the North Pacific at 0.74 and highest in the North Atlantic at 2.3.

Mg/Ca ratios for the eight new sites in the subpolar North Pacific ranged from 0.70 mmol/mol at site SO202-04-13 to 1.33 mmol/mol at site HLY0902-19 (Table 4.1). Within the entire dataset Mg/Ca ratios ranged between 0.34 mmol/mol and 2.48 mmol/mol; the average for the whole dataset was 0.98 mmol/mol. The Mg/Ca dataset was regressed against a range of hydrographic parameters including temperature (0-50 m); 0-50 m pH; 0-50 m CO_3^{2-}; 0-50 m $\Omega_{calcite}$; bottom

water $\Omega_{calcite}$ (core depth) and water depth (Figure 4.1). The form of our linear, non-linear, and multiple regression analysis can be seen in table 4.2.

Form	**a**	±2σ	ρ	**b**	±2σ	ρ	**c**	±2σ	ρ	**RSE**	AIC	r^2	n
Mg/Ca = a * exp(b * T)	0.641	0.025	**$<10^{-16}$**	**0.061**	0.003	**$<10^{-16}$**	NA	NA	NA	0.250	12.535	NA	140
Mg/Ca = a * exp(b * T_{winter})	0.636	0.027	**$<10^{-16}$**	**0.662**	0.004	**$<10^{-16}$**	NA	NA	NA	0.261	25.615	NA	140
Mg/Ca = (a * T) + c	**0.062**	0.004	**$<10^{-16}$**	NA	NA	NA	0.618	0.032	$<10^{-16}$	0.272	36.550	0.640	140
Mg/Ca = exp(a * S + b * T + c)	0.009	0.037	0.82	**0.060**	0.005	**$<10^{-16}$**	-0.736	1.254	0.558	0.250	14.478	NA	140
Mg/Ca = exp(a * (pH-8) + b * T + c)	0.626	0.804	0.44	**0.062**	0.004	**$<10^{-16}$**	-0.535	0.124	$<10^{-5}$	0.250	13.933	NA	140
Mg/Ca = exp(a * $CO_3^{2-}{}_{surf}$ + b * T + c)	2.6E-03	0.002	0.22	**0.048**	0.011	**$<10^{-5}$**	-0.724	0.233	0.002	0.249	13.019	NA	140
Mg/Ca = exp(a * $CO_3^{2-}{}_{surf}$ + 0.06 * T + c)	3.7E-04	0.001	0.53	NA	NA	NA	-0.495	0.099	$<10^{-6}$	0.249	12.226	NA	140
Mg/Ca = exp(a * (1/Ωc) + b * T + c)	-0.407	0.135	**0.003**	**0.061**	0.003	**$<10^{-16}$**	-0.147	0.103	0.157	0.242	5.496	NA	140

Table 4.3: Equations from single and multiple regression analysis. RSE = Relative Standard Error. AIC refers to "Akaike information criterion" a method with which to compare our regression models. The small difference between model AIC (>30) suggests little difference in variance explained by different models.

	Mg/Ca = B exp(AT)					
Species	B	A	R^2	T range	Region	Reference
Multispecies	0.520 (±0.010)	0.1		0 - 20°C	Global	Elderfield and Ganssen (2000)
N. pachyderma	0.406 (±0.032)	0.083		0 - 15°C	Norwegian Sea	Nürnberg (1995)
N. pachyderma	0.580 (±0.016)	0.084 (±0.006)	0.7	(-1) - 9°C	Southern Ocean	Vazquez Riveiros et al., (2016)
N. pachyderma	0.641 (±0.025)	0.061 (±0.003)		(-2) - 20°C	Global (incl. North Pacific)	This Study

Table 4.2: Comparison of published Mg/Ca calibrations involving N. pachyderma.

4.3 Discussion

4.3.1 A global Mg/Ca temperature calibration for *N. pachyderma*

The sensitivity of our exponential fit Mg/Ca to temperature is 6.1 ± 0.3 % per °C, with a residual standard error (RSE) of 0.25 (Figure 4.3, Table 4.2). Using a linear fit yields very similar results, with an $r^2 = 0.64$ and a sensitivity of 0.062 ± 0.004 mmol/mol per °C (Figure 4.3, Table 4.2). The RSE of our linear fit is higher than that of our exponential regression at 0.272. We also present further multiple regression analysis to assess the impact of other surface and bottom water parameters on our Mg/Ca ratios and temperature calibration. The results and implications of these are discussed in section 4.5.1.

We propose a new global calibration for *N. pachyderma* with a temperature sensitivity of 6.1 ± 0.3 %/°C (Figure 4.3), defined by the exponential equation

$$Mg/Ca = 0.641(\pm 0.025)\, e^{0.061\,(\pm 0.003) * T} \quad (4.1)$$

(RSE = 0.250). This sensitivity is slightly lower than that of some other published calibrations for this species (Table 4.2) where a sensitivity between 8-10 % was suggested (Nürnberg, 1995;

Elderfield and Ganssen, 2000; Anand *et al.*, 2003; Vazquez Riveiros *et al.*, 2016). This difference is likely due in part to the fact that our calibration encompasses a global sample set and, as discussed in more detail below, uses hydrographic data rather than $\delta^{18}O_{calcite}$ - $\delta^{18}O_{sw}$ derived isotopic temperatures.

Two primary methods exist for acquiring temperatures for use in geochemical calibrations. The first, and the method employed in this study, involves the use of hydrographic data, collected during ocean cruises or compiled into gridded datasets for global estimation. The second, uses the relationship between $\delta^{18}O_{calcite}$, $\delta^{18}O_{sw}$, and ocean temperature to calculate isotopic temperatures for a given sample; examples of calibrations using isotopic temperature can be seen in table 4.3. Both methods have their advantages and shortfalls. For example, the use of hydrographic data depends on the accuracy of measurement and the resolution of the dataset itself. It also requires knowledge of the depth habitat of the foraminifera species, so that temperatures can be calculated for the appropriate depth. However, it is relatively easy to calculate consistently for each site and does not require further analysis (c.f. $\delta^{18}O_{calcite}$). The calculation of isotopic temperatures benefits

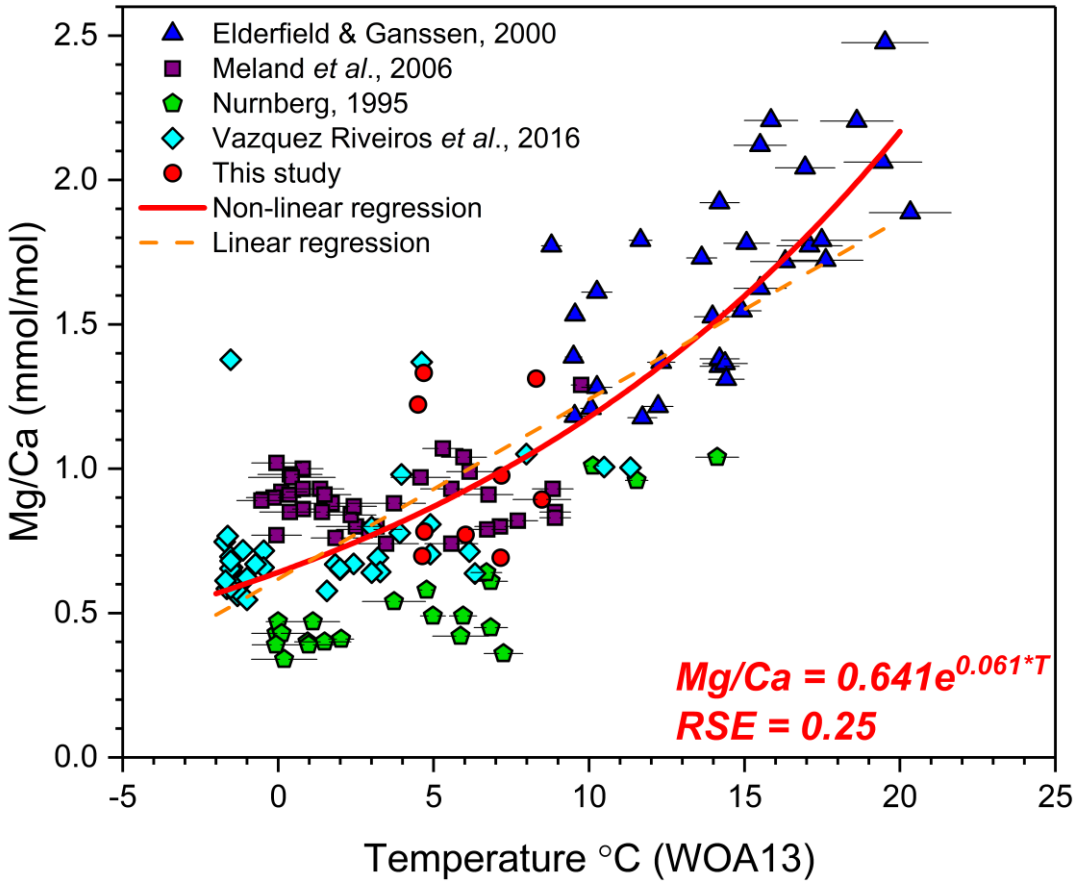

Figure 4.3: N. pachyderma Mg/Ca ratios (mmol/mol) vs WOA13 derived temperatures for all sites in our compiled global dataset. The red line shows the exponential relationship between Mg/Ca and temperature. The orange dashed line shows the linear fit. Error bars indicate 2SD uncertainty calculated for WOA13 data.

from being independent of foraminifera depth as it essentially attempts to calculate calcification temperatures from $\delta^{18}O$ values. This can be done through the relationship between temperature and $\delta^{18}O$ in foraminifera ($\delta^{18}O_{calcite}$), also taking into account variability in $\delta^{18}O$ of seawater ($\delta^{18}O_{sw}$), as described by Shackleton (1974):

$$T_{iso} = 16.0 - 4.38 * (\delta^{18}O_{calcite} - \delta^{18}O_{sw}) + 0.10 * (\delta^{18}O_{calcite} - \delta^{18}O_{sw})^2 \quad (4.2)$$

This method is only viable if both Mg/Ca and $\delta^{18}O_{calcite}$ are measured on the same foraminifera samples. Crucially, it also requires accurate determination of $\delta^{18}O_{sw}$, which is usually taken from the gridded dataset of Legrande and Schmidt (2006). However, the resolution of this dataset means that estimation of $\delta^{18}O_{sw}$ may be subject to considerable error, which affects the accuracy of isotopic temperature calibrations. Legrande and Schimdt (2006) also note that in some regions, particularly where sea ice is present, data may be seasonally biased, adding further uncertainty in the calculation of isotopic temperatures. In addition, uncertainty introduced when calculating isotopic temperatures is observed to be systematic (Figure 4.4) and therefore could induce bias into the reconstructions, whereas hydrographic temperature estimates used in our study will reflect normally distributed annual means and any uncertainty will be random error (noise) (Gray *et al.*, 2018a). Our approach of using hydrographic data derived from WOA13 (Locarnini *et al.*, 2013; Zweng *et al.*, 2013) provides a consistent attempt to estimate temperatures for each site in our compilation, and also means we can include data for which there are no $\delta^{18}O_{calcite}$ measurements available (our data and that of Nurnberg, 1995). Our WOA13 is calculated using monthly means to produce annual average data therefore avoiding seasonal bias which may affect isotopic temperatures. Finally, it allows for future Mg/Ca measurements to be easily added to this compilation without the need for additional analysis.

To test how our WOA13 derived temperatures compare with available isotopic temperatures from the same sites, we plot the relationship between the two datasets in figure 4.4. We note that this relationship is not 1:1. Although both sets of data compare well at the lower temperature end, at higher temperatures the relationship is weaker. This is primarily due to samples from Elderfield and Ganssen (2000), which have a latitudinal range of 35-60° N. At these latitudes, core-top samples of *N. pachyderma* are unlikely to live in high numbers throughout the year and are more likely to reflect winter populations (Schiebel and Hemleben, 2017). To address this, we calculated winter (DJF) temperatures for the sites of Elderfield and Ganssen (2000) (Figure 4.4) and used these to re-run our temperature regression.

$$Mg/Ca = 0.636(\pm 0.027)\, e^{0.066\,(\pm 0.004) * T} \quad (4.3)$$

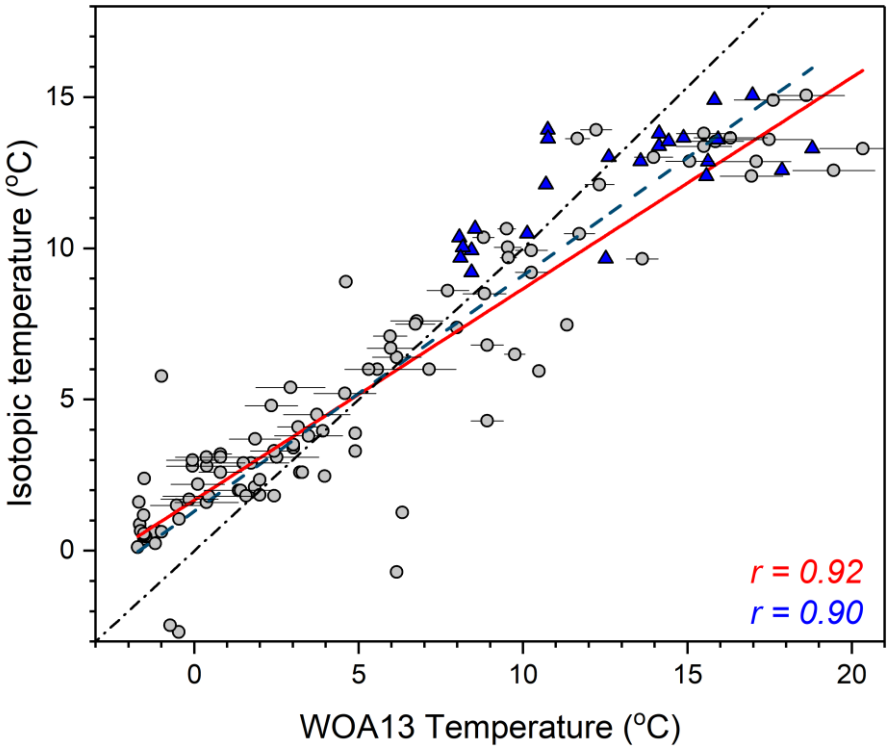

Figure 4.4: Comparison of available $\delta^{18}O$ isotopic temperatures against calculated WOA13 temperature. $\delta^{18}O$ values come from Elderfield and Ganssen (2000), Vazquez-Rivieros et al., (2016), and Meland et al., (2006). Blue triangles indicate winter temperatures calculated for lower latitude sites in our compilation. The red line shows the fit between $\delta^{18}O$ data and annual average data, whilst the blue dashed line shows uses winter values instead. The black dot dash line shows the 1:1 line. Error bars indicate 2SD uncertainty calculated for WOA13 data.

RSE = 0.261. We find that even when we include winter temperatures for the lower latitude sites in our compilation we see only a small change in our Mg/Ca sensitivity. Sensitivity increases slightly to 6.6 % per °C and RSE is higher at 0.261. In order to ensure consistency within calculated hydrographic variables we use our annual average temperature estimates throughout the remainder of the discussion.

4.3.2 Additional surface controls on Mg/Ca in *N. pachyderma*

In addition to temperature, other surface water parameters have been known to influence Mg/Ca ratios in planktic foraminifera. In particular, surface salinity and surface carbonate conditions have the potential to add complexity to the interpretation of Mg/Ca ratios (Nürnberg *et al.*, 1996; Lea *et al.*, 1999; Russell *et al.*, 2004; Kisakurek *et al.*, 2008; Hönisch *et al.*, 2013; Allen *et al.*, 2016; Evans *et al.*, 2016; Gray *et al.*, 2018a). To fully investigate the relationship between Mg/Ca ratios in *N. pachyderma* and water column properties we employed multiple regression analysis to assess the influence of multiple variables at once. Our multiple regressions follow the formula,

$$Mg/Ca = \exp(a * Var + b * T + c) \quad (4.4)$$

Where *Var* is the additional water column variable, *T* is temperature, and *a, b and c* are the exponential coefficients.

We first analyse the effect of salinity on Mg/Ca ratios and on the relationship between Mg/Ca and temperature. Regressing against both temperature and salinity results in a temperature sensitivity of 6.0 ± 0.5 % per °C,

$$Mg/Ca = \exp(0.009 \pm 0.004 * Sal + 0.060 \pm 0.005 * T - 0.736 \pm 1.25) \quad (4.5)$$

(RSE = 0.250). We see a 0.9 ± 0.004 %/°C sensitivity of Mg/Ca to salinity, however this relationship is not significant (ρ = 0.82). Salinity and temperature correlate in our dataset with an r = 0.64 (Figure 4.2); however, the insignificant change in temperature sensitivity with the inclusion of salinity indicates this covariance is not affecting our results.

Next, we analyse the impact of surface water pH and CO_3^{2-} on Mg/Ca and our temperature calibration. When regressing against CO_3^{2-} and temperature we find temperature sensitivity of 4.8 ± 1.1 % per °C and an insignificant positive term for CO_3^{2-} (ρ = 0.22),

$$Mg/Ca = \exp(0.003 \pm 0.002 * CO_3^{2-} + 0.048 \pm 0.011 * T - 0.724 \pm 0.23) \quad (4.6)$$

(RSE = 0.249). This decrease in the Mg/C temperature sensitivity is primarily caused by the strong co-variance of CO_3^{2-} and temperature in the surface ocean (Figure 4.2). We find it unlikely that CO_3^{2-} exerts a control on Mg/Ca in our dataset due to culture studies on other species of planktic foraminifera (*G. bulloides* and *O. universa*) which suggest that Mg/Ca and CO_3^{2-} should exhibit a negative relationship (Russell *et al.*, 2004), whereas our model finds no correlation (ρ = 0.22). If we prescribe our temperature coefficient to 6% to overcome the covariance between temperature and CO_3^{2-}, our results still indicate no significant correlation between $CO_3^{2-}$and Mg/Ca (ρ = 0.53).

Assuming pH, rather than CO_3^{2-}, is the controlling carbonate system variable gives the following equation:

$$Mg/Ca = \exp(0.626 \pm 0.804 * (\mathrm{pH} - 8) + 0.062 \pm 0.004 * T - 0.54 \pm 0.12) \quad (4.7)$$

(RSE = 0.250). From equation 4.7 we see no significant correlation between surface ocean (0-50 m) pH and Mg/Ca ratio (ρ = 0.44). The temperature sensitivity of Mg/Ca remains at 6 %, and there is no covariance between pH and temperature in the dataset. Although we see no significant correlation between pH and Mg/Ca in our multiple regression, recent culture and sediment trap studies suggest a sensitivity of -5 to -10% per 0.1 pH unit for the majority of planktic foraminiferal species (Lea *et al.*, 1999; Russell *et al.*, 2004; Kisakurek, 2008; Evans 2016; Gray 2018a). We

hypothesise that there is likely to be a pH control on Mg/Ca in *N. pachyderma*, however, it is not detectable due to the low range of pH and relatively small number of samples within our dataset.

4.3.3 Bottom water controls on Mg/Ca ratios

Several studies have indicated a possible diagenetic or dissolution effect on Mg/Ca ratios in planktic foraminifera (Rosenthal and Boyle, 1993; Brown and Elderfield, 1996; Elderfield and Ganssen, 2000; Meland et al., 2006). To test this, we use a multiple regression to regress Mg/Ca ratios against bottom water $\Omega_{calcite}$ and temperature for our new and compiled sites, which is expressed by the following equation:

$$Mg/Ca = \exp(-0.407 \pm 0.135 * 1/\Omega_{cal} + 0.061 \pm 0.003 * T - 0.147 \pm 0.157) \quad (4.8)$$

(RSE = 0.242). We use 1/ $\Omega_{calcite}$ to account for the non-linear nature of $\Omega_{calcite}$. Our multiple regression indicates a -41% sensitivity of Mg/Ca to changes in bottom water $1/\Omega_{calcite}$ suggesting that changes in bottom water carbonate chemistry do exert an influence on Mg/Ca ratios. There is no covariance between temperature and $\Omega_{calcite}$ and there is no change in the sensitivity of Mg/Ca

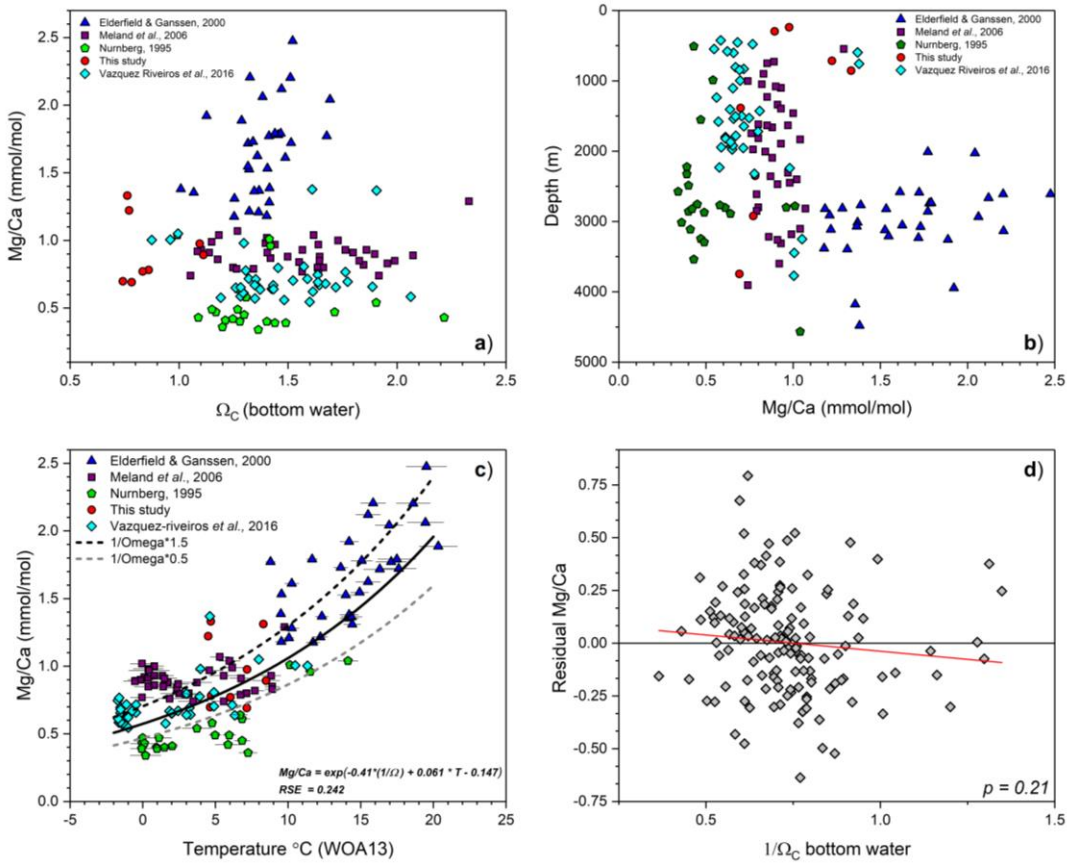

Figure 4.5: a) Cross-plot of Omega calcite vs Mg/Ca (mmol/mol) for all sites in our compiled dataset. b) Depth (m) vs Mg/Ca (mmol/mol) for all sites in our compiled dataset. c) Mg/Ca (mmol/mol) vs temperature with the addition of multiple regression fits incorporating bottom water Omega calcite at different magnitudes (1.5 and 0.5). d) Residual Mg/Ca from our exponential regression (equation 4.1) vs 1/Omega calcite of bottom water.

to temperature (which remains at 6 %). When comparing the residual Mg/Ca from our temperature calibration (equation 4.1) against bottom water $\Omega_{calcite}$ we also see no noticeable correlation between the two variables ($p = 0.21$).

The effect of this $\Omega_{calcite}$ sensitivity on apparent temperature is shown in figure 4.5, where we plot our multiple regression of $\Omega_{calcite}$ and temperature at $\Omega_{calcite}$ values between 1.5 and 0.5 (roughly the range in the entire deep ocean today). This shows our $\Omega_{calcite}$ sensitivity has only a relatively minor influence at the range of $\Omega_{calcite}$ in the deep ocean today. Our multiple regression does indicate a bottom water carbonate chemistry effect on the Mg/Ca ratios within *N. pachyderma*, something also highlighted by Meland *et al.*, 2006. However, even the relatively large changes in bottom water carbonate ion seen between the Last Glacial Maximum and the Holocene (between +20 to -35 µmol/kg; Yu *et al.*, 2014) would not greatly influence our Mg/Ca regression, giving further confidence in the use of this calibration to reconstruct past temperatures.

Our regression analyses clearly suggest that temperature is the dominant control on Mg/Ca ratios in *N. pachyderma* globally, and that a sensitivity of 6.1 % per °C (equation 4.1) can be used to reconstruct SSTs in the past. A sensitivity of 6 % was also recently demonstrated in a global calibration of *G. ruber* by Gray *et al.*, (2018a), indicating that it may be ubiquitous to planktic foraminifera.

4.4 Conclusions

Our new Mg/Ca temperature calibration for the planktic foraminifera *N. pachyderma* provides a robust global calibration based on hydrographic measurements. We find a global sensitivity of Mg/Ca ratios to temperature of 6.1 % per °C, defined by the equation $Mg/Ca = 0.641*e^{0.061 \pm 0.003*T}$ (RSE = 0.250). Our new calibration removes some of the uncertainty surrounding the use of isotopic temperature, namely the estimation of seawater $\delta^{18}O$ (Legrand and Schmidt, 2006; Gray *et al.*, 2018a), and provides a calibration based on a large dataset (140 sites), which is particularly useful when reconstructing temperatures within regions that do not have a previously published regional calibration. Finally, our new calibration is structured such that additional Mg/Ca and hydrographic data can easily be assimilated even if foraminifera $\delta^{18}O$ has not been measured. Although not enough data is currently available to produce a robust regional calibration for the North Pacific, this should be the goal of future studies. Despite this, the similarity of the global and North Pacific data suggests different genotypes of *N. pachyderma* may calcify in a similar manner.

We analysed the impact of additional surface water parameters on Mg/Ca ratios in *N. pachyderma* through multiple regression analysis. Multiple regression analysis showed temperature as the

dominant control on Mg/Ca ratios with the no correlations observed between Mg/Ca and surface salinity, pH, or CO_3^{2-}. We suggest that although the relationship observed between Mg/Ca and pH is not significant ($p = 0.44$), the sensitivities observed in culture studies suggests with a greater range of pH values, or a larger dataset, a significant correlation may be observed.

Finally, we analysed the potential for dissolution bias in Mg/Ca ratios. Our multiple regression analysis of surface temperature and bottom water $1/\Omega_{calcite}$ indicated some sensitivity of Mg/Ca to bottom water $1/\Omega_{calcite}$ throughout our sites. This has only a small effect on Mg/Ca over the range of $\Omega_{calcite}$ in the deep ocean and thus, although bottom water $\Omega_{calcite}$ may affect Mg/Ca ratios in *N. pachyderma*, it is likely to only have a limited effect on the reconstruction past ocean temperatures.

4.5 References

Allen, K.A. et al., 2016. Trace element proxies for surface ocean conditions: A synthesis of culture calibrations with planktic foraminifera. *Geochimica et Cosmochimica Acta*, 193, pp.197–221.

Anand, P., Elderfield, H. & Conte, M.H., 2003. Calibration of Mg/Ca thermometry in planktonic foraminifera from a sediment trap time series. *Paleoceanography*, 18(2).

Barker, S. et al., 2005. Planktonic foraminiferal Mg/Ca as a proxy for past oceanic temperatures: A methodological overview and data compilation for the Last Glacial Maximum. *Quaternary Science Reviews*, 24(7–9 SPEC. ISS.), pp.821–834.

Barker, S. et al., 2009. Interhemispheric Atlantic seesaw response during the last deglaciation. *Nature*, 457, pp.1097–1102.

Brown, S.J. & Elderfield, H., 1996. Variations in Mg/Ca and Sr/Ca ratios of planktonic foraminifera caused by postdepositional dissolution: Evidence of shallow Mg-dependent dissolution. *Paleoceanography*, 11(5), pp.543–551.

Elderfield, H. & Ganssen, G., 2000. Past temperature and δ18O of surface ocean waters inferred from foraminiferal Mg/Ca ratios. *Nature*, 405(6785), pp.442–445.

Erez, J., 1978. Vital effect on stable-isotope composition seen in foraminifera and coral skeletons. *Nature*, 273, pp.199–202.

Evans, D. et al., 2015. Mg/Ca-temperature and seawater-test chemistry relationships in the shallow-dwelling large benthic foraminifera Operculina ammonoides. *Geochimica et Cosmochimica Acta*, 148, pp.325–342.

Evans, D. et al., 2016. Revisiting carbonate chemistry controls on planktic foraminifera Mg / Ca: Implications for sea surface temperature and hydrology shifts over the Paleocene-Eocene Thermal Maximum and Eocene-Oligocene transition. *Climate of the Past*, 12(4), pp.819–835.

Fenton, I.S. et al., 2016. Environmental Predictors of Diversity in Recent Planktonic Foraminifera as Recorded in Marine Sediments. Plos One, 11(11).

Gebhardt, H. et al., 2008. Paleonutrient and productivity records from the subarctic North Pacific for Pleistocene glacial terminations I to V. *Paleoceanography*, 23(4).

Gersonde, R., 2012. The Expedition of the Research Vessel " Sonne ", 2009, pp.127–282.

Gray, W.R. et al., 2018a. The effects of temperature, salinity, and the carbonate system on Mg/Ca in Globigerinoides ruber (white): A global sediment trap calibration. *Earth and Planetary Science Letters*, 482, pp.607–620.

Gray, W.R. et al., 2018b. Deglacial upwelling, productivity and CO2 outgassing in the North Pacific Ocean. *Nature Geoscience*.

Hönisch, B. et al., 2013. The influence of salinity on Mg/Ca in planktic foraminifers - Evidence from cultures, core-top sediments and complementary δ18O. *Geochimica et Cosmochimica Acta*, 121, pp.196–213.

Jonkers, L. et al., 2010. Seasonal stratification, shell flux, and oxygen isotope dynamics of leftcoiling N. pachyderma and T. quinqueloba in the western subpolar North Atlantic. *Paleoceanography*, 25(2), pp.1–13.

Jonkers, L. et al., 2013. Seasonal Mg/Ca variability of *N. pachyderma* (s) and *G. bulloides*: Implications for seawater temperature reconstruction. *Earth and Planetary Science Letters*, 376, pp.137–144.

Kisakürek, B. et al., 2008. Controls on shell Mg/Ca and Sr/Ca in cultured planktonic foraminiferan, Globigerinoides ruber (white). *Earth and Planetary Science Letters*, 273(3–4), pp.260–269.

Kozdon, R. et al., 2009. Reassessing Mg/Ca temperature calibrations of Neogloboquadrina pachyderma (sinistral) using paired ??44/40Ca and Mg/Ca measurements. *Geochemistry, Geophysics, Geosystems*, 10(3).

Lea, D.W., Pak, D.K. & Spero, H.J., 2000. Climate Impact of Late Quaternary Equatorial Pacific Sea Surface Temperature Variations. *Science*, 289(5485), pp.1719–1724.

Lea, D.W., Mashiotta, T.A. & Spero, H.J., 1999. Controls on magnesium and strontium uptake in planktonic foraminifera determined by live culturing. *Geochimica et Cosmochimica Acta*, 63(16), pp.2369–2379.

LeGrande, A.N. & Schmidt, G.A., 2006. Global gridded data set of the oxygen isotopic composition in seawater. *Geophysical Research Letters*, 33(12), pp.1–5.

Locarnini, R.A. et al., 2013. *World Ocean Atlas 2013. Vol. 1: Temperature.*,

Lombard, F. et al., 2009. Modelling the temperature dependent growth rates of planktic foraminifera. *Marine Micropaleontology*, 70(1–2), pp.1–7.

Martínez-Botí, M.A. et al., 2011. Mg/Ca in foraminifera from plankton tows: Evaluation of proxy controls and comparison with core tops. *Earth and Planetary Science Letters*, 307(1–2), pp.113–125.

Meland, M.Y. et al., 2006. Mg/Ca ratios in the planktonic foraminifer Neogloboquadrina pachyderma (sinistral) in the northern North Atlantic/Nordic Seas. *Geochemistry, Geophysics, Geosystems*, 7(6).

Nürnberg, D., 1995. Magnesium in tests of Neogloboquadrina pachyderma sinistral from high northern and southern latitudes. *Journal of Foraminiferal Research*, 25(4), pp.350–368.

Nürnberg, D., Bijma, J. & Hemleben, C., 1996. Assessing the reliability of magnesium in foraminiferal calcite as a proxy for water mass temperatures. *Geochimica et Cosmochimica Acta*, 60(5), pp.803–814.

Pak, D.K., Lea, D.W. & Kennett, J.P., 2004. Seasonal and interannual variation in Santa Barbara Basin water temperatures observed in sediment trap foraminiferal Mg/Ca. *Geochemistry, Geophysics, Geosystems*, 5(12).

Regenberg, M. et al., 2014. Global dissolution effects on planktonic foraminiferal Mg/Ca ratios controlled by the calcite-saturation state of bottom waters. *Paleoceanography*, 29(3), pp.127–142.

Riethdorf, J.R. et al., 2013. Deglacial development of (sub) sea surface temperature and salinity in the subarctic northwest Pacific: Implications for upper-ocean stratification. *Paleoceanography*, 28(1), pp.91–104.

Rosenthal, Y. & Boyle, E., 1993. Factors controlling the floride content of planktonic foraminifera: An evaluation of its paleoceanographic applicability. *Geochimica et Cosmochimica Acta*, 57(2), pp.335–346.

Rutherford, S., D'Hondt, S. & Prell, W., 1999. Environmental controls on the geographic distribution of zooplankton diversity. Nature, 400(6746), pp.749–753.

Schlitzer, R., 2017. Ocean Data View.

Shackleton, N.J., 1974. Attainment of isotopic equilibrium between ocean water and the benthonic foraminifera geuns *Uvigerina*: Isotopic changes in the ocean during the last glacial. *Colloques Internationaux du C.N.R.S.*, 219, pp.203–210.

Stott, L.D. et al., 2004. Decline of surface temperature and salinity in the western tropical Pacific Ocean in the Holocene epoch. *Nature*, 431(September 2004), pp.56–59.

Taylor, B.J. et al., 2018. Distribution and ecology of planktic foraminifera in the North Pacific: Implications for paleo-reconstructions. *Quaternary Science Reviews*, 191, pp.256–274.

Thornalley, D.J.R., Elderfield, H. & McCave, I.N., 2011. Reconstructing North Atlantic deglacial surface hydrography and its link to the Atlantic overturning circulation. *Global and Planetary Change*, 79(3–4), pp.163–175.

Thornalley, D.J.R., Elderfield, H. & McCave, I.N., 2009. Holocene oscillations in temperature and salinity of the surface subpolar North Atlantic. *Nature*, 457(7230), pp.711–714.

Ujiié, Y. et al., 2016. Evolution of the North Pacific Subtropical Gyre during the past 190 kyr through the interaction of the Kuroshio Current with the surface and intermediate waters. *Paleoceanography*, 31(11), pp.1498–1513.

Vazquez Riveiros, N. et al., 2016. Mg/Ca thermometry in planktic foraminifera: Improving paleotemperature estimations for G. bulloides and N. pachyderma. *Geochemistry, Geophysics, Geosystems*, 17.

Visser, K., Thunell, R. & Stott, L.D., 2003. Magnitude and timing of temperature change in the Indo-Paci c warm pool during deglaciation. *Nature*, 421(JANUARY), pp.3667–3670.

Yu, J., Anderson, R.F. & Rohling, E.J., 2014. Deep ocean carbonate chemistry and glacial-interglacial atmospheric CO2 changes. Oceanography, 27(1), pp.16–25.

Zeebe, R.E and Wolf-Gladrow, D., 2001. *CO2 in Seawater: Equilibrium, Kinetics, Isotopes*,

Zweng, M.M. et al., 2013. World Ocean Atlas 2013, Volume 2: Salinity. *NOAA Atlas NESDIS*, 2(1), p.39.

4.6 Supplementary figures

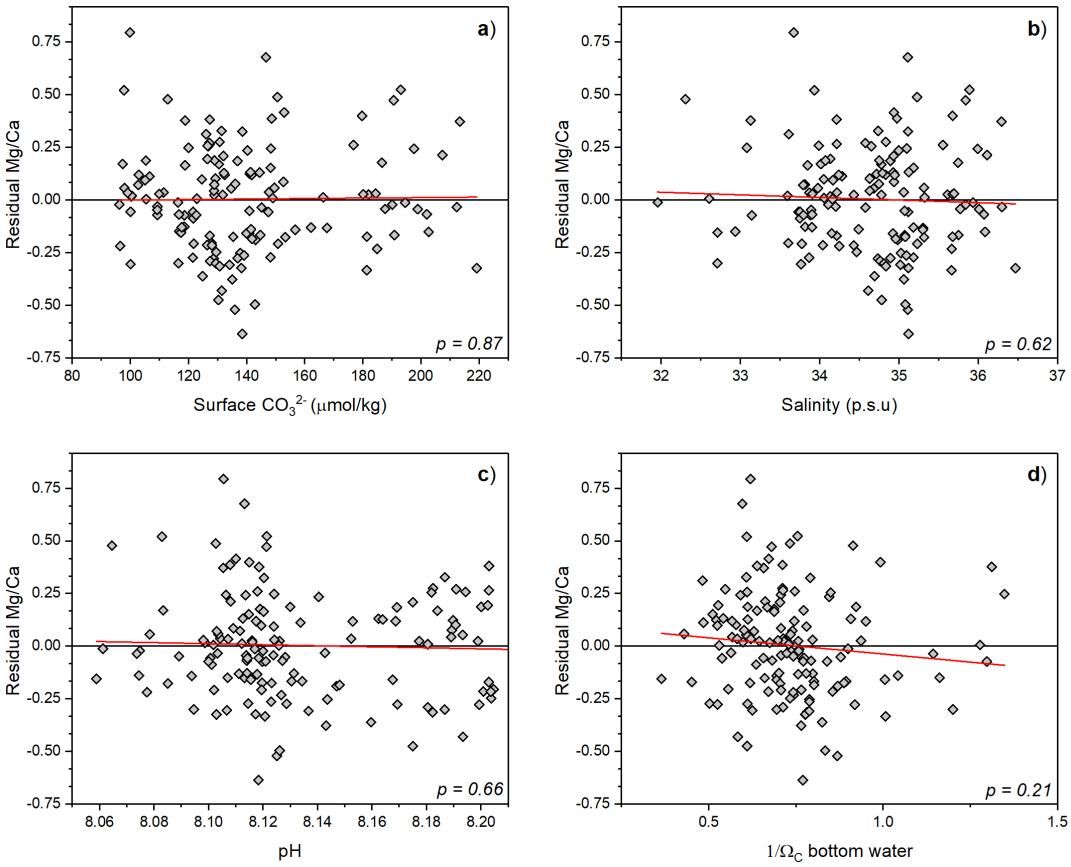

Figure 4.6: Residual Mg/Ca from our exponential regression (equation 4.1) plotted against surface CO_3^{2-} (a), surface salinity (b), surface pH (c), and 1/ bottom water Omega calcite (d).

Chapter 5

5. Pulses of deglacial CO_2 release from the sub-polar North Pacific

This chapter is for submission to Paleoceanography with the author list: ***Taylor, B.J.,*** *Rae, J.W.B., Gray, W., Sarnthein, M. Burke, A. Taylor performed the analyses, made the figures, and wrote the chapter, with input and comments from all other authors.*

Abstract

The role of North Pacific in CO_2 release during the last deglaciation is widely debated. Some recent research has suggested large changes in ocean stratification, nutrient levels, and CO_2 supply took place during Heinrich Stadial 1 and the Bølling-Allerød, driving changes in productivity and CO_2 outgassing, while other authors have suggested that the glacial North Pacific was even more stratified than it is today. Here we present new boron isotope surface pH and CO_2 reconstructions, sea surface temperature reconstructions, and planktic foraminifera census data from the last deglaciation in the North East Pacific. Our record shows two key intervals of decreased surface pH and increased surface water CO_2. The first, between 17-15.5 ka, occurs at a time of increased ventilation in the deep North Pacific and supports suggestions that enhanced North Pacific overturning, combined with a weak biological pump, may have contributed to CO_2 release from the North Pacific at the onset of the last deglaciation. The second and most dramatic shift in surface CO_2 occurs at the onset of the Bølling-Allerød at ~14.7 ka, where surface CO_2 increases by ~70 ppm in ~600 years. At this time, stratified conditions pool nutrients and CO_2 in subsurface waters, while enhanced Ekman suction helps bring them into the mixed layer. Combined with published data from the North West Pacific, this suggests a prominent role for the North Pacific in CO_2 release during the Bølling-Allerød, which may help counter Southern Ocean stratification and allow elevated atmospheric CO_2 levels to persist and deglaciation to continue. Overall, our geochemical and census records coupled with published proxy data on circulation and nutrients suggest a more dynamic overturning regime operated in the North Pacific during the last deglaciation and that the North Pacific made a prominent contribution towards deglacial CO_2 rise.

5.1 Introduction

5.1.1 Deglacial CO_2 in the North Pacific

The last deglaciation saw the largest recent change in CO_2 and climate prior to the Anthropocene (Jouzel *et al.,* 2007; Marcotte *et al.,* 2015). Deglacial CO_2 rise occurred in a series of steps associated with rapid changes in circulation in the North Atlantic (Thornalley *et al.,* 2010; Thornalley *et al.,* 2011) and biological pump efficiency in the Southern Ocean (Watson *et al.,* 2000; Sigman *et al.,* 2010). The Southern Ocean has thus been recognised as a likely source of deglacial CO_2 release (Burke and Robinson, 2012; Ferrari *et al.,* 2014; Martinez-Boti *et al.,* 2015). However, the North Pacific also has the potential to play a role in deglacial CO_2 release, due to the large reservoir of dissolved inorganic carbon (DIC) that exists in its interior waters. In the modern ocean, this deep store of CO_2 is cut off from the atmosphere because of strong surface stratification in the North Pacific caused by low salinity surface waters, mild summer temperatures, and enhanced precipitation over evaporation (Warren, 1983; Emile-Geay *et al.,* 2003). This is in contrast to the modern North Atlantic, where warm salty water from the tropics cools and sinks at high latitudes to form North Atlantic Deep Water (NADW). Recent research has suggested that North Pacific stratification may have changed dramatically, providing a potential route for the outgassing of previously sequestered CO_2 into the atmosphere (Okazaki *et al.,* 2010; Max *et al.,* 2014; Rae *et al.,* 2014; Maier *et al.,* 2015; Gray *et al.,* 2018). This is particularly thought to occur during Heinrich Stadial 1 (HS1) and the Bølling-Allerød (B/A), though with different characteristics. During HS1, a cold stadial interval with reduced overturning in the North Atlantic, radiocarbon data from the North Pacific suggests a period of local deepwater formation (Okazaki *et al.,* 2010, Max *et al.,* 2014, Rae *et al.,* 2014), which may have mixed CO_2 and nutrients throughout the water column, leading to CO_2 outgassing (Rae *et al.,* 2014). During the B/A, a Northern Hemisphere warm period with enhanced overturning in the North Atlantic, the stratification of the North Pacific has been hypothesised to increase (Kennet and Ingram, 1995; Okazaki *et al.,* 2010; Lam *et al.,* 2013; Rae *et al.,* 2014), pooling nutrients and CO_2 in the upper ocean, leading to basin-wide productivity and CO_2 outgassing (Gray *et al.,* 2018).

Here we assess the changing nature of North Pacific overturning through new planktic foraminifera $\delta^{11}B$, trace element, and census data from the North East Pacific (sites MD02-2489 and ODP 887B), to better constrain North Pacific biogeochemistry and its role in deglacial CO_2 release. We use the $\delta^{11}B$ of planktic foraminifera *Neogloboquadrina pachyderma* to calculate surface water pH and pCO_2 from 21.5 - 6.4 ka, comparing our results with similar data from the North West Pacific produced by Gray *et al.,* (2018). Our results, alongside published data, suggest the North Pacific played an active role in CO_2 storage and release during the last deglaciation, driven by pronounced changes in circulation and productivity.

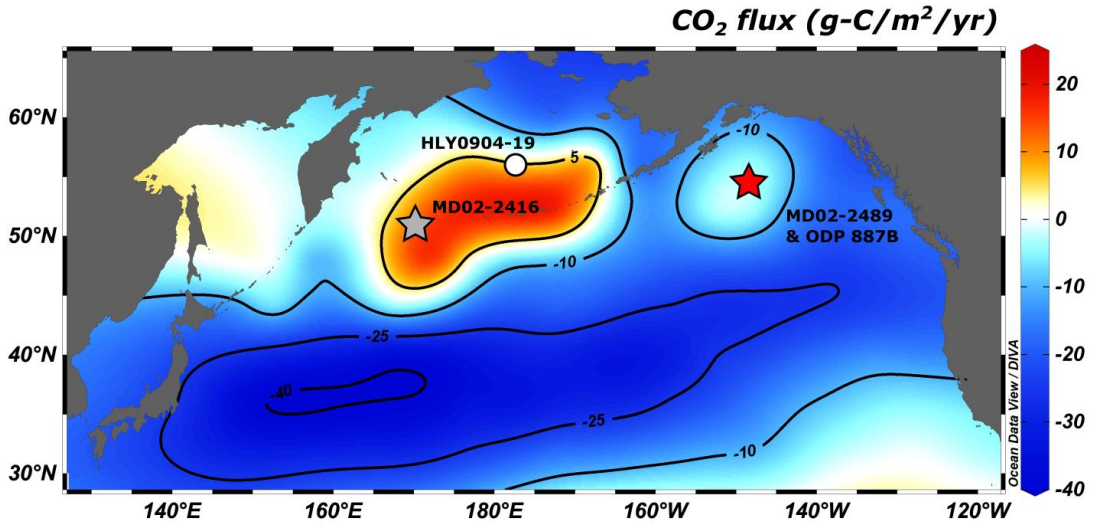

Figure 5.1: Map of surface ocean CO_2 flux from Takahashi et al., (2009). The red star denotes the location of new data generated by this study at sites MD02-2489 and ODP 887B. The grey star shows the location of sediment core MD02-2416 from Gray et al., (2018). The white circle shows core-top HLY0904-19 used to better calibrate our $\delta^{11}B$ record.

5.1.2 Regional Oceanography

Surface circulation in the North Pacific is dominated by two contrasting gyres: the warm, salty and nutrient poor subtropical gyre, and the cold, fresh, and nutrient rich subpolar gyre (see supplementary figure 5.8). The low salinity (32.5-33.5) of the sub-polar North Pacific surface – lower than any other open ocean basin (Zweng *et al.*, 2014) – results in highly stratified conditions, with little interaction between surface and deep water and only limited intermediate water formation (Warren, 1983). The cause of this subpolar low salinity pool is threefold: firstly, it is related to the isolated nature of the subpolar gyre, with little input from salty subtropical waters; secondly, high rates of precipitation compared with evaporation (Warren, 1983; Emile-Geay *et al.*, 2003) help to dilute subpolar waters; thirdly, large-scale atmospheric circulation patterns make the North Pacific as a whole fresher than equivalent latitudes in the North Atlantic.

The stratification of the subpolar North Pacific has a major effect on regional ventilation and, in turn, water column geochemistry. The lack of substantial regional deep-water ventilation is clearly observed within water column radiocarbon ventilation ages, which show some of the oldest deep waters found in the global ocean. Mid-depth waters also have extremely low pH and O_2 levels due to poor ventilation and large-scale organic matter remineralisation (Garcia *et al.*, 2013). In contrast, the deep North Pacific has higher alkalinity and pH due to the deep dissolution of $CaCO_3$ (Sarmiento and Gruber, 2013).

Despite the surface stratification, wind driven upwelling and winter mixing bring nutrient and CO_2-rich waters into the subpolar surface ocean (Ayers and Lozier, 2010). The entirety of the subpolar gyre is a high nutrient low chlorophyll zone (HNLC), with high phosphate and nitrate levels sourced via upwelling and seasonal mixing from nutrient-rich waters in the subsurface (Ayers and Lozier, 2010), and low primary productivity due to limited availability of light and iron (Boyd and Harrison, 1999). This is particularly prevalent in the North West Pacific, where annual average surface phosphate levels exceed 1.5 µmol/kg (Garcia *et al.,* 2014).

Sea surface temperatures in the subpolar gyre vary spatially and seasonally. Annual average temperatures range from 3-12 °C (Locarnini *et al.,*2013) with coolest temperatures seen in the most northerly reaches of the Bering Sea. The North West Pacific is colder than the North East which is fed partially by warmer waters from the Kuroshio extension.

5.2 Methods

5.2.1 Sediment core and age control

Sediment core MD02-2489 was raised from the Patten seamount (54.39° N, 148.92° W) at a depth of 3640 m (Figure 5.1). Core sedimentology is described in detail in Gebhardt *et al.,* (2008) and consists of a mixture of siliceous and calcareous oozes with high levels of ice rafted debris (IRD), lithic fragments carried and deposited by icebergs, seen within some sections of the core. The top 50 cm of the core was noted to have experienced some slumping and was therefore judged not to be useful for paleo-reconstructions. Our samples span from 50-298 cmbsf, equivalent to 6.4-21.5 kyr when applying the age model from Rae *et al.,* (2014). This age model ties high resolution planktic foraminifera $\delta^{18}O$ (Gebhardt *et al.,* 2008) with $\delta^{18}O$ values from the NGRIP ice core (NGRIP members, 2004) and the Hulu Cave speleothem records (Wang *et al.,* 2001; Southon *et al.,* 2012; Wu *et al.,* 2009) and produces values similar to plateau-tuned age models (Sarnthein *et al.,* 2007; Gebhardt *et al.,* 2008; Rae *et al.,* 2014). MD02-2489 has a particularly high sedimentation rate of around 20 cm/ky. This high sedimentation rate has allowed us to produce high resolution geochemical and planktic census records across key intervals of the last deglaciation.

Sediment core ODP 887B was raised from on the Patten seamount (54.37° N, 148.45° W) at a depth of 3647 m (Figure 5.1). Core sedimentology is described in detail in Shipboard Scientific Party (1993) and is noted to contain siliceous and calcareous oozes with clay and IRD deposits. Our samples span from 35.5-125 cmbsf, equivalent to 8.4-20 ky when applying the updated age model from Rae *et al.,* (2014). This age model synchronises the chronology of the two cores by tying the % $CaCO_3$ and ^{14}C between the two closely-spaced sites (Rae *et al.,* 2014). Following the application of this age model, tie points are still within 2σ uncertainties presented in the

original age model by Galbraith *et al.,* (2007). The sedimentation rate of ODP 887B ranges from 4-15 cm/ky.

5.2.2 Planktic foraminifera census counts

Relative abundance and planktic foraminifera per gram calculations were made on 38 samples from sediment core MD02-2489 and on 42 samples from sediment core ODP 887B. Samples were initially freeze dried for 12-24 hours and weighed to ascertain their dry weight. Following this, samples were disaggregated on a shaker table and sieved through a 63 μm sieve to remove clay material and retrieve the coarse fraction. Samples were sieved through a 150 μm sieve and split using a micro-splitter so that >300 foraminifera were present in each sample. Each split was counted for planktic foraminifera abundance and the relative abundance of each species was calculated. Split counts were scaled up to calculate total foraminifera abundance and through combination with sample dry weight, planktic foraminifera per gram was calculated.

5.2.3 Trace element and boron isotope analysis

We analysed 28 down-core samples of the planktic foraminifera *N. pachyderma*. We picked ~400 *N. pachyderma* per sample from the 150-250 μm size fraction, before crushing and oxidatively cleaning samples to remove clay and organic material following Rae *et al.,* (2011), modified from Barker *et al.,* (2003). An aliquot of 5 % of the dissolved solution was analysed for trace elements using an Agilent 7500 Inductively Coupled Plasma Mass Spectrometer in the STAiG laboratory at the University of St Andrews and sample-standard bracketing. Typical analytical uncertainty was ~0.03 mmol/mol for Mg/Ca (1.9 %) and ~0.005 μmol/mol (3.8 %) for Cd/Ca, based on 2SD of long-term analysis of consistency standards. Two samples were removed due to high Al/Ca and Mn/Ca ratios (see supplementary figure 5.9). For our boron isotope analysis 27 dissolved samples were put through column chromatography using an Amberlite resin to concentrate their boron content and remove matrix material. Samples were then analysed on a Neptune Multi-Collector Inductively Coupled Plasma Mass Spectrometer (MC-ICPMS) in the STAiG laboratory at the University of St Andrews following Foster *et al.,* (2008) and Rae *et al.,* (2011), though with the addition of trace hydrofluoric acid used to improve washout (Rae *et al.,* in review). Samples were run alongside matrix-matched standards using standard-sample bracketing. Uncertainty is reported at 95 % confidence based on long-term machine reproducibility and the size of the sample in question.

We converted our Mg/Ca ratios to temperature using the new global temperature calibration (Taylor *et al., in prep;* see chapter 4). This follows the equation:

$$Mg/Ca = 0.641(\pm 0.025)\, e^{0.061\,(\pm 0.003) * T} \quad (5.1)$$

These temperatures were also used to calculate pH and $pCO_{2(sw)}$ when combined with our boron isotope record.

We also present 30 benthic Cd/Ca analyses from sediment core MD02-2489, from the same *C. wuellerstorfi* specimens analysed for $\delta^{11}B$ by Rae et al., (2014). Samples were prepared using the same cleaning method as our planktic records and were analysed on an Element 2 Inductively Coupled Mass Spectrometer at the University of Bristol, using the same standards as used for our planktic data.

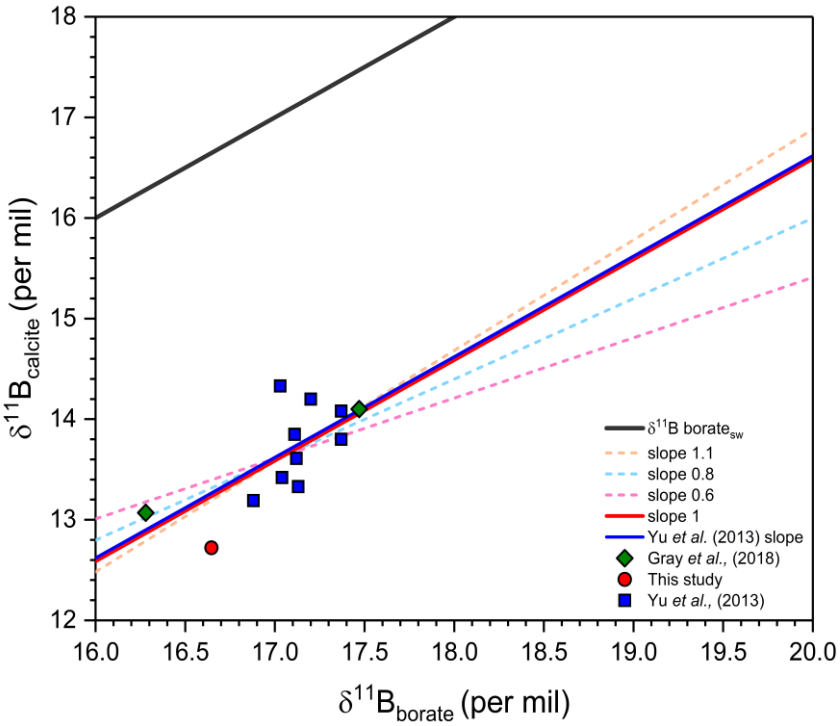

Figure 5.2: Sensitivity test for the calibration of $\delta^{11}B$ in N. pachyderma. Measured $\delta^{11}B$ of calcite is plotted against calculated $\delta^{11}B_{borate}$ from Yu et al., (2013) (blue squares), Gray et al., (2018) (green diamonds) and a new site in the Bering Sea (red circle, HLY0904-19). Dashed lines show different slopes for the relationship between $\delta^{11}B_{calcite}$ and $\delta^{11}B_{borate}$ which covers encompasses the range seen within other calibration studies.

5.2.4 pH and CO_2 calibration and calculations

The boron isotope composition ($\delta^{11}B$) of foraminifera is increasingly used to reconstruct ocean pH and CO_2 in the past (Foster and Rae, 2016; Rae, 2018). The calculation of pH from boron isotopes in planktic foraminifera requires an adjustment of measured $\delta^{11}B$ to ascertain the $\delta^{11}B$ of borate ($\delta^{11}B_{B4}$) in seawater, the parameter that is directly linked to ocean pH (Foster and Rae, 2016). In planktic foraminifera, there is an offset between measured $\delta^{11}B_{calcite}$ and seawater $\delta^{11}B_{B4}$

depending on the presence or absence of photosynthetic algae. Non-symbiont bearing species fall below the seawater borate curve, whilst symbiont bearing species plot above the curve (Hönisch *et al.*, 2004; Henehan *et al.*, 2013). Because of this offset, species-specific calibrations are required. To date, only Yu *et al.*, (2013) provide core-top data for the non-symbiont bearing polar species *N. pachyderma*. Yu *et al.*, (2013) propose an average $\delta^{11}B_{calcite\text{-}B4}$ offset of -3.38 ± 0.71 ‰ based on nine North Atlantic samples, but cover a limited $\delta^{11}B_{B4}$ range (16.88 - 17.37 ‰), increasing the uncertainty of pH reconstructions from lower pH sites.

To add confidence to low pH reconstructions, Gray et al. (2018) provided two Holocene $\delta^{11}B$ values from the North Pacific, one from sediment core MD02-2489 (North East Pacific) and one from sediment core MD02-2416 (North West Pacific) (Figure 5.1). Additionally, we add a further low pH core-top (MUC) from the Bering Sea core HLY0902-19 (54.61° N, 178.72° E, 855 m water depth) (Figure 5.1). These three points significantly increase the range of $\delta^{11}B_{B4}$ values within the calibration. To add these points to calibration curve of Yu *et al.*, (2013) we calculate pre-industrial (PI) $\delta^{11}B_{B4}$ for each site using the GLODAP database (Key *et al.*, 2004) and ODV's 3D estimation tool (Schiltzer, 2006) to attain PI-DIC values for each site. We then use PI-DIC and alkalinity (estimated in the same way) to calculate pH and $\delta^{11}B_{B4}$ using the suite of equations set out in Zeebe and Wolf-Gladrow (2001) and Rae (2018).

To test the sensitivity of $\delta^{11}B_{calcite}$ to a change in pH we use the values from Yu *et al.*, (2013), Gray *et al.*, (2018), and our new Bering Sea site. Yu *et al.*, (2013) assume a slope of 1 when calculating their intercept. We adjust the sensitivity by modelling the intercept under different slopes, encompassing the range of slopes seen within other planktic foraminifera species (0.6-1.1) (Figure 5.2). Our sensitivity tests suggest that the slope of *N. pachyderma* $\delta^{11}B_{B4}$ does not profoundly impact that $\delta^{11}B_{B4}$ intercept. Furthermore, as our new values have good consistency with those from Yu *et al.*, (2013), we do not propose a new offset for *N. pachyderma* from $\delta^{11}B_{B4}$ and support the continued use of -3.81 ± 0.71 ‰ (2σ).

Following $\delta^{11}B_{calcite}$ conversion to $\delta^{11}B_{B4}$, using the calibration discussed above, pH was then calculated by combining Mg/Ca temperature estimates from the same samples, surface salinity of 33 p.s.u, and surface pressure. A modern ocean alkalinity value of 2200 µmol/kg ± 175 was used to converted $pH_{(sw)}$ to $pCO_{2(sw)}$. We use a conservative uncertainty (equivalent to the range across the whole modern surface ocean) as alkalinity is poorly constrained; however, due to relationships within the carbonate system, uncertainty in $CO_{2(sw)}$ calculations remains driven primarily by our $\delta^{11}B$ and pH data (Rae, 2018). Confidence intervals of 66 % (1σ) and 95 % (2σ) were fully propagated through a Monte Carlo simulation of 10,000 repetitions.

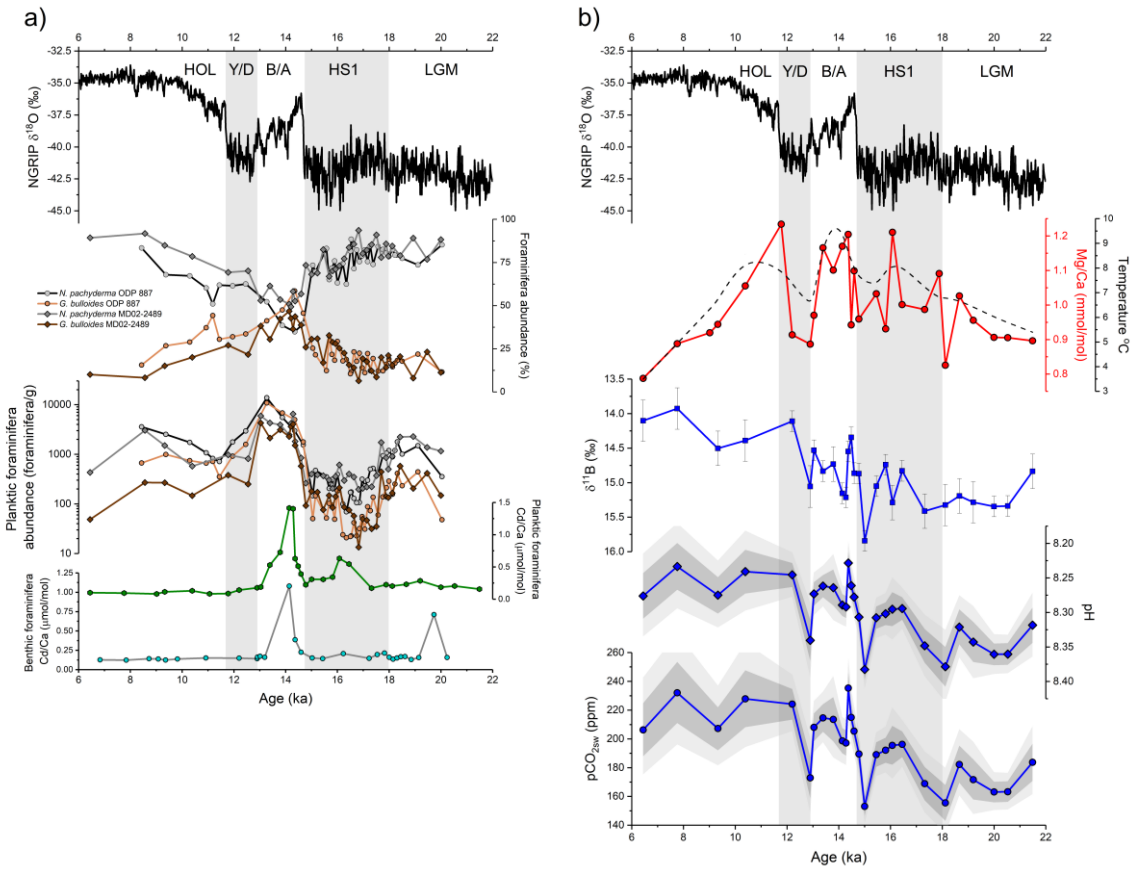

Figure 5.3: Census, trace element, and $\delta^{11}B$ analyses from sediment core MD02-2489 and ODP 887B plotted alongside the $\delta^{18}O$ record from NGRIP members (2004). ***a)*** *The relative abundance of N. pachyderma and G. bulloides as well as planktic foraminifera per gram of sediment (log scale) for both species. Cd/Ca ratios in benthic (C. wuellerstorfi) and planktic (N. pachyderma) foraminifera are also shown. Benthic trace element data was analysed at the University of Bristol.* ***b)*** *Mg/Ca ratios from N. pachyderma and smoothed temperature calculated using the new calibration from chapter 4. In addition, new raw boron isotope data (blue squares), calculated pH (blue diamonds), and calculated $pCO_{2(sw)}$ are shown. Uncertainty in our pH and $pCO_{2(sw)}$ records was fully propagated using a Monte Carlo simulation of 10,000 repetitions and is presented at both 1σ (dark grey) and 2σ (light grey) confidence limits. Shaded bars highlight key intervals during the last deglaciation: LGM is the Last Glacial Maximum; HS1 is Heinrich Stadial 1; B/A is the Bölling-Alleröd; Y/D is the Younger Dryas and HOL is the Holocene.*

5.3 Results

5.3.1 Planktic foraminifera census data

Nine species of planktic foraminifera were present within our samples from both core sites: *N. pachyderma; G. bulloides; T. quinqueloba; N. incompta; G. glutinata; G. siphonifera; O. universa; N. dutertrei* and *G. scitula*. Of these, *N. pachyderma* and *G. bulloides* dominate

throughout, with the sum of the remaining species not exceeding 15 % abundance at any point in either core.

The relative abundance of *N. pachyderma* and *G. bulloides* covary inversely with one another through the last deglaciation at both MD02-2489 and ODP 887B (Figure 5.3). During the latter stages of the last glacial maximum (LGM) and the early parts of Heinrich Stadial 1, *N. pachyderma* abundance is high and stable (>70%), whilst *G. bulloides* abundance is low and does not exceed 30 % relative abundance (Figure 5.3). This changes around 16.5 ka, when the percentage abundance of *G. bulloides* begins to increase, prompting a concurrent reduction in percentage *N. pachyderma* (Figure 5.3). The largest step change in % abundance is observed at the onset of the B/A. Here, *G. bulloides* abundance rises rapidly to greater than 50 % in both cores whilst *N. pachyderma* drops in the same fashion. This period is also marked by higher planktic foraminifera diversity, with the abundance of other species rising to 8 % in MD02-2489 and 15 % in ODP 887B. The remainder of the record sees *N. pachyderma* abundance recover in both cores, eventually reaching relative abundances higher than seen during the LGM (Figure 5.3).

The abundance of planktic foraminifera to the sediment (planktics/g) is shown for both cores in figure 5.3. At the onset of HS1, both species see decreases in abundance, particularly *G. bulloides* whose numbers are dramatically reduced in both cores (Figure 5.3). *G. bulloides* abundances then recover through HS1, reaching a peak around 16 ka. At the onset of the B/A *G. bulloides* and *N. pachyderma* abundances increase dramatically, before decreasing once more at the onset of the Younger Dryas, and then increasing slightly into the early Holocene.

5.3.2 Trace element data

Trace element to calcium ratios and Mg/Ca derived temperatures are shown in Figure 5.3. Notably, temperatures based on Mg/Ca are higher during the LGM than in the late Holocene and increase further during mid HS1 (Figure 5.3). Higher temperatures are observed again at the onset of the B/A and remain stable for the remainder of the interval (Figure 5.3). They then drop rapidly to low values during the Younger Dryas (Y/D) before rising once more to mark the onset of the Holocene (Figure 5.3). The Holocene section of our record is characterised by a downward trend in Mg/Ca ratios and temperature, in which values drop to below that of the LGM (Figure 5.3).

Planktic Cd/Ca ratios show two key excursions to high values within our record (Figure 5.3). The first peak occurs between 17.5 and 16 ka, where Cd/Ca ratios rise to 0.6 µmol/mol. The second peak occurs at the onset of the B/A, where Cd/Ca ratios rise dramatically to 1.4 µmol/mol between 14.7-14.1 ka before dropping to previous levels before the start of the Y/D. Benthic Cd/Ca ratios from the same core (MD02-2489) are also presented (Figure 5.3). These provide a test of the potential influence of post-depositional coatings, given that the planktic and benthic specimens

grow in different waters, but may acquire a similar post-depositional coating. Covariation of benthic and planktic Cd/Ca indicates an influence from authigenic coatings during the B/A excursion, a time where various other records indicate profound changes in sediment redox conditions (Figure 5.3) (Jaccard *et al.*, 2009; Jaccard and Galbraith, 2011; Galbraith and Jaccard, 2015). In contrast, benthic and planktic Cd/Ca ratios do not co-vary during HS1, suggesting high planktic values during this interval reflect elevated surface nutrient conditions (Figure 5.3).

5.3.3 Boron isotope data

Boron isotope data show a general trend from LGM to Holocene of decreasing $\delta^{11}B$, indicating decreasing surface pH and increasing surface CO_2 (Figure 5.3). Our record is punctuated by two abrupt shifts in $\delta^{11}B$, firstly between 17.5 and 15.5 ka where $\delta^{11}B$ and pH drop, and $pCO_{2(sw)}$ rises to ~190 ppm. $\delta^{11}B$ and pH then recover to higher values at the end of HS1, before dropping dramatically into the B/A, indicating a $pCO_{2(sw)}$ rise of ~70 ppm in ~600 years (Figure 5.3). $\delta^{11}B$ ratios and pH remain low throughout the B/A before decreasing during the Younger Dryas (Figure 5.3). Following this decrease, $\delta^{11}B$, pH, and $pCO_{2(sw)}$ values stabilise for the remainder of the Holocene, with a slight trend towards increasing $pCO_{2(sw)}$ (Figure 5.3).

5.4 Discussion

The role of the North Pacific in deglacial CO_2 rise has recently received increased attention (Galbraith *et al.*, 2008; Gebhardt *et al.*, 2008; Okazaki *et al.*, 2010; Jaccard and Galbraith, 2013; Max *et al.*, 2014; Rae *et al.*, 2014; Maier *et al.*, 2015; Gray *et al.*, 2018), and our new data help further this discussion. Our boron isotope reconstructions of pH and $pCO_{2(sw)}$ from the North East Pacific are notably similar to the recently published North West Pacific record from Grey *et al.*, (2018). Our higher resolution record confirms the large excursion during the B/A as well as highlighting a second prominent excursion during HS1. The signals in our data are lower in amplitude than in the North West Pacific record, which also exhibits lower pH and higher CO_2. This is not unexpected, given the high surface CO_2 values around the centre of upwelling in the modern North West Pacific, and suggests that much of the action during deglaciation is centred on the North West Pacific, but that changes in pH and pCO_2 are consistently felt across the whole subpolar gyre.

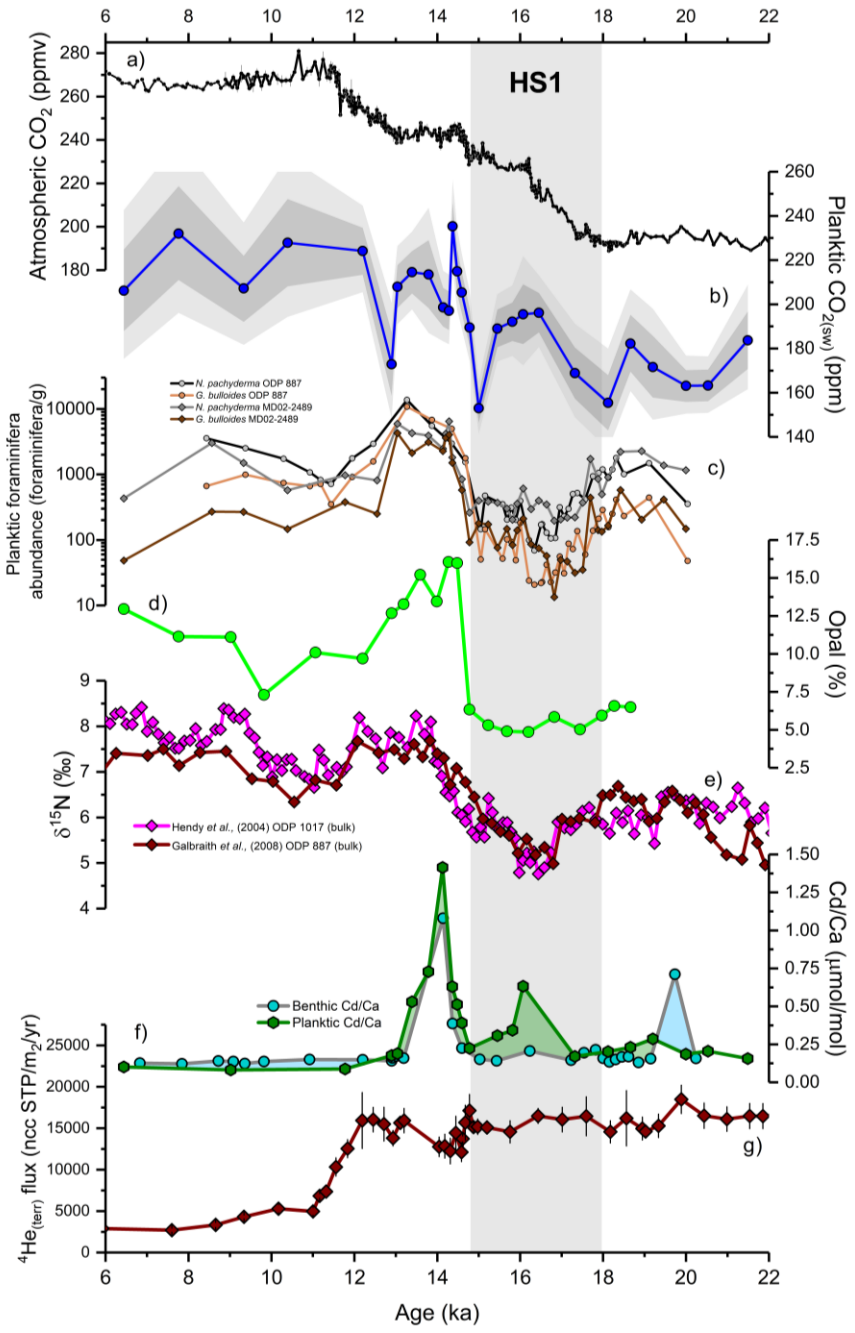

Figure 5.4: Productivity, nutrients and CO_2 in the North Pacific during HS1. ***a)*** *Atmospheric CO_2 record from Marcott et al., (2014) and Berieter et al., (2015).* ***b)*** *New $pCO_{2(sw)}$ calculated from $\delta^{11}B$ and Mg/Ca temperatures from ODP 887B in the North East Pacific. Confidence bands are giving at 1σ (dark grey) and 2σ (light grey).* ***c)*** *Planktic foraminifera per gram of sediment for two species N. pachyderma (grey and black lines) and G. bulloides (light and dark brown lines) from two adjacent sediment cores in the North Pacific, MD02-2489 (diamonds) and ODP 887B (circles).* ***d)*** *Percentage opal from sediment core MD02-2489 (Gebhardt et al., 2008), a proxy for productivity.* ***e)*** *$\delta^{14}N$ data from two North East Pacific cores, ODP 1017 (purple) from Hendy et al., (2004) and ODP 887 (brown) from Galbraith et al., 2008.* ***f)*** *New benthic and planktic Cd/Ca ratios from MD02-2489, Cd/Ca ratios in planktic foraminifera are a proxy for surface nutrient levels (Yu et al., 2013).* ***g)*** *Terrestrial ^4He flux (a dust flux proxy) from Serno et al., (2015).*

The two intervals of high surface CO_2 during HS1 and the BA occur alongside distinct biogeochemical and circulation conditions. During HS1, high surface CO_2 is combined with increased regional ventilation (Okazaki *et al.,* 2010; Rae *et al.,* 2014), whilst productivity remains low (Figures 5.4 and 5.5). In contrast, the abrupt increase in surface CO_2 seen at the onset of the B/A is associated with increased surface stratification and large increases in productivity across the North Pacific (Gebhardt *et al.,* 2008; Gray *et al.,* 2018) (Figures 5.6 and 5.7). To reconcile these opposing circulation regimes alongside high surface CO_2 during both events, we discuss in detail our new records of $pCO_{2(sw)}$, foraminiferal census, and trace elements, alongside a range of published records from the region.

5.4.1 CO_2, circulation, and productivity during Heinrich Stadial 1

Our planktic $\delta^{11}B_{(sw)}$ data show that pH decreased, and surface water CO_2 increased between 17.5-15.5 ka in the North East Pacific (Figure 5.4). Our planktic Cd/Ca record shows a positive excursion between 17.5-15.5 ka, concurrent with the increase in $pCO_{2(sw)}$ (Figure 5.4) suggesting a simultaneous increase in surface nutrient content (Delaney, 1989; Boyle, 2006; Yu *et al.,* 2013). Although only a few studies highlight the relationship between Cd/Ca and nutrient contents, Yu *et al.,* 2013 show a strong relationship exists within *N. pachyderma.*

Several recent studies suggest a more dynamic North Pacific overturning regime existed during HS1, with increased ventilation indicated by ^{14}C data across the interval (Okazaki *et al.,* 2010; Max *et al.,* 2014; Rae *et al.,* 2014). This breakdown of stratification is particularly pronounced between ~17.5-16 ka, with benthic-planktic (B-P) radiocarbon offsets from Rae *et al.,* (2014) showing a decrease in B-P ages to <500 yrs, suggesting a pulse of local deep-water formation (Figure 5.5). Benthic $\delta^{11}B$ and $\delta^{13}C$ data from the same core also show a concurrent step change towards lower $\delta^{11}B$ and $\delta^{13}C$ values during this interval (Figure 5.5), suggested by Rae et al. (2014) to reflect mixing of CO_2-rich low $\delta^{13}C$ water from intermediate depths throughout the water column. The similarity between our surface water CO_2 reconstructions and the benthic boron isotope record supports the idea that CO_2-rich water was mixed throughout the water column at this time. An increase in overturning circulation during HS1 may be expected to bring in warm waters from the subtropics. This is supported by our Mg/Ca temperature record, which shows a small increase in surface temperatures between 17.5 and 16 ka (Figure 5.5), as previously observed in several other subpolar North Pacific records (Kiefer and Kienast, 2005).

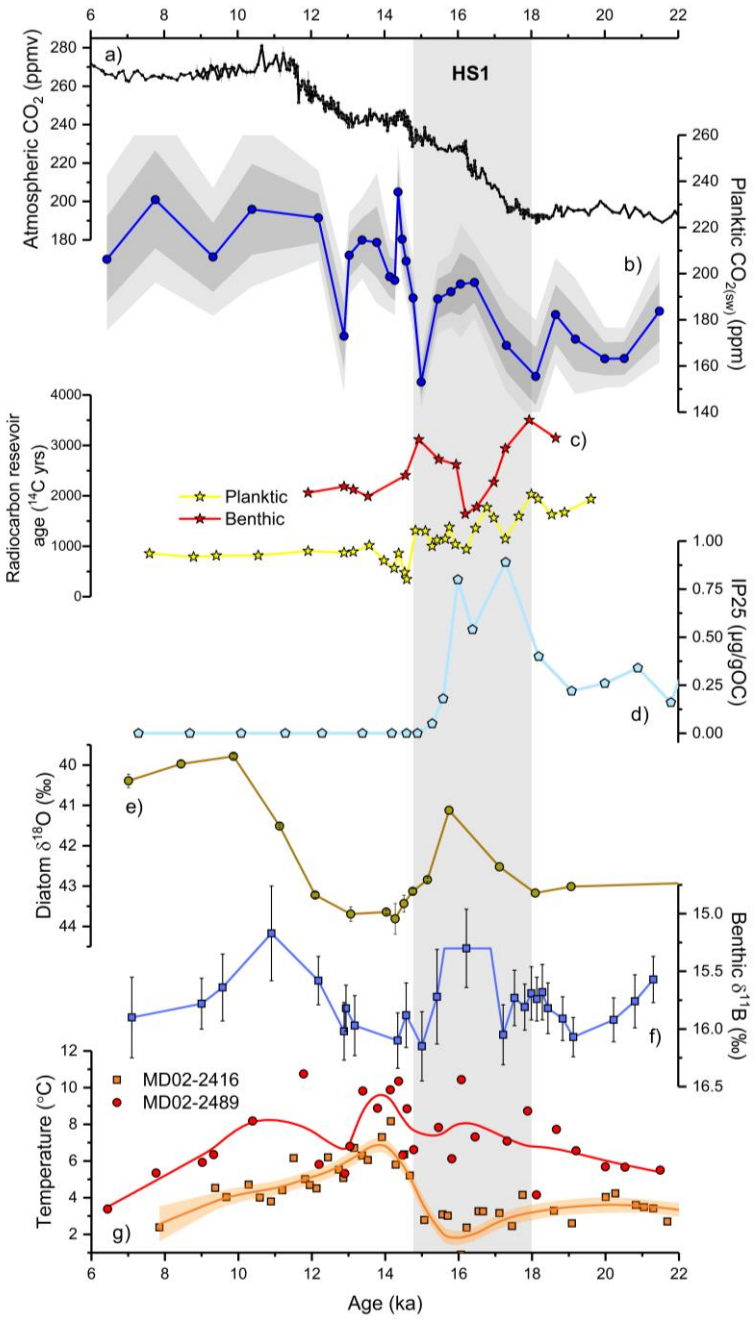

Figure 5.5: Ventilation and CO_2 changes during HS1. ***a)*** *Atmospheric CO_2 record generated from Antarctic ice cores (Marcott et al., 2014; Bereiter et al., 2015).* ***b)*** *New $pCO_{2(sw)}$ calculated from $\delta^{11}B$ and Mg/Ca temperatures from ODP 887B in the North East Pacific. Confidence bands are giving at 1σ (dark grey) and 2σ (light grey).* ***c)*** *Benthic (red stars) and planktic (yellow stars) radiocarbon reservoir ages (^{14}C yrs) from Rae et al., (2014) from sediment core MD02-2489 highlighting a reduction in the Benthic-Planktic offset during the middle of HS1.* ***d)*** *IP25 per gram of organic carbon (a sea ice proxy) from sediment core SO202-27-6 in the North East Pacific (Méheust et al., 2018).* ***e)*** *Diatom $\delta^{18}O$ from sediment core SO202-27-6 (Maier et al.,2015).* ***f)*** *Benthic $\delta^{11}B$ data from MD02-2489 showing low $\delta^{11}B$ (high CO_2) during the middle of HS1 (Rae et al., 2014).* ***g)*** *New SST estimates from MD02-2489 (red circles) calculated using the new calibration from Chapter 4, alongside published SST estimates from MD02-2489 from Gray et al., (2018).*

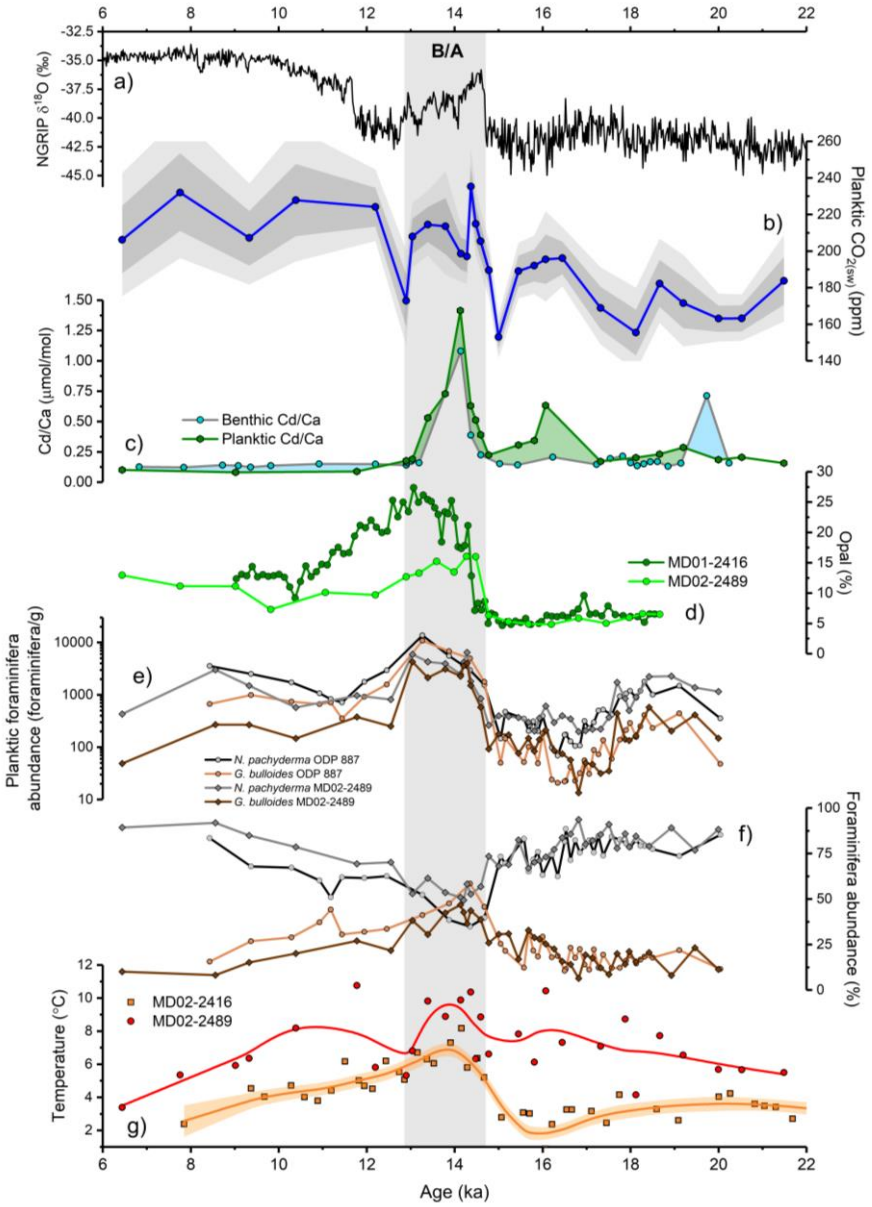

Figure 5.6: Changes in deglacial CO_2, nutrients, and temperature during the B/A in the North Pacific. ***a)*** *d18O record from the Greenland Ice Core (NGRIP members, 2004).* ***b)*** *New $pCO_{2(sw)}$ calculated from $\delta^{11}B$ and Mg/Ca temperatures from ODP 887B in the North East Pacific. Confidence bands are giving at 1σ (dark grey) and 2σ (light grey).* ***c)*** *New benthic and planktic Cd/Ca ratios from MD02-2489, Cd/Ca ratios in planktic foraminifera are a proxy for surface nutrient levels (Yu et al., 2013).* ***d)*** *Percentage opal from sediment core MD02-2489 (Gebhardt et al., 2008) and ODP 887B (Galbraith et al., 2007), a proxy for productivity.* ***e)*** *Planktic foraminifera per gram of sediment for two species N. pachyderma (grey and black lines) and G. bulloides (light and dark brown lines) from two adjacent sediment cores in the North Pacific, MD02-2489 (diamonds) and ODP 887B (circles).* ***f)*** *Relative abundance of N. pachyderma (grey and black lines) and G. bulloides (brown lines) from two adjacent sediment cores in the North Pacific, MD02-2489 (diamonds) and ODP 887B (circles).* ***g)*** *New SST estimates from MD02-2489 (red circles) calculated using the new calibration from Chapter 4, alongside published SST estimates from MD02-2489 from Gray et al., (2018).*

In contrast to the emerging picture of enhanced ventilation during HS1 in the North Pacific, Maier *et al.,* (2015) argue for increased stratification. They compare $\delta^{18}O_{diatom}$, used as an indicator of fresh surface waters, and $\delta^{18}O_{NPS}$, suggesting that the lack of coherence between these two records indicates isolation between surface and sub-surface waters (Maier *et al.,* 2015). Additionally, Maier *et al.,* (2015) suggest melting sea ice could provide the mechanism for this enhanced surface stratification. We reject this view based on two factors. Firstly, recent work by Iwasaki *et al.,* (2017) and Taylor *et al.,* (2018) suggest that *N. pachyderma* in the North Pacific are predominantly found in the top 50 m of the water column and are often associated with the chlorophyll maximum. This suggests $\delta^{18}O_{NPS}$ and $\delta^{18}O_{diatom}$ would both reflect surface water conditions at this site. Secondly, the presence of sea ice in the region is indicated by the sea ice proxy IP25 (Figure 5.5), a biomarker produced by diatoms when they are living beneath sea ice (Méheust *et al.,* 2018). Rather than sea ice melt leading to enhanced stratification, we find it more likely that winter sea ice formation and coupled brine rejection would increase surface water density and drive enhanced ventilation (Shcherbina *et al.,* 2003). Maier *et al.,* (2015)'s $\delta^{18}O_{diatom}$ record may instead reflect spring/summer values, where melting sea ice increases surface water freshness following winter brine rejection and deeper mixing. Studies from across the polar North Pacific have noted an apparent increase in North Pacific Intermediate Water formation during the late LGM and HS1 (Okazaki *et al.,* 2010; Jaccard and Galbraith, 2013; Max *et al.,* 2014). Our records of $\delta^{11}B$ agree with this view and support a further period of localised deep-water formation, which initiated at 17 ka (Rae *et al.,* 2014), supplying the surface North Pacific with CO_2 and nutrients (Figures 5.4 and 5.5).

Our Cd/Ca records suggest the nutrient content of North East Pacific waters was increased during HS1 (Figure 5.4). Despite this, data from several sites in the region indicate muted surface ocean productivity during this time (Gebhardt *et al.,* 2008; Galbraith *et al.,* 2008; Maier *et al.,* 2015) (Figure 5.4). This is in part reflected in our planktic foraminifera census data, with an overall decrease in planktic abundance between 17.5-15.5 ka compared with the LGM and B/A (Figure 5.4), though this is likely also driven in part by low pH deep waters (Rae *et al.,* 2014) which enhance dissolution of calcium carbonate. Interestingly, a small increase in flux of the opportunistic species *G. bulloides* during mid HS1 is suggestive of increased nutrient levels but low overall productivity (Figure 5.4). This lapse in productivity could have been driven by an increase in mixed layer depth, linked to enhanced overturning (Okazaki *et al.,* 2010; Max *et al.,* 2014; Rae *et al.,* 2014). This would remove primary producers from the photic zone (Lam *et al.,* 2013), driving a decrease in productivity despite abundant major nutrients (Gebhardt *et al.,* 2008; Galbraith *et al.,* 2008; Maier *et al.,* 2015) and iron (Serno *et al.,* 2015). Together, this availability of nutrients and high CO_2 alongside low productivity implies an inefficient biological pump,

which is further supported by a decrease in $\delta^{15}N$ indicating reduced nitrate utilization (Galbraith *et al.,* 2008; Hendy *et al.,* 2004), though foraminifera bound $\delta^{15}N$ data from the North West Pacific, which do not show this trend, remain a point of interest (Ren *et al.,* 2015). Alongside low productivity and increased surface nutrients and CO_2, the majority of $\delta^{15}N$ data supports our conclusion that a weak biological pump dominated the North East Pacific at this time.

A weak biological pump combined with high $pCO_{2(sw)}$ during this mid HS1 interval of deep-water formation would have allowed CO_2 to outgas from the deep ocean into the atmosphere. Although this CO_2 anomaly in the North East Pacific is relatively small in magnitude, a pulse of deep water in this region has the potential to ventilate a large volume of deep CO_2 and provide a source of high preformed nutrient North Pacific deep water to the oceans' interior (Hain *et al.,* 2010; Hain *et al.,* 2011), and thus could have had a major impact on atmospheric pCO_2 levels. The ability of North Pacific deep-water formation to contribute to early deglacial CO_2 rise is further supported by experiments with a biogeochemistry enabled Earth System model, which show that this process can also explain the concurrent drop in atmospheric $\delta^{14}C$ and $\delta^{13}C$. While the Southern Ocean likely plays a crucial role in deglacial CO_2 rise, most changes in Southern Ocean ventilation occur somewhat later in HS1.

5.4.2 Stratification, nutrients and CO_2 during the Bølling-Allerød

Our $\delta^{11}B$, pH, and $pCO_{2(sw)}$ records show that the most rapid increase in North Pacific surface CO_2 occurred at the onset of the B/A (Figure 5.6), with a $pCO_{2(sw)}$ increase of ~70 ppm in ~600 years. This was accompanied by a simultaneous increase in planktic Cd/Ca ratios, which may indicate an increase in surface nutrient concentrations, though may also be impacted by post-depositional coatings at this time, given the concurrent increase in benthic Cd/Ca (Delany, 1989; Boyle, 2006) (Figure 5.6). Our planktic foraminifera census data show increases of several thousand planktic foraminifera per gram in both *G. bulloides* and *N. pachyderma* (Figure 5.6). As the flux of these species is controlled heavily by food availability (Taylor *et al.,* 2018), the parallel increase in both species suggests an increase in primary productivity, as previously inferred from opal, organic carbon, and chlorin contents in sediments at this site (Gebhardt *et al.,* 2008, Galbraith *et al.,* 2008). In addition, the relative abundance of the opportunistic species *G. bulloides* increases dramatically at the onset of the B/A, further supporting an increase in productivity and food availability (Figure 5.6). Bottom water pH, inferred from benthic boron isotope data (Rae *et al.,* 2014), shows no change at the onset of the B/A, suggesting that the signals in our census data are not primarily controlled by bottom water dissolution at this time. Increased nutrient availability during the B/A is also supported by Maier *et al.,* (2015) who cite a decrease in $\delta^{30}Si_{(diat)}$ as an indicator of increased Si supply during this time.

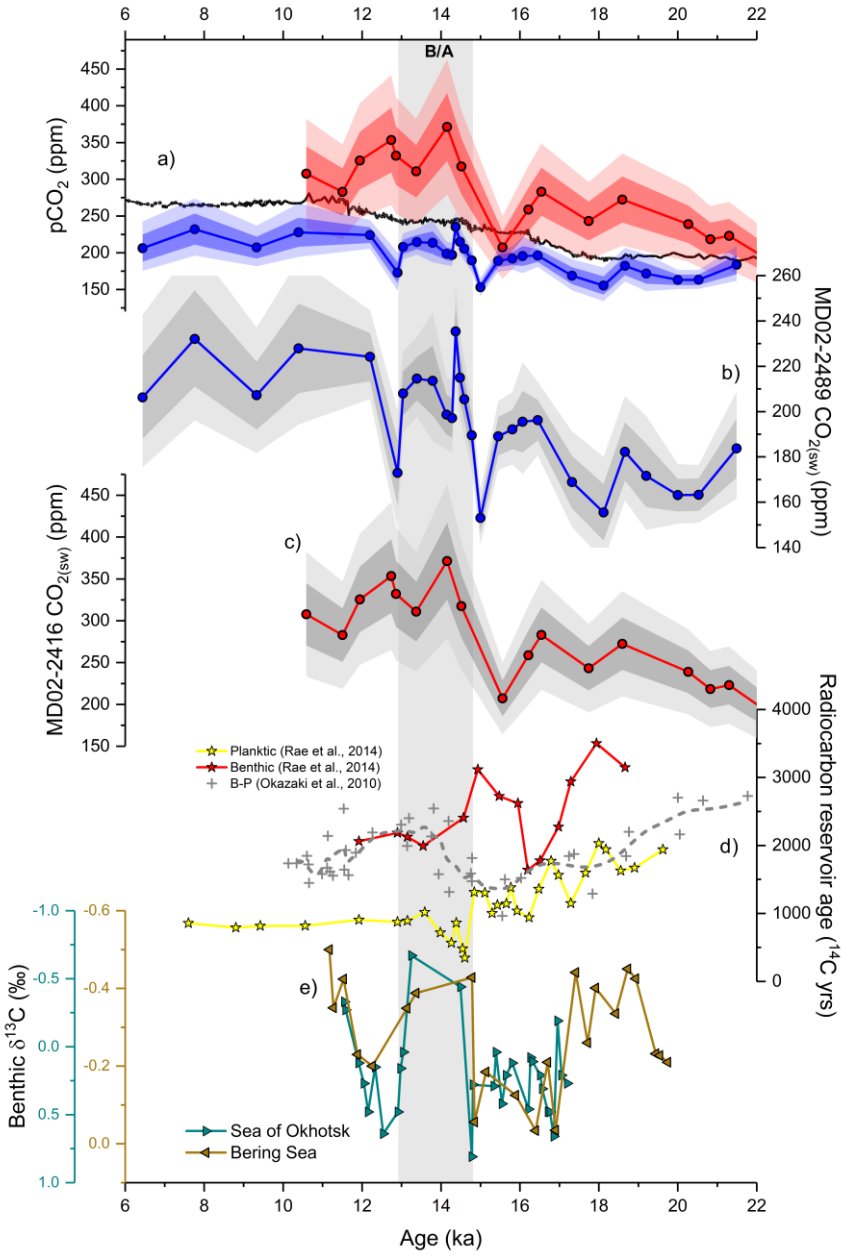

Figure 5.7: Changes in CO_2 and stratification during the B/A. ***a)*** *Atmospheric CO_2 (black line) (Marcott et al., 2014; Bereiter et al., 2015) plotted alongside surface ocean CO_2 records from the North East Pacific (this study, blue circles) and the North West Pacific (Gray et al., 2018).* ***b)*** *New $pCO_{2(sw)}$ calculated from $\delta^{11}B$ and Mg/Ca temperatures from ODP 887B in the North East Pacific. Confidence bands are giving at 1σ (dark grey) and 2σ (light grey).* ***c)*** *Published $pCO_{2(sw)}$ based on boron isotope data from sediment MD02-2416 in the North West Pacific (Gray et al., 2018). Confidence bands are given at 1σ (dark grey) and 2σ (light grey).* ***d)*** *Benthic (red stars) and planktic (yellow stars) radiocarbon reservoir ages (^{14}C yrs) from Rae et al., (2014) from sediment core MD02-2489 alongside compiled North Pacific intermediate depth B-P offsets from Okazaki et al., (2010) (grey crosses and dashed line).* ***e)*** *Benthic $\delta^{13}C$ records from the Sea of Okhotsk (green triangles) and the Bering Sea (Brown triangles) produced by Max et al., (2014).*

Our high $pCO_{2(sw)}$ values confirm the finding of Gray et al. (2018), that increased nutrient and CO_2 supply drove the regional productivity peak during the B/A. Although availability of iron and light, due to high dust fluxes (Serno *et al.*, 2015) and stratified surface waters (Lam *et al.*, 2013), may have contributed, they cannot be the primary cause of the productivity pulse, as a net increase in biological pump efficiency would drive a decrease in surface water CO_2.

Basin-wide intermediate water records of ^{14}C and $\delta^{13}C$ suggest reduced ventilation at the onset of the B/A (Okazaki *et al.*, 2010; Rae *et al.*, 2014; Max *et al.*, 2014). This is also reflected in widespread anoxia observed through benthic foraminifera oxygenation indexes, laminations, and trace element analysis (Keigwin and Jones, 1990; Kennett and Ingram, 1995; Zheng *et al.*, 2000; Crusuis *et al.*, 2004; Jaccard and Galbraith, 2011; Praetorius *et al.*, 2015), likely a consequence of both reduced regional ventilation (Kennet and Ingram, 1995; Okazaki *et al.*, 2010; Max *et al.*, 2014; Rae *et al.*, 2014) and increased respiration of organic matter due to the productivity pulse (Grey *et al.*, 2018). Enhanced stratification during the B/A would have facilitated the pooling of nutrients and CO_2 in subsurface waters in the North Pacific, but for this to drive high surface productivity, these high nutrient, high CO_2 waters would have to be supplied to the surface. Gray *et al.*, (2018) present a mechanism in which high nutrient and carbon subsurface waters are brought to the surface via winter mixing and enhanced Ekman suction. Their analysis of the PMIP3 model ensemble shows that the presence of ice on North America dramatically increases the wind stress curl and associated Ekman suction over the subpolar North Pacific (Gray *et al.* 2018). This would drive increased upwelling, tapping into the shallow potent reservoirs of nutrients and carbon (Rae *et al.*, 2014; Gray *et al.*, 2018) and enhancing surface productivity.

Despite increased productivity during the B/A, our $pCO_{2(sw)}$ record alongside that of Grey *et al.*, (2018) show that CO_2 and nutrient supply to surface waters through Ekman suction overwhelmed the productivity spike observed within opal and planktic foraminifera records (Figure 5.7). The synchronous nature of the peaks in pCO_2 in both North West and North East Pacific suggest a basin-wide reduction in the efficiency of the biological pump, though higher pCO_2 in the North West Pacific suggests that outgassing of CO_2 was centred on this region. $\delta^{15}N$ data from across the North Pacific show increased $\delta^{15}N$ values at the onset of the B/A (Hendy *et al.*, 2004; Galbraith *et al.*, 2008) (Figure 5.4). These are thought to predominantly reflect high rates of denitrification brought on by increased anoxia, making these records difficult to interpret in terms of nutrient utilization. Recent work by Maier *et al.*, (2015) showing a decoupling between $\delta^{30}Si_{(diat)}$ and opal deposition, also suggests a reduction in the efficiency of the biological pump during the B/A.

The simultaneous increase in atmospheric CO_2 at 14.7 ka (Marcott *et al.*, 2014) and surface water CO_2 from both sides of the North Pacific basin, combined with increased nutrient/carbon supply

and a reduction in biological pump efficiency, suggest a possible role for the North Pacific during this abrupt event. The high surface water pCO_2 values seen throughout the B/A suggests the North Pacific played a key role in maintaining high CO_2 during the B/A when other ocean basins would likely have contributed to CO_2 drawdown (McManus *et al.,* 2004). By comparing our $pCO_{2(sw)}$ data from the North East Pacific with that of Gray *et al.,* (2018)'s we can conclude that, in a similar fashion to the modern ocean (Takahashi *et al.,* 2009), CO_2 leakage during the B/A was centred around the North West Pacific.

In addition to high productivity, an increase in sea surface temperature of ~2°C is also seen at the onset of the B/A in the North East Pacific. This is a muted response compared with a 4°C rise seen in the North West Pacific (Grey *et al.,* 2018) (Figure 5.6). Sea surface temperature reconstructions by Maier *et al.,* (2015) and Gebhardt *et al.,* (2008) also show limited North East Pacific temperature rise during the B/A. Whilst the North West Pacific was cool during HS1 (Gray *et al.,* 2018) and was able to warm rapidly in response to atmospheric teleconnections and warming in the North Atlantic, the North East Pacific, which had already experienced warming throughout HS1, only displays a muted signal likely propagated through the inflow of warm waters along the Kuroshio extension.

5.4.3 Younger Dryas and Holocene in the North Pacific

The Younger Dryas (Y/D) marks a return to cooler Northern Hemisphere conditions following a warm B/A period (NGRIP members, 2004). Our Mg/Ca temperature reconstructions from the North East Pacific suggest a decrease of ~5°C at the end of the B/A (Figure 5.6). Surface water temperatures then increase towards the start of the Holocene (although resolution in our record is limited through this period) (Figure 5.6). In the North West Pacific, a high ratio of *N. pachyderma* to *N. incompta* at the onset of the Y/D is also suggestive of cold conditions, followed by a reduction of 30% by the start of the Holocene at 11.7 ka (Kallel *et al.,* 1998). Mg/Ca temperatures from Gray *et al.* (2018) indicate cooling in the North West Pacific following the end of the B/A and throughout the Y/D (Figure 5.6). Once again, the different temperature trends seen between the North West and North East Pacific may be due to the varying influence of atmospheric teleconnections with the North Atlantic versus local changes in ocean circulation in the North Pacific. The fact that cooling is now more pronounced in the NE than NW Pacific hints at differences between this stadial event and HS1, perhaps explained by changing atmospheric teleconnections as the ice sheets recede, or a less pronounced change in North Pacific overturning in the Y/D compared to HS1.

Our results also suggest a reduction in productivity occurred at the onset of the Y/D. This is primarily seen within our planktic foraminifera abundance data (Figure 5.6), where both *N.*

pachyderma and *G. bulloides* abundance decrease, indicating reduced food availability (Taylor *et al.,* 2018). Reduced productivity in comparison to the B/A is seen throughout the North Pacific during the Y/D, particularly in opal records (Hendy *et al.,* 2004; Gebhardt *et al.,* 2008; Maier *et al.,* 2015). In addition, $\delta^{13}C$ records from Max *et al.,* (2014) and ^{14}C data from Kennet and Ingram (1995) suggest a return to better ventilated conditions, flushing out the subsurface nutrients and CO_2 that accumulated during the BA (Figure 5.7). This flushing event could contribute to the small jump in $pCO_{2(sw)}$ observed during the YD, but this is less pronounced than the HS1 event, perhaps due to a less pronounced increase in overturning, and an already depleted subsurface CO_2 reservoir.

At the start of the Holocene, North East Pacific sea surface temperatures rise, and then decrease steadily between 10.5 and 6.4 ka. Whilst the initial rise in SSTs is at odds with similar records from the North West Pacific (Sarnthein *et al.,* 2004; Gray *et al.,* 2018), following 10.5 ka the general trend throughout the basin is one of decreasing SST. In addition to falling SSTs, Sarnthein *et al.,* (2004) suggest a major reduction in surface salinity took place over this period, with salinity dropping 2-3 p.s.u between 12 and 4 ka. These shifts in temperature and salinity are more akin to the modern day sub-polar North Pacific and suggest that the transition towards today's fresh, stratified surface waters occurred progressively through the Holocene. In terms of surface CO_2, no significant changes are seen following the end of the Y/D (Figure 5.7), further supporting a stabilisation of surface ocean conditions in this region during the Holocene.

5.5 Conclusion

Our new downcore planktic foraminifera census, $\delta^{11}B$, and trace element records suggest the North Pacific played a key role in CO_2 release during the last deglaciation. During HS1, our $pCO_{2(sw)}$ reconstruction indicates high surface water CO_2 in the North East Pacific. Coupled with benthic $\delta^{11}B$ and ^{14}C data, these data suggest a period of local deep-water formation existed during mid HS1, mixing CO_2 rich waters throughout the water column. Increased sea-ice brine rejection alongside changes to the hydrological cycle may have facilitated this increase in ventilation (Shcherbina *et al.,* 2003; Okazaki *et al.,* 2010). New Cd/Ca data also suggests increased nutrients in surface waters despite muted productivity (Gebhardt *et al.,* 2008; Galbraith *et al.,* 2008; Maier *et al.,* 2015). Combined with high CO_2 surface waters, this suggests an inefficient biological pump existed during mid HS1 in the North East Pacific, which, alongside formation of high preformed nutrient North Pacific Deep Water, helped drive net outgassing of CO_2 from this region.

During the B/A, our Cd/Ca and $\delta^{11}B$ records suggest nutrients and CO_2 increased in North Pacific surface waters. This was driven by collapse in ventilation, allowing nutrients and carbon to pool in the subsurface, from where they can be brought to the surface by enhanced Ekman suction

(Gray *et al.,* 2018). These high nutrient waters and stratified conditions contributed to the dramatic increase in surface water productivity seen throughout the region during this time (Gebhardt *et al.,* 2008; Maier *et al.,* 2015; Gray *et al.,* 2018). Our $\delta^{11}B$ record confirms the signal of pH and $pCO_{2(sw)}$ seen in the North West Pacific (Gray *et al.,* 2018) but at higher resolution, and suggests that much of the CO_2 released during the B/A was centred around the North West Pacific, due to the higher $pCO_{2(sw)}$ values and higher amplitude signals seen in that region. Comparison of Mg/Ca data from the NE and NW Pacific during HS1 and the BA suggests that the North West Pacific is more directly affected by North Atlantic climate through atmospheric teleconnections, while the North East Pacific may feel a greater influence from regional changes in ocean circulation. Overall, our new data suggests the North Pacific played a crucial role in regulating atmospheric CO_2 during the last deglaciation, contributing to early deglacial CO_2 rise during HS1, and maintaining high atmospheric CO_2 throughout the B/A.

These findings may have significant implications for studying previous glacial terminations. Our data suggests a more dynamic North Pacific during the last deglaciations, however this only represents one glacial cycle. Future work should focus on assessing the role of the North Pacific further back in time particularly during large terminations such as termination IV (Jouzel *et al.,* 2007) where even greater volumes of CO_2 were exchanged between oceanic and atmospheric reservoirs.

5.6 References

Ayers, J.M. & Lozier, M.S., 2010. Physical controls on the seasonal migration of the North Pacific transition zone chlorophyll front. *Journal of Geophysical Research: Oceans*, 115(5), pp.1–11.

Barker, S., Greaves, M. & Elderfield, H., 2003. A study of cleaning procedures used for foraminiferal Mg/Ca paleothermometry. *Geochemistry, Geophysics, Geosystems*, 4(9).

Boyd, P. & Harrison, P.J., 1999. Phytoplankton dynamics in the NE subarctic Pacific. *Deep-Sea Research Part II: Topical Studies in Oceanography*, 46(11–12), pp.2405–2432.

Boyle, E.A., 2006. A Direct Proxy for Oceanic Phosphorus? *Science*, 312(5781), pp.1758–1759.

Burke, A. & Robinson, L.F., 2012. The Southern Ocean's Role in Carbon Exchange During the Last Deglaciation. *Science*, 335, pp.557–561.

Crusius, J. et al., 2004. Influence of northwest Pacific productivity on North Pacific Intermediate Water oxygen concentrations during the Bølling-Ållerød interval (14.7-12.9 ka). *Geology*, 32(7), pp.633–636.

Delaney, M., 1989. Uptake of cadmium into calcite shells by planktonic foraminifera. *Chemical Geology*, 78(2).

Deutsch, C. et al., 2004. Isotopic constraints on glacial/interglacial changes in the oceanic nitrogen budget. *Global Biogeochemical Cycles*, 18(4), pp.1–22.

Elderfield, H. & Ganssen, G., 2000. Past temperature and $\delta^{18}O$ of surface ocean waters inferred from foraminiferal Mg/Ca ratios. *Nature*, 405(6785), pp.442–445.

Elderfield, H. & Rickaby, R., 2000. Oceanic Cd/P ratio and nutrient utilization in the glacial Southern Ocean. *Nature*, 405(6784), pp.305–10.

Emile-Geay, J., 2003. Warren revisited: Atmospheric freshwater fluxes and "Why is no deep water formed in the North Pacific." *Journal of Geophysical Research*, 108.

Ferrari, R. et al., 2014. Antarctic sea ice control on ocean circulation in present and glacial climates. *Proceedings of the National Academy of Sciences of the United States of America*, 111(24), pp.8753–8.

Foster, G.L., Pogge Von Strandmann, P.A.E. & Rae, J.W.B., 2010. Boron and magnesium isotopic composition of seawater. *Geochemistry, Geophysics, Geosystems*, 11(8).

Foster, G.L. & Rae, J.W.B., 2016. Reconstructing Ocean pH with Boron Isotopes in Foraminifera. *Annual review of Earth and Planetary Science*, 44, 1, pp.207–237.

Galbraith, E.D. et al., 2007. Carbon dioxide release from the North Pacific abyss during the last deglaciation. *Nature*, 449(7164), pp.890–3.

Galbraith, E.D. & Jaccard, S.L., 2015. Deglacial weakening of the oceanic soft tissue pump: global constraints from sedimentary nitrogen isotopes and oxygenation proxies. *Quaternary Science Reviews*, 109, pp.38–48.

Garcia, H.E. et al., 2014. World Ocean Atlas 2013, Volume 4: Dissolved Inorganic Nutrients (phosphate, nitrate, silicate). *NOAA Atlas NESDIS 76*, 4(September).

Garcia, H.E. et al., 2013. World Ocean Atlas 2013. Volume 3: dissolved oxygen, apparent oxygen utilization, and oxygen saturation. *NOAA Atlas NESDIS 75*, 3(September), p.27.

Gebhardt, H. et al., 2008. Paleonutrient and productivity records from the subarctic North Pacific for Pleistocene glacial terminations I to V. *Paleoceanography*, 23(4).

Gray, W.R. et al., 2018. Deglacial upwelling, productivity and CO_2 outgassing in the North Pacific Ocean. *Nature Geoscience*.

Hain, M.P., Sigman, D.M. & Haug, G.H., 2010. Carbon dioxide effects of Antarctic stratification, North Atlantic Intermediate Water formation, and subantarctic nutrient drawdown during the last ice age: Diagnosis and synthesis in a geochemical box model. *Global Biogeochemical Cycles*, 24(4), pp.1–19.

Hain, M.P., Sigman, D.M. & Haug, G.H., 2011. Shortcomings of the isolated abyssal reservoir model for deglacial radiocarbon changes in the mid-depth Indo-Pacific Ocean. *Geophysical Research Letters*, 38(4), pp.1–6.

Heinrich, H., 1988. Origin and consequences of cyclic ice rafting in the Northeast Atlantic Ocean during the past 130,000 years. *Quaternary Research*, 29(2), pp.142–152.

Hemming, N.G. & Hanson, G.N., 1992. Boron isotopic composition and concentration in modern marine carbonates. *Geochimica et Cosmochimica Acta*, 56(1), pp.537–543.

Hendy, I.L. et al., 2004. Intermittent existence of a southern Californian upwelling cell during submillennial climate change of the last 60 kyr. *Paleoceanography*, 19(3), pp.1–15.

Henehan, M.J. et al., 2013. Calibration of the boron isotope proxy in the planktonic foraminifera Globigerinoides ruber for use in palaeo-CO_2 reconstruction. *Earth and Planetary Science Letters*, 364, pp.111–122.

Hönisch, B. & Hemming, N.G., 2004. Ground-truthing the boron isotope-paleo-pH proxy in planktonic foraminifera shells: Partial dissolution and shell size effects. *Paleoceanography*, 19(4), pp.1–13.

Iwasaki, S. et al., 2017. Horizontal and vertical distributions of planktic foraminifera in the subarctic North Pacific. *Marine Micropaleontology*.

Jaccard, S.L. et al., 2009. Subarctic Pacific evidence for a glacial deepening of the oceanic respired carbon pool. *Earth and Planetary Science Letters*, 277(1–2), pp.156–165.

Jaccard, S.L. & Galbraith, E.D., 2011. Large climate-driven changes of oceanic oxygen concentrations during the last deglaciation. *Nature Geoscience*, 5(2), pp.151–156.

Jaccard, S.L. & Galbraith, E.D., 2013. Direct ventilation of the North Pacific did not reach the deep ocean during the last deglaciation. *Geophysical Research Letters*, 40(1), pp.199–203.

Jouzel, J. et al., 2007. Orbital and millennial Antarctic climate variability over the past 800,000 years. *Science (New York, N.Y.)*, 317(5839), pp.793–796.

Kallel, N. et al., 1988. Evidence of cooling during the Younger Dryas in the western North Pacific. *Oceanologica acta*, 11(4), pp.369–375.

Keigwin, L.D. & Jones, G.A., 1990. Deglacial climatic oscillations in the Gulf of California. *Paleoceanography*, 5(6), pp.1009–1023.

Keigwin, L.D., 1998. Glacial-age hydrography of the far northwest Pacific Ocean. *Paleoceanography*, 13(4), p.323.

Kennett, J.P. & Ingram, B.L., 1995. A 20,000 year record of ocean circulation and climate-change from the Santa-Barbara basin. *Nature*, 377(6549), pp.510–514.

Key, R.M. et al., 2004. A global ocean carbon climatology: Results from Global Data Analysis Project (GLODAP). *Global Biogeochemical Cycles*, 18(4), pp.1–23.

Kiefer, T. et al., 2001. North Pacific response to millennial-scale changes in ocean circulation. *Paleoceanography*, 16(2), pp.179–189.

Kohfeld, K. & Ridgwell, A., 2009. Glacial-Interglacial Variability in Atmospheric CO_2. *Surface ocean-lower atmosphere processes*, 187, pp.251-286.

Lam, P.J. et al., 2013. Transient stratification as the cause of the North Pacific productivity spike during deglaciation. *Nature Geoscience*, 6(8), pp.622–626.

Lembke-jene, L. et al., 2018. Rapid shift and millennial-scale variations in Holocene North Pacific Intermediate Water ventilation. *PNAS*, (18).

Lembke-Jene, L. et al., 2017. Deglacial variability in Okhotsk Sea Intermediate Water ventilation and biogeochemistry: Implications for North Pacific nutrient supply and productivity. *Quaternary Science Reviews*, 160, pp.116–137.

Locarnini, R.A. et al., 2013. *World Ocean Atlas 2013. Vol. 1: Temperature.*

Maier, E. et al., 2015. Deglacial subarctic Pacific surface water hydrography and nutrient dynamics and links to North Atlantic climate variability and atmospheric CO_2. pp.1–20.

Marchitto, T.M. et al., 2007. Marine radiocarbon evidence for the mechanism of deglacial atmospheric CO2 rise. *Science (New York, N.Y.)*, 316(5830), pp.1456–9.

Marcott, S.A. et al., 2014. Centennial-scale changes in the global carbon cycle during the last deglaciation. *Nature*, 514(7524), pp.616–619.

Martínez-Botí, M. A. et al., 2015. Boron isotope evidence for oceanic carbon dioxide leakage during the last deglaciation. *Nature*, 518(7538), pp.219–222.

Max, L. et al., 2014. Pulses of enhanced north Pacific intermediate water ventilation from the Okhotsk Sea and Bering Sea during the last deglaciation. *Climate of the Past*, 10(2), pp.591–605.

McManus, J.F. et al., 2004. Collapse and rapid resumption of Atlantic meridional circulation linked to deglacial climate changes. *Nature*, 428(6985), pp.834–837.

Méheust, M. et al., 2018. Sea-ice variability in the subarctic North Pacific and adjacent Bering Sea during the past 25 ka: new insights from IP 25 and U k′ 37 proxy records. *arktos*, 1(48), p.0.

Meyer, V.D. et al., 2016. Glacial-to-Holocene evolution of sea surface temperature and surface circulation in the subarctic Northwest Pacific and the Western Bering Sea. *Paleoceanography*, pp.916–927.

NGRIP Members et al., 2004. High-resolution record of Northern Hemisphere climate extending into the last interglacial period. *Nature*, 431(7005), pp.147–151.

Okazaki, Y. et al., 2010. Deepwater formation in the North Pacific during the Last Glacial Termination. *Science (New York, N.Y.)*, 329(5988), pp.200–4.

Praetorius, S.K. et al., 2015. North Pacific deglacial hypoxic events linked to abrupt ocean warming. *Nature*, 527(7578), pp.362–366.

Rae, J.W.B. et al., 2014. Deep water formation in the North Pacific and deglacial CO_2 rise. *Paleoceanography*, 29, pp.645–667.

Rae, J.W., 2018. Boron Isotopes in Foraminifera: Systematics, Biomineralisation, and CO_2 Reconstruction. In Boron Isotopes (pp. 107-143). Springer, Cham.

Ren, H. et al., 2015. Glacial-to-interglacial changes in nitrate supply and consumption in the subarctic North Pacific from microfossil-bound N isotopes at two trophic levels. *Paleoceanography*, 30(9), pp.1217–1232.

Riethdorf, J.R. et al., 2013. Deglacial development of (sub) sea surface temperature and salinity in the subarctic northwest Pacific: Implications for upper-ocean stratification. *Paleoceanography*, 28(1), pp.91–104.

Sarmiento, J. & Gruber, N., 2013. Ocean biogeochmical dynamic, Princton University Press.

Sarnthein, M. et al., 2004. Mid Holocene origin of the sea-surface salinity low in the subarctic North Pacific. *Quaternary Science Reviews*, 23(20–22 SPEC. ISS.), pp.2089–2099.

Sarnthein, M. et al., 2007. 14C reservoir ages show deglacial changes in ocean currents and carbon cycle. In Geophysical Monograph Series. pp. 175–196.

Schlitzer, R., 2017. Ocean Data View.

Shackleton, N.J., 1974. Attainment of isotopic equilibrium between ocean water and the benthonic foraminifera geuns *Uvigerina*: Isotopic changes in the ocean during the last glacial. *Colloques Internationaux du C.N.R.S.*, 219, pp.203–210.

Shcherbina, A.Y., Talley, L.D. & Rudnick, D.L., 2003. Direct Observations of North Pacific Ventilation: Brine Rejection in the Okhotsk Sea. *Science*, 302(5652), pp.1952–1955.

Sigman, D. & Boyle, E., 2000. Glacial/interglacial variations in atmospheric carbon dioxide. *Nature*, 407(October), pp.859–869.

Sigman, D.M., Hain, M.P. & Haug, G.H., 2010. The polar ocean and glacial cycles in atmospheric CO_2 concentration. Nature, 466(7302), pp.47–55.

Southon, J. et al., 2012. A high-resolution record of atmospheric ^{14}C based on Hulu Cave speleothem H82. *Quaternary Science Reviews*, 33, pp.32–41.

Stott, L.D. et al., 2004. Decline of surface temperature and salinity in the western tropical Pacific Ocean in the Holocene epoch. *Nature*, 431(September 2004), pp.56–59.

Takahashi, T. et al., 2009. Climatological mean and decadal change in surface ocean pCO_2, and net sea-air CO2 flux over the global oceans. *Deep-Sea Research Part II: Topical Studies in Oceanography*, 56(8–10), pp.554–577.

Talley, L.D., 1993. Distribution and Formation of North Pacific Intermediate Water. *Journal of Physical Oceanography*, 23(3), pp.517–537.

Taylor, B.J. et al., 2018. Distribution and ecology of planktic foraminifera in the North Pacific: Implications for paleo-reconstructions. *Quaternary Science Reviews*, 191, pp.256–274.

Thornalley, D.J., Elderfield, H. and McCave, I.N., 2011. Reconstructing North Atlantic deglacial surface hydrography and its link to the Atlantic overturning circulation. *Global and Planetary Change*, 79(3-4), pp.163-175.

Visser, K., Thunell, R. & Stott, L.D., 2003. Magnitude and timing of temperature change in the Indo-Paci c warm pool during deglaciation. *Nature*, 421(JANUARY), pp.3667–3670.

Wang, Y.J., 2001. A High-Resolution Absolute-Dated Late Pleistocene Monsoon Record from Hulu Cave, China. *Science*, 294(5550), pp.2345–2348.

Watson, A.J. et al., 2000. Effect of iron supply on Southern Ocean CO_2 uptake and implications for glacial atmospheric CO2. Nature, 407(October), pp.730–733.

Warren, B. a., 1983. Why is no deep water formed in the North Pacific? *Journal of Marine Research*, 41(2), pp.327–347.

Wu, J.Y. et al., 2009. An exceptionally strengthened East Asian summer monsoon event between 19.9 and 17.1 ka BP recorded in a Hulu stalagmite. *Science in China, Series D: Earth Sciences*, 52(3), pp.360–368.

You, Y. et al., 2000. Roles of the Okhotsk Sea and Gulf of Alaska in forming the North Pacific Intermediate Water. *Journal of Geophysical Research*, 105(C2), pp.3253–3280.

Yu, J. et al., 2013. Calibration and application of B/Ca, Cd/Ca, and $\delta^{11}B$ in Neogloboquadrina pachyderma (sinistral) to constrain CO_2 uptake in the subpolar North Atlantic during the last deglaciation. *Paleoceanography*, 28(2), pp.237–252.

Zeebe, R.E. and Wolf-Gladrow, D.A., 2001. CO_2 in seawater: equilibrium, kinetics, isotopes (No. 65). Gulf Professional Publishing.

Zheng, Y. et al., 2000. Intensification of the northeast Pacific oxygen minimum zone during the Bolling-Allerod warm period. *Paleoceanography*, 15(5), pp.528–536.

Zweng, M.M. et al., 2013. World Ocean Atlas 2013, Volume 2: Salinity. *NOAA Atlas NESDIS*, 2(1), p.39.

5.7 Supplementary information

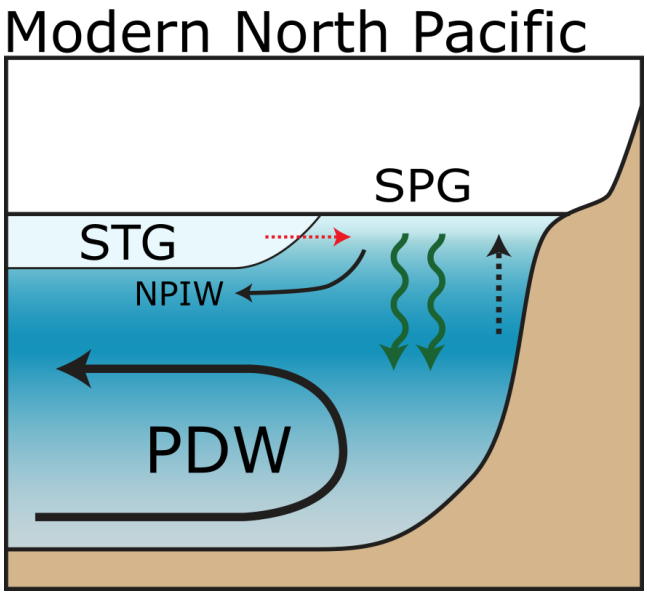

Figure 5.8: Schematic image highlighting modern North Pacific circulation. STG is Sub-tropical gyre; SPG is Sub-polar gyre; PDW is Pacific Deep Water; NPIW is North Pacific Deep Water. The red arrow indicates limited exchange between the two gyres. The solid black arrows indicate ocean circulation. The dashed black arrow indicates limited seasonal upwelling. The green arrows show moderate productivity (this is focused in the North West Pacific).

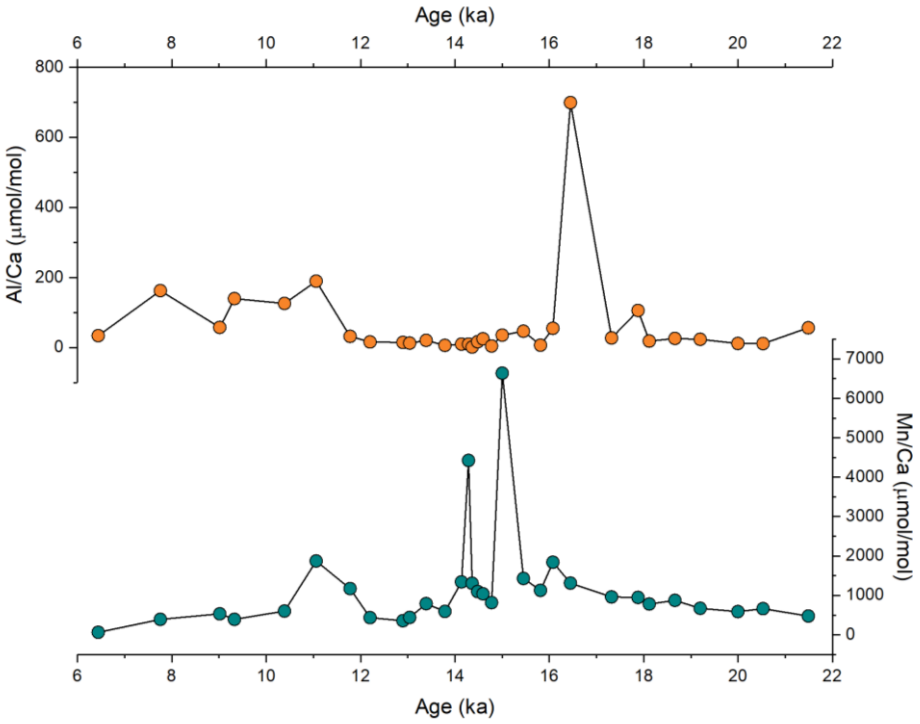

Figure 5.9: Possible contaminant phases for trace element data. Orange circles indicate Al/Ca ratios whilst blue circles show Mn/Ca. Samples with high Al/Ca (>200 µmol/mol) were removed from interpretation. Samples with >2000 µmol/mol Mn/Ca were also removed from interpretation.

Chapter 6

6. Summary and outlook

This thesis has improved the use of planktic foraminifera in the reconstruction of past ocean environments and climate through census data and geochemistry. Focusing on the North Pacific (Chapter 2), two key proxy carriers, *G. bulloides* and *N. pachyderma*, have been observed to live predominantly in the upper 50 m water of the water column, with their abundance closely linked to food availability. *N. pachyderma* shows an additional strong temperature control, highlighting its qualitative use in reconstructing past changes in SST. Across the whole North Pacific, six faunal zones have been identified: the sub-polar zone; the sub-tropical zone; the transitional zone; the upwelling zone; the west equatorial zone and the east equatorial zone. Changes in the abundance of key species within these zones could be used to reconstruct changes in surface ocean ecology, as well as the movement of gyre boundaries.

The global distribution and ecology of planktic foraminifera was addressed in Chapter 3. Twelve key species of planktic foraminifera are most abundant in assemblages across the world's oceans: *N. pachyderma; N. incompta; G. bulloides; T. quinqueloba; G. inflata; G. glutinata; G. ruber; G. menardii; T. sacculifer; N. dutertrei; G. tumida* and *P. obliquiloculata.* Through redundancy analysis, it is clear that the dominant control on variance within an assemblage is temperature, whilst secondary controls are likely to be associated with upwelling and nutrient availability. Both Chapters 2 and 3 highlight the importance of recognising dissolution within planktic foraminifera assemblages. This is seen within the North Pacific, where offsets between core-tops and multinets suggest that *N. pachyderma* may exhibit a dissolution bias over *G. bulloides* which could affect the interpretation of downcore records. Globally, dissolution resistant foraminifera such as *G. tumida*, *N. pachyderma*, and *P. obliquiloculata* are found in high abundance (>75 %) in sediment cores where bottom water Omega is low, whilst dissolution prone species like *G. ruber*, *T. sacculifer* and *G. bulloides* are found in lower abundances at these sites. It is, therefore, key that dissolution is incorporated into downcore interpretations of census data, and that further research is required to better quantify the effects of dissolution on planktic foraminifera assemblages.

Geochemical reconstructions of temperature and pH from Mg/Ca ratios and boron isotopes are covered in detail in Chapters 4 and 5. A new global temperature calibration for Mg/Ca ratios in *N. pachyderma* is presented, which shows a temperature sensitivity of 6 % per °C (Chapter 4). No significant relationships are seen between Mg/Ca and other surface parameters, however a weak correlation with bottom water Omega calcite is observed. This temperature calibration is

used to calculate past SSTs, and combined with new boron isotope data from the North East Pacific to reconstruct deglacial ocean pH and $CO_{2(sw)}$. Two periods of enhanced surface water CO_2 suggest a dynamic role for the North Pacific during the last deglaciation (Chapter 5). During Heinrich Stadial 1 (HS1), deepwater formation mixed nutrients and CO_2 throughout the water column, removed primary producers from the photic zone, and led to muted productivity and potential CO_2 outgassing. During the Bølling-Allerød (B/A), the North Pacific is characterised by dramatically increased primary productivity and high $CO_{2(sw)}$ in both the east and west subpolar gyre. Although North Pacific waters were stratified during the B/A, enhanced Ekman suction supplied surface waters with nutrients and CO_2, leading to high productivity and CO_2 outgassing. Overall, this thesis suggests a dynamic role for the North Pacific in deglacial climate change, caused by abrupt changes in circulation and the cycling of nutrients and CO_2.

Chapter 7

7. Appendix

7.1 Appendix 1: Trace element ratios from North Pacific core-tops

Introduction

Planktic foraminifera produce calcium carbonate tests using the chemistry of the seawater in which they live. These tests are deposited on the seafloor when the foraminifera die and are buried and preserved in marine sediments over time. Several trace elements can be readily incorporated into foraminiferal calcite (Lea, 1999), these include Li, B, Mg, Na, U, Nd, Sr, Cd, Mn, Al, and Ba among others (Allen *et al.*, 2016). Through careful analytical geochemistry the concentrations of these trace elements can be attained and are often reported as a ratio against Ca in foraminifera tests (Lea *et al.*, 1999). The ratio of different trace elements (TE) to Ca (TE/Ca) have been observed to vary depending on environmental conditions such as temperature, salinity and pH. They thus present a unique opportunity to reconstruct ocean climates in the past and understand regional and global environmental change. For TE/Ca ratios to be useful downcore, ground truthing studies are required. Ground truthing studies usually take the form of laboratory culture studies or core-top analysis and have lead to a wide variety of TE/Ca associations with ocean conditions such as temperature, nutrients, salinity, pH and CO_3^{2-} (Lea *et al.*, 1999; Anand *et al.*, 2003; Russell *et al.*, 2004; Yu *et al.*, 2013; Allen *et al.*, 2016).

Methods

We analysed the relationship between TE/Ca ratios and environmental parameters for the subpolar North Pacific species *N. pachyderma* and *G. bulloides*. Both species of planktic foraminifera are commonly used to reconstruct past climates particularly in polar and subpolar regions where they are most abundant (see chapter 2 and 3). We used core-top material from nine sites in the North Pacific and one multinet site (Table 7.1). Planktic foraminifera were picked from the 150-250 µm size fraction of washed marine sediment and cleaned in accordance with Barker *et al.*, (2003). Trace element to calcium ratios of Li, B, Na, Mg, Al, Mn, Sr, Cd, Ba, Nd and U were analysed on an Agilent 7500 ICP-MS in the STAiG laboratory at the University of St Andrews. Machine sensitivity was below 1 % 2*RSD for seven trace elements (Li, B, Na, Mg, Mn, Sr, Ba). For U, Nd, Al and Cd percentage 2*RSE were 8.67, 1.99, 1.43, and 33.01 respectively. The large error associated with Cd/Ca ratios may be due to one sample (SO27MN) containing much higher Cd/Ca ratios than the rest, which could have influenced Cd/Ca ratios for

the remainder of the sequence. Three samples containing trace element data for the species *N. incompta* were also produced, however, due to the lack of samples, this species is not discussed in detail.

Hydrographic data for each site was calculated using ODV's 3D estimation tool (Schlitzer, 2006) using annual averages from the World Ocean Atlas 2013 (1955-2012) (WOA13) (Boyer *et al.*, 2013). Annual average estimates of temperature (Locarnini *et al.*, 2013), salinity (Zweng *et al.*, 2013), oxygen (Garcia *et al.*, 2013), and phosphate (Garcia *et al.*, 2013) were calculated for the top 50 m of the water column. pH was calculated using GLODAP V2 (Olsen *et al.*, 2016). A depth habitat of 0-50 m has been observed for both species in the North Pacific (Iwasaki *et al.*, 2017; Taylor *et al.*, 2018).

Linear regression analysis was conducted to assess the relationship between certain environmental parameters and TE/Ca ratios. In some cases, outliers were removed from statistical analysis where a good reason existed. Where this is the case, outliers have been highlighted and the reason for omission is clearly stated. Where confidence bands are given, they are reported at 95 % (2σ).

Results

Detailed results for trace element ratios can be seen in table 7.1. Li/Ca ratios for all species of planktic foraminifera ranged between 9.44 and 19.86 µmol/mol with an average of 13 µmol/mol. In general, ratios in *N. pachyderma* and *N. incompta* were higher than those of *G. bulloides*. For B/Ca, ratios ranged from 18.29 - 59.18 µmol/mol. Again, ratios for *N. pachyderma* and *N. incompta* were significantly highly (44.42 - 56.85 µmol/mol) when compared to *G. bulloides* (18.29 - 34.88). Mg/Ca ratios in all species analysed ranged from 0.69 and 1.64 mmol/mol with an average of 1.04 mmol/mol. No differences in ranges were observed between species. Al/Ca ratios, usually used as a measure of sample cleanliness, ranged from -4.91 (below blank levels) to 847.55 µmol/mol. Samples with very high Al/Ca (>200 µmol/mol) were flagged and used with caution. For Mn/Ca ratios, values ranged from 4.55 to 61.08 µmol/mol with an average of 19.73 µmol/mol. Sr/Ca ratios ranged from 1.3 to 1.46 mmol/mol in our samples with an average of 1.37. *N. pachyderma* Sr/Ca were noticeably highly than those of *G. bulloides* with a range of 1.39 to 1.46 mmol/mol compared to 1.30 - 1.34 mmol/mol. Cd/Ca were generally low in our core-top samples ranging from 0.06 – 0.15 µmol/mol. Conversely the single multinet sample (*N. pachyderma*) we analysed was high with a Cd/Ca ratio of 0.87 µmol/mol. Ba/Ca ratios ranged between 1.40 and 68.83 µmol/mol and showed no distinction between species. The average was 19.28. For Nd/Ca ratios the average was 2.55 and ranged fro 0.01 to 4.86 with no species

distinction. Finally, U/Ca ratios ranged between 2.92 and 313.14 nmol/mol with an average of 77.50 nmol/mol.

Hydrographic data was estimated between 0-50 m for temperature, salinity, phosphate, oxygen and pH. Temperature at our sites ranged from 4.67 to 14.95 °C with an average of 8.56°C. Salinity ranged from 32.15 to 33.47 p.s.u with an average of 32.91 p.s.u. Phosphate ranged from 0.48 to 1.88 µmol/kg with an average of 1.29 µmol/kg. Oxygen content ranged from 5.70 to 7.28 ml/L with an average of 6.62 ml/L. pH ranged from 7.99 to 8.09 with an average of 8.05.

Discussion and conclusions

Trace element ratios in N. pachyderma

The polar to subpolar species *N. pachyderma* is commonly used to reconstruct past ocean temperatures through Mg/Ca ratios (Nurnberg, 1995; Elderfield and Ganssen, 2000; Vazquez Rivieros *et al.,* 2016; Allen *et al.,* 2016). Mg/Ca ratios in *N. pachyderma* is covered in detail in chapter 4, and instead we focus here on the application of alternative trace element ratios (B/Ca, Sr/Ca, U/Ca and Na/Ca) in the reconstruction of past environmental change.

B/Ca

B/Ca in *N. pachyderma* has received much attention in recent literature due to the relationship between seawater borate and ocean pH (see chapter 1) (Hemming and Hanson, 1992). In our core-tops, B/Ca exhibits a weak negative correlation with pH ($R^2 = 0.45$) (Figure 7.1). This is at odds with culture studies that suggest B/Ca in planktic foraminifera increases with pH under laboratory conditions (Sanyal *et al.,* 2001; Allen *et al.,* 2011; Allen *et al.,* 2012; Henehan *et al,* 2015). In core-tops from Yu *et al.,* (2013), B/Ca also shows a positive with carbonate parameters. It is important to note that much of the trend observed in our data is driven by a signal low pH point which is highlighted (Figure 7.1). When this point is removed the relationship breaks down. We find a stronger positive relationship between B/Ca and temperature in our samples ($R^2 = 0.65$) (Figure 7.1). This is the first noted correlation between this *N. pachyderma* B/Ca and temperature with Allen *et al.,* (2012) noting no relationship between *O. universa, G. ruber and G. sacculifer*, and temperature but rather a linear relationship with salinity. B/Ca ratios in planktic foraminifera remain an interesting proxy for past ocean conditions, particularly carbonate parameters, but require further investigation and analysis.

Sr/Ca

Our Sr/Ca ratios in *N. Pachyderma* show a negative relationship with temperature ($R^2 = 0.78$) except for two outliers highlighted in figure 7.1. These were not included in statistical analysis due to their large digression from the other samples. Previous studies of Sr/Ca within planktic

foraminifera have highlighted some positive correlation with temperature in the species *G. inflata* and *G. trunculatulinoides* (Elderfield *et al.,* 2000; Cleroux *et al.,* 2008). *N. pachyderma* samples from Elderfield *et al.,* (2000) show no correlation with temperature. Allen *et al.,* (2016) also note that several culture and core-top studies show relationships between Sr/Ca ratio and calcification rate as opposed to a temperature calibration. Changes in Sr/Ca downcore have also been used to track changes in past ocean CO_3^{2-} and nutrients (Stoll *et al.,* 1999; Billups *et al.,* 2004). The relationship observed in our North Pacific samples alongside our downcore record of Sr/Ca (see Appendix 2) suggests North Pacific *N. pachyderma* may be controlled by temperature to some extent and warrant further investigation and ground truthing.

U/Ca

We find a strong ($R^2 = 0.83$) positive correlation between U/Ca ratios at our sites and temperature between 0-50 m (Figure 7.1). Despite the relationship being heavily dependent on a single high temperature site (highlighted, site NV12) (Figure 7.1) this relationship is consistent with other studies of core-top U/Ca (Yu *et al.,* 2008). In particular, Yu *et al.,* (2008) highlight an exponential relationship between U/Ca in *N. pachyderma* and temperature from samples in the North Atlantic. In addition to a temperature relationship, our samples display negative relationship with pH ($R^2 = 0.89$). Again, this relationship is heavily dependent on a single low pH site (NV12) and further sampling and analysis would help to better constrain this relationship. Allen *et al.,* (2016) highlight the fact that the relationship between temperature and U/Ca has only been observed in core-top samples and has not been recreated under laboratory conditions. Yu *et al.,* (2008) also note a linear relationship between *N. pachyderma* shell weight and U/Ca ratio hinting that calcification may affect the uptake of uranium into calcium carbonate.

Na/Ca

The relationship between Na/Ca in planktic foraminifera and environmental parameters is not well tested in recent literature. Our Na/Ca ratios in *N. pachyderma* suggest a negative associated with salinity ($R^2 = 0.61$). We removed the multinet sample from our statistical analysis as it likely reflects seasonal salinity rather than annual average (Figure 7.1). Na/Ca ratios from sub-tropical species *G. ruber* (pink) have been show a positive linear relationship with salinity, however this is only based on three cultured samples (Allen *et al.,* 2016).

Trace element ratios in *G. bulloides*

G. bulloides is commonly used in geochemistry to reconstruct past climates due to its wide latitudinal range (see chapter 3). In addition, it also frequents upwelling regions across the globe which are important for tracking CO_2 exchange with the atmosphere in the past.

Mg/Ca

G. bulloides is most commonly used in geochemistry to reconstruct past ocean temperatures through Mg/Ca ratios. Our Mg/Ca ratios in *G. bulloides* show a strong linear relationship with temperature ($R^2 = 0.84$) (Figure 7.2). We removed two samples from our statistical analysis due to Al/Ca ratios greater than 200 µmol/mol, these are highlighted in blue in figure 7.2. Most published literature using Mg/Ca ratios in *G. bulloides* suggest an exponential relationship between Mg/Ca and temperature (Mashiotta *et al.,* 1999; Elderfield and Ganssen, 2000; Jonkers *et al.,* 2013; Vazquez Riveiros *et al.,* 2016). Mashiotta *et al.,* (1999) describe a sensitivity of Mg/Ca to temperature of 10 % based on culture studies whilst new and compiled core-top data from Vazquez Riveiros *et al.,* (2016) suggest a sensitivity closer to 6.5 %. Seasonal data from Jonkers *et al.,* (2013) also suggests a sensitivity of 10 % for the relationship between Mg/Ca and temperature. Our samples represent the first core-top Mg/Ca records produced from the North Pacific. More core-top analysis from this region will provide additional constraints on this relationship, improving global calibrations and reconstructions of temperature from *G. bulloides* in the North Pacific.

Li/Ca and Na/Ca

Li/Ca in *G. bulloides* at our site shows a weak positive relationship with temperature ($R^2 = 0.56$). Previous studies of Li/Ca in planktic foraminifera have shown little correspondence between the two (Hall and Chan, 2004), whilst benthic foraminifera are known to exhibit a negative relationship between their Li/Ca and temperature (Marriott *et al.,* 2004). Na/Ca has been shown to correlate with salinity in the global ocean (Allen *et al.,* 2016). Our Na/Ca ratios in *G. bulloides* show no affinity to salinity, rather a negative correlation with surface oxygen content is observed ($R^2 = 0.67$). This trend has not been observed in other ocean regions and differs to our Na/Ca data from *N. pachyderma*.

Sr/Ca

In a similar fashion to Sr/Ca in our samples of *N. pachyderma*, Sr/Ca in *G. bulloides* shows a negative correlation with temperature ($R^2 = 0.44$) (Figure 7.2). This is at odds with culture studies of *G. bulloides* from Lea *et al.,* (1999b) who show a positive correlation between temperature and Sr/Ca ratio. It is important to note that the culture work of Lea *et al.,* (1999b) was conducted at higher temperatures than are present in our study, with theirs ranging between 15-30 °C compared to 4-9 °C at our sites. One very high temperature value was not included in our statistical analysis and is highlighted in figure 7.2. Lea *et al.,* (1999b) also note a positive correlation between Sr/Ca and pH which is not seen within our data.

U/Ca

U/Ca in *G. bulloides* at our sites correlates with a number of environmental parameters (Figure 7.2). It shows a positive correlation with temperature ($R^2 = 0.87$), at odds with work by Allen *et al.,* (2016) and Russell *et al.,* (2004) who show a negative correlation and no relationship respectively. However, Yu *et al.,* (2008) show a strong positive temperature control on U/Ca in planktic foraminifera including *G. bulloides*. U/Ca is negatively correlated with phosphate ($R^2 = 0.71$), oxygen content ($R^2 = 0.94$), and pH ($R_2 = 0.91$). Whilst both Allen *et al.*, (2016) and Yu *et al.*, (2008) highlight a possible influence on carbonate ion on *G. bulloides* U/Ca, Yu *et al.*, (2008) suggest this is only applicable to higher temperatures and that U/Ca may provide a promising proxy for evaluating glacial temperatures.

References

Allen, K.A. et al., 2016. Trace element proxies for surface ocean conditions: A synthesis of culture calibrations with planktic foraminifera. *Geochimica et Cosmochimica Acta*, 193, pp.197–221.

Allen, K.A. et al., 2012. Environmental controls on B/Ca in calcite tests of the tropical planktic foraminifer species Globigerinoides ruber and Globigerinoides sacculifer. *Earth and Planetary Science Letters*, 351–352, pp.270–280.

Allen, K.A. et al., 2011. Controls on boron incorporation in cultured tests of the planktic foraminifer Orbulina universa. *Earth and Planetary Science Letters*, 309(3–4), pp.291–301.

Anand, P., Elderfield, H. & Conte, M.H., 2003. Calibration of Mg/Ca thermometry in planktonic foraminifera from a sediment trap time series. *Paleoceanography*, 18(2).

Barker, S., Greaves, M. & Elderfield, H., 2003. A study of cleaning procedures used for foraminiferal Mg/Ca paleothermometry. *Geochemistry, Geophysics, Geosystems*, 4(9).

Billups, K., Rickaby, R.E.M. & Schrag, D.P., 2004. Cenozoic pelagic Sr/Ca records: Exploring a link to paleoproductivity. *Paleoceanography*, 19(3), pp.1–11.

Boyer, T.P. et al., 2013. World Ocean Database 2013.

Cléroux, C. et al., 2008. Mg/Ca and Sr/Ca ratios in planktonic foraminifera: Proxies for upper water column temperature reconstruction. *Paleoceanography*, 23(3), pp.1–16.

Elderfield, H., Cooper, M. & Ganssen, G., 2000. Sr/Ca in multiple species of planktonic foraminifera: Implications for reconstructions of seawater Sr/Ca. *Geochemistry, Geophysics, Geosystems*, 1(11).

Elderfield, H. & Ganssen, G., 2000. Past temperature and $\delta^{18}O$ of surface ocean waters inferred from foraminiferal Mg/Ca ratios. *Nature*, 405(6785), pp.442–445.

Garcia, H.E. et al., 2013. World Ocean Atlas 2013. Volume 3: dissolved oxygen, apparent oxygen utilization, and oxygen saturation. *NOAA Atlas NESDIS 75*, 3(September).

Hall, J.M. & Chan, L.H., 2004. Li/Ca in multiple species of benthic and planktonic foraminifera: Thermocline, latitudinal, and glacial-interglacial variation. *Geochimica et Cosmochimica Acta*, 68(3), pp.529–545.

Hemming, N.G. & Hanson, G.N., 1992. Boron isotopic composition and concentration in modern marine carbonates. *Geochimica et Cosmochimica Acta*, 56(1), pp.537–543.

Henehan, M.J. et al., 2015. Evaluating the utility of B/Ca ratios in planktic foraminifera as a proxy for the carbonate system: A case study of Globigerinoides ruber. *Geochemistry, Geophysics, Geosystems*, 16, pp.1052–1069.

Jonkers, L. et al., 2013. Seasonal Mg/Ca variability of *N. pachyderma* (s) and *G. bulloides*: Implications for seawater temperature reconstruction. *Earth and Planetary Science Letters*, 376, pp.137–144.

Lea, D.W., 1999. Trace elements in foraminiferal calcite. In *Modern foraminifera*. Springer, Dordrecht, pp. 259–277.

Lea, D.W., Mashiotta, T.A. & Spero, H.J., 1999. Controls on magnesium and strontium uptake in planktonic foraminifera determined by live culturing. *Geochimica et Cosmochimica Acta*, 63(16), pp.2369–2379.

Locarnini, R.A. et al., 2013. *World Ocean Atlas 2013. Vol. 1: Temperature.*

Marriott, C.S. et al., 2004. Effect of mineralogy, salinity, and temperature on Li/Ca and Li isotope composition of calcium carbonate. *Chemical Geology*, 212(1–2), pp.5–15.

Mashiotta, T.A., Lea, D.W. & Spero, H.J., 1999. Glacial-interglacial changes in Subantarctic sea surface temperature and δ18O-water using foraminiferal Mg. *Earth and Planetary Science Letters*, 170(4), pp.417–432.

Nürnberg, D., 1995. Magnesium in tests of Neogloboquadrina pachyderma sinistral from high northern and southern latitudes. *Journal of Foraminiferal Research*, 25(4), pp.350–368.

Olsen, A. et al., 2016. The global ocean data analysis project version 2 (GLODAPv2) - An internally consistent data product for the world ocean. *Earth System Science Data*, 8(2), pp.297–323.

Russell, A.D. et al., 2004. Effects of seawater carbonate ion concentration and temperature on shell U, Mg, and Sr in cultured planktonic foraminifera. *Geochimica et Cosmochimica Acta*, 68(21), pp.4347–4361.

Sanyal, A. et al., 2001. Empirical relationship between pH and the boron isotopic composition of Globigerinoidessacculifer: Implication for the boron isotope paleo-pH proxy. *Paleoceanography*, 16(5), pp.515–519.

Schlitzer, R., 2017. Ocean Data View.

Stoll, H.M., Schrag, D.P. & Clemens, S.C., 1999. Are seawater Sr/Ca variations preserved in Quaternary foraminifera? *Geochimica et Cosmochimica Acta*, 63(21), pp.3535–3547.

Taylor, B.J. et al., 2018. Distribution and ecology of planktic foraminifera in the North Pacific: Implications for paleo-reconstructions. *Quaternary Science Reviews*, 191, pp.256–274.

Yu, J. et al., 2008. A strong temperature effect on U/Ca in planktonic foraminiferal carbonates. *Geochimica et Cosmochimica Acta*, 72(20), pp.4988–5000.

Yu, J. et al., 2013. Calibration and application of B/Ca, Cd/Ca, and δ11B in Neogloboquadrina pachyderma (sinistral) to constrain CO2 uptake in the subpolar North Atlantic during the last deglaciation. *Paleoceanography*, 28(2), pp.237–252.

Zweng, M.M. et al., 2013. World Ocean Atlas 2013, Volume 2: Salinity. *NOAA Atlas NESDIS*, 2(1), p.39.

Site	Species	lat (dec)	long (dec)	depth (m)	Li/Ca µmol/mol	B/Ca µmol/mol	Na/Ca mmol/mol	Mg/Ca mmol/mol	Sr/Ca mmol/mol	Ba/Ca µmol/mol	Nd/Ca µmol/mol	U/Ca nmol/mol	Al/Ca µmol/mol	Mn/Ca µmol/mol	Temp °C	Sal p.s.u	Phos µmol/kg	Oxy ml/L	pH
EW0408-68	*G. bulloides*	55.55	-134.71	296	11.27	21.45	4.807	1.04	1.317	2.43	2.362	128.02	205.76	15.19	8.48	32.15	1.27	6.58	8.06
EW0408-15	*G. bulloides*	59.44	-140.25	238	10.79	23.55	4.691	1.12	1.302	2.37	3.816	94.82	193.42	41.44	7.65	32.24	1.36	6.80	8.06
HLY0902-24	*G. bulloides*	54.00	-179.59	714	11.23	23.78	4.825	1.47	1.339	30.29	2.384	34.01	224.22	13.07	4.81	33.10	1.88	7.15	8.08
NV12	*G. bulloides*	32.99	-118.40	920	12.90	34.88	5.056	1.64	1.341	5.24	2.376	313.14	130.77	13.81	14.77	33.47	0.50	5.70	8.00
SO202-02-07	*G. bulloides*	51.27	167.69	2349	9.44	18.29	4.617	0.69	1.323	3.28	2.604	5.16	47.84	16.76	4.92	32.99	1.87	7.15	8.07
SO202-04-27	*G. bulloides*	54.29	-149.59	2921	9.78	27.85	4.744	0.93	1.321	40.74	4.855	5.72	91.34	26.95	6.60	32.71	1.38	6.95	8.07
SO202-05-31	*G. bulloides*	49.67	-152.54	3744	9.86	22.07	4.647	0.73	1.314	68.83	3.826	8.72	98.01	33.77	7.34	32.67	1.37	6.99	8.08
NV10	*N. incompta*	32.84	-118.33	760	13.64	55.15	5.052	1.27	1.336	16.09	1.765	171.97	217.16	5.56	14.95	33.47	0.48	5.70	8.00
NV12B	*N. incompta*	32.99	-118.40	920	12.85	56.85	4.909	1.04	1.374	32.18	1.731	244.07	120.24	9.49	14.77	33.47	0.50	5.70	8.00
NV26	*N. incompta*	33.47	-120.46	1095	12.88	54.16	5.038	1.08	1.373	17.69	1.378	161.94	25.52	7.89	14.51	33.39	0.49	5.77	7.99
EW0408-15	*N. pachyderma*	55.55	-134.71	296	13.81	55.38	5.903	0.89	1.392	2.25	1.987	64.52	42.14	8.75	8.48	32.15	1.27	6.58	8.06
EW0408-68	*N. pachyderma*	59.44	-140.25	238	13.53	48.89	5.709	0.98	1.385	4.26	3.299	45.43	93.31	31.46	7.65	32.24	1.36	6.80	8.06
HLY0902-19	*N. pachyderma*	54.61	-178.72	855	14.32	48.29	5.433	1.33	1.423	33.24	2.148	20.56	260.49	34.21	4.79	33.11	1.88	7.16	8.09
HLY0902-24	*N. pachyderma*	54.00	-179.59	714	13.48	47.19	5.540	1.22	1.407	19.34	1.880	13.83	142.93	8.37	4.81	33.10	1.88	7.15	8.08
NV12B	*N. pachyderma*	32.99	-118.40	920	16.26	59.18	5.528	1.08	1.411	7.12	1.897	200.29	163.55	10.82	14.77	33.47	0.50	5.70	8.00
SO202-02-07	*N. pachyderma*	51.27	167.69	2349	12.95	48.70	5.386	0.78	1.411	35.82	3.515	2.92	75.01	61.08	4.92	32.99	1.87	7.15	8.07
SO202-04-13	*N. pachyderma*	54.97	177.95	1386	13.06	46.77	5.427	0.70	1.428	9.29	2.368	5.45	31.47	10.20	4.67	33.11	1.88	7.28	8.09
SO202-01-27 (MN)	*N. pachyderma*	54.29	-149.59	0-500	19.86	53.40	6.557	1.31	1.377	1.40	0.009	23.52	-4.91	4.55	8.28	32.89	1.28	6.24	8.07
SO202-04-27	*N. pachyderma*	54.29	-149.59	2921	12.76	44.42	5.558	0.77	1.398	17.61	3.839	3.01	847.55	10.53	6.60	32.71	1.38	6.95	8.07
SO202-05-31	*N. pachyderma*	49.67	-152.54	3744	15.43	53.88	5.666	0.69	1.461	36.20	2.996	2.96	89.64	30.72	7.34	32.67	1.37	6.99	8.08

Table 7.1: New trace element data for G. bulloides, N. incompta, and N. pachyderma in the North Pacific.

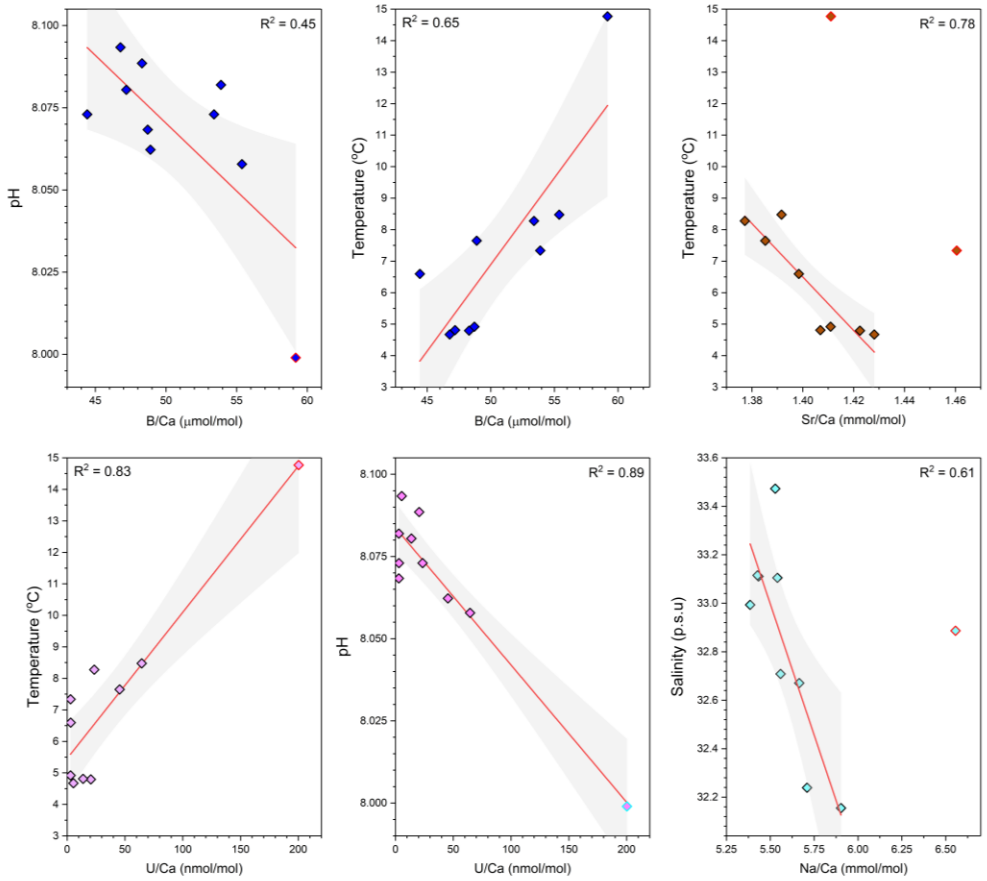

Figure 7.1: Trace element calcium ratios in N. pachyderma plotted against surface ocean temperature (Locarnini et al., 2013); pH (Key et al., 2004); Salinity (Zweng et al., 2014); Phosphate (Garcia et al., 2014). Samples that were excluded from statistical analysis have highlighted borders, confidence bands for linear regressions are given at 95 % limits.

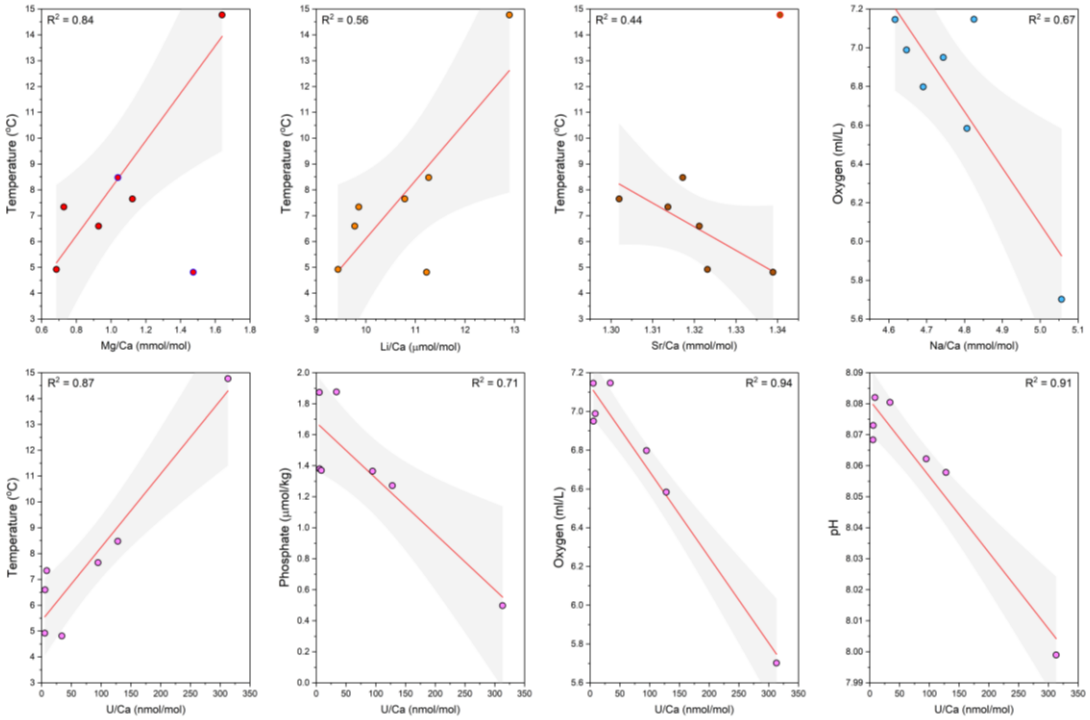

Figure 7.2: Trace element calcium ratios in G. bulloides plotted against surface ocean temperature (Locarnini et al., 2013); pH (Key et al., 2004); Salinity (Zweng et al., 2014); Phosphate (Garcia et al., 2014); Oxygen (Garcia et al., 2013). Samples that were excluded from statistical analysis have highlighted borders, confidence bands for linear regressions are given at 95 % limits.

7.2 Appendix 2: Trace element ratios from glacial to Holocene

Introduction

Trace element ratios in planktic foraminifera have been used to reconstruct a variety of environmental parameters in the past. Commonly used TE/Ca ratios include Mg/Ca to reconstruct past ocean temperatures (Elderfield and Ganssen, 2000; Gray *et al.,* 2018); B/Ca records to look at carbonate chemistry (Yu *et al.,* 2013) and Cd/Ca ratios to track changes in surface nutrient content (Rickaby and Elderfield, 1999; Yu *et al.,* 2013). Appendix 1 highlights some of the associations of various TE/Ca ratios with environmental parameters in the North Pacific, particularly an inverse relationship between Sr/Ca and temperature. In addition to our Mg/Ca record of deglacial temperature in the North Pacific (see chapter 5) we present downcore records for six other TE/Ca ratios including: Sr/Ca; Li/Ca; Ba/Ca; B/Ca; Na/Ca and Nd/Ca. These downcore records allow us to speculate on the drivers of environmental change during the last deglaciation, as well as interpret the potential influencers of trace element incorporation into planktic foraminifera tests for future calibration purposes.

Methods and results

We analysed the trace element to calcium ratio of 31 samples from site MD02-2489 (54.39° N, 148.92° W) located on the Patten seamount at a depth of 3640 m. The samples spanned from 50-298 cmbsf reflecting an age range of 6.4-21.5 ka based on the age model by Rae *et al.,* (2014) which ties planktic foraminifera $\delta^{18}O$ from Gebhardt *et al.,* (2008) to $\delta^{18}O$ records from NGRIP (NGRIP members, 2004) and the Hulu Cave speleothem records (Wang *et al.,* 2001; Southon *et al.,* 2012; Wu *et al.,* 2009). The high sedimentation rate of site MD02-2489 (up to 20 cm/ky) allows for high resolution records to be produced. Samples were washed and sieved greater than >150 µm and ~400 specimens of *N. pachyderma* from the 150-250 µm size fraction were picked from each sample. Each sample was oxidatively cleaned following the cleaning procedure of Barker *et al.,* (2003) to remove clay material and organic matter. Samples were then analysed on an Agilent 7500 ICP-MS and long-term machine sensitivity was below 1 % for 2*RSD.

Downcore records for Sr/Ca, Li/Ca, Ba/Ca, B/Ca, Na/Ca and Nd/Ca can be seen in figure 7.3. Our Sr/Ca record ranges from 1.37 to 1.47 mmol/mol and show an overall decrease in Sr/Ca value from LGM to Holocene (Figure 7.3). There is a significant jump to lower Sr/Ca values at 14.7 ka in our record. For Li/Ca, ratios range from 11.98 to 20.56 µmol/mol and depict a general and consistent trend of decreasing Li/Ca ratios from the LGM through the Holocene (Figure 7.3). Our Ba/Ca record consists of very low Ba/Ca ratios which range between 2.5 and 20 µmol/mol between 21.5 and 12 ka. Following this, Ba/Ca rises dramatically to 59.23 µmol/mol at 11.8 ka and remains high until 6.44 ka where it drops down to below 10 µmol/mol once more. B/Ca ratios

ranged from 41.70 to 75.17 µmol/mol again indicating a general trend of decreasing ratio over time (Figure 7.3. A small peak in B/Ca occurs at 20 ka with values rising to 75 µmol/mol. Apart from this B/Ca values remain below 70 µmol/mol. For Na/Ca, ratios range between 5.18 and 6.19 mmol/mol and are highest during the LGM and HS1 (Figure 7.3). Ratios start to drop at 14.7 ka before stabilising between 5.2 and 5.4 mmol/mol for the latter part of the record (Figure 7.3). Nd/Ca ratios range between 17.01 µmol/mol and 2.01 µmol/mol. During the LGM and HS1, Nd/Ca is consistently high, between 10 and 15 µmol/mol (Figure 7.3). Following the onset of the B/A, Nd/Ca drops abruptly to <5 µmol/mol by 14 ka. It then remains low for the remainder of the record (Figure 7.3).

Discussion

Figure 7.3 depicts our TE/Ca ratios from LGM to Holocene against the NGRIP $\delta^{18}O$ record (NGRIP members, 2004). Also highlighted are the key intervals associated with the last deglaciation which provide useful place markers when interpreting our trace element ratios, these are: The last glacial maximum (~23-18 ka); Heinrich stadial 1 (18-14.7 ka); the Bølling-Allerød (14.7-12.9 ka); the Younger-Dryas (12.9-11.7 ka) and the Holocene (11.7 ka to modern). The boundaries between these intervals are associated with abrupt reorganisation of North Pacific circulation, nutrient, and carbon cycling (Galbraith *et al.,* 2007; Okazaki *et al.,* 2010; Rae *et al.,* 2014; Maier *et al.,* 2015; Gray *et al.,* 2018; see chapter 5).

The most abrupt change in ocean conditions occurs at the B/A where the North Pacific becomes warm, stratified, and highly productive (Gray *et al.,* 2018), as well as a leak of CO_2 to the atmosphere (see chapter 5). Two of our TE/Ca ratios also show abrupt changes at the onset of the B/A: Sr/Ca, which is shown on an inverse scale, shows a rapid decrease in ratios at 14.7 ka, whilst our Nd/Ca starts to decrease towards the end of HS1 followed by an abrupt shift to lower values at 14.7 ka. Our Sr/Ca record depicts the most interesting deglacial trend due primarily to its similarity to the NGRIP record and our core-top study (Appendix 1) (Figure 7.3). We note in appendix 1 that our core-top Sr/Ca in *N. pachyderma* shows a strong inverse correlation to temperature ($R^2 = 0.78$). Increases in North Pacific SST of 4-8°C at the onset of the B/A has been noted from recent Mg/Ca paleothermometry (Gray *et al.,* 2018; see chapter 5). Increases in global atmospheric temperatures are also demonstrated by the increase in $\delta^{18}O$ from the NGRIP record (NGRIP members, 2004). Our Sr/Ca record not only suggests that this increase in SST temperature was as abrupt as the atmospheric shift, but it also highlights the potential use of Sr/Ca ratio in future paleothermometry studies. Our Nd/Ca record is more difficult to interpret as a single driver of Nd/Ca ratios in planktic foraminifera is yet to be identified despite a recent study by Martinez-Boti *et al.,* (2009) suggesting that Nd/Ca in planktic foraminifera may reflect

seawater Nd. One clue to a possible influence on Nd/Ca ratios is the fact that our one multinet (surface water) *N. pachyderma* sample contained negligible Nd/Ca (0.01 µmol/mol) compared to those samples from core-top material (1.8-3.8 µmol/mol). This suggests that bottom/pore water chemistry may exert an influence on Nd/Ca ratios in planktic foraminifera. The shift from high Nd/Ca (~10-15 µmol/mol) ratios to low Nd/Ca ratios (~1-5 µmol/mol) seen at 14.7 ka may well reflect changes in bottom water chemistry. It is well documented that during the B/A productivity was high (Gebhardt *et al.,* 2008; Gray *et al.,* 2018) and that oxygen content in waters down to 3000 m were greatly reduced due to enhanced remineralisation (Jaccard and Galbraith, 2011). This could have affected bottom water redox conditions which may explain the abrupt shift in our Nd/Ca record.

Our record of Li/Ca over the last deglaciation indicates a steady decrease in Li/Ca ratios from LGM to Holocene (Figure 7.3). We see no affinity of Li/Ca ratios to any environmental parameter in *N. pachyderma* making the interpretation of this record somewhat difficult. Interestingly work by Hall and Chan (2004) found a similar deglacial trend in samples from the Bahamas with Li/Ca ratios in multiple species of planktic foraminifera a decrease in Li/Ca ratios from glacial to Holocene. Due to the long residence time of Li/Ca in seawater Hall and Chan (2004) suggest it is unlikely that Li/Ca ratios reflect changes in seawater Li/Ca but rather reflect environmental changes which affect the incorporation of lithium into foraminiferal calcite. Based on the comparison of our record, alongside known changes in the North Pacific during the deglaciation, it is possible our Li/Ca record reflects a combination of increasing deglacial temperatures and increased CO_2 levels. These two environmental effects were also suggested by Hall and Chan (2004) as potential drivers of Li/Ca change in planktic foraminifera.

Our Ba/Ca record is stable and low throughout the major transitional periods of the last deglaciation. Very small shifts in Ba/Ca are seen during late HS1 and the beginning of the B/A, however our record is dominated by a large abrupt shift occurring during the Y/D where Ba/Ca increases from 15 µmol/mol to ~60 µmol/mol. Ba/Ca in planktic foraminifera has been thought to reflect a suite of environmental variables such as salinity, temperature and the carbonate system (Allen *et al.,* 2016). It has also been suggested that Ba/Ca may be influenced by changes in the [Ba] of seawater, particularly the influence of freshwater runoff (which has a higher [Ba] than seawater) (Allen *et al.,* 2016). The influence of freshwater runoff could explain the trend seen in our deglacial Ba/Ca record. As the Cordilleran ice sheet reduced in size during the latter stages of the deglaciation, increased freshwater runoff from the North American continent could have increased the [Ba] content of seawater leading to an enrichment of Ba/Ca during the Y/D and much of the Holocene.

The two most difficult TE/Ca ratios to interpret from our deglacial records and Na/Ca and B/Ca. Na/Ca ratios, which have been known to show a positive correlation with salinity (Allen *et al.*, 2016), show the opposite trend in our North Pacific core-tops (Appendix 1). The gradual reduction in Na/Ca over the B/A and Y/D may suggest a switch to lower salinity conditions as the Cordilleran Ice Sheet melted and flushed the North Pacific basin with freshwater. However, several documented shifts in ventilation during HS1 and the B/A (Rae *et al.*, 2014; Maier *et al.*, 2015, see chapter 5), which would require substantial changes in salinity, to not appear to influence our Na/Ca record (Figure 7.3). Further investigation of the incorporation of Na into planktic foraminifera tests is required to better interpret this record. With regards to our B/Ca record, no major shifts in B/Ca are observed apart from an initial LGM peak in B/Ca at 20 ka. Following this, B/Ca gently decreases towards the Holocene and doesn't appear to reflect changes in CO_2 or carbonate chemistry, its primary use as a proxy, limiting its use in interpreting deglacial changes in North Pacific circulation and CO_2.

Conclusion and future work

Overall, our additional deglacial TE/Ca records from the North Pacific can help reinforce some of the environmental changes thought to occur during this period of earth's history. Our Sr/Ca records seem to reflect SST temperatures, adding weight to the idea of rising temperatures at the onset of the B/A and the use of Sr/Ca ratios as a paleothermometer (subject to further ground truthing studies). Nd/Ca ratios may also track changes in bottom water redox state thought to occur due to basin wide changes in bottom water oxygenation caused by enhanced productivity during the B/A (Jaccard and Galbraith, 2011). Ba/Ca ratios may be used to track influences of freshwater flux into the North Pacific, but this again requires further investigation, whilst the remaining TE/Ca ratios presented also require further study to interpret fully. We hope that these records may provide the basis for future work to better clarify and understand the incorporation of less commonly utilised trace elements into planktic foraminifera tests.

References

Allen, K.A. et al., 2016. Trace element proxies for surface ocean conditions: A synthesis of culture calibrations with planktic foraminifera. *Geochimica et Cosmochimica Acta*, 193, pp.197–221.

Barker, S., Greaves, M. & Elderfield, H., 2003. A study of cleaning procedures used for foraminiferal Mg/Ca paleothermometry. *Geochemistry, Geophysics, Geosystems*, 4(9).

Elderfield, H. & Ganssen, G., 2000. Past temperature and $\delta^{18}O$ of surface ocean waters inferred from foraminiferal Mg/Ca ratios. *Nature*, 405(6785), pp.442–445.

Galbraith, E.D. et al., 2007. Carbon dioxide release from the North Pacific abyss during the last deglaciation. *Nature*, 449(7164), pp.890–3.

Gebhardt, H. et al., 2008. Paleonutrient and productivity records from the subarctic North Pacific for Pleistocene glacial terminations I to V. *Paleoceanography*, 23(4).

Gray, W.R. et al., 2018. Deglacial upwelling, productivity and CO2 outgassing in the North Pacific Ocean. *Nature Geoscience*.

Hall, J.M. & Chan, L.H., 2004. Li/Ca in multiple species of benthic and planktonic foraminifera: Thermocline, latitudinal, and glacial-interglacial variation. *Geochimica et Cosmochimica Acta*, 68(3), pp.529–545.

Hall, J.M. et al., 2005. Determination of the lithium isotopic composition of planktic foraminifera and its application as a paleo-seawater proxy. *Marine Geology*, 217(3–4), pp.255–265.

Jaccard, S.L. & Galbraith, E.D., 2011. Large climate-driven changes of oceanic oxygen concentrations during the last deglaciation. *Nature Geoscience*, 5(2), pp.151–156.

Maier, E. et al., 2015. Deglacial subarctic Pacific surface water hydrography and nutrient dynamics and links to North Atlantic climate variability and atmospheric CO_2, pp.1–20.

Martínez-Botí, M.A., Vance, D. & Mortyn, P.G., 2009. Nd/Ca ratios in plankton-towed and core top foraminifera: Confirmation of the water column acquisition of Nd. *Geochemistry, Geophysics, Geosystems*, 10(8).

NGRIP Members et al., 2004. High-resolution record of Northern Hemisphere climate extending into the last interglacial period. *Nature*, 431(7005), pp.147–151.

Okazaki, Y. et al., 2010. Deepwater formation in the North Pacific during the Last Glacial Termination. *Science (New York, N.Y.)*, 329(5988), pp.200–4.

Rae, J.W.B. et al., 2014. Deep water formation in the North Pacific and deglacial CO2 rise. *Paleoceanography*, 29, pp.645–667.

Rickaby, R.E.M. & Elderfield, H., 1999. Planktonic foraminiferal Cd/Ca. *Paleoceanography*, 14(3), pp.293–303.

Wang, Y.J., 2001. A High-Resolution Absolute-Dated Late Pleistocene Monsoon Record from Hulu Cave, China. *Science*, 294(5550), pp.2345–2348.

Wu, J.Y. et al., 2009. An exceptionally strengthened East Asian summer monsoon event between 19.9 and 17.1 ka BP recorded in a Hulu stalagmite. *Science in China, Series D: Earth Sciences*, 52(3), pp.360–368.

Yu, J. et al., 2013. Calibration and application of B/Ca, Cd/Ca, and δ11B in Neogloboquadrina pachyderma (sinistral) to constrain CO2 uptake in the subpolar North Atlantic during the last deglaciation. *Paleoceanography*, 28(2), pp.237–252.

Core	Depth (m)	Age (ka)	Li/Ca µmol/mol	B/Ca µmol/mol	Na/Ca mmol/mol	Sr/Ca mmol/mol	Ba/Ca µmol/mol	Nd/Ca µmol/mol
MD02-2489	50	6.44	13.19	41.70	5.422	1.398	6.16	4.79
MD02-2489	60	7.76	12.46	48.78	5.265	1.395	51.25	4.52
MD02-2489	70	9.02	11.98	45.26	5.227	1.372	50.05	3.57
MD02-2489	75	9.33	12.95	44.65	5.365	1.394	43.96	4.08
MD02-2489	85	10.39	12.91	56.68	5.235	1.383	49.69	4.14
MD02-2489	90	11.06	12.48	59.51	5.184	1.389	50.73	3.42
MD02-2489	95	11.78	13.94	45.84	5.617	1.417	59.23	3.00
MD02-2489	100	12.20	14.44	47.94	5.682	1.406	15.00	3.51
MD02-2489	110	12.90	15.51	55.72	5.901	1.427	4.41	2.78
MD02-2489	115	13.04	15.87	45.47	5.947	1.413	4.88	2.01
MD02-2489	125	13.39	17.00	50.92	6.028	1.409	16.46	2.58
MD02-2489	135	13.79	16.58	48.89	6.037	1.418	5.08	2.40
MD02-2489	145	14.14	16.31	58.66	5.996	1.401	2.97	2.48
MD02-2489	151.5	14.29	17.09	52.96	6.067	1.398	10.77	3.72
MD02-2489	155	14.37	16.92	60.98	6.136	1.423	3.00	3.95
MD02-2489	160	14.48	17.41	56.67	6.122	1.421	6.67	7.49
MD02-2489	165	14.59	15.24	49.24	5.870	1.434	6.43	9.38
MD02-2489	170	14.78	14.80	63.41	5.888	1.456	5.89	8.96
MD02-2489	175	15.00	17.27	63.80	6.056	1.437	15.45	13.72
MD02-2489	185	15.45	16.42	54.95	5.985	1.437	18.70	14.85
MD02-2489	193	15.81	16.63	66.11	6.189	1.460	6.25	10.27
MD02-2489	198	16.07	17.40	55.13	6.161	1.449	11.08	17.06
MD02-2489	204	16.45	16.33	54.92	6.053	1.467	4.74	13.73
MD02-2489	218	17.32	18.55	51.77	6.019	1.442	8.68	11.36
MD02-2489	227	17.88	20.26	54.70	5.964	1.458	8.69	12.65
MD02-2489	235	18.12	19.29	51.13	6.015	1.456	9.29	10.60
MD02-2489	250	18.66	20.56	51.19	6.107	1.444	11.90	14.32
MD02-2489	260	19.20	19.59	56.64	5.999	1.437	2.65	11.07
MD02-2489	275	20.00	19.95	75.17	6.064	1.451	6.61	10.96
MD02-2489	285	20.53	19.42	59.74	5.901	1.438	4.66	13.53
MD02-2489	298	21.49	18.10	52.25	5.757	1.446	7.35	11.26

Table 7.2: Trace element calcium ratios from sediment core MD02-2489 in the North East Pacific.

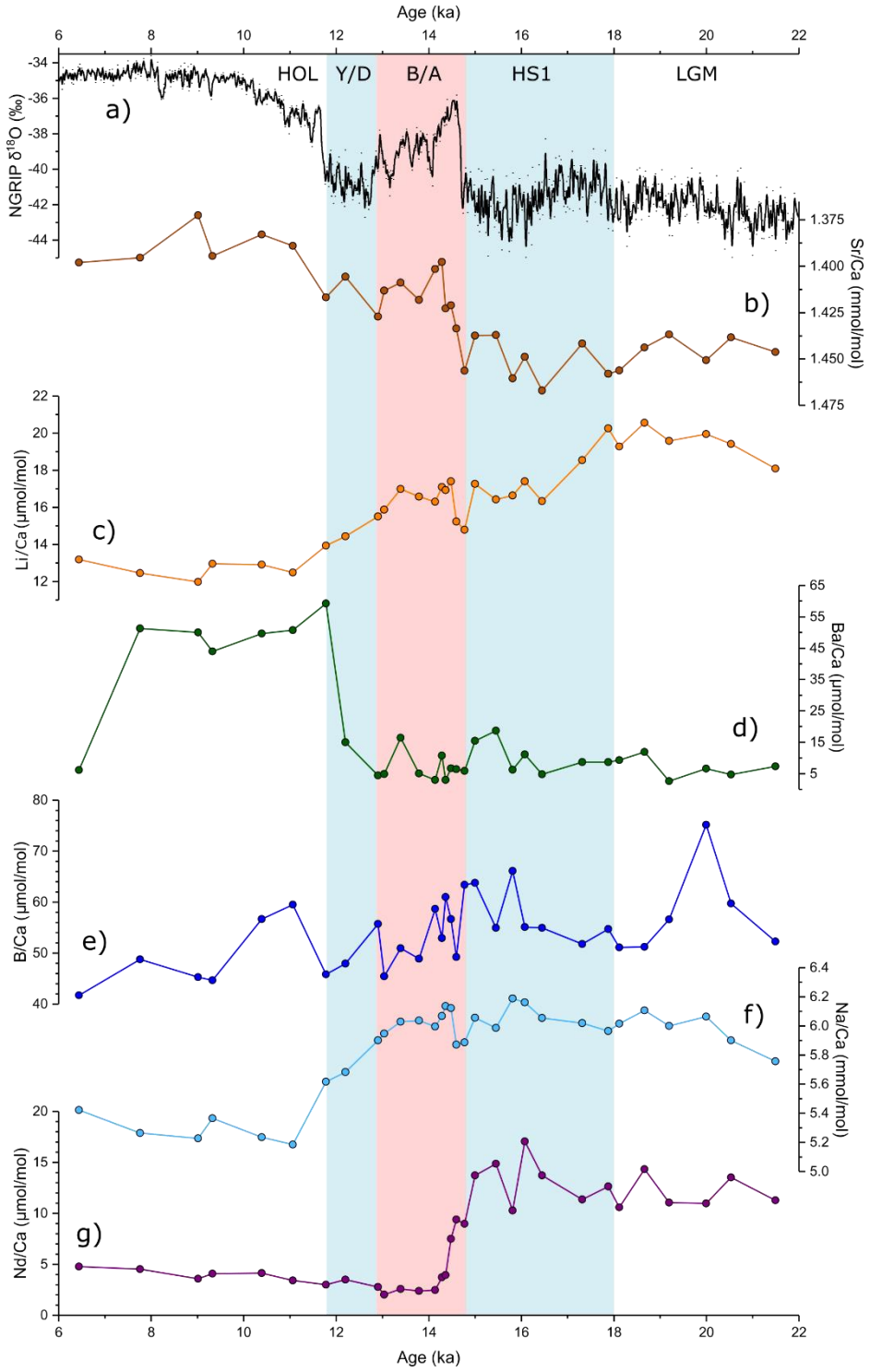

Figure 7.3: Deglacial T/E data from sediment core MD02-2489. a) d18O record from the Greenland ice (NGRIP members, 2004). b) Sr/Ca (mmol/mol) ratios from MD)2-2489. c) Li/Ca ratios (µmol/mol) from MD02-2489. d) Ba/Ca ratios (µmol/mol) from MD02-2489. e) B/Ca ratios (µmol/mol) from MD02-2489. Na/Ca ratios (mmol/mol) from MD02-2489. g) Nd/Ca ratios from MD02-2489. Shaded bars represent key time intervals during the last deglaciation. LGM is the Last Glacial Maximum; HS1 (blue) is Heinrich Stadial 1; B/A (red) is the Bølling-Allerød; Y/D (blue) is the Younger Dryas; HOL is the Holocene.

7.3 Appendix 3: Glacial sedimentology of marine sediment core ODP 887

Introduction

Sediment core ODP 887 (54.37° N, 148.45° W) is located on the Patton-Murray Seamount at a depth of 3674 m. The North East Pacific core has been widely used to reconstruct past climate in the region over the past 500,000 years (Galbraith *et al.,* 2007; Galbraith *et al.,* 2008; Gebhardt *et al.,* 2008; Rae *et al.,* 2014). The most extensive work associated with ODP 887 is Galbraith *et al.,* (2008)'s 500 kyr record of bulk nitrogen isotopes which assessed the relationship between nitrate utilization and changes in global climate. On shorter timescales, it has been used to track changes in the deglacial evolution of the region through radiocarbon ventilation records and measurements of opal accumulation to determine productivity changes (Galbraith *et al.,* 2007). Its location on the Patton-Murray Seamount allows for the comparison with other nearby sediment cores, particularly MD02-2489 (54.39° N, 148.92° W, 3640 m) (Rae *et al.,* 2014) and SO202-27-6 (54.30° N, 149.6° W, 2929 m) (Maier *et al.,* 2015).

My initial aim was to produce several high-resolution records spanning the entire last glacial from ~125 kyr to modern. These records would include planktic foraminifera boron isotope and surface CO_2 reconstructions, as well as planktic foraminifera census data to investigate environmental change. Unfortunately, after the initial preparation of the core material I discovered much of the core material was barren of planktic foraminifera with only a few sites containing enough specimens for geochemical analysis. Interestingly, I also noted several horizons within the core where core material was dominated by "fluffy" siliceous material, these appear to be synchronous with diatom horizons noted by McDonald *et al.,* (1999). Although my initial project aims could not be addressed, I present coarse fraction data from ODP 887 spanning the last glacial. In addition, I highlight the distribution of siliceous horizons and presence of planktic foraminifera for use in future studies.

Methods and Results

In total, 57 samples from sediment core ODP 887B were obtained and prepared for foraminiferal geochemistry and census analysis. The samples spanned from 1.75 cm to 1048 cm below sea floor (cmbsf). Samples were washed, dried and sieved above 63 μm to attain the coarse faction. Samples were then sieved >150 μm and analysed under light microscope to identify samples containing planktic foraminifera and those with high amounts of siliceous.

The coarse fraction of sediment core ODP 887B ranged from 2.4 % to 34.2 % with an average of 13.7 %. Siliceous layers were predominantly found in deeper sections of the core commonly between 470 and 940 cmbsf (Figure 7.4). A horizon with increased numbers of planktic

foraminifera was also identified between 160 and 415 cmbsf, however this is punctuated by a hiatus in ODP 887B between 174.5 and 375.5 cmbsf (Figure 7.4). No obvious trend in percentage coarse fraction is observed in the deeper sections of our record (Figure 7.4). Coarse fraction shifts rapidly between 650 and 900 cmbsf before a peak in % coarse fraction is observed at 600 cmbsf (Figure 7.4). Above 200 cmbsf, coarse fraction drops steadily towards lower values near the surface (Figure 7.4).

Discussion and future work

I plot my coarse fraction data, siliceous horizons, and foraminifera data alongside the percentage $CaCO_3$ content of ODP 887B (McDonald *et al.,* 1997) (Figure 7.4). No clear relationship is seen between coarse fraction and percentage calcium carbonate. This is expected due to a lack of planktic foraminifera and suggests that carbonate content (foraminifera and coccolithophores) does not control coarse fraction in this sediment core. Instead, other factors such as export production or the inclusion of IRD is likely to control the coarse fraction at this site. Records of IRD from this region are already known to influence sediments during the middle stages of the last deglaciation (Hewitt *et al.,* 1997; Maier *et al.,* 2015). This is exemplified in the top 2 m of the sediment core where percentage coarse fraction and percent $CaCO_3$ display an inverse relationship with peaks in $CaCO_3$ % associated with troughs in % coarse fraction.

The siliceous layers observed in the sediment core predominantly occur where coarse fraction is between 10-30 % during the middle section of our record (4.5-7 m) suggesting high levels of export production may exert an influence over coarse fraction at this point. Through detailed analysis of the core material, previous literature (Shipboard Scientific Party, 1993; McDonald *et al.,* 1997; Galbraith *et al.,* 2006) and discussions with Eric Galbraith, it was noted that a 3.37 m section of core ODP 887B was lost during coring and that to achieve a full glacial stratigraphy ODP 887B would have to be spliced with sections of ODP 887C or 887A (McDonald *et al.,* 1997). The depth range of the section lost appears to be 174.5 cm to 375.5 cmbsf. Samples obtained to fill this gap from ODP 887C are shown in Figure 7.4 and covered a depth range of 174.5 to 412 cmbsf.

Although the planned project for ODP 887 was unsuccessful, I hope that this section adds useful information for anybody looking to utilise this core in the future and allows for improved project planning on this well positioned and highly useful core.

References

Galbraith, E.D. et al., 2008. Consistent relationship between global climate and surface nitrate utilization in the western subarctic Pacific throughout the last 500 ka. *Paleoceanography*, 23(2), pp.1–11.

Galbraith, E.D. et al., 2007. Carbon dioxide release from the North Pacific abyss during the last deglaciation. *Nature*, 449(7164), pp.890–3.

Gebhardt, H. et al., 2008. Paleonutrient and productivity records from the subarctic North Pacific for Pleistocene glacial terminations I to V. *Paleoceanography*, 23(4).

Hewitt, A.T., McDonald, D. & Bornhold, B.D., 1997. Ice-rafted debris in the North Pacific and correlation to North Atlantic climatic events. *Geophysical Research Letters*, 24(24), pp.3261–3264.

Maier, E. et al., 2015. Deglacial subarctic Pacific surface water hydrography and nutrient dynamics and links to North Atlantic climate variability and atmospheric CO2. pp.1–20.

McDonald, D., 1997. The late Quaternary history of primary productivity in the subarctic east Pacific. M.S.c. Thesis, University of British Columbia, Canada.

McDonald, D., Pedersen, T.F. & Crusius, J., 1999. Multiple late Quaternary episodes of exceptional diatom production in the Gulf of Alaska. *Deep-Sea Research Part II: Topical Studies in Oceanography*, 46(11–12), pp.2993–3017.

Rae, J.W.B. et al., 2014. Deep water formation in the North Pacific and deglacial CO_2 rise. *Paleoceanography*, 29, pp.645–667.

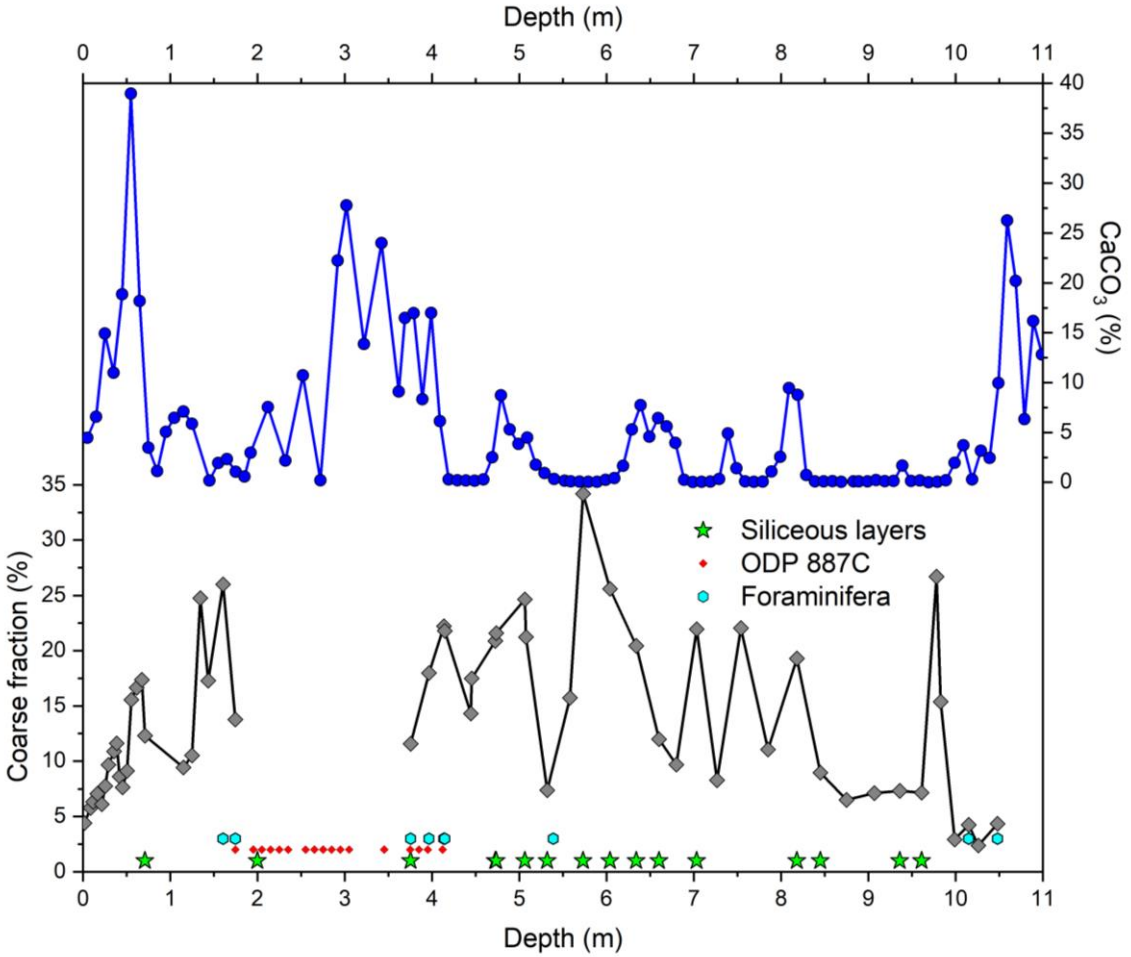

Figure 7.4: Full glacial cycle from sediment core ODP 887B. Percent $CaCO_3$ for ODP 887 is from McDonald et al., (1997) (dark blue circles). New % coarse values are in grey, the gap in data highlights the hiatus within sediment core ODP 887B. Green stars show the layers of siliceous fluff found within the core, whilst light blue circles denote depths where foraminifera were present. Red diamonds indicate samples from ODP 887C which are yet to be processed.

Site	Hole	Core	Section	Working/ Archive	Top (cm)	Bottom (cm)	Mean Composite Depth (cm)	Age (ka) McDonald (1997)	Coarse Fraction (%)	S*	F[1]
887	B	1	1	A	1	2.5	1.75	0.4	4.39		
887	B	1	1	W	8	9	8.5	1.8	5.76		
887	B	1	1	W	11	12	11.5	2.4	6.33		
887	B	1	1	W	16	17	16.5	3.4	7.06		
887	B	1	1	W	21	22	21.5	4.4	6.11		
887	B	1	1	W	25	26	25.5	5.3	7.75		
887	B	1	1	W	28.5	29.5	29	6.0	9.68		
887	B	1	1	W	35	36	35.5	7.4	10.88		
887	B	1	1	W	38	39	38.5	8.0	11.61		
887	B	1	1	W	41.5	42.5	42	8.8	8.61		
887	B	1	1	A	45	46	45.5	9.6	7.62		
887	B	1	1	W	50	51	50.5	10.6	9.11		
887	B	1	1	A	55	56	55.5	11.7	15.55		
887	B	1	1	A	61	62	61.5	13.2	16.65		
887	B	1	1	A	67	68	67.5	13.9	17.36		
887	B	1	1	W	70.5	71.5	71	14.1	12.31	*	
887	B	1	1	W	113.5	114.5	114	18.1			
887	B	1	1	W	114.5	115.5	115	18.2	9.44		
887	B	1	1	W	124.5	125.5	125	19.2	10.52		
887	B	1	1	W	134	135	134.5	20.3	24.75		
887	B	1	1	W	143	144	143.5	21.7	17.27		
887	B	1	2	W	10	11	160.5	24.3	26.00		1
887	B	1	2	W	24	25	174.5	25.2	13.77	*	1
887	B	2	1	W	11	12	375.5	53.7	11.57	*	1
887	B	2	1	W	32	33	396.5	56.5	17.98		1
887	B	2	1	W	49	50	413.5	58.8	22.22		1
887	B	2	1	W	50	51	414.5	58.9	21.78		1
887	B	2	1	W	80	81	444.5	64.2	14.30		
887	B	2	1	W	81	82	445.5	64.4	17.49		
887	B	2	1	W	108	109	472.5	69.1	20.87	*	
887	B	2	1	W	109	110	473.5	69.3	21.57	*	
887	B	2	1	W	141.5	143	506.25	73.1	24.63	*	
887	B	2	1	W	143	144	507.5	73.2	21.22		
887	B	2	2	W	17	19	532	75.4	7.37	*	
887	B	2	2	W	24	26	539	76.0			1
887	B	2	2	W	43	45	558	77.7	15.74	*	
887	B	2	2	W	58	60	573	79.1	34.19	*	
887	B	2	2	W	89	91	604	81.8	25.59	*	
887	B	2	2	W	119	121	634	85.4	20.43	*	
887	B	2	2	W	145	147	660	89.1	11.98		
887	B	2	3	W	15	17	680	91.9	9.70	*	
887	B	2	3	W	38.5	40	703.25	95.1	21.93		
887	B	2	3	W	61.5	63.5	726.5	98.1	8.28		
887	B	2	3	W	89	91	754	101.7	22.05		
887	B	2	3	W	120	122	785	104.9	11.05	*	
887	B	2	4	W	3	5	818	107.0	19.28	*	
887	B	2	4	W	30	32	845	108.8	8.96		
887	B	2	4	W	60	62	875	110.8	6.49		
887	B	2	4	W	92	94	907	112.9	7.12	*	
887	B	2	4	W	121	123	936	114.9	7.31	*	
887	B	2	4	W	146	148	961	118.0	7.15		
887	B	2	5	W	13	15	978	120.2	26.70		
887	B	2	5	W	18	20	983	120.9	15.37		
887	B	2	5	W	34	36	999	122.9	2.91		
887	B	2	5	W	50	52	1015	125.0	4.23		1
887	B	2	5	W	61	63	1026	126.4	2.37		
887	B	2	5	W	83	85	1048	129.4	4.33		1

Table 7.3: Downcore percent coarse for sediment core ODP 887B. The dashed line represents a hiatus within sediment core ODP 887B.

7.4 Appendix 4: Benthic-planktic radiocarbon offsets from ODP 887B

Introduction

A popular method with which to assess changes in deep ocean ventilation is the use of benthic and planktic radiocarbon offsets. This involves the comparison of radiocarbon measurements from benthic and planktic foraminifera to calculate a ventilation age or Benthic-Planktic offset (B-P offset). Planktic foraminifera record the radiocarbon content of surface waters which reflect the exchange of CO_2 between the ocean and the atmosphere. In contrast, benthic foraminifera radiocarbon ages reflect the time since a parcel of water has been in contact with the atmosphere. When B-P offsets are low, it suggests increased interaction between surface and deep waters, whilst higher B-P offsets are suggestive of a more stratified water column.

Benthic-planktic radiocarbon offsets have been used to assess changes in North Pacific ventilation during the last deglaciation (Galbraith *et al.,* 2007; Okazaki *et al.,* 2010; Rae *et al.,* 2014). At intermediate depths during the last deglaciation, Okazaki *et al.,* (2010) showed that B-P offsets decreased during HS1 suggesting increased ventilation of intermediate waters. This was followed by a substantial increase in B-P offsets at the onset of the B/A signalling enhanced stratification (Okazaki *et al.,* 2010). In addition, B-P offsets from MD02-2489 (3640 m) show a large decrease in ventilation age during the middle of HS1 (Rae *et al.,* 2014) (Figure 7.5). Rae *et al.,* (2014) used this to suggest a pulse of deepwater formation, which ventilated intermediate and deep water in the North East Pacific leading to high CO_2 surface waters and deglacial CO_2 rise (see chapter 5). Whilst radiocarbon data from the adjacent site ODP 887B analysed by Galbraith *et al.,* (2007) do not show this excursion, the sample resolution from their record is such that the interval of low B-P offsets seen in MD02-2489 is not covered (Figure 7.5).

To address this, we present new radiocarbon B-P offsets from ODP 887B to fill the gap in the record of Galbraith *et al.,* (2007). We use this data to compare changes in radiocarbon B-P offsets and potential sediment core bioturbation between the two cores.

Methods

Fourteen samples from sediment core ODP 887B (54.37° N, 148.45° W) were analysed for radiocarbon. Of these, six samples comprised of mixed benthic foraminifera with the exclusion of deep-dwelling species (Magana *et al.,* 2010) (Table 7.4). Of the remaining samples, six samples of the planktic foraminifera *N. pachyderma* and two samples of *G. bulloides* were picked for analyses. The samples of *G. bulloides* were picked for comparison and are not discussed below. Samples were analysed by Accelerator Mass Spectrometry (AMS) at the University of California Irvine. Radiocarbon uncertainties are given at 1 SE. Uncertainty on our samples ranged from 70

^{14}C yrs to 310 ^{14}C yrs, the large uncertainty on some of our samples is due primarily to the small sample size and lack of foraminifera across this interval in the core (Figure 7.5).

Results and Discussion

In order to assess our new radiocarbon data, we combined it with the previously published radiocarbon values from Galbraith *et al.,* (2007) (Figure 7.5). The large excursion seen within B-P data from MD02-2489 during HS1 is not seen within our new radiocarbon data (Figure 7.5). Instead we see a small decrease in B-P offset during the middle of the excursion but, predominantly due to young planktic values, the magnitude of this change does not compare to that observed by Rae *et al.,* (2014). Although this may initially cast doubt on the hypothesis of increase North Pacific deepwater formation during HS1, when compared with new foraminifera abundance data from the same core it seems more likely that radiocarbon differences observed between the two cores are due to sedimentation and bioturbation.

The newly generated foraminifera abundance data from ODP 887B show dramatic decreases in abundance of both benthic and planktic foraminifera during the middle of HS1 (Figure 7.5). This is in line with low benthic boron isotope values from Rae *et al.,* (2014) suggesting corrosive deep waters existed during this interval. Whilst benthic abundance drops at the onset of the B-P excursion seen in MD02-2489, planktic abundance decline occurs slightly earlier and does not reach its lowest values until 16.5 ka (Figure 7.5). Compared with MD02-2489, ODP 887B has a lower sedimentation rate and is therefore likely to be more influenced by bioturbation (Trauth *et al.,* 1997; Rae *et al.,* 2014). In addition, due to the "Barker effect" in this corrosive environment the only planktic foraminifera likely to be preserved are those quickly mixed into the sediment (Barker *et al.,* 2007; Broecker and Clark, 2011). If we assume the MD02-2489 record shows little or no bioturbation (Rae *et al.,* 2014), a smoothed recorded of this may show a signal similar to that expected of a bioturbated core (Figure 7.5). Indeed, various degrees of smoothing to point towards a trend similar to that seen in ODP 887B suggesting bioturbation may cause the old radiocarbon ages observed in benthic foraminifera and the young ages seen in the planktic data from this site. Simple smoothing only represents a very basic bioturbation model, a more complex model, alongside further radiocarbon data from across the interval may shed more light on the radiocarbon discrepancies between the two sediment cores.

References

Barker, S. et al., 2007. Radiocarbon age offsets of foraminifera resulting from differential dissolution and fragmentation within the sedidmentary bioturbated zone. Paleoceanography, 22(2), pp.1–11.

Broecker, W. & Clark, E., 2011. Radiocarbon-age differences among coexisting planktic foraminifera shells: The barker effect. Paleoceanography, 26(2), pp.1–7.

Magana, A.L. et al., 2010. Resolving the cause of large differences between deglacial benthic foraminifera radiocarbon measurements in Santa Barbara Basin. *Paleoceanography*, 25(4), pp.1–8.

Trauth, M.H., Sarnthein, M. & Arnold, M., 1997. Bioturbation mixing depth and carbonate flux at the seafloor. *Paleoceanography*, 12(3), pp.517–526.

Galbraith, E.D. et al., 2007. Carbon dioxide release from the North Pacific abyss during the last deglaciation. *Nature*, 449(7164), pp.890–3.

Okazaki, Y. et al., 2010. Deepwater formation in the North Pacific during the Last Glacial Termination. *Science (New York, N.Y.)*, 329(5988), pp.200–4.

Rae, J.W.B. et al., 2014. Deep water formation in the North Pacific and deglacial CO2 rise. *Paleoceanography*, 29, pp.645–667.

UCIAMS #	Sample name	Fraction Modern	±	$D^{14}C$ (‰)	±	^{14}C age (BP)	±
156825	ODP887B 1H1W 102.5-103.5 pachy .16mgC	0.1322	0.0018	-867.8	1.8	16260	110
156826	ODP887B 1H1W 102.5-103.5 benth .075mgC	0.1000	0.0032	-900.0	3.2	18490	270
156827	ODP887B 1H1A 94-95 pachy .15mgC	0.1527	0.0017	-847.3	1.7	15100	90
156828	ODP887B 1H1A 94-95 benth .058mgC	0.1220	0.0041	-878.0	4.1	16900	280
156829	ODP 887B 1H1W 91-92 pachy .13mgC	0.1623	0.0019	-837.7	1.9	14610	100
156830	ODP 887B 1H1W 91-92 bull .077mgC	0.1673	0.0030	-832.7	3.0	14360	150
156831	ODP 887B 1H1W 91-92 benth .075mgC	0.1233	0.0032	-876.7	3.2	16810	210
156832	ODP887B 1H1A 87.5-89 pachy .14mgC	0.1691	0.0018	-830.9	1.8	14280	90
156837	ODP887B 1H1A 87.5-89 benth .073mgC	0.1370	0.0033	-863.0	3.3	15970	200
156838	ODP887B 1H1A 86-87.5 pachy .10mgC	0.1716	0.0023	-828.4	2.3	14160	110
156839	ODP887B 1H1A 86-87.5 benth .044mgC	0.1426	0.0055	-857.4	5.5	15650	310
156840	ODP887B 1H1A 80-81 pachy .16mgC	0.1730	0.0015	-827.0	1.5	14090	70
156841	ODP887B 1H1A 80-81 bull .15mgC	0.1735	0.0015	-826.5	1.5	14070	80
156842	ODP887B 1H1A 80-81 benth .11mgC	0.1429	0.0021	-857.1	2.1	15630	120

Table 7.4: Radiocarbon analyses from sediment core ODP 887B. Samples were analysed by AMS at the University of California, Irvine.

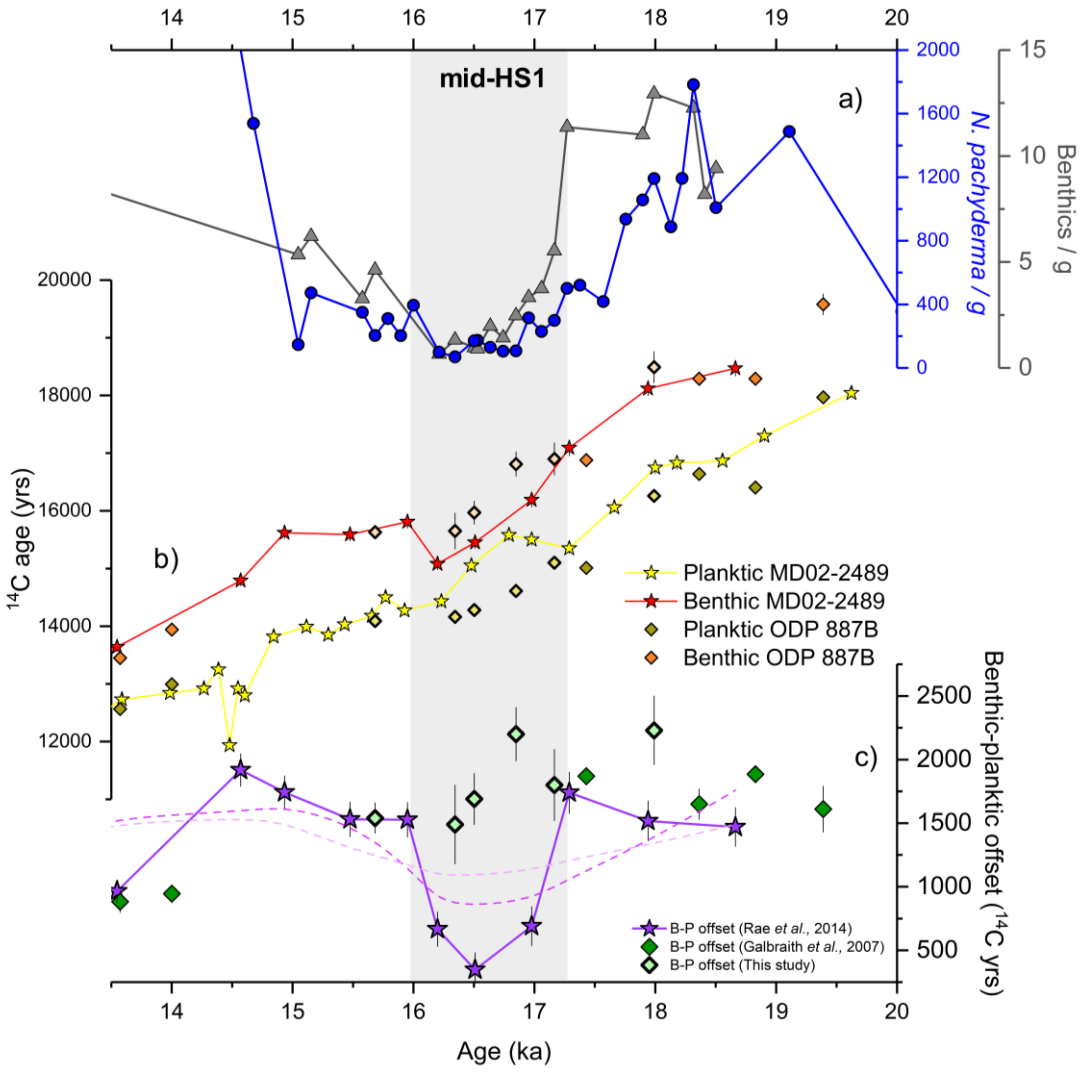

Figure 7.5: New radiocarbon and census data from ODP 887B alongside published radiocarbon records from Rae et al., (2014). ***a)*** *N. pachyderma per gram of sediment (blue circles) alongside benthic foraminifera per gram of sediment (grey triangles).* ***b)*** *New benthic (light red diamonds) and planktic (light yellow diamonds) from ODP 887B alongside published data from Galbraith et al., (2007) (orange and gold diamonds) and from Rae et al., (2014) from MD02-2489 (red and yellow stars).* ***c)*** *B-P offsets for ODP 887B and MD02-2489 (Rae et al., 2014). New B-P offsets are shown in light green, with those from Galbraith et al., (2007) in dark green. B-P offsets from Rae et al., (2014) are shown in purple, dashed lines represent smoothed curves of different strengths to demonstrate the possible effects of bioturbation.*